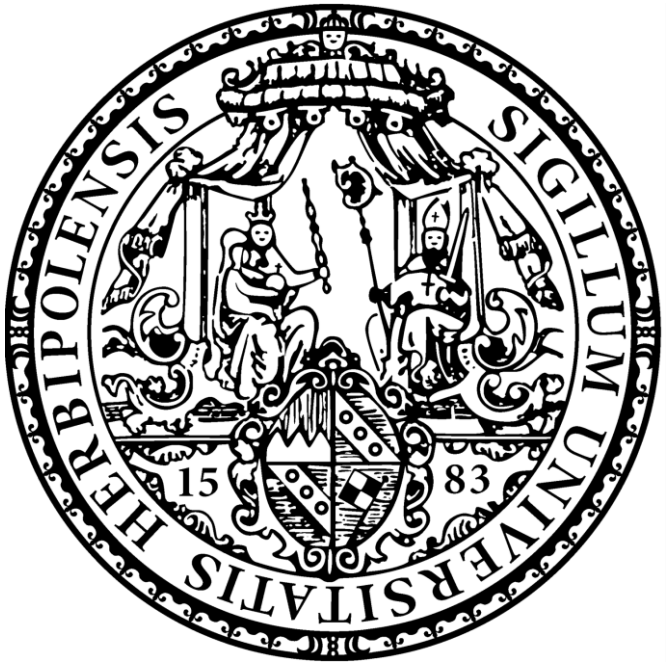

Induction of ectopic bone formation by site directed immobilized BMP2 variants *in vivo*

Induktion ektoper Knochenbildung durch gerichtet immobilisierte BMP2-Varianten *in vivo*

Doctoral thesis for a doctoral degree
at the Graduate School of Life Sciences,
Julius-Maximilians-Universität Würzburg,
Section Biomedicine

submitted by

Claudia Siverino

from Catania (Italy)

Würzburg 2018

Submitted on:

……..……..

Office stamp

Members of the Committee

Chairperson: Prof. Dr.

Primary Supervisor: Prof. Dr. Heike Walles

Supervisor (Second): Prof. Dr. Thomas Müller

Supervisor (Third): Dr. Joachim Nickel

Supervisor (Fourth): Dr. Tessa Lühmann

Date of Public Defense: ……..……

Date of Receipt of Certificates: …….

Dedicated to my parents

Dedicato ai miei genitori

“Intelligence is the ability to adapt to change”

-Stephen Hawking-

“L’intelligenza è la capacità di adattarsi al cambiamento”

Table of contents

Abstract

In contrast to common bone fractures, critical size bone defects are unable to self-regenerate and therefore external sources for bone replacement are needed. Currently, the gold standard to treat critical size bone fractures, resulting from diseases, trauma or surgical interventions, is the use of autologous bone transplantation that is associated with several drawbacks such as postoperative pain, increased loss of blood during surgery and extended operative time.

The field of bone tissue engineering focuses on the combination of biomaterials and growth factors to circumvent these adverse events and thereby to improve critical size bone defects treatment.

To this aim, a promising approach is represented by using a collagen sponge soaked with one of the most powerful osteoinductive proteins, the bone morphogenetic protein 2 (BMP2). After the approval by the Food and Drug Administration (FDA), BMP2 was used to successfully treat several severe bone defects. However, the use of BMP2 delivery systems is associated with severe side effects such as inflammation, swelling, ectopic bone formation outside of the site of implantation and breathing problems if implanted in the area of the cervical spine. The occurrence of severe side effects is related to the supraphysiological amounts of the applied protein at the implantation site. The BMP2 is typically adsorbed into the scaffold and diffuses rapidly after implantation. Therefore, intensive research has been conducted to improve the protein's retention ability, since a prolonged entrapment of the BMP2 at the implantation site would induce superior bone formation *in vivo* due to a minimized protein release. By controlling the release from newly designed materials or changing the protein immobilization methods, it seems possible to improve the osteoinductive properties of the resulting BMP2-functionalized scaffolds.

The combination of biocompatible and biodegradable scaffolds functionalized with a covalently immobilized protein such as BMP2 would constitute a new alternative in bone tissue engineering by eliminating the aforementioned severe side effects. One of the most common immobilization techniques is represented by the so-called EDC/NHS chemistry. This coupling technique allows covalent biding of the growth factor but in a non-site direct manner, thus producing an implant with uncontrollable and unpredictable osteogenic activities. Therefore, the generation of BMP2 variants harboring functional groups that allow a site-directed immobilization to the scaffold, would enable the production of implants with reproducible osteogenic activity.

The new BMP2 variants harbor an artificial amino acid at a specific position of the mature polypeptide sequence. The presence of the unnatural amino acid allows to use particular covalent immobilization techniques in a highly specific and site directed manner. The two selected BMP2 variants, BMP2 E83Plk and BMP2 E83Azide, were expressed in *E. coli*, renatured and purified by cation exchange chromatography. The final products were intensively analyzed in terms of purity and biological activity *in vitro*. The two BMP2 variants enabled the application of different coupling techniques and verify the possible options for site directed immobilization to the scaffold.

Intensive analyses on the possible side effects caused by the coupling reactions and on the quantification of the coupled protein were performed. Both click chemistry reactions showed high reaction efficacies when the BMP2 variants were coupled to functionalized fluorophores. Quantification by ELISA and scintillation counting of radioactively labeled protein revealed different outcomes. Moreover, the amounts of protein detected for the BMP2 variants coupled to microspheres were similar to that of the wild type protein. Therefore, it was not possible to conclude whether the BMP2 variants were covalently coupled or just adsorbed.

BMP2 variants being immobilized to various microspheres induced osteogenic differentiation of C2C12 cells *in vitro*, but only in those cells that were located in close proximity to the functionalized beads. This selectivity strongly indicates that the protein is for a great portion covalently coupled and not just adsorbed. Moreover, the difference between the covalently coupled BMP2 variants and the adsorbed BMP2 WT was confirmed *in vivo*. Injection of the BMP2-functionalized microspheres in a rat model induced subcutaneous bone formation.

The main aim of the animal experiment was to prove whether covalently coupled BMP2 induces bone formation at significant lower doses if compared to the amount being required if the protein is simply adsorbed. To this aim, several BMP2 concentrations were tested in this animal experiment. The BMP2 variants, being covalently immobilized, were hypothesized to be retained and therefore bio-available at the site of implantation for a prolonged time. However, in the animal experiments, lower doses of either coupled or adsorbed protein were unable to induce any bone formation within the 12 weeks.

In contrast, the highest doses induced bone formation that was first detected at week 4. During the 12 weeks of the experiment, an increase in bone density and a steady state bone volume was observed. These results were obtained only for the covalently coupled BMP2 E83Azide but not for BMP2 E83Plk that did not induce bone formation in any condition. The negative outcome after application of BMP2 E83Plk suggested that the coupling reaction might have

provoked changes in the protein structure that extremely influenced its osteogenic capabilities *in vivo*.

However, the histological examination of the different ossicles induced either by BMP2 WT or BMP2 E83Azide, revealed clear morphological differences. BMP2 WT induced a bone shell-like structure, while the covalently coupled protein induced uniform bone formation also throughout the inner part. The differences between the two newly formed bones can be clearly associated with the different protein delivery mechanisms. Thus, the developed functionalized microspheres constitute a new interesting strategy that needs further investigations in order to be able to be used as replacement of the currently used BMP2 WT loaded medical devices.

Zusammenfassung

Knochendefekte kritischer Größe sind im Vergleich zu normalen Knochenfrakturen nicht in der Lage selbst zu heilen. Daher werden zusätzlich Knochenersatzmaterialien zu deren Heilung benötigt. Der derzeitige Goldstandard in der Behandlung dieser Defekte, die durch Krankheiten, Traumata oder durch chirurgische Eingriffe hervorgerufen werden können, ist Transplantation autologen Knochens, was jedoch mit einigen Nachteilen verbunden ist. Als Alternative können neuartige biokompatible Materialien mit intrinsischem osteogenen Potential verwendet werden. Solche Materialien können Wachstumsfaktoren beinhalten welche aktiv die Heilung des beschädigten Knochens fördern.

Ein vielversprechender Ansatz um dieses Ziel zu erreichen, ist der Einsatz eines Kollagenträgers, welcher mit einem der stärksten osteoinduktiven Proteine, dem Bone Morphogenic Protein 2 (BMP2) dotiert ist. Nach der Genehmigung durch die Food and Drug Administration (FDA), wurde BMP2 erfolgreich bei der Behandlung von schwerwiegenden Knochendefekten eingesetzt. Daher wird es als bisher beste Alternative zu autologen Transplantaten sowie als beste Möglichkeit zur Anregung der Knochenneubildung angesehen. Nichtdestotrotz geht der Einsatz von mit BMP2 beladenen Trägersystemen mit Nebenwirkungen, wie Entzündungen Schwellungen, Knochenwucherungen abseits des behandelten Defektes sowie Atembeschwerden bei Behandlungen im Bereich der Halswirbelsäule einher. Die Nebenwirkungen werden durch die supraphysiologische Menge an Protein, mit der die Trägerstruktur beladen wird hervorgerufen. Jedoch ist solch eine Menge an Protein nötig, da die Abgabe des Proteins an der Transplantationsstelle sehr schnell abläuft. Deshalb konzentriert sich die Forschung auf die Verbesserung der Freisetzungskinetik, da ein längerer Verbleib des BMP2 an der Implantationsstelle sowie eine verringerte Freisetzung des Proteins eine bessere Knochenbildung *in vivo* herbeiführt. Die Freisetzungskinetik kann durch die Eigenschaften neu entwickelter Materialien selbst oder durch alternative Methoden der Kopplung des Proteins an die Trägerstruktur verändert werden.

Die Kombination aus biokompatiblen sowie biodegradierbaren Trägerstrukturen, an die über kovalente Bindungen BMP2 gebunden wird, stellt eine vielversprechende Alternative dar, welche die vorgenannten Nebenwirkungen bei der Knochenregeneration eliminiert. Die am häufigsten eingesetzte Methode zur kovalenten Anbindung von Proteinen an Trägerstukturen erfolgt über die sogenannte EDC/NHS-Chemie. Diese Technik erlaubt die allerdings nur eine ungerichtete Anbindung wodurch die standardisierte Reproduktion eines möglichen

Medizinproduktes erschwert wird. Als Resultat entstehen sehr wahrscheinlich Implantate mit unvorhersehbaren osteogenen Eigenschaften. Die Herstellung von BMP2-Varianten, welche gerichtet an Trägerstrukturen gekoppelt werden können, ermöglicht die Herstellung von Implantaten mit reproduzierbarer osteogener Aktivität.

Alle hier vorgestellte Varianten beinhalten eine artifizielle Aminosäure an einer bestimmten Stelle in der Polypeptidsequenz. Die künstliche Aminosäure ermöglicht den Einsatz spezieller Kopplungschemien für kovalente Bindungen, welche dadurch per Definition spezifisch und gerichtet sind. Für weiterführende Experimente wurden die folgende BMP2-Varianten ausgewählt: BMP2 E83Plk und BMP2 E83Azide. Diese wurden durch Expression in *E. coli* gewonnen, renaturiert und mittels Ionenchromatographie aufgereinigt. Die gewonnenen Produkte wurden hinsichtlich ihrer Reinheit und biologischen Aktivität *in vitro* untersucht. Beide BMP2 Varianten ermöglichen den Einsatz verschiedener Kopplungstechniken an geeignete Trägerstrukturen.

Analysen hinsichtlich möglicher Nebenwirkungen aufgrund der Kupplungsreaktion sowie die genaue Quantifizierung der gekoppelten Proteine auf den Mikrosphären wurden durchgeführt. Beide Kopplungsstrategien zeigten eine hohe Effizienz wobei für die Quantifizierung der Proteinmengen mittels ELISA und Szintillationszählung unterschiedliche Werte gemessen wurden. Des Weiteren war die gemessene Proteinmenge von an Mikrosphären gekoppelten BMP2 Varianten in einem ähnlichen Bereich, wie die bei der ungekoppelten BMP2 WT Kontrolle gemessen wurden. Daher war es nicht möglich zu bestimmen, inwieweit die verwendeten BMP2-Varianten kovalent gebunden oder lediglich adsorbiert waren.

Die BMP2 Varianten, die anhand der verwendeten Kopplungschemie in kovalent gebundener Form vorliegenden sollten, induzierten unabhängig vom jeweils verwendeten Material der Sphären die osteogene Differenzierung von C2C12 Zellen die in unmittelbarem Kontakt zu diesen Sphären standen. Im Falle von BMP2 WT beinhaltenden Sphären wurde auch Zelldifferenzierung in Distanz zu den einzelnen Sphären beobachten, was auf Diffusionsprozesse hindeutet. Da dies im Falle der kovalent gekoppelten BMP-2 Varianten nicht beobachtet werden konnte zeigt, dass das Protein hier zum Großteil kovalent gebunden vorliegt und nicht nur adsorbiert wird. Unterschiede zwischen den kovalent gebundenen BMP2 Varianten und dem adsorbierten Wildtyp zeigten sich auch in den Tierexperimenten. Mikrosphären, welche mit BMP2 WT oder einem der beiden BMP2 Varianten beladenen waren, wurden einer Ratte subkutan injiziert, was zu einer ektopen Knochenbildung führte. Das Ziel des Tierversuches war, zu überprüfen, ob geringere Dosen an kovalent gebundenem BMP2, verglichen mit der hohen benötigten Menge an adsorbiertem Protein diese

Knochenneubildung induzieren kann. Dabei wurden verschiedene BMP2 Konzentrationen getestet.

Die Hypothese war, dass die kovalent gebundenen BMP2 Varianten zurückgehalten werden beziehungsweise langsamer freigesetzt werden und daher über einen längeren Zeitraum an der Implantationsstelle wirksam sind. Allerdings konnte im Tierversuch weder durch niedrig dosiertes (< 10 µg) kovalent gebundenes noch durch adsorbiertes Protein innerhalb von 12 Wochen ektope Knochenbildung induziert werden.

Dagegen konnte mit der höchsten Dosis bereits nach 4 Wochen Knochenbildung nachgewiesen werden. Während des zwölfwöchigen Experiments konnte ein Anstieg der Knochendichte und ein Steady State des Knochenvolumens beobachtet werden. Dies traf jedoch nur für das kovalent gebundene BMP2 E83Azide zu, jedoch nicht für das BMP2 E83Plk, welches bei allen Dosen kein Knochenwachstum hervorrufen konnte. Das negative Ergebnis nach der Gabe von BMP2 E83Plk deutet darauf hin, dass die hier verwendete Kopplungschemie möglicherweise eine Veränderung der Proteinstruktur bewirkt und dadurch die biologische Aktivität des Proteins verloren geht.

Allerdings zeigten histologische Untersuchungen der gebildeten Knochenstrukturen, welche durch BMP2 WT oder durch BMP2 E83Azide hervorgerufen wurden, deutliche morphologische Unterschiede. BMP2 WT erzeugt eine solide schalenförmige Strukturen während das kovalent gebundene Protein ein eher gleichförmiges Knochenwachstum induziert, auch im Inneren der gebildeten Knochenstruktur, welches hier Reste implantierten Mikrosphären umschließt. Dies konnte nicht in den durch BMP2 WT induzierten Knochenstrukturen nachgewiesen werden. Der Unterschied zwischen den zwei Formen neu gebildeten Knochens kann mit den verschiedenen Freisetzungsmechanismen in Verbindung gebracht werden. Daher stellt die Entwicklung funktionalisierter Mikrosphären eine neue interessante Strategie dar, welche weiterführende Untersuchungen benötigt, um die aktuell genutzten BMP2 WT beinhaltenden Medizinprodukte zu ersetzen.

List of Figures

List of Tables

Abbreviation

^{3}H	Tritium
α-SMA	alpha-smooth muscle actin
AaRS	aminoacyl-tRNA-synthetase
ALIF	anterior lumbar interbody fusion
ALP	alkaline phosphatase
AMH	anti-Müllerian hormone
amber stop codon	TAG stop codon
APS	Ammonium persulfate
β-TCP	β-tri-calcium phosphate
BCA	bicinchoinic acid
BCP	biphasic calcium phosphate
BISC	BMP-induced signaling complex
BMP2 E83Azide	BMP2 variant containing Azide in place of glutamic acid 83
BMP2 K3Plk	BMP2 variant containing Plk in place of lysine 3 (K3)
BMP2 E83Plk	BMP2 variant containing Plk in place of glutamic acid (E83)
BMP2 E94Plk	BMP2 variant containing Plk in place of glutamic acid (E94)
BMP2 WT	wild type BMP2
BMPRIA (Alk3)	bone morphogenetic protein receptor, type IA
BMPRIB	bone morphogenetic protein receptor, type IB
BMPRII	bone morphogenetic protein receptor, type II
BMPs	bone morphogenetic proteins
BMSCs	bone marrow derived mesenchymal stem cells
BMU	basic multicellular unit
BRC	bone remodeling compartment
BSP I/II	bone sialoprotein I/II
C2C12	mouse myoblast cell line
CHAPS	3-[(3-Cholamidopropyl)dimethylammonio]-1-propanesulfonate
CHES	2-(Cyclohexylamino)ethanesulfonic acid
CKGF	cysteine know growth factor
Col1	collagen 1
cpm	counts per minutes

CuAAC	Copper(I)-catalyzed alkyne-azide cycloaddition
DBCO	dibenzocyclooctyne
dH_2O	deionized water
DHT	dehydrothermal
Dlx5	distal-less homeobox 5
DMEM	Dulbecco's Modified Eagle Medium
DTT	dithiothreitol
EC_{50}	half maximal effective concentration
EDC	1-ethyl-3-(3-dimethylaminopropyl)carbodiimide hydrochloride
EDTA	ethylenediaminetetraacetic acid
EMT	epithelial to mesenchymal transition
EndMT	endothelial to mesenchymal transition
ESI-MS	elektrospray-Ionisation mass spectrometry
FCS	fetal calf serum
FDA	Food and Drug Administration
FGF2	fibroblast growth factor 2
FPLC	fast protein liquid chromatography
FOP	fibrodysplasia ossificans progressive
GDF	Growth and Differentiation Factors
GDNF	glial-derived neurotrophic factors
GSH	glutathione
GSSG	glutathione disulfide
GuCl	guanidinium chloride
HA	hyaluronic acid
HAp	hydroxyapatite
HMDIC	hexamethylene diisocyanide
HPLC	high-performance liquid chromatography
HO	heterotopic ossification
IBs	inclusion bodies
IEX	ion exchange chromatography
IGF	insulin growth factor
IPTG	isopropyl β-D-1-thiogalactopyranoside
LB	lysogeny broth
M-CSF	macrophage colony stimulating factor

MIS	Müllerian inhibiting substance
MSCs	mesenchymal stem cell
MWCO	molecular weight cut-off
NaAsc	sodium ascorbate
NBT/BCIP	combination of nitro-blue tetrazolium chloride and 5-bromo-4-chloro-3'-indolyphosphate p-toluidine salt)
NHS	N-hydroxysuccinimide
NMWL	Nominal Molecular Weight Limit
OCN	osteocalcin
OD	optical density
OP1	osteogenic protein 1
OPG	osteoprotegerin
Osx	osteoblast-specific transcription factor Osterix
p38/MAPK	mitogen-activated protein kinases
PEG	polyethylene glycol
PBS	phosphate-buffered saline
Pen/Strep	penicillin/streptomycin
pET11a-pyrtRNA	plamid construct encoding BMP2 variants
PFC	preformed BMP complex
PLA	poly (lactic acid)
PLG	poly (glycolic acid)
PLGA	poly (lactic-co-glycolic) acid
Plk	N-Propargyl-lysine
pNPP	paranitrophenyl-phosphate
pRSFduet-pyrtRNAsynth	plasmid construct encoding pyrrolysyl tRNA synthetase
RCP	recombinant collagen like peptide
RANK	activator of nuclear factor kappa B
RANKL	Receptor Activator of Nuclear Factor-κB Ligand
ROS	reactive oxygen species
Runx2	Runt releated transcription factor 2
RT	room temperature
SDS	sodium dodecyl sulfate
SDS-PAGE	sodium dodecyl sulfate polyacrylamide gel electrophoresis
SEC	size exclusion chromatography

SPAAC	strain-promoted azide–alkyne cycloaddition
TB	terrific broth
TGF- β	transforming growth factor β
THPTA	tris(3-hydroxypropyltriazolylmethyl)amine
TNBS	2,4,6-trinitrobenzenesulfonic acid
TRAP	tartrate resistant alkaline phosphatase
Tris	tris(hydroxymethyl)aminomethane
VEGF	Vascular Endothelial Growth Factor
WB	Western blot

I. Introduction

1. The discovery of BMP2: how a simple molecule generates the complex bone tissue

The discovery of Bone Morphogenetic Protein (BMP) was a breakthrough in orthopedic surgeries and has revolutionized the study of bone biology. The history of BMPs starts in 1960, when Marshall R. Urist suggested the presence of osteoinductive molecules in demineralized bone matrix extracts (Urist 1965). He prepared a demineralized bone matrix from various vertebrates, implanted it in rabbits´ muscle pockets and observed the ectopic formation of new bone. Urist described this phenomenon with the term "bone induction principle", envisioning the process of osteogenesis as a cell to cell interaction with "inducing cells" and "responding cells" (Urist et al. 1967). Already in 1971 the "specific diffusible chemical agent" (Murray et al. 2016) started to be called bone morphogenetic protein (Urist and Strates 1971). By the end of the 19th century, the phenomenon of osteogenesis and ectopic bone formation were well accepted and investigated by several researchers (Murray et al. 2016).

However, the BMP induced bone formation process described by Urist does not correspond with the contemporary understanding one. Urist's BMP was not a single purified protein but was a partially purified mixture of bone matrix proteins. The BMP was described as being composed of "multiple components" (Murray et al. 2016). Whether this phenomenon of bone induction was due to diffusible factors, extracellular matrix components, cell-cell interactions or combination of these remained elusive at that time.

The work of different groups aimed to isolate, characterize, and sequence "the real BMPs". This intense research resulted in the discovery of the complete sequences of new clones named: BMP1, BMP2A (later named BMP2), BMP3 (osteogenin) and osteogenic protein 1 (OP1) (Wang et al. 1988, Wozney et al. 1988, Ozkaynak et al. 1990).

The discovery of the clones, the possibility to express, isolate the recombinant human proteins, and the ability to independently induce cartilage and bone formation *in vivo* constituted a step forward in understating the bone inducing mechanisms and how those are orchestrated by the novel regulators of bone formation (Wozney et al. 1988, Wang et al. 1990).

The newly discovered molecules were identified as members of the large transforming growth factor-β (TGF-β) family. Only BMP1 has a distinct structure and belongs to the

metalloproteinase family (Wozney et al. 1988), while the other BMPs are structurally related and can be divided into multiple subclasses of the TGF-β super family (Celeste et al. 1990).

The TGF-β superfamily comprises 33 growth and differentiation factors that, share remarkable structural similarities, they act as regulators of a variety of processes in development, maintenance and regeneration of tissues and organs (Massague 1998, Reddi 2005).

The TGF-β family is formed by the TGF-βs (TGF-β 1, 2 and 3), the subclass of Bone Morphogenetic Proteins (BMPs), the Growth and Differentiation Factors (GDFs), activins/inhibins, 1 nodal, 2 leftys (A and B), Müllerian inhibiting substance (MIS) or anti-Müllerian hormone (AMH) and glial-derived neurotrophic factors GDNF (Horbelt et al. 2012, Hinck 2012).

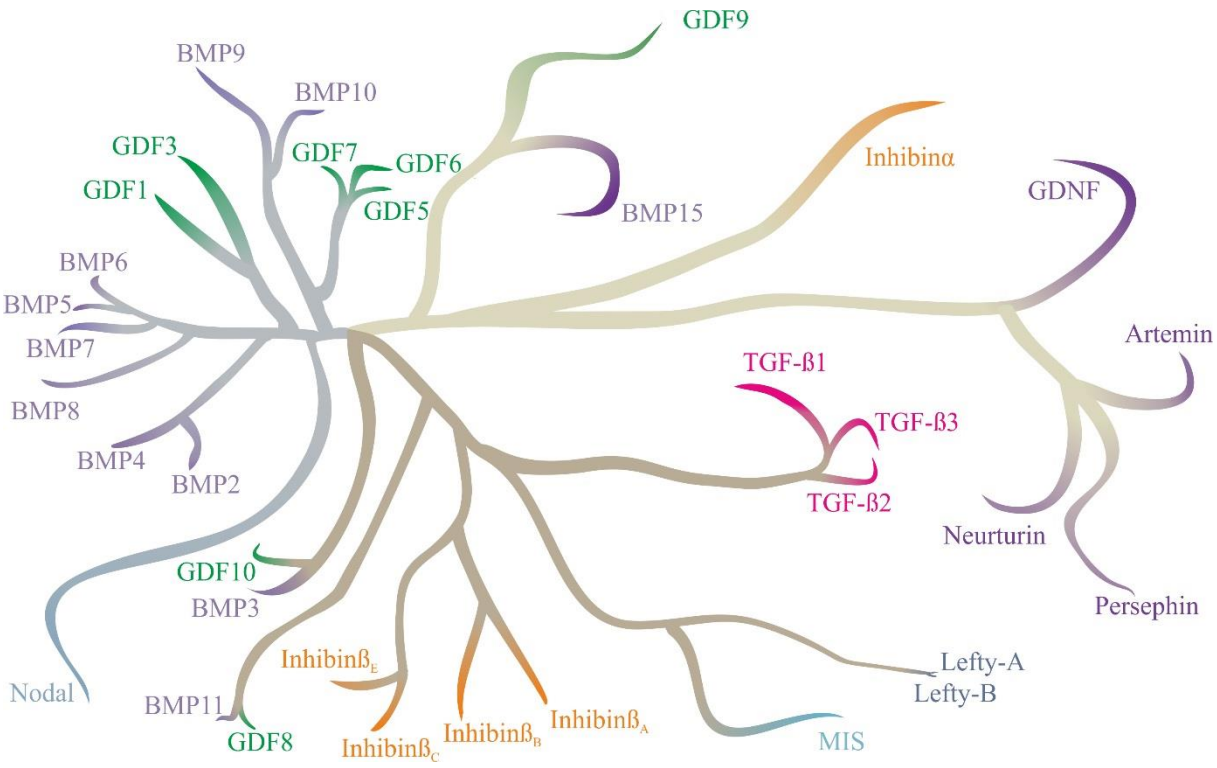

Figure 1: Phylogenetic tree of TGF-β superfamily proteins.
The branches of the phylogenetic tree represent divergence of each branch member from a common ancestor. The branch lengths reflect the number of amino acid changes between each protein and that hypothetical ancestor, and imply how much time has passed since the divergence. BMP = Bone Morphogenetic Protein, GDF = Growth Differentiation Factor, GDNF = Glial cell line-derived Neurotrophic Factor, MIS = Muellerian inhibiting substance. Image was readapted from R&D Systems.

1.1 BMPs: the regulatory molecules in bone formation

Within the TGF-β family, several BMPs and GDFs were shown to induce the formation of bone and/or cartilage tissue not only through the implantation of recombinant proteins (Wang et al. 1990) but also through the transduction of individual BMP/GDF encoding cDNAs using viral vectors (Cheng et al. 2003, Kang et al. 2004). In *vitro* activities of 14 types of BMPs (BMP2 through BMP15) were directly compared using an adenoviral-expression system and among these factors, BMP2, BMP6 and BMP9 induced high activity levels of the osteogenic marker alkaline phosphatase (ALP) in the murine myogenic cell line C2C12 (Cheng et al. 2003). Moreover, C2C12 cells transduced with viruses encoding for BMP2, BMP6, BMP7 or BMP9 induced bone formation *in vivo* (Kang et al. 2004). Recent studies suggested that BMP6 and 9 may be more effective in promoting ectopic bone formation when compared to BMP2 and 7 (Lamplot et al. 2013).

However, not all members of the BMP subfamily are solely osteogenic. For example, BMP7 is involved in kidney, eye, and limb development; BMP4, 7, and 14 are important for proper reproductive tissue development; BMP2, 3, and 7 contribute to cartilage regeneration; and BMP12 and 13 are required for tendon healing (Rahman et al. 2015).

TGF-β1 and TGF-β2 were identified as cartilage inducing factor-A (CIF-A) and CIF-B in bone extracts in an *in vitro* chondrogenesis assay of muscle cells (Seyedin et al. 1985). However, the *in vivo* implantation of TGF-β1 alone failed to induce ectopic bone formation (Sampath et al. 1987), while a combination of TGF-β1 or TGF-β2 or activin with BMP2 showed potent heterotopic bone-inducing activity *in vivo* (Katagiri et al. 2015). These findings suggest that the TGF- β family members synergistically enhance the heterotopic bone-inducing activity of BMPs. Therefore, the potential of BMPs alone or in concert with each other, as well as with other members of the TGF-β superfamily, has been intensively investigated *in vivo* in order to understand how these molecules can trigger a cascade of events that promote the complex biological process of bone formation.

1.2 Bone formation: an intimate cross-talk between osteoblast, osteoclasts and the myriad of cellular activities

Bone matrix is a composite of protein and mineral, which is continuously molded, shaped and repaired in order to fulfil its role in mineral homeostasis. Bone remodeling is the predominant metabolic process regulating bone structure and function during adult life. Additionally, bone has a substantial capacity for repair in response to fracture, involving the complex integration of cells, growth factors, and the extracellular matrix.
To understand the complex process of fracture healing, it is required a first insight into bone remodeling mechanism focusing on cells and their cross-talk during the bone remodeling process.

The process of bone remodeling is tightly coordinated by a myriad of cellular activities. The intimate cross-talk between osteoblasts and osteoclasts is a crucial element in bone remodeling, that is also influenced by the activities of other cells like osteocytes, bone lining cells, and osteomacs (Sanchez-Duffhues et al. 2015). An imbalance in the coordination of these cellular activities often leads to bone diseases. The two key cell types are the bone resorbing osteoclasts and bone forming osteoblasts. The misbalanced turnover rate and ratio between bone formation and resorption during remodeling leads to a number of clinical disease conditions including osteopenia, osteoporosis and osteopetrosis (Kular et al. 2012).
Bone remodeling occurs through the synergistic action of a functional cohort of cells termed the basic multicellular unit (BMU). The BMU consists of osteoclasts resorbing bone, osteoblasts replacing bone, osteocytes within the bone matrix, the bone lining cells and capillaries-forming endothelial cells. The BMU is covered by a canopy of cells that form the bone remodeling compartment (BRC) that is connected to the bone lining cells which are interacting with the osteocytes embedded in the bone matrix (Florencio-Silva et al. 2015).
The bone remodeling cycle begins with an initiation phase, where osteoclast precursor cells are recruited and then differentiated into mature osteoclasts. In the transition or reversal phase osteoclast formation is inhibited and osteoclasts undergo apoptosis, while osteoblasts are recruited and differentiate. The cycle is completed by coordinated actions of osteocytes and bone lining cells (Kular et al. 2012).
Osteoclasts are terminally differentiated multinucleated cells which originate from mononuclear cells of the hematopoietic stem cell lineage. Osteoclasts are located on the

endosteal surfaces within the Haversian system and on the periosteal surface beneath the periosteum. They exist in two functional states: the motile and the resorptive stage.

Motile osteoclasts are flattened and non-polarized cells and they are characterized by the presence of membrane protrusions called lamellipodia. Upon reaching the resorptive site they become polarized, through a cytoskeleton reorganization, acquiring a dome shape and lacking lamellipodia. Four different membrane domains are created during the resorptive stage in order to separate the acid resorptive environment (sealing zone) from the rest of the cell (ruffled border, functional secretory domain and basolateral membrane) (Charles and Aliprantis 2014). The two factors necessary and sufficient to promote osteoclastogenesis are macrophage colony stimulating factor (M-CSF), secreted by osteoprogenitor mesenchymal cells and osteoblasts, and Receptor Activator of Nuclear Factor-κB Ligand (RANKL), secreted by osteoblasts, osteocytes, and stromal cells. M-CSF, upon binding to its receptor on osteoclasts precursors, stimulates proliferation and inhibits apoptosis. When RANKL bind to its receptor RANK in osteoclast precursors, osteoclast formation is induced. An inhibitory factor called osteoprotegerin (OPG), can prevent RANK/RANKL interaction and consequently inhibit osteoclastogenesis. The RANKL/OPG expression ratio determines the degree of osteoclast formation and activity. The RANK/RANKL interaction also promotes the expression of osteoclast-specific genes including tartrate resistant alkaline phosphatase (TRAP) (Raggatt and Partridge 2010).

The resorption operated by the osteoclasts causes a release of bone matrix derived factors that might regulate bone formation. BMPs and other growth factors such as TGF-β and insulin growth factor (IGF) initiate the recruitment of mesenchymal osteoblasts precursors.

Osteoblasts originate from mesenchymal stem cells (MSC) and are the only cells being directly responsible for bone formation. The differentiation of MSC toward osteoblasts requires the expression of specific genes. There are four different maturational stages of osteoblasts: preosteoblast, osteoblast, osteocyte and bone lining cell. The expressions of Runt related transcription factor 2 (Runx2), Distal-less homeobox 5 (Dlx5) and osterix (Osx) are crucial for osteoblast differentiation. *Runx2* is the master gene of osteoblast differentiation. Preosteoblasts express alkaline phosphatase but they lack the ability to produce mineralized tissue. The transition to osteoblasts is characterized by an increased expression of Osx, and in the secretion of bone matrix proteins like collagen type I, osteocalcin (OCN), bone sialoprotein (BSP) I/II and a characteristic cuboidal morphology (Clarke 2008).

The new bone matrix is generated in two steps, a first deposition phase followed by a mineralization phase. Osteoblasts secrete all the above mentioned proteins, collagen I, OCN,

osteonectin, BSP I/II, osteopontin and proteoglycans, to create the organic matrix. Mineralization starts when vesicles (called matrix vesicles) are released from osteoblasts into the newly formed bone matrix, where they bind to proteoglycans that immobilize the calcium ions due to their negative charge. When osteoblasts secrete enzymes that are able to degrade the proteoglycans, the calcium ions are released and cross the calcium channels on the matrix vesicles. On the other side, osteoblasts release ALP that degrades phosphate containing compounds releasing phosphate ions inside the matrix vesicles. Phosphate and calcium ions nucleate inside the vesicles and create hydroxyapatite crystals, and as soon as a high saturation is reached inside the matrix vesicles, they break diffusing hydroxyapatite crystals in the matrix. Mature osteoblasts can undergo three different fates: apoptosis, differentiation to osteocytes or quiescent lining cells. Around 50 % to 70 % of osteoblasts undergo apoptosis (Lynch et al. 1998).

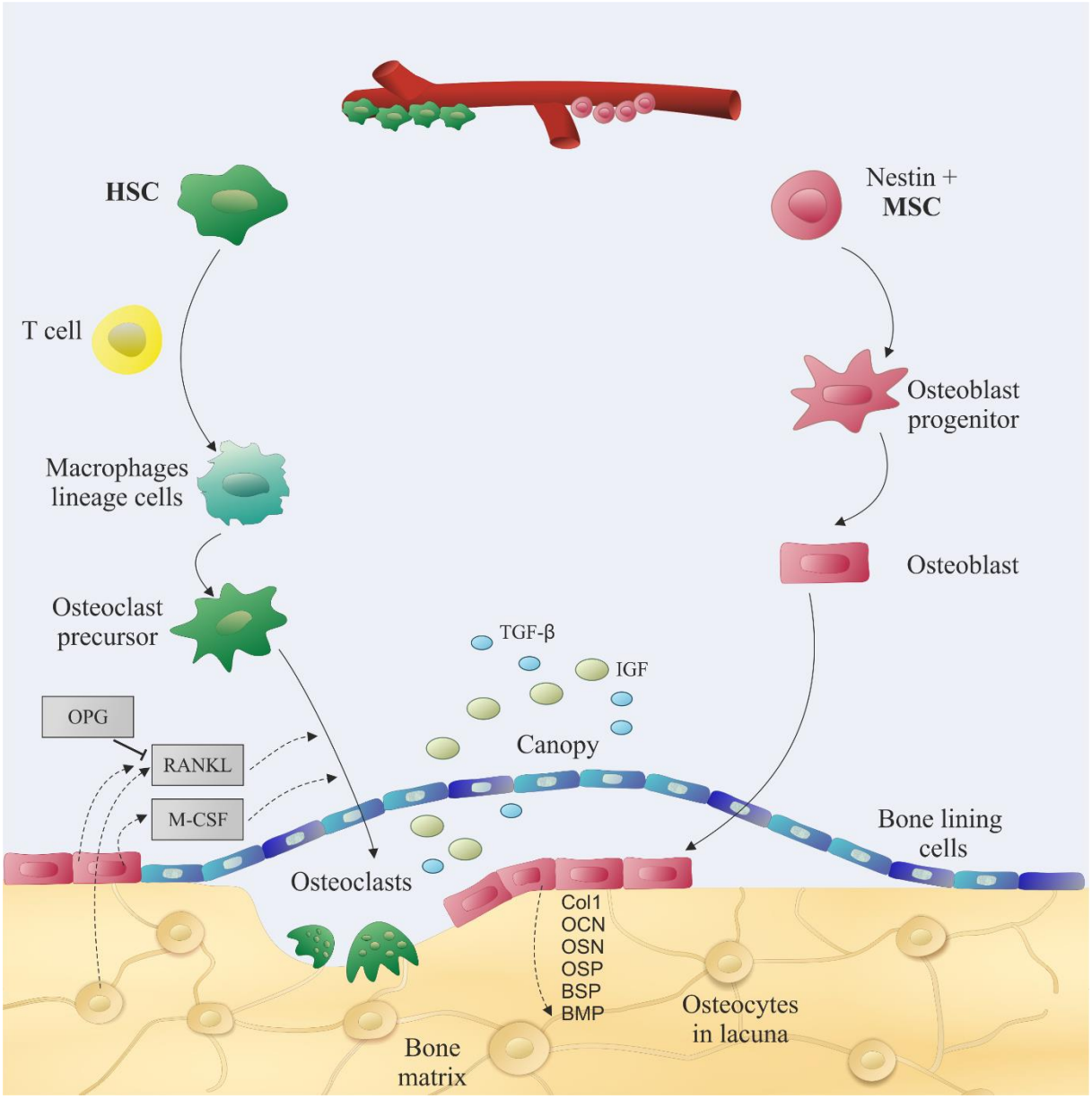

Figure 2: Schematic summary of bone tissue showing bone cells and the relationships among them and with bone matrix

Osteoclasts originate from mononuclear cells of the hematopoietic stem cell lineage. Osteoclast activation occurs after binding of RANKL its receptor RANK, present in the membrane of osteoclast precursors. Osteoblasts also produce RANKL and osteoprotegerin (OPG), which increase and decrease osteoclastogenesis, respectively. Osteoblasts secrete collagen (Col1), osteocalcin (OCN), osteopontin (OSP), osteonectin (OSN), and bone morphogenetic proteins (BMP). Osteocytes are located within lacunae surrounded by mineralized bone matrix. Its cytoplasmic processes cross canaliculi to make connection with other neighboring osteocytes processes by gap junctions. RANKL secreted by osteocytes stimulates osteoclastogenesis, while insulin-like growth factor (IGF) and TGF-β stimulate osteoblast activity. Activation of TGF-β recruits MSCs during bone remodeling. TGF-β is released from the bone matrix and activated during osteoclast-mediated bone resorption. TGF-β induces migration of MSCs to the bone remodeling sites to couple bone resorption and formation. The bone-resorptive microenvironment also provides signals that direct the cell lineage–specific differentiation of MSCs.

Osteocytes are terminally differentiated osteoblasts that are incorporated into the newly formed bone matrix. The mature osteocytes trapped in the lacunae show a down-regulation of osteoblast markers (OCN, Col I, BSP II, and ALP) and an upregulation of dentine matrix

protein 1 (DMP1) and sclerostin. They are spatially isolated between each other but they present long filipodial extensions (up to 50 per cell), called canaliculi, that allows them to be connected to each other as well as to bone lining cells and osteoblasts on the bone surface (Tanaka-Kamioka et al. 1998). This intricate network forms the osteocyte lacunocanalicular system (Manolagas 2006).
Using the lacunocanalicular system osteocytes act as regulators of the bone structure and as mechano-sensor cells that transduce musculo-skeletally derived mechanical input into biological output (Bonewald 2007).
Bone lining cells are flat shaped osteoblasts that cover bone surfaces and are in a quiescent status in which no bone resorption or bone formation occurs. Their cytoplasm extends along the bone surface and it presents processes reaching the canaliculi, also the presence of gap junctions is observed between bone lining cells (Miller et al. 1989).
Osteomacs are resident tissue macrophages present in close proximity of periosteal and endosteal surfaces. During bone modelling, osteomacs form a canopy-like structure over mature osteoblasts. They regulate osteoblast mineralization playing a role in bone homeostasis (Chang et al. 2008).

Bone homeostasis, regulated by this intricate cross-talk within cells, is of course based also on the complex cross-talk within the key molecules responsible for keeping this cellular activities in balance, the TGF-βs and BMPs (Crane and Cao 2014). Specific members of the TGF-β family, such as BMPs (2, 8), GDF (1, 5, 8 and 10), and TGF- β1, 2 and 3, promote various stages of intramembranous and endochondral bone ossification during fracture healing (Cho et al. 2002).

Fractures normally heal by the combination of both, intramembranous and endochondral ossification. Endochondral bone formation usually occurs externally to the periosteum in regions that are mechanically less stable and immediately adjacent to the fracture site, whereas intramembranous ossification occurs internal to the periosteum at the proximal and distal edges of the callus and forms hard callus (Ai-Aql et al. 2008).
The repair process comprises a series of overlapping phases. The first phase is constituted by an inflammatory response, which leads to the recruitment of mesenchymal stem cells and the subsequent differentiation into chondrocytes that produce cartilage and osteoblasts which form bone. The newly produced cartilage starts to mineralize and through a resorption phase

the cartilage is transformed into bone. In the following remodeling stage, this initial bony callus is reshaped by secondary bone formation and resorption.

This biological process of bone healing is orchestrated by an intense activity of cell signaling molecules, which can be categorized into three groups: (1) pro-inflammatory cytokines, (2) TGF-β members, and (3) angiogenic factors (Ai-Aql et al. 2008).

Immediately after the fracture, bleeding from the ruptured bone and the periosteal vessels induces the formation of a hematoma in the injured bone. The levels of several inflammatory mediators, including cytokines such as interleukin-1 (IL-1), IL-6, IL-11, IL-18, and tumor necrosis factor-α (TNF-α) are significantly elevated within the first few days after the injury. These pro-inflammatory mediators are believed to play the main role in the cascade activation after injury and overall they have chemotactic effects on other inflammatory cells, such as the one involved in osteoclastogenesis, during the removal of mineralized cartilage or others involved in last phase of remodeling.

After injury the fracture site becomes hypoxic and the osteocytes at the ends of the fracture undergo necrosis. Macrophages phagocytize the necrotic areas and facilitate the regeneration stage by releasing signaling factors such as BMPs, TGF-βs, platelet-derived growth factor (PDGF), and IGF. These growth factors are responsible for migration, recruitment, and proliferation of mesenchymal stem cells and their differentiation to angioblasts, chondroblasts, fibroblasts, and osteoblasts (Oryan et al. 2015). Moreover, these growth factors exhibit different temporal patterns of expression at different stages of fracture healing (Cho et al. 2002).

The hematoma transforms therefore into granulation tissue. This phase of soft callus (cartilage formation) involves a periosteal response with angiogenesis and formation of connective tissue. This soft callus is gradually replaced by the immature woven bone formed by endochondral ossification. The mineralized callus is then replaced with mineralized bone, shaping the bone back to its original shape, size, and biomechanical competency via modeling and remodeling (Oryan et al. 2015) In this phase, osteoclasts resorb the newly woven bone and osteoblasts replace this matrix with the lamellar bone. The process of replacement and repair is continuously ongoing in the normal skeleton.

Focusing more in details on which factors are involved in particular phases of fracture repair, BMP2 is the earliest gene to be induced, showing a second peak in the osteogenic period (day 14 – 21), while BMP3, 4, 7, and 8 show only a restricted period of expression between day 14 through 21, when the resorption of calcified cartilage and osteoblastic recruitment are most active, and coupled bone formation takes place. BMP5 and 6 and other members of the TGF-

β superfamily, such as GDF10, are constitutively expressed throughout the healing period, suggesting that they have a regulatory effect on both intramembranous and endochondral ossification. The TGF-β2 and 3 are expressed after fracture with a peak at day 7, while the TGF-β1 is constant throughout the healing process (Cho et al. 2002).

Fracture healing as all the complex physiological processes, involves all the structural levels, down to the cellular and molecular mechanisms. Between the several growth factors and signaling molecules involved in this process, BMP is the most important one.

1.3 Canonical and non-canonical signaling pathways: the receptors decide

In general, binding of TGF-β ligands to specific receptors at the cell membrane triggers the recruitment of signaling complexes responsible to transduce the signal into the nucleus to regulate bone homeostasis related genes. Almost all members of the TGF-β family are synthesized as precursor molecules, with the pro-peptide being clipped from the mature protein during secretion from the cell (Wozney 2002).

All TGF-β superfamily members form dimeric molecules. In detail, BMP2 is synthesized as a 453 residue pro-protein, which becomes glycosylated, proteolytically cleaved and dimerized to yield the mature homodimeric protein (Scheufler et al. 1999). Each monomer represents a single-domain protein consisting of 114 residues, and contains a so-called cysteine knot motif which is formed by six cysteine residues forming three intra-chain disulfide bridges. Further stabilization of the BMP2 structure is achieved by dimerization, which creates a hydrophobic core inside of the two monomers (Scheufler et al. 1999).

The intra-chain disulfide bond that the majority of TGF-β family factors share in their structure, is referred to a cysteine-knot folding motif. This cysteine knot (CK) growth factor (CKGF) domain has a specific three-dimensional structure and sequence. Having a CKGF does not necessary grant growth factor activity, and most TGF-β family members for instance act as differentiation factors rather than growth factors (Hinck et al. 2016).

Differently from TGF-βs, BMPs assemble their receptor in a distinct manner (Hinck 2012). The BMP type I and type II receptors bind to the ‘‘wrist’’ and ‘‘knuckle’’ epitopes, respectively, and do not contact one another. The knuckle epitope is formed by four anti-parallel β-sheets and the wrist epitope is formed by a four-turn α helix (Scheufler et al. 1999).

Ternary crystal structure analysis of BMP – BMP receptor complexes shows that BMP type II receptors utilize the concave surface of their β-sheet to complement the convex surface of the knuckle epitope of the BMP. The BMP type I receptors bind to the wrist epitope and have extensive contact with both BMP monomers (Nickel et al. 2009, Mueller and Nickel 2012, Hinck 2012).

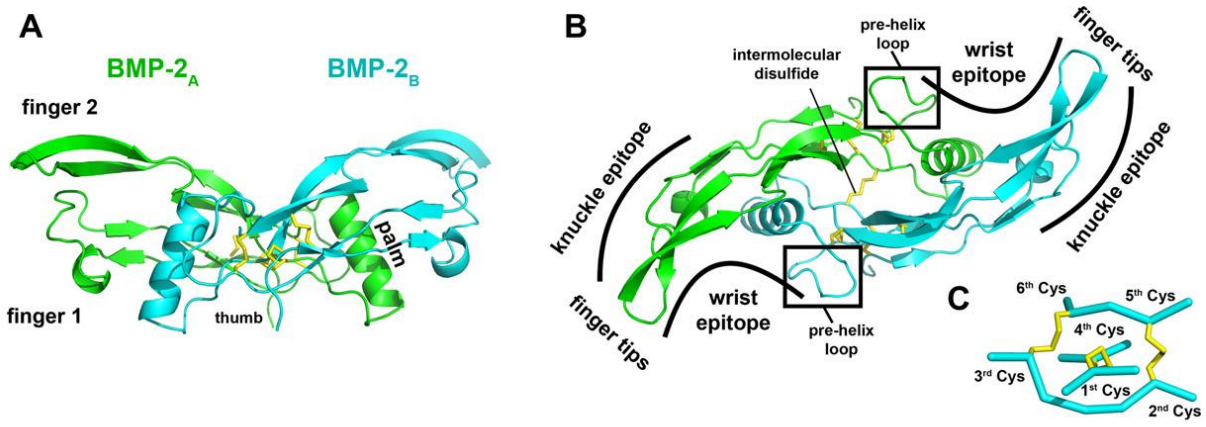

Figure 3:BMP2 structure – Details on knuckle and wrist epitopes
(A) Ribbon representation of BMP2. The butterfly-shaped architecture of the dimeric ligand resembles two hands assembled palm-to-palm, with the β-sheets representing fingers 1 and 2, the α-helix and the dimer interface forming the palm, and the N-terminus described as thumb. The convex side of the fingers termed knuckle epitope is the binding interface for type II receptors in the BMP/GDF and Activin subgroups, TGF-βs bind their type II receptors at the finger tips. Type I receptor binding occurs in the so-called wrist epitope formed by the concave side of the fingers and the palm of the ligand. (B) As in (A) but viewed along the ligand's 2-fold symmetry axis. (C) Close-up of the cysteine-knot, which is formed by two disulfide bridges between Cys2-Cys5 and Cys3-Cys6 building a ring-like structure, and a third disulfide bond between Cys1 and Cys4 penetrating this ring. Image from (Mueller and Nickel 2012).

The identification of BMP receptors and intracellular signal transduction components is still an area of intensive research. Since the development of expression cloning methods for TGF-β receptors in 1992 (Lin and Wang 1992), deep investigation on the particular molecular mechanisms have been conducted.

TGF-βs family members bind to and oligomerize two different types of single transmembrane serine/threonine kinase receptor chains named type I and type II (Wrana et al. 1992) (ten Dijke et al. 1996). There are seven type I (ALK1–7) and four type II (TβRII, BMPRII, ActRII A/B) receptors identified to date with different binding affinities for individual ligands thus contributing to signaling specificity (Nickel et al. 2009).

The concerted actions of both receptor types are needed for BMPs to activate specific signaling pathways. The receptors contain an extracellular ligand binding domain, and in

intracellular serine/threonine kinase domain. Furthermore, the type I, but not type II, receptors contain a characteristic SGSGSG sequence, termed the GS domain. The activation of the type I receptor involves the phosphorylation of its GS domain by the type II receptor; hence an active receptor signaling complex comprises both types of receptors bound to the ligand (Shi and Massague 2003). The activated type I receptor then phosphorylates receptor mediated SMAD proteins (R-SMADs), which translocate into the nucleus where they regulate gene expression.

There are two different SMAD pathways that transduce the signal from the cell surface into the nucleus. Which of the two pathways is activated depends on the capabilities of the individual type I receptor (the signaling receptor) to phosphorylate either SMAD-2/3 (which are activated by TGF-β/activin/nodal ligands by the type I receptors ALK4, -5, or -7) or SMAD-1/5/8 (being activated by BMP/GDF/MIS by ALK1, ALK2 (ActRIa), ALK3 (BRIa), and ALK6 (BRIb)) (Shi and Massague 2003). This specificity is thought to be determined by the compatibility of the loop (L45) between β-sheets β4 and β5 in the type I receptor and the L3 loop in SMADs (Mueller and Nickel 2012). BMP ligands, such as BMP2 and 4, exhibit higher affinity for the type I receptors and a lower affinity for the type II receptors (Knaus and Sebald 2001, Nickel et al. 2005).

There are two modes of BMP receptor oligomerization: one, which occurs prior to ligand binding, where BMP bind to preformed complex (PFC) of type I and type II receptors, and the other, which is ligand-mediated, called BMP-induced signaling complex (BISC) (Mueller and Nickel 2012, Ehrlich et al. 2011, Nohe et al. 2002). BMP signaling via PFCs was shown to be associated with clathrin-mediated endocytosis, while signaling originating from BMP-mediated oligomers correlated with caveolar uptake (Hartung et al. 2006).

Binding of BMPs to their receptors may trigger SMAD as well as non-SMAD signaling cascade. In the SMAD pathway, upon phosphorylation of the type I receptor kinase by the type II receptor kinase, the SMAD proteins 1, 5 and 8 are phosphorylated and activated. The SMAD proteins assemble with so-called co-SMAD 4 forming a heterotrimer required for nuclear translocation (Chacko et al. 2001). In parallel to canonical SMAD pathways, the receptors can trigger an independent pathway mediated through the activation of p38, ERK or JNK (Sieber et al. 2009, Nohe et al. 2002).

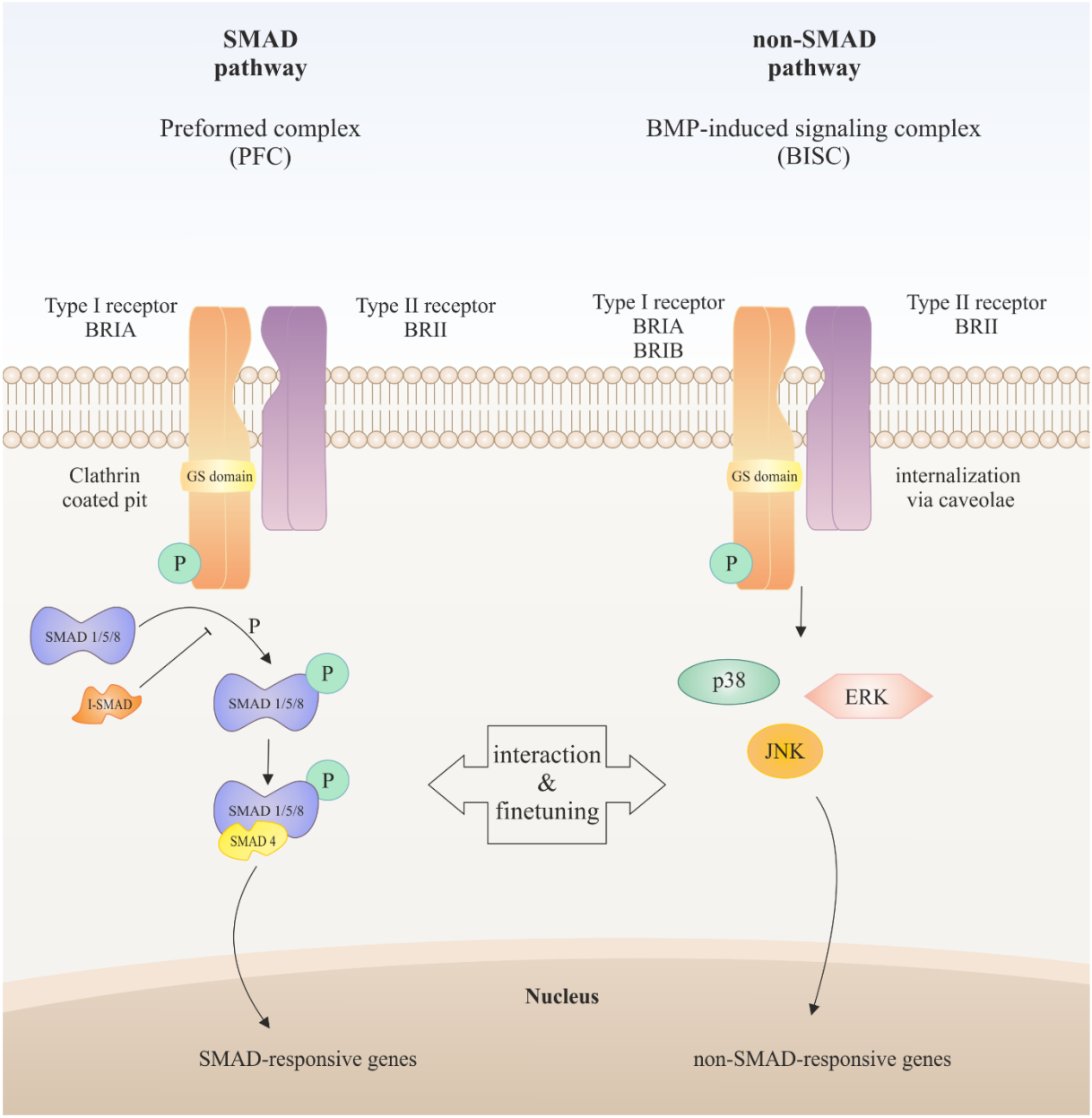

Figure 4: Schematic representation of the BMP signaling cascade.
BMP signaling elicit diverse cellular responses through SMAD and non-SMAD pathways. Binding of BMP to cognate receptors induces the formation of active receptor signaling complexes in which the type I receptor is phosphorylated and thus activated by the type II receptor. Subsequently, R-SMAD proteins (SMAD 1/5/8) are phosphorylated by the type I receptor, associate with SMAD 4, and translocate into the nucleus and regulate gene transcription. Besides the canonical SMAD pathway, other signaling cascades have been described for BMP signaling. For instance the MAP kinase pathway (p38, ERK or JNK kinases).
Represented also the two mode of BMP receptor oligomerization: BMP-induced signaling complex (BISC) and the preformed complex (PFC). In BISC BMP2 binds to its high affinity type I receptor (BRI) upon which the type II receptor (BRII) is recruited into the complex. This oligomerization mode results in caveolae-dependent internalization and activation of non-SMAD pathways. Signaling via PFC, BMP2 binds to a PFC of type I and type II receptors, which targets the Clathrin-dependent internalization into endosomes. This signaling route is required for progression of the SMAD pathway. Interaction, fine-tuning and non-transcriptional responses are initiated at both sides.

Among other SMAD family members, SMAD6 and SMAD7, are classified as inhibitory SMADs (I-SMADs) because they block the phosphorylation of the R-SMADs by competitive binding to the activated type I receptors (Heldin et al. 1997).
BMP signal transduction is also antagonized by inhibitory modulator proteins such as noggin, chordin, gremlin or follistatin that are able to bind to BMPs directly (Brazil et al. 2015). The antagonistic activity of different modulators involved in the BMP pathway is a broad field including several mechanisms and therefore out of scope for this work.

The interactions of particular ligands with different receptor assemblies generate highly specific cellular signals, which are especially required during development but also for tissue homeostasis (Mueller and Nickel 2012). Altered BMP signaling affects most tissue types of the skeletal system causing abnormal formation and growth of bones, joints or connective tissues. At least 436 distinct disorders have been identified, resulting from mutations in 364 genes (Bonafe et al. 2015). Skeletal dysplasias have been separated into several groups of phenotypically similar but genetically distinct skeletal disorders, also trying to understand whether an excess or deficiency of signaling, through specific branches of BMP–GDF or TGF-β–activin signaling pathways, is involved (Salazar et al. 2016). Reduced BMP signaling is associated with acromelic dysplasias, acromesomelic dysplasias and brachydactylies, characterized by severe longitudinal growth defects that manifest at distal sites of the limb while skeletal structures of the skull and spine are reasonably normal. On the other side an excess of BMP signaling causes brachydactyly, Klippel – Feil anomaly, or fibrodysplasia ossificans progressive (FOP) (Shore et al. 2006). Excess of TGF-β signaling is associated with the Loeys-Dietz syndrome (LD), Camurati-Engelmann disease and the Marfran syndrome. Affected patients suffer from craniosynostoses, scoliosis, a sunken or bulging chest, club or flat feet, and/or contractures of the joints.

1.4 Clinical use of BMPs as osteoinductive agent: how a discovery became a clinical product

Although many BMPs share osteogenic properties, recombinant human BMP2 (rhBMP2) was the first and to be introduced as a bone graft substitute. OP1 (BMP7) received FDA Humanitarian Device Exemption approval in 2004. Additionally GDF5 was also preliminarily tested in humans (Hustedt and Blizzard 2014).

The intense research on bone graft substitutes derives from the need of an alternative for the historically used technique of autologous bone grafting performed to enhance the healing of spinal fusions, bone defects, fractures of the long bones and to augment skeletal reconstruction in the treatment of maxillofacial injuries and conditions.

The osteogenic properties induced by the multitude of cells and growth factors present in these grafts, make the autologous bone still the gold standard for these types of procedures. However, harvesting of autologous bone is associated with increased postoperative pain, increased loss of blood during surgery and extended operative time. In addition, complications such as injury to sensory or motor nerves, major blood vessel injury, hematoma, infection and postoperative problems may occur after these procedures (Bishop and Einhorn 2007). The development of a readily available graft material could limit the need for harvesting autologous bone and represent a potential major advance in the treatment of skeletal conditions.

One of these graft substitute, containing rhBMP2 was introduced commercially in the United States in 2002. Since its approval by the FDA, it was first introduced for single-level anterior lumbar interbody fusion (ALIF) within a specific threaded titanium tapered cage, named InFUSE™ Bone Graft (Burkus et al. 2002). BMP2 was later also approved for the treatment of tibial non-unions (2004) (Govender et al. 2002) and for oral maxillofacial reconstructions (2007) (Boyne et al. 1997).

Between 2002 and 2006, the USA's nationwide use of BMP2 increased from 0.7 % to 24.9 % in clinical practice (Cahill et al. 2009). The effectiveness of the product (McKay et al. 2007), compared to autogenous bone grafts, was also related with the reduction in duration and operation time and length of hospitalization (Garrison et al. 2007).

Indeed, BMP2 was promoted as a much needed clinical alternative to autograft bone, being considered to be nearly perfect in achieving bone formation without causing harmful side effects. Several small and large trials reported the use of rhBMP2 in a large number of patients undergoing a variety of spinal fusion techniques, but no adverse events were reported

and observed. Remarkably, these initial industry-sponsored trials reported a combined risk to less than 0.5 % in the early 2000s (Carragee et al. 2011).

Beginning from 2006, several studies were conducted in patients that underwent anterior spinal fusion, reporting complications associated with swelling of neck and throat tissue, causing compression of the airway and/or neurological structures in the neck (Shields et al. 2006, Vaidya et al. 2007). Other reports described difficulties in swallowing, breathing or speaking. Most complications occurred between 2 and 14 days post-operatively and in case of airway complications, additional necessary treatments included respiratory support with intubation, anti-inflammatory medication or tracheotomy (FDA Public health notification 2014).The use of BMP2 in lumbar spine surgery caused retrograde ejaculation, antibody formation, postoperative radiculitis, postoperative nerve root injury, ectopic bone formation, and/or vertebral osteolysis/edema (Tannoury and An 2014).

The intricate stories that included severe side effects around the use of rhBMP2 could be linked to trials with inappropriate indication or anatomical location and to the required supraphysiological doses, arising suspicions of a more marketing oriented strategy than an objective scientific study (Fauber 2010).

The current FDA approved concentration for medical use in patients is 1.5 mg/ml (FDA InFUSE™ Bone Graft/LT-CAGE™ Lumbar Tapered Fusion Device 2002). The severe side effects observed upon rhBMP2 use are mainly related to the high doses of protein. These supraphysiological amounts of protein are indeed needed in such rhBMP2 loaded implant to induce bone formation. This necessity comes from premature leakage of rhBMP2 during manual manipulation while implantation and from a fast release of the protein at the implant site causing ectopic bone formation at a rate of nearly six times more than in control patients (Carragee et al. 2011). Ectopic bone formation in the spinal canal leads to root compression of nerves with a rate of 14 % of postoperative ridiculitis (Rihn et al. 2009). Moreover, increase rhBMP2 doses did not necessarily result e.g. in higher fusion rates in spine procedures or long bone non-unions (Lee et al. 2013). Today, the most recognized adverse event associated with rhBMP2 is caused by the high doses used (James et al. 2016).

The observed side effects can be decreased or completely avoided by improving particular characteristics of the newly developed bone-inducing clinical devices such as, the biomaterial used and the delivery system chosen, and which growth factor or combination of growth factors to implement.

Figure 5: Milestones in BMP research.
Timeline of the most important discoveries in BMP research starting from 1965 with the discovery from Urist to the latest news in 2013.

2. The effectiveness of an optimal bone-inductive product depends on the intrinsic activity of the bone inducing factor, the choice of delivery system, the material, the dose and the implementation with additional growth factors

A clinical osteoinductive product must comply with safety aspects that include purity, localized activity, systemic availability, immunogenicity, and biocompatibility. The intrinsic stability of BMP proteins is partly given from their tightly folded and disulfide bond-stabilized structure. Moreover, the original protein purification process required the extraction of BMPs from the bone mineral component with hydrochloric acid and in presence of strongly chaotropic agents such as urea, still resulting in a biologically active protein (Bessho et al. 1989). The use of recombinant production system of BMPs allows if established, high yields of produced protein (Wozney 2002).
BMP2 itself presents all the characteristics required in bone tissue regeneration, but the drawbacks connected to its use, bring the necessity to intensively focus on improving delivery carriers and materials in order to achieve a higher qualified osteoinductive products.

2.1 Delivery of growth factors: always a balance of pros and cons

The different techniques developed for BMP2 delivery extend from viral and non-viral gene therapy to covalent and non-covalent coupling approaches. The main role of a delivery system is to retain the growth factor at the site of injury for the necessary time frame needed to induce cell proliferation and new bone formation (Seeherman and Wozney 2005).

Gene delivery offers a promising possibility to enable protein expression for an extended period of time and temporal regulation of the transgene expression. The protein expressed by gene delivery undergoes authentic posttranslational modification and the use of tissue-specific promoters may allow spatial control of gene expression (Evans 2012). A number of different viruses, such as adenovirus and lentivirus, have been modified and used to generate proteins at bone defect sites *in vivo*. The different vectors differ in immunogenicity and manufacturing ability (Evans 2011).

The problem of adenovirus delivered BMP2 was proven in a murine model, where the immune-deficient group showed superior level of bone formation compared to the immune-competent group (Musgrave et al. 1999). Of course, this reveals the main disadvantage of using adenovirus *in vivo* by highlighting their tendency to incite immunological responses in the host organism. Even though the use of viral vectors provided high promises in the bone regeneration field and showed higher transfection efficiencies than non-viral vectors, their use still provokes debates regarding safety (Niyibizi et al. 1998, Baltzer et al. 2000, Betz et al. 2006). Major concerns regard inflammatory or antigenic reactions and potential insertional mutagenesis (Warnock et al. 2011).

A promising alternative is the use of liposome-based or polymer-based compounds that act as vehicle for the introduction of genetic material into cells (Elsabahy et al. 2011).

The most common method for the application of the vectors at the fraction site is by direct injection. However, this could lead to dispersion of the vector outside of the desired area. Several studies focused on the use of "scaffolds", gene-activated matrices (GAMs), which are decorated with the vector allowing a more controlled release in the host tissue (Jang et al. 2011).

Another alternative is *ex vivo* gene therapy, in which cells are explanted from the patient, genetically modified in cell culture, and then re-introduced into the patient. This technique can overcome many of the safety issues, but it is expensive, time consuming and not easy to perform (Tarassoli et al. 2013).

Both *in vivo* and *ex vivo* techniques show promising results, nevertheless safety still remains the most important factor to overcome and up to date few studies are investigating gene therapy in larger animals. For further applications in bone healing it is necessary that both parameters, efficacy and safety are proved.

The promising but problematic protein expression by gene delivery technologies finds an opponent in the less controversially discussed recombinant protein delivery systems. The retention of rhBMP2 in a delivery carrier can be performed by different methods like adsorption, encapsulation or covalent binding.

Independently from the method used, the carrier or scaffold should be biocompatible, provoking an optimal inflammatory response, and biodegradable allowing infiltration of cells and formation of blood vessels into the newly formed bone (Gothard et al. 2014). Suitable scaffolds are thought to be those that mimic the highly complex structural hierarchy of native bone, such as porosity and the microstructure of the host tissue (Bonfield 2006). Furthermore,

the carrier should protect the BMPs from degradation and maintain their bioactivity whilst releasing the protein in a spatial-temporal manner controlled way to promote the formation of new bone at the treatment site.

Scaffolds should be favorably bioactive in terms of promoting the desired cellular response *in vivo* (Green et al. 2002). The morphology, as well as the microtopography and chemistry of the scaffolds´ surface, determine the cellular response and differentiation in the osteoblastic lineage (Boyan et al. 1996, Schwartz et al. 1999).

The material, together with the bone inducing growth factor, are major determinants of the success of the bone regeneration outcome. It is then fundamental to use a suitable material and delivery technique that ideally control the release kinetics to maximize osseointegration (Agarwal and Garcia 2015).

The most commonly used biomaterials for bone tissue engineering are natural polymers (collagen, hyaluronans, fibrin, chitosan, silk alginate and agarose), synthetic polymers such as poly (lactic acid) (PLA), poly (glycolic acid) (PLG), and copolymers such as poly (lactic-co-glycolic acid) (PLGA)), and ceramics such as (hydroxyapatite (HAp), β-tri-calcium phosphate (β-TCP), biphasic calcium phosphate (BCP)). By fine tuning the material's characteristics such as porosity, wettability, roughness, surface charge, charge density and crosslinking methods, it is possible to control the initial burst release of the adsorbed protein that usually occurs after implantation (King and Krebsbach 2012) causing the already mentioned inflammatory and osteoclastic activities.

Collagen is the most wildly used scaffold material among the natural polymers. As the major non-mineral component of bone and the most abundant protein in connective tissue, it is extremely biocompatible and produces physiologically compatible products after degradation. It is suitable for interaction with cells and other macromolecules, very versatile, wettable and can be manipulated easily. It is not surprising that has been so intensively used (MEDTRONIC InFUSE™).

Albeit successfully used, collagen possess the risk of certain immunogenic reactions, as it is animal derived, exhibits batch-to-batch variability, and comprises possible risk of pathogen transmission (Bessa et al. 2008, Glowacki and Mizuno 2008). Other natural polymers were recently investigated (Begam et al. 2017), but the main disadvantage of potential disease transmission remains. The use of BMP2 loaded synthetic polymers such as PLGA has demonstrated bone formation in rats (Shimazu et al. 2006), or in a canine model (Jones et al. 2006). Other synthetic polymers, such as PEGylated fibrinogen hydrogel matrices loaded with BMP2 have shown bone formation in rat critical size defects (Ben-David et al. 2013) and

tibial segmental defects (Peled et al. 2007). However, a major disadvantage of the use of synthetic polymers is the risk of an inflammatory response, due to acidic degrading products (Winet and Hollinger 1993), which may also affect the stability of BMP2. Ceramics, such as calcium phosphates, share similarities with human bone in terms of structure and composition and additionally possess osteoinductive properties and strong binding capabilities (Louis-Ugbo et al. 2002). Yet issues that must be considered for the effective application of bioceramics in the field of tissue engineering rely on the degree of bioresorption and the poor mechanical strength (El-Ghannam 2005).

Having listed the possible advantages and disadvantages related to the most commonly used materials for bone regeneration, different delivery methods have to be likewise examined. As BMP2 is a soluble and highly diffusible protein, non-covalent techniques have mainly been investigated. Most research approaches focused on adsorption of BMPs together with other therapeutic molecules and drugs to enhance osseointegration (Seeherman et al. 2002). This method is chemically simple but it might cause a decreased biological activity of the protein caused by the possible masking of the receptor binding sites (Roach et al. 2006). Furthermore, delivery by adsorbed growth factors often results in an initial burst release (Bessa et al. 2008). Slower release rates without a reduction in biological activity were achieved by enhancing the binding ability of BMP2 to scaffolds by chemical modification of collagen (Zhang et al. 2012), tailoring physical and chemical activities of hyaluronic acid hydrogels (Todeschi et al. 2017) or mixing thiolated chitosan scaffold with collagen (Bae et al. 2013).

The hydrophobic nature of BMP2 leads to strong adhesion to solid material surfaces thus inducing conformational changes which lead to protein precipitation and thus decrease protein's bioavailability. An additional layer between implant and protein was proposed to overcome this issue. A modified BMP2 variant, containing three N-terminal material binding motifs for titanium was produced and immobilized onto a titanium surfaces. The BMP2-functionalized titanium surfaces showed maintained biological activity *in vitro*, as proved by cell-based assays and receptor accessibility assay by BMPRIA/Fc chimera (Kashiwagi et al. 2009) and also *in vivo* (Yuasa et al. 2014).

Insertion of a multitude of affinity tags at the N-terminus of BMP2 has been intensively investigated due to the resulting advantages in the highly specific interaction, mild coupling conditions and in the availability of a broad variety of different commercially available affinity tag systems. However, this approach comprises several limitations, such as laborious protein production, a possible influence of the tag on folding and protein properties, the costs

of affinity ligands, and an unpredictable release of the immobilized protein from solid phases (Mumcuoglu et al. 2017). Common approaches can be performed using small charged affinity tags such as poly-arginin or poly-histidine, FLAGs, Myc, calmodulin binding peptide (CBP), cellulose and chitin binding domain, maltose binding protein (MBP) and many others (Terpe 2003). Use of anti-polyhistidine monoclonal antibodies immobilized on collagen scaffolds enhanced the loading capacity of His-tagged BMP2, if compared to not-tagged BMP2. His-tagged BMP2 bound to the scaffolds showed maintained biological activity *in vitro* and ectopic bone formation *in vivo* identified by thick layers of bone tissues and increased calcification, as compared to the control (Zhao et al. 2010).

Another approach to directly couple BMPs to scaffolds by means of bi-functional peptides. These peptides simultaneously bind to scaffolds and to the proteins to be immobilized (Hamilton et al. 2013). Identification of peptides that bind with high affinity to BMP2 and to collagen was performed using the phage display method. *In vivo* data of BMP2 coupled to collagen using these peptides which were identified by this approach, demonstrated increased osteogenic activity, area of formed bone and bone maturity if compared to the controls.

All these immobilization strategies by affinity interaction allows binding and/or release of proteins in a controlled manner, being related to the reversibility of the bonds involved like hydrogen bonds, electrostatic bonds, Van der Waals forces and hydrophobic bonds. However, the strength of the reversible affinity is much weaker than covalent linkage. Moreover, there is still a need to characterize the release kinetics of the protein in detail, especially *in vivo*, to better understand these effects on bone growth and osseointegration.

The release of a protein can be measured *in vivo* by near infra-red dye labels by monitoring alterations in fluorescence over time in a non-invasive manner (Boerckel et al. 2011). Other approaches such as the quantification of remnants protein, which is still available in an implant at certain time points, can be performed if for instance the protein is radioactively labeled (Hulsart-Billstrom et al. 2013).

Beside the above discussed release strategies for BMPs in bone tissue engineering, an alternative approach is the covalent coupling method. The loss of almost 50 % of protein after a few days *in vivo*, the necessity to modify the materials to decrease the release rate of the growth factor and the other above mentioned limitations are avoided by using covalent methods.

Covalent immobilization of BMP2 to 1,1’-carbonyl diimidazole (CDI) activated titanium surfaces showed enhanced peri-implant osseointegration and gap healing. The rhBMP2 coated

surfaces showed high biological activity *in vitro* and high osteoinductive activity *in vivo* with trabecular bone formation in 4 weeks together with a significant increase in bone density and in bone-implant contact (Chatzinikolaidou et al. 2010). In another approach BMP2 coating of gold surfaces was performed by a two-step approach: first by functionalizing the surface with a N-hydroxysuccinimide (NHS) ester containing linker, and second by coupling the protein to the linker by classical 1-Ethyl-3-(3-dimethylaminopropyl) carbodiimide (EDC) / NHS coupling chemistry (Pohl et al. 2013). The covalently coupled BMP2 showed maintained biological activity *in vitro*, as proved by alkaline phosphatase assays. The reaction with the surface-immobilized NHS groups takes place with any lysine residues of the BMP2 protein and with the free amine available at the N-terminal residues. As shown for other ligands, the length and the flexibility of the linker might enable interaction with otherwise sterically hindered binding sites, thus compensating for unfavorable orientation (Hu et al. 2010).

Chitosan films were used to covalently couple BMP2 via EDC/NHS chemistry, which resulted in higher loading efficacy if compared to a simple protein adsorption. Since the adsorbed BMP2 diffused more rapidly, the films with covalently immobilized BMP2 stimulated osteoblast attachment, proliferation, and differentiation to a greater extent than the films with just adsorbed BMP2 (Park et al. 2006, Budiraharjo et al. 2013).

The use of fibrin was also explored as matrix for BMP2 covalent immobilization (Karfeld-Sulzer et al. 2015). Fibrin is one the extracellular matrix proteins and is also a key component of wound healing, which is part of the process of bone regeneration. By inclusion of a transglutaminase amino acid sequence at the N-terminal of BMP2, the molecule (named TG-BMP2) was covalently attached to lysine residues present on fibrin. This reaction was performed by Factor XIII that is indeed able to create a bridge between the side chain of lysine and glutamine (Karfeld-Sulzer et al. 2015). In addition, the use of BMP heterodimers has been investigated. Being the BMP molecule formed of two identical polypeptide chains (homodimer); in the heterodimer conformation each chain belongs to a different BMP type. BMP2/BMP7 heterodimers have already demonstrated greater activity compared to the corresponding homodimers (Israel et al. 1996, Sun et al. 2012, Zheng et al. 2010). In the study of Karfeld-Sulzer, a single TG-BMP2 polypeptide chain was coupled to a single BMP7 polypeptide chain, creating the TG-BMP2/BMP7. The release of the newly engineered heterodimers is almost identical to the TG-BMP2 homodimers, while *in vivo* the TG-BMP2/BMP7 showed higher bone formation in critical calvarial size defects in rats compared to the homodimer molecule (Karfeld-Sulzer et al. 2015).

All these examples require a certain chemistry to activate the scaffold´s surface and/or the protein, resulting finally in a covalent immobilization of the growth factor. In certain cases, the use of a particular chemistry showed no improvements on cells attachment, adhesion or proliferation (Bauer et al. 2011) indicating that random, non-site directed chemically triggered reactions might result in deactivation or denaturation of the coupled proteins.

In this context, the use of site directed immobilization techniques was investigated by creating BMP2 variants harboring artificial amino acid that enable the covalent binding of the protein to the scaffold by a click chemistry reaction (Tabisz et al. 2017). The constructed BMP2 variant showed the same bioactivity compared to the wild type protein and showed maintained bioactivity after being treated in an environment required to perform the desired click chemistry reaction. The coupled protein was able to bind the Texas Red labeled BMP receptor IA (BMPRIA) *in vitro* and also induced alkaline phosphatase expression *in vitro*. The use of site directed mutagenesis at the BMP2 DNA level allows to place the artificial amino acid at the desired position of the expressed BMP2 variant. By this method the receptor binding sites are available for signal transduction upon cell-protein interaction.

Differently from the previously presented cases with tags, which can be added only to restricted positions, or with randomly occurring covalent reactions, the use of this technique allows the protein coupling via a site directed method using the functional group introduced in any desired peptide positions.

The different studies presented on immobilized growth factors showed a maintained bioactivity, indicating that the release of the proteins and their subsequent internalization by the cells are not essential for cell stimulation (Hartung et al. 2006). In fact, the covalent immobilization of growth factors allows the sustained stimulation of the target cells while maintaining an effective dosage because of an enhanced occupancy of different types of receptors at the cell membrane (Masters 2011, Pohl et al. 2013, Uludag et al. 2000).

The various immobilization techniques can be adapted according to the needs of the individual approach, such as targeting of different reactive groups or including spacers, but each method is accompanied by advantages as well as limitations.

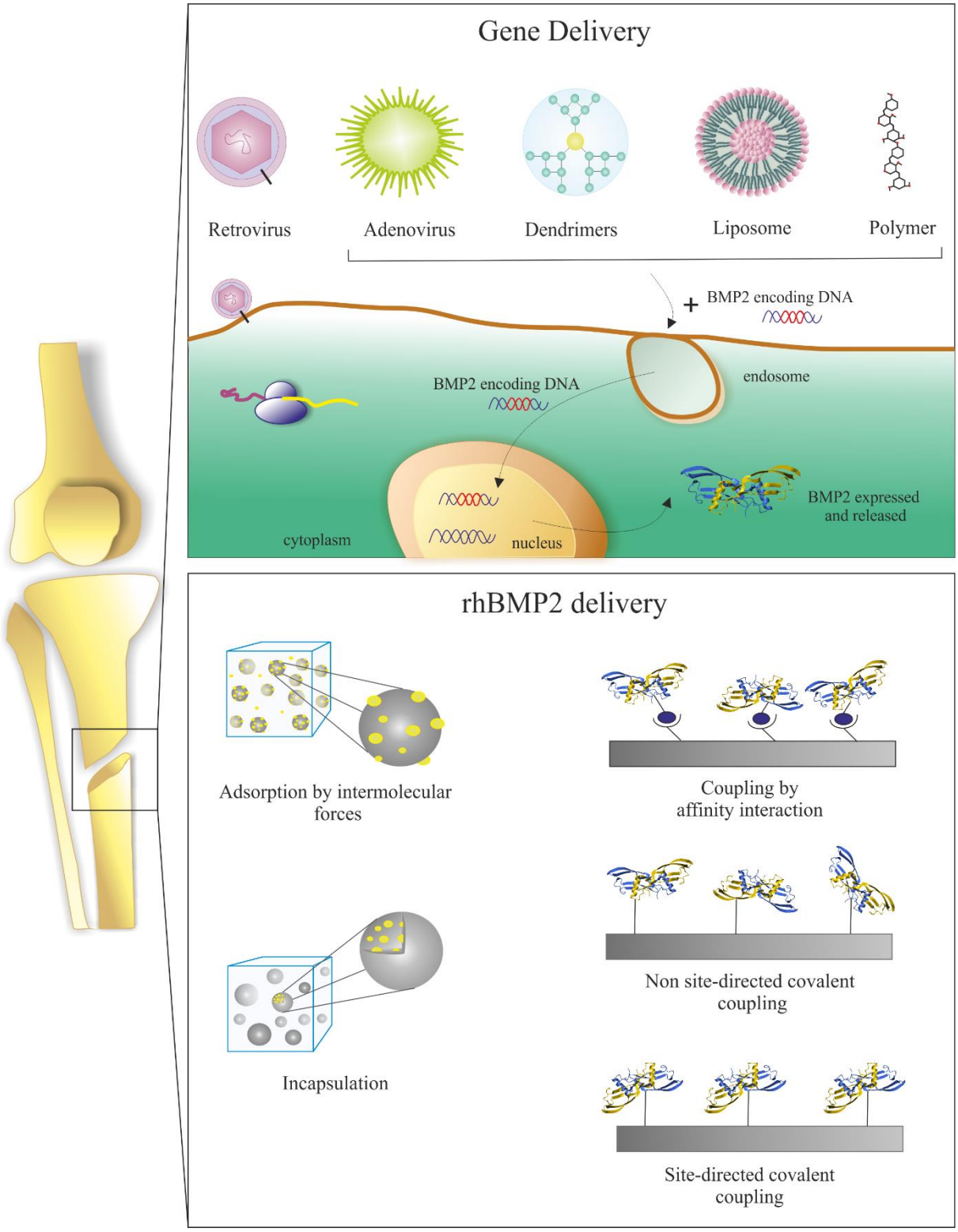

Figure 6: BMP delivery systems

Gene delivery: cDNA encoding for the desired growth factor is introduced into the cells e.g. via viral vectors or dendrimers, liposomes or polymers and is translated and secreted at the site of injury. Instead in the lower panel the different immobilization strategies for rhBMP2 are indicated. BMP2 can be adsorbed to solid surfaces or encapsulated into e.g. hydrogels. Higher coupling specificities can be achieved by affinity interactions e.g. using biotinylated BMP2 being coupled to streptavidin coated matrices, or by covalent coupling achieved in a non-site-directed manner to structures being activated e.g. by NHS esters or site-directed via click chemistry. Figure readapted from (Mumcuoglu et al. 2017).

2.2 Pharmacokinetic profiles of released BMPs: the connection between dose and activation of different signaling molecules in animal studies.

Maintaining a critical threshold concentration of the rhBMP2 at the defect site during the necessary period of time required for bone repair is crucial. Approximately 0.002 mg of BMP2 can be extracted from one kilogram of powdered bovine bone (Wang et al. 1990). These amounts appear to be sufficient for normal fracture healing. In contrast, the supraphysiological doses required to accelerate or induce fracture healing range from 0.01 mg/ml in small animal models (rats) to 0.4 mg/ml in rabbit to more than 1.5 mg/ml in non-human primates (Haidar et al. 2009). Different anatomical sites require different therapeutic doses depending on the degree of vascularization, defect size and the number of resident responding cells. Seeherman et al. presented different idealized scenarios to illustrate the requirements that BMP carriers need to accomplish in order to induce tissue repair (Seeherman and Wozney 2005). These scenarios assume that there is a baseline concentration of BMP responsive cells required for effective bone formation, but in addition they assume that there is a minimal concentration of exogenous BMPs required to generate the desired newly bone tissue. Without the presence of exogenous BMPs, repair would occur at a slower rate or segmental defect bridging would be impeded. Appropriate tissue formation occurs once the critical density of cells is achieved, independent from a continued presence of exogenous BMP (Seeherman and Wozney 2005). A higher starting BMP concentration, applied with a given BMP carrier, will maintain the minimum exogenous BMP concentration for a longer period of time allowing a smaller initial cell population or slower responding cell population to reach the critical cell density for tissue formation (Seeherman et al. 2002). On the other side, there is also a threshold on the optimal concentration for bone induction. Different studies showed that beyond a certain value of applied protein, bone healing and quality do not further improve. Administration of high doses of protein in critical size rat femoral bone defects induced bone regeneration in a nonlinear dose-dependent manner when evaluated for bridging rate, bone volume, connectivity and mechanical properties (Boerckel et al. 2011). The decrease in BMP2 responsiveness associated to higher dose is likely due to saturation of BMP receptors and responding cells. The histological examination highlighted the presence of fatty bone marrow filling these defects. These results were also shown in another rat- femoral-segmental defect study, where high doses of BMP2 induced formation of cyst-like bone voids filled with fatty marrow instead of a normal trabecular bone structure

(Zara et al. 2011). These findings are also in line with those found in Canine radii treated with high doses of BMP2 (Sciadini and Johnson 2000).

BMP2 induces peroxisome proliferatoractivated receptor gamma (PPARγ) expression, a key regulator of adipogenesis, in a dose-dependent manner (Takada et al. 2012). Bone marrow stem cell differentiation into adipocytes rather than osteoblasts is controlled by PPARγ activation and down-regulation of Wnt signaling. Additionally, published studies showed that BMP receptors direct the fate towards adipogenesis or osteogenesis (Chen et al. 1998). BMPR-IA and BMPR-IB exhibited versatile and divergent effects on the process of osteogenesis both *in vitro* and *in vivo* (Zhang et al. 2014b, Kaps et al. 2004). Their exact functions are highly dependent on factors including cell type and differentiation stage (Mishina et al. 2004).

In addition, the use of supraphysiological amounts of BMP2 can modify the balance between pro-inflammatory and anti-inflammatory cytokines. The well-orchestrated bone regeneration events comprise several physiological processes which are initiated with a local inflammation step followed by mobilization, proliferation and differentiation of stem cells such as hematopoietic (HSC) and mesenchymal stem cells (MSC). An insufficient or an excessive inflammation would affect some signaling molecules and consequently inhibit or delay the bone regeneration process (Mountziaris and Mikos 2008).

The high dose of BMP2 applied in a femoral onlay model, induced inflammation at early time points with increased presence of immune cells (Zara et al. 2011). Different studies suggest that BMP2 induces osteoclastic activity through direct and indirect mechanisms. BMP2 directly stimulates osteoclastogenesis in bone marrow macrophage cultures treated with RANKL and M-CSF, essential cytokines for inducing osteoclast differentiation (Itoh et al. 2001). Additionally, high doses of BMP2 affects osteoclast activity by upregulation of the PPARγ pathway, either directly or and as result of Wnt signaling pathway repression (Wan et al. 2007). High doses of BMP2 not only induce significant tissue inflammation but also increase osteoclastogenesis that may cause bone subsidence by an excessive bone resorption (Zara et al. 2011).

The positive and negative effects related to the different doses of rhBMP2 used represent the core of the whole bone regeneration discussion. To understand and recapitulate the healing cascade, suitable bone defects models should be established *in vivo* by using appropriate animal models. The use of animals allows the elimination of variables which contribute to the success or failure of tissue engineered materials. However, it must be taken into account that

currently no single animal model provides a representative comparison for human bone repair; rather each animal model is selected to address a particular research question (Gothard et al. 2014). Up to date, small animals are mainly preferred for fracture related studies, constituting 72 % of them (rat 38 %, rabbit 19 % mouse 15 %) and leaving the rest to sheep 11 %, dog 9 % and goat 4 % (O'Loughlin et al. 2008). Usually preliminary investigations of new delivery systems or the combination of different growth factors should be evaluated in small animals such as rats or mouse, since higher throughputs can be achieved with such kind of animal models which share enough biochemical similarity to humans, and the considerable existing literature facilitates and supports data interpretation. Positive data can lead to verify these results in larger animal models, which resemble humans by scale, mechanical loading and bone composition (Pearce et al. 2007).

Intense studies were performed to investigate how to decrease the numerous adverse side effects associated with the application of recombinant BMP2. Beneficial in this context was the combination of BMP2 with additional proteins or other growth factors in order to avoid the non-specific and adverse events of the osteoinductive protein. Local inflammation suppression was evaluated in a critical size bone defect by the controlled co-release of a immunosuppressive drug (triptolide) and BMP-2 (Ratanavaraporn et al. 2012). The release of the incorporated triptolide was timed to be during the initial inflammation period (< 7 days) in order to reduce the inflammation but still to be sufficient to initiate the regenerative process. Bone formation was enhanced in implants were triptolide and BMP2 were mixed (Ratanavaraporn et al. 2012).

Apart from the inhibition of the inflammatory response, also other growth factors have been investigated as a helpful tool to increase their bone inducing capability. For example, as angiogenesis is a crucial part in bone regeneration, vascular endothelial growth factor (VEGF) was used in combination with BMP2 in bone fractures. The angiogenic factor in combination with BMP2 induced an increase in blood vessel formation and a greater defect coverage (Kaigler et al. 2006). However, in another study the same VEGF-BMP2 combination did not induce higher bone volume or bone density compared to the BMP2 wild type alone (Patel et al. 2008). Also fibroblast growth factor 2 (FGF2) was used in bone tissue engineering. Administration of FGF2 resulted in blood vessel ingrowth and ossification at the defect site (Guo et al. 2006). However, another group reported the opposite outcome, since FGF2 together with BMP2 or VEGF induced less bone formation (Behr et al. 2012). Therefore, the outcome of these synergistic effects still needs some detailed research.

Previous studies clearly demonstrated the crucial role of BMP2 as the triggering molecule for bone regeneration. However, further studies are needed to investigate the regenerative outcome if BMP2 is combined with additional growth factor.

Aim of the study

By screening the literature of the last 20 years of BMP2 research, it became more obvious, that BMP as a single molecule is sufficient to induce ectopic bone formation. However, in case of critical size bone defects, the bone is not able to self-regenerate and several BMPs release systems were investigated in order to test the necessary conditions to obtain bone formation. Application of the recombinant protein in delivery systems such as adsorbed in collagen scaffold causes several severe side effects. This main limit is connected to the use of supraphysiological doses needed to maintain the protein at the implantation site for a period of time long enough for bone regeneration to occur. This requirement comes from the fast clearance of the protein at the implantation site. Therefore, it is necessary to improve the delivery carrier systems by investigating new bio materials with improved release kinetics or developing new BMP2 variant able to be covalently immobilized to solid scaffold. The covalently coupled protein would be available at the implantation site for longer time since the burst release, usually observed in the common adsorbed delivery techniques, is avoided. This also implicates that lower amount of protein might be enough to induce bone formation therefore reducing the severe side effects.

Starting from previous findings on covalent immobilization methods of BMP2 variant by click chemistry technique, this work aimed to investigate covalent coupling of new BMP2 variants to collagen-based microspheres, to quantify and evaluate the efficiency of the covalent reaction technique with the final aim to prove osteogenic activity *in vivo*.

II. Materials and Methods

1. Cloning two new BMP2 constructs: BMP2 E83amber and BMP2 E94amber

The first BMP2 variant into which an artificial amino acid i.e. N-Propargyl-lysine (Plk) was introduced by so-called codon-usage expansion, was constructed by replacing the codon encoding for lysine at position 3 (K3) of the human mature BMP2 (hmBMP2) by that of an amber stop codon (Tabisz 2016). This position was chosen in order to prevent problems which might occur upon protein refolding since this part of the molecule appears unstructured (Scheufler et al. 1999). Introduction of N-Propargyl-lysine at position 3 yielded the variant BMP2 K3Plk, which showed unaltered biological activities *in vitro* if compared to wild type BMP2 (BMP2 WT). Coupling of a bulky fluorophore to Plk at this position did not impede the BMP2 K3Plk-mediated induction of alkaline phosphatase expression in C2C12 cells thus excluding inhibitory effects caused by steric hindrance.
To further optimize the geometric orientation of the ligand after coupling to solid scaffolds, new BMP2 variants were designed and cloned.

Amber stop codons replacing either glutamic acid (E) 83 or E94 in hmBMP2 were introduced by cyclic mutagenesis using the plasmid p25N-hmBMP2 (see Figure 7) as template and the forward and reverse primers listed in Table 1 were used, respectively.

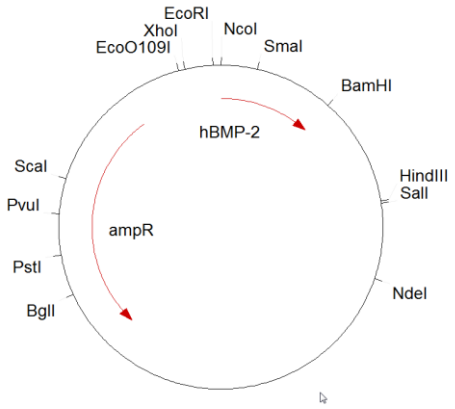

Figure 7: p25N-hmBMP2 vector used for site directed mutagenesis
Human mature BMP2 (hmBMP2) sequence was amplified from p25N-hmBMP2 vector introducing an amber stop codon (TAG) at position glutamic acid (E) 83 or E 94.

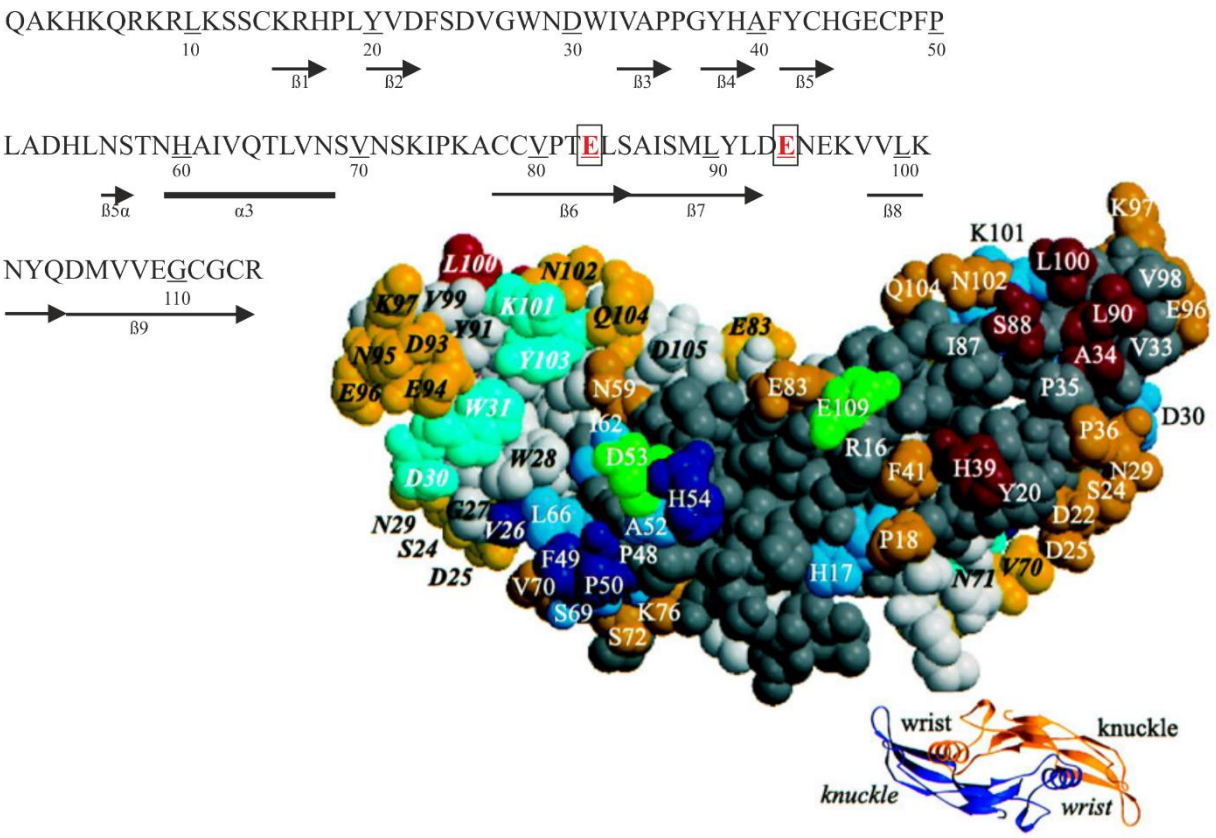

Figure 8: hmBMP2 sequence and BMP2 residues substituted in this study.
Scheme shows the hmBMP2 amino acid sequence, location of secondary structure elements as β-sheets (β1-β9) and α-helix (α3). Glutamic acid (E) 83 or E94, indicated in red, were substituted with a TAG codon. The ribbon structure shows where the substituted residues are located in the 3D structure.

Primer name	Sequence
E83amber_forward	5’ TGCTGTCCCGACA**TAG**CTCAGTGCTATCTCG 3’
E83amber_reverse	5’ CGAGATAGCACTGAGCTATGTCGGGACAGCA 3’
E94amber_forward	5’ATGCTGTACCTTGAC**TAG**AATGAAAAGGTTGTA 3’
E94amber_reverse	5’ TACAACCTTTTCATTCTAGTCAAGGTACAGCAT 3’

Table 1: Primers used for site directed mutagenesis on p25N-hmBMP2

KAPA HiFi DNA polymerase (Kapa Biosystems) was used for the PCR amplification, according to the manufacturer’s protocol. Amplification was performed by an initial denaturation step for 5 min at 95 °C; followed by 30 cycles of denaturation at 95 °C for 1 min, 1 min annealing at 60 °C, and 1 min elongation at 72 °C. Reactions were completed by a final extension step for 10 min at 72 °C. The PCR product was subsequently purified with the

Wizard® SV Gel and PCR Clean-Up System (Promega), according to the manufacturer's protocol.

For subcloning the resulting PCR products were used as template and the BMP2 encoding sequences were amplified using the primers listed in Table 2 in order to introduce NdeI and BamHI restriction sites (bold, underlined) and to replace the TAG stop codon contained in the p25N-hmBMP2 by the stop codon TAA (italic). PCR was performed as described before.

Primer name	**Sequence**
F_BMP2 NdeI	5´ GACCAGGA**CATATG**GCTCAAGCCAAACACAAACAGC 3´
R_BMP2_BamHI	5´ CCAGGA**GGATCC***TTA*GCGACACCCACAACCCT 3´

Table 2: Primers used to introduce the restriction sites, NdeI and BamHI into the p25N-hmBMP2

The resulting PCR products were subcloned into the EcoRV restriction site of pBluescript II SK (+). For this purpose the plasmid was digested with the restriction enzyme EcoRV (Fast Digest, Fermentas) for 15 min at 37 °C and heat inactivated for 20 min at 80 °C. The 5'-phosphate groups were then dephosphorylated using Antartic phosphatase (New England Biolabs), according to the manufacturer's protocol, and the enzyme inactivated at 70 °C for 5 min. The linearized product was separated by agarose gel electrophoresis and purified using the Wizard® SV Gel and PCR Clean-Up System (Promega).

Ligation of inserts with the digested pBluescript II SK (+) vector was performed using Quick T4 DNA Ligase (NEB Quick Ligation) at a 5:1 ratio for 5 min at RT. Chemically competent NovaBlue bacteria (Novagen) were transformed with the ligation products according to the standard protocol (Table 3) plated on ampicillin/IPTG/XGal agar plates (100 µg/ml ampicillin, 50 µg/ml IPTG, 40 µg/ml XGal). Plates were incubated overnight at 37 °C. For sequence verification white colonies (most likely positive clones) were isolated, propagated in LB medium and plasmid DNA isolated using the Wizard® Plus SV Minipreps DNA Purification System (Promega) according to the manufacturer's protocol.

Bacteria transformation protocol
Thaw competent bacteria on ice
Add plasmid DNA to the bacteria (10 – 100 ng)

Incubate 30 min on ice
Incubate 1 minute at 42 °C (heat shock transformation)
Incubate 5 mintes on ice
Add 800 µl LB medium without antibiotic to 200 µl bacteria
Incubate for 1 hour at 37 °C at 300 rpm
Plate 200 µl bacteria solution onto agar plate containing the antibiotic

Table 3: Bacteria transformation protocol

The final target vector pET11a-pyrtRNA was double-digested with the restriction enzymes NdeI and BamHI for 20 min at 37 °C, according to the manufacturer's protocol. The product was dephosphorylated with Antarctic phosphatase (New England Biolabs) in order to further reduce self-ligation of vectors being incompletely digested. The enzymes were subsequently inactivated at 65 °C for 10 min.
The plasmids pBluescript II SK (+) BMP2 E83amber and pBluescript II SK (+) BMP2 E94amber were both double-digested with the restriction enzymes NdeI and BamHI (Fast Digest, Fermentas) for 20 min at 37 °C. The digested inserts were separated from the vector backbone by agarose gel electrophoresis and purified using the Wizard® SV Gel and PCR Clean-Up System (Promega). The inserts encoding BMP2 E83amber or BMP E94amber were ligated into the digested pET11a-pyrtRNA vector at a 5:1 molar ratio using Quick T4 DNA Ligase (NEB Quick Ligation) for 5 min at RT to generate the final constructs pET11a-pyrtRNA BMP2 E83amber or pET11a-pyrtRNA BMP2 E94amber, respectively.

Chemically competent NovaBlue cells (Novagen) were transformed with the ligation reaction according to the standard protocol (Table 3), seeded on ampicillin agar plates (100 µg/ml ampicillin), and incubated overnight at 37 °C. Transformants were isolated, propagated, and plasmids were isolated using the Wizard® Plus SV Minipreps DNA Purification System (Promega) according to the manufacturer's protocol. As control step, clones were digested with NdeI and BamHI restriction enzymes and then DNA was sequenced to confirm the presence of the mutation in the inserts. NovaBlue cells were transformed with the plasmid, propagated, and DNA was isolated using the Wizard® Plus SV Minipreps DNA Purification System (Promega), according to manufacturer's protocol.

2. Protein production of the new BMP2 variants

2.1 Expression of BMP2 E83Plk, BMP2 E94Plk and BMP2 E83Azide

Two different BMP2 variants were produced, containing N-Propargyl-lysine (Plk, kindly provided by Prof. Lorenz Meinel, Chair for Pharmaceutics and Biopharmacy, Institute for Pharmacy and Food Chemistry, University of Würzburg) and another one containing H-L-Lys(EO-N3)-OH (Azide) (Iris Biotech, GmbH).

In order to test whether both plasmids are appropriate to express the particular proteins at high yields, BL21(DE3) bacteria were double transformed with either pET11a-pyrtRNA BMP2 E83amber or pET11a-pyrtRNA BMP2 E94amber and pRSFduet-pyrtRNAsynth according to standard protocols (Table 3). The latter plasmid, encodes for pyrrolysyl-tRNA synthetase (kindly provided by Prof. Lorenz Meinel, Chair for Pharmaceutics and Biopharmacy, Institute for Pharmacy and Food Chemistry, University of Würzburg).

Incorporation of artificial amino acids, like N-Propargyl-lysine and H-L-Lys(EO-N3)-OH is performed by reprogramming the cell's translational machinery by evolving additional tRNA/aminoacyl-tRNA synthetase (aaRS) pairs that site-specifically incorporate the artificial amino acid in response to amber codons. When the amino acid is added to the growth medium, it must be efficiently transported into the cytoplasm, where tRNA/aaRs, the amino acid and the amber codon start the incorporation system.

Bacteria were plated on kanamycin (50 µg/ml) / ampicillin (100 µg/ml) plates and incubated overnight at 37 °C. Several colonies were selected and propagated individually overnight at 37 °C in LB medium supplemented with antibiotics (kanamycin 50 µg/ml / ampicillin 100 µg/ml). On the next day, overnight cultures were transferred into TB medium (dilution: 1:20) supplemented with Phosphate buffer (170 mM KH_2PO_4, 720 mM K_2HPO_4) and antibiotics (kanamycin 50 µg/ml / ampicillin 100 µg/ml), and grown until OD_{600} 0.5 was reached. Artificial amino acids N-Propargyl-lysine (= 264.71 g/mol) or H-L-Lys(EO-N3)-OH (= 259.26*36.46 g/mol) were individually dissolved in 0.5 ml of TB medium and cultures were further incubated until OD_{600} 0.7-0.8 was reached. To initiate protein expression IPTG at a final concentration of 1 mM was added and cultures incubated overnight at 37 °C.

The validation of the optimal artificial amino acid concentration was performed in a small scale culture (4 mL volume). Two different concentrations of Plk were tested: 10 mM and 20 mM, according to former experiments (Tabisz 2016). For the production of BMP2 variants

harboring H-L-Lys(EO-N3)-OH (Azide), 3mM, 5 mM, 10 mM, 15 mM, and 20 mM concentrations were tested.
Samples (100 µl) were collected before adding the artificial amino acid at OD_{600} ~ 0.5, before IPTG induction at OD_{600} ~ 0.8 and after IPTG induction after overnight incubation at 37 °C. Samples were centrifuged at 20000 x g and bacterial culture pellets were resuspended with 20 µl deionized water (dH_2O) and 4 µl 5x reducing loading buffer were added to each sample.
The expressed proteins were named: BMP2 E83Plk, BMP2 E94Plk and BMP2 E83Azide.

2.1.1 SDS-PAGE Electrophoresis and Western Blot analyses of expressed BMP2 variants

Samples were separated by SDS-PAGE Electrophoresis (12 % Gel) (SDS-PAGE chamber system, Peqlab) and stained by Coomassie Brilliant Blue (2.5 g Coomassie Brilliant Blue R-250, 450 ml Ethanol, 100 ml Acetic acid, 400 ml dH_20) for 2 h or overnight, and destained with (10 % Isopropanol, 10 % Acetic acid, 80 % dH_20) until the excess of dye was completely removed. In parallel samples separated by SDS-PAGE Electrophoresis (12 % Gel) were afterwards transferred onto nitrocellulose membranes using a semi-dry Western blot system (Semi-Dry Electroblotter Sedec™,Peqlab) applying 1 mA per cm^2 of membrane surface for 90 min. The membrane was blocked with 5 % milk for 60 min, washed 3 times for 10 min with TBST (2.5 mM Tris base pH 7.6; 15 mM NaCl; 0.1 % Tween) and incubated overnight with an anti-human/murine/rat BMP2 polyclonal antibody (PeproTech) at a dilution of 1:1000 in 5 % milk at 4 °C on a tube roller mixer. On the following day the membrane was washed 3 times for 10 min with TBST buffer and incubated for 1 h at RT with a secondary antibody (HRP coupled goat anti rabbit antibody, ab97051, Abcam) at a dilution of 1:10000 in 5 % milk. Afterwards the membrane was again washed 3 times for 10 min with TBST. Blots were developed using the WesternBright Chemiluminescence substrate Quantum (Biozym). The chemiluminescence signal was detected using the imaging system FluorChemQ (Biozym Scientific GmbH) and the AlphaView FluorChemQ software.

The optimal concentrations being identified (10 mM N-Propargyl-lysine and 15 mM H-L-Lys(EO-N3)-OH) were subsequently used for large scale (800 ml total volume) protein expression.

2.2 Purification of BMP2 variants

2.2.1 Inclusion Body (IBs)

After expression, bacterial cultures were centrifuged at 9000 x g for 30 min (centrifuge Avanti J-26 XP). Each pellet was resuspended in 30 ml TBSE buffer (10 mM Tris, 150 mM NaCl, 1 mM EDTA, 1:1000 β-mercaptoethanol, freshly added) and then centrifuged at 6360 x g for 20 min. Whenever necessary, BMP2 purification could be paused here by storing the bacterial pellet at -20 °C for short term or -80 °C for long term storage. Bacterial pellets were suspended in STE buffer (10 mM Tris pH 8.0; 150 mM NaCl; 1 mM EDTA; 375 mM Sucrose; 1:1000 β-mercaptoethanol freshly added) and subjected to sonication (10 min with: 40 sec pulse, 20 sec break and 30 % amplitude) using a Branson Digital Sonifier 250. Afterwards, the sonicated bacteria were centrifuged at 6360 x g for 20 min. This process of sonication and centrifugation was repeated 4 times in total. IBs were resuspended with benzonase buffer (100 mM Tris pH 7.1; 1 mM EDTA; 3 mM $MgCl_2$, 80 U/mL benzonase) using 10 ml/g of pellet, and incubated overnight at room temperature while stirring. 0.5 volume parts of Triton buffer (60 mM EDTA pH 7.0; 6 % (v/v) Triton X-100; 1.5 M NaCl) were added and the suspension was further incubated for 20 min at RT. The suspension was then centrifuged for 20 min at 6360 x g, pellets were resuspended again in TE buffer (100mM Tris pH 7.0; 20 mM EDTA) using 8 mL/mg pellet, and centrifuged. The pellets were resuspended in extraction buffer (25 mM NaAc pH 5.0; 3 M GuCl; 1 mM DTT freshly added) and incubated overnight at 4°C while stirring. Extracts were centrifuged at 75500 x g and the supernatant was concentrated to approximately OD_{280} 20 units/ml with an Amicon® concentrating cell using a 3 kDa MWCO membrane.

2.2.2 Size Exclusion Chromatography

Concentrated protein extracts (approximately OD_{280} 20 units/ml) were centrifuged in order to pellet insoluble cellular debris. Size Exclusion Chromatography (SEC) separates molecules based on their size by filtration through a gel. The gel of the column (Sephacryl^{TM} – S-300 High Resolution, GE Healthcare) consists of spherical beads containing pores of a specific size distribution. Separation occurs when molecules of different sizes are included or excluded from the pores within the matrix. This separation step allows the purification of the

target proteins from other component significantly differing in molecular weight that could still be present in the extract.

The column was equilibrated using buffer A_0 (6 M GuCl, 20 mM NaAc, pH 5.2; 1 mM DTT freshly added). A volume of 20 ml of concentrated protein extract was loaded onto the column (maximum column volume: approx. 30 ml) and buffer A_0 flow rate maintained constant (2 ml /min). Protein containing fractions were pooled and concentrated with an Amicon® concentrating cell using a 3 kDa MWCO membrane (approximately OD_{280} 20 units/ml).

2.3 Renaturation process and validation of refolding efficacy of the new BMP2 variants

The BMP2 isolated from E.coli inclusion bodies represents an unfolded monomeric protein, and hence does not exhibit the tertiary structure essential for its biological activity. Thus, dimerization and correct refolding needs to be initiated.

The concentrated protein solution obtained from SEC was drop wise added to the refolding buffer (50 mM Tris, 2 M LiCl, 5 mM EDTA, 25 mM CHAPS, 2 mM glutathione (GSH), and 1 mM glutathione disulfide (GSSG)) under high speed stirring, and afterwards incubated at RT in the dark for at least 5 days. A second refolding buffer was used for one of the batches of BMP2 E83Plk produced. This buffer contained 50 mM Tris, 1 M NaCl, 5 mM EDTA, 0.5 M GuCl, 0.75 M Ches, pH 8.5, 2 mM GSH, and 1 mM GSSG.

During this period of time refolding occurs which was monitored by SDS-PAGE Electrophoresis and Coomassie Brilliant Blue staining.

2.4 Purification of BMP2 variants by Ion Exchange Chromatography

After refolding the pH of the refolding buffer was adjusted to 3.0 using a 6 M HCl solution. Proteins were repeatedly concentrated using a QuickStand Benchtop System (Hollow Fiber Cartridge, 5000 NMWC, surface 650cm2) while being adjusted to 1 mM HCl.

Ion Exchange Chromatography (IEX) involves separation of ionic and polar analytes using functional groups that have opposite charges to that of the analyte ions. The analyte ions and similarly charged ions of the eluent compete to bind to the oppositely charged group on the

surface of the stationary phase. The refolded BMP2 variants were separated from unfolded or monomeric protein species by cation exchange chromatography using either COO^- (weak cation exchange, Fractogel ® EMD COO^- (M), Merck KGaA) or SO_3^- (strong cation exchange, Fractogel ® EMD SO_3^- (M)) column. Before applying the protein to the column, proteins were concentrated by an Amicon® concentrating cell using a 10 kDa MWCO membrane and then centrifuged for 10 min at 4700 x g at RT, to pellet any residual precipitate.

For the COO^- column buffer A_1 (20 mM NaAc; 30 % isopropanol) and buffer B_1 (20 mM NaAc; 30 % isopropanol, 2 M NaCl) were used, while for the SO_3^- column buffer A_2 (4 M Urea, 20 mM NaAc pH 4.5) and buffer B_2 (4 M Urea, 20 mM NaAc, 2 M NaCl pH 4.5) were used.

The first experiments (first batch of BMP2 E83Plk and BMP2 E94Plk) of IEX were performed using the COO^- column (buffer A_1 and B_1) and only in this case the protein was adjusted to buffer A_1 before loading it onto the column. In order to increase the separation between dimers and monomers, the protocol was switched to the use of a SO_3^- cation exchange chromatography (BMP2E83Plk and BMP E83Azide).

In general, the column was equilibrated to buffer A_1 or A_2 (depending on the column) and the protein applied. 2 ml fractions were eluted using a linear gradient of buffer B_1 or B_2, and analyzed by SDS-PAGE Electrophoresis and Coomassie Brilliant Blue staining. Dimer containing fractions were pooled and dialyzed to 5 liters of 1 mM HCl for 2 days, then to 5 liters of dH_20 for 24 hours. The dialyzed product was concentrated using an Amicon® concentrating cell with a 10 kDa MWCO membrane.

The concentration of the final product was measured by UV spectrophotometry using the following calculation:

$$\frac{\left(\frac{OD/_{ml}}{\varepsilon_{coeff.}}\right)}{2}$$

where, $\varepsilon_{coeff} = 18825\ L \cdot mol^{-1} \cdot cm^{-1}$.

2.5 Evaluation of BMP2 variants

2.5.1 SDS-PAGE Electrophoresis and Western blot

3 to 5 µg of each BMP2 variant was separated by SDS-PAGE Electrophoresis (12 % Gel) and stained by Coomassie Brilliant Blue for 2 h or overnight, and destained until the excess of dye was completely removed. In parallel 1 µg of each BMP2 variant was separated by SDS-PAGE Electrophoresis and transferred onto nitrocellulose membranes and Western blotting proceeded like described in 2.1.1

2.5.2 Mass Spectrometry analyses

To determine the mass of the BMP2 variants electrospray ionization mass spectrometry (ESI-MS) was performed using an APEX-II Fourier Transform Ion Cyclotron Resonance (FT-ICR) mass spectrometer (Bruker Daltonic GmbH, Bremen) equipped with a 7.4 T magnet and an Apollo ESI ion source in positive mode.

Mass spectrometry is an analytical technique that can provide both qualitative (structure) and quantitative (molecular mass or concentration) information on analyte molecules after their conversion to ions. The molecules of interest are first introduced into the ionization source of the mass spectrometer, where they are first ionized to acquire positive or negative charges. The ions then travel through the mass analyzer and arrive at different parts of the detector according to their mass/charge (m/z) ratio. After the ions make contact with the detector, useable signals are generated and recorded by a computer system. The computer displays the signals graphically as a mass spectrum showing the relative abundance of the signals according to their m/z ratio (Ho et al. 2003).

Desalted proteins were dissolved in MeOH/H_2O/HAc (49.5/49.5/1) at a concentration ranging from 1 – 5 µM. 2 µL/min of sample were injected using a Hamilton syringe. BMP2 wild type protein was also analyzed as control. Detection range was set to 750 - 3000 m/z according to earlier measurements with other BMP variants. The detection range was optimized to the signal containing area afterwards. 256 scans were recorded at a resolution of 256 K.

The mass spectrometry analyses were performed by Dr. Werner Schmitz, Department of Biochemistry and Molecular Biology, Würzburg.

2.5.3 Biological activity determination by alkaline phosphatase (ALP) expression

Myoblast progenitor C2C12 cells were used as BMP2-responsive cell line to test BMP variant's biological activity. Cells were seeded onto 96-well plates at a concentration of 10^4 cells/well. Cells were cultured in DMEM medium containing 10 % FCS and 1 % of Pen/Strep in a volume of 100 µl/well. After 12 hours of incubation the medium was replaced by 100 µl of DMED medium containing 2 % FCS and 1 % Pen/Strep which additionally contained either BMP2 WT or one of the BMP variants at different concentrations. The proteins were applied in 3 replicates at a concentration of 200 nM and diluted in a log-2 serial dilution (200 nM, 100 nM, 50 nM, 25 nM etc…). DMEM medium containing 2 % FCS and 1 % Pen/Strep served as negative control. The plate was incubated for 72 hours at 37 °C.

For alkaline phosphatase detection by a spectrophotometric assay, after incubation the medium was removed, the cells were washed with PBS, lysed with 100µl of lysis buffer (0.1 M Glycin pH 8.5, 1 % TritonX-100, 1 mM $MgCl_2$, 1 mM $ZnCl_2$, pH 9.6) and incubated at RT on an orbital shaker for 2 h. Paranitrophenyl-phosphate (pNPP) solution (2 mg/ml of paranitrophenyl-phosphate in the reaction buffer (0.1 M Glycin pH 8.5, 1 mM $MgCl_2$, 1 mM $ZnCl_2$, pH 9.6)) was added in order to start the reaction. Absorption at 405 nm was measured every 5 min until extinction reached a values of 2 using a Tecan infinite M200 (Tecan) reader. Dose-response curves were generated using the software OriginPro9.1. EC_{50} values and values for maximal ALP activity were obtained by fitting the data to a logistic dose-response function, which produce a sigmoidal curve:

$$y = \frac{A_1 - A_2}{1 + \left(\frac{x}{x_0}\right)^p} + A_2$$

where, A_1 is the initial value, A_2 the final values, x_0 the center, and p the power.

The spectrophotometric assay is based on the ability of phosphatases to catalyze the hydrolysis of pNPP to p-nitrophenol, a chromogenic product that absorbs maximally at 405 nm.

Instead for the alkaline phosphatase detection based on a staining procedure, after the 72 h incubation, the cells were washed with PBS and successively stained by the application of 100 µl of a 1-Step™ nitro-blue tetrazolium chloride /5-bromo-4-chloro-3'-indolyphosphate p-toluidine salt (NBT/BCIP) substrate solution (Thermo Fisher Scientific). The plates were

incubated in the dark at RT for 15 min. Upon color development the staining solution was removed, replaced with PBS, and plates were analyzed microscopically. The combination of NBT and BCIP yields an intense, insoluble black-purple precipitate when reacted with alkaline phosphatase.

List of buffers and solutions – Protein production

Buffer name	Composition
Ampicillin	1 g Ampicillin 10 ml Millipore water
APS 40 % (w/v)	400 mg ammonium persulfate Dissolve in 1 ml of dH_2O
Benzonase buffer	100 mM Tris pH 7.1 1 mM EDTA 3 mM $MgCl_2$ 80 U/mL Benzonase (final concentration)
Blocking buffer	5 % (w/v) milk powder in TBST
Coomassie Brilliant Blue staining solution	2.5 g Coomassie Brilliant Blue R-250 450 ml Ethanol 100 ml Acetic acid 400 mL dH_2O
Coomassie Brilliant Blue destainer solution	10 % Isopropanol 10 % Acetic acid 80 % dH_2O
Extraction buffer	50 mM NaAc pH 5.0 1 mM EDTA 6 M GuCl 1mM DTT (fresh)
IEX buffer A_1	20 mM NaAc pH 4.5 30 % Isopropanol
IEX buffer B_1	20 mM NaAc pH 4.5 30 % Isopropanol 2M NaCl
IEX buffer A_2	4 M Urea 20 mM NaAc pH 4.5
IEX buffer B_2	4 M Urea 20 mM NaAc 2 M NaCl pH 4.5

Kanamycin 50 mg/mL	0.5 g Kanamycin 10 mL Millipore water
LB agar	5 g Trypton 2.5 g Yeast extract 5 g NaCl 7.5g Agar Ad 0.5 L pH 7.5
LB medium	50 g Trypton 25 g Yeast extract 50 g NaCl Add 5 L pH 7.5
Phosphate buffer	170 mM KH_2PO_4 720 mM K_2HPO_4
Refolding buffer	50 mM Tris pH 8.0-8.2 2 M LiCl 5 mM EDTA 25 mM CHAPS 2 mM GSH 1 mM GSSG
Running buffer 10X	30.3 g Tris base 144.0 g Glycine 10.0 g SDS ad 1 L with dH_2O
SDS-PAGE sample buffer	3.55 ml dH_2O 1.25 ml 0.5M tris-HCl, pH 6.8 2.5 ml Glycerol 2.0 ml 10 % (w/v) SDS 0.2 ml 0.5 % (w/v) bromophenol blue ad 9.5 ml For reducing SDS-PAGE add 50µl β-mercaptoethanol to 950 µl buffer prior to use

Size Exclusion Chromatography buffer A_0	6 M GuCl 20 mM NaAc pH 5.2 1 mM DTT (fresh)
STE buffer	10 mM Tris pH 8.0 150 mM NaCl 1 mM EDTA 375 mM D(+)Saccharose 1:1000 β-mercaptoethanol (fresh)
TAE buffer 1x	40 mM tris acetate 1 mM EDTA pH 8.2 - 8.4
TB medium	60 g Bacto Trypton 120 g Yeast 20 ml Glycerol Ad 5 L Millipore water
TBS buffer	10 mM Tris pH 8.0 150 mM NaCl
TBS buffer 10x	25 mM Tris base pH=7.6 150 mM NaCl
TBSE buffer	10 mM Tris pH 8.0 150 mM NaCl 1 mM EDTA 1:1000 β-mercaptoethanol (fresh)
TBST buffer 1x	100 ml of 10X TBS buffer 1 ml Tween® 20 Fill up to 1 L
TE buffer	100 mM Tris pH 7.0 20 mM EDTA
Transfer buffer 10x	1.92 M Glycine 0.25 M Trizma base
Transfer buffer 1x	100 ml of 10X Transfer buffer 20 % Methanol Ad 700 ml with Millipore water
Triton buffer	60 mM EDTA pH 7.0

	6 % (v/v) Triton X-100 1.5 M NaCl
TSS buffer	2.5 ml 1 M $MgCl_2$ 5 g PEG_{3000} 2.5 ml DMSO Ad 50 ml LB medium pH 6.5 sterilize and store at -20 °C
Tris-HCl 0.5M, pH 6.8	0.5 M Tris Base pH to 6.8 0.4 % SDS
Tris-HCl 1.5M; pH 8.8	1.5 M Tris Base pH to 8.8 0.4 % SDS

Table 4: List of buffers and solutions - Protein production

SDS-PAGE Gel formulation					
12 % Gel	Tris – HCl 0.5M pH 6.8	Tris – HCl 1.5M pH 8.8	Acrylamide 30 %	Glycerin	dH_2O
Stacking Gel	1.25 ml	-	0.5 ml	-	3.2
Running Gel	-	2.5 ml	4 ml	2	1.5 ml
Add 14 µl APS 40 % and 14 µl TEMED to the running gel. Add 12 µl APS 40 % and 12 µl TEMED to the stacking gel.					

Table 5: SDS-PAGE Gel formulation

List of materials – Protein production

Chemicals	Suppliers
1,4 –Dithiothreitol (DTT)	Carl Roth GmbH
Acetic acid (100 %)	Carl Roth GmbH
Acrylamide 30 %	Carl Roth GmbH
Ampicillin sodium salt	Carl Roth GmbH
Antartic phosphatase	New England Biolabs GmbH
BamHI (Fast digest enzyme)	Thermo Fisher Scientific
Benzonase	Merck KGaA
BL21(DE3)	Stratagene
Bromphenol blue Na-salt	Carl Roth GmbH
CHAPS	Merck KGaA
CHES	Merck KGaA
Chloroform	Sigma-Aldrich GmbH
Coomassie Brillant Blue R-250	Thermo Fisher Scientific
D(+) Saccharose	Carl Roth GmbH
Disodium phosphate (Na_2HPO_4)	Hartenstein
DMSO	Sigma-Aldrich GmbH
EcoRV (Fast digest enzyme)	Thermo Fisher Scientific
EDTA	Sigma-Aldrich GmbH
Ethanol, absolute	Sigma-Aldrich GmbH
Glycerin	Carl Roth GmbH
Glycine	Carl Roth GmbH
Guanindin - hydrochlorid	Carl Roth GmbH
H-L-Lys(EO-N3)-OH (Azide)	Iris Biotech GmbH
HEPES	Sigma-Aldrich GmbH
HRP coupled goat anti rabbit antibody ab97051	Abcam
Hydrochloric acid (37 %)	Carl Roth GmbH
Hydrochloric acid 1 N	Carl Roth GmbH
Hydrochloric acid 6 N	Carl Roth GmbH
Isopropyl β-D-1-thiogalactopyranoside	Carl Roth GmbH

(IPTG)	
Isopropanol	Sigma-Aldrich GmbH
Kanamycin Sulfate	Carl Roth GmbH
KAPA HiFi PCR Kit	Kapa Biosystems
L-Ariginin	Carl Roth GmbH
Lamda DNA/Pstl Marker	ThemoScientific
L-Cysteine hydrochloride	Roth
L-Glutathione oxidized (GSSG)	Sigma-Aldrich GmbH
L-Glutathione reduced (GSH)	Sigma-Aldrich GmbH
Lithium Chloride (LiCl)	Carl Roth GmbH
Methanol	Sigma-Aldrich GmbH
Milk powder	Carl Roth GmbH
Monosodium phosphate (NaH_2PO_4)	Carl Roth GmbH
N-Propargyl-lysine	Provided by the Chair for Pharmaceutics and Biopharmacy, University Wuerzburg
NdeI	Thermo Fisher Scientific
NovaBlue cells	Novagen
p25N-hmBMP2 vector	Plasmid kindly provided from W. Sebald to J. Nickel
pET11a-pyrtRNA vector	Provided by the Chair for Pharmaceutics and Biopharmacy, University Wuerzburg
pBluescript II SK (+) vector	Novagen
Potassium Chloride	Sigma-Aldrich GmbH
Potassium dihydrogen phosphate (H_2KO_4P)	Sigma-Aldrich GmbH
ProSieve QuadColor Protein Marker	Biozym
pRSFduet-pyrtRNAsynth	Provided by the Chair for Pharmaceutics and Biopharmacy, University Wuerzburg
Rabbit polyclonal antibody Anti-Human/Murine/Rat BMP-2	PeproTech
Sodium Acetate	Sigma-Aldrich GmbH
Sodium Carbonate (Na_2CO_3)	Carl Roth GmbH
Sodium Chloride	Sigma-Aldrich GmbH
Sodium Dodecyl sulfate (SDS)	Carl Roth GmbH

Sodium hydroxide solution (NaOH)	Carl Roth GmbH
Sodium thiosulfate pentahydrate ($Na_2S_2O_3$)	Merck KGaA
T4 DNA Ligase Kit (Quick Ligation)	New England Biolabs GmbH
TEMED	Carl Roth GmbH
Triton-X-100	Sigma-Aldrich GmbH
Trizma Base (Tris(hydroxymethyl)-aminomethan)	Sigma-Aldrich GmbH
Trypan blue	Sigma-Aldrich GmbH
Trypton/Pepton aus Casein	Carl Roth GmbH
Tween® 20	Sigma-Aldrich GmbH
Urea	Sigma-Aldrich GmbH
WesternBright Chemiluminescence substrate Quantum	Biozym
Wizard ® Plus SV Minipreps DNA Purification System	Promega
Wizard® SV Gel and PCR Clean-Up System	Promega
Yeast extract	Roth/Applichem
β-mercaptoethanol	Carl Roth GmbH

Table 6: List of materials – Protein production

List of equipment – Protein production

Laboratory material	**Supplier**
Amicon Ultra-15 Centrifugal Filter Unit with Ultracel-10 membrane	Merck KGaA
Fractogel ® EMD COO^- (M)	Merck KGaA
Fractogel ® EMD $SO3^-$ (M)	Merck KGaA
Sephacryl™ – S-300 High Resolution	GE Healthcare
Ultrafiltration regenerated cellulose Discs 3kDa, 10kDa MWCO	Merck KGaA

Table 7: List of equipment – Protein production

List of buffer – Cell culture

Buffer	Composition
Lysis buffer ALP assay	0.1 M Glycine pH 8.5 1 % Triton-X-100 1 mM $MgCl_2$ 1 mM $ZnCl_2$
Reaction buffer ALP assay	0.1 M Glycine pH 8.5 1 mM $MgCl_2$ 1 mM $ZnCl_2$
Paranitrophenyl-phosphate solution	20 mg/ml paranitrophenyl-phosphate in H_2O diluted 1:10 in reaction buffer.

Table 8: List of buffer – Cell culture

List of materials – Cell culture

Chemicals	Suppliers
4-Nitrophenyl phosphate disodium salt hexahydrate	Sigma-Aldrich GmbH
DMEM (1X) GlutaMAX™	Gibco
Dulbecco's Phosphate Buffered Saline 1x	Sigma-Aldrich GmbH
FCS	Lonza
Glycine	Carl Roth GmbH
Magnisium chloride hexahydrate	Carl Roth GmbH
Penicillin/Streptomycin 100X	PAA
Trypsin (10x)	Invitrogen GmbH
Zinc chloride	Roth/Applichem

Table 9: List of materials – Cell culture

3. Coupling reactions: Copper (I) - catalyzed alkyne - azide cycloaddition (CuAAC) and strain-promoted azide–alkyne cycloaddition (SPAAC)

3.1 CuAAC using $CuSO_4$ and CuBr as catalysts: the reaction of BMP2 E83Plk

Solutions of 20 µM BMP2 E83Plk were prepared and added to reaction buffer (0.1 M HEPES pH 7.0; 3.9 M Urea final concentrations). $CuSO_4$ CuAAC click reactions were carried out in 50 µM $CuSO_4$, 5 mM Sodium Ascorbate (NaAsc) and 250 µM THPTA. CuBr CuAAC reaction 100 µM CuBr and 250 µM THPTA. The reactions were performed in a final volume of 50 µL. The reaction buffer was the same in both CuAAC reactions.
Both reactions were performed using 100 µM azide-functionalized fluorophores, Sulfo-Cy5-Azide or 5/6-Texas Red-PEG_3-Azide (Jena Bioscience). The use of a functional fluorophore allows the visualization of the coupled protein after the reaction under different detection channels (e.g. Cy5 and Cy3, respectively) using the imaging system FluorChemQ (Biozym Scientific GmbH) and the AlphaView FluorChemQ software.

Reaction mixtures using Sulfo-Cy5-Azide were incubated for 15 min, 30 min, 60 min, and 120 min at room temperature on a rotating platform. As negative controls, BMP2 E83Plk samples without copper ions (no $CuSO_4$ or no CuBr) or without THPTA (no THPTA) were used. BMP2 WT was also used as negative control. Reactions were stopped by addition of 100 mM EDTA (5 mM final concentration). 20 µl samples were separated by SDS-PAGE Electrophoresis and visualized under Cy5 detection channel. Gels were then stained with Coomassie Brilliant Blue.

In order to test possible side effects influencing the integrity or stability of the different BMP variants which are caused by the chemicals used for click reactions, CuAAC reactions using $CuSO_4$ or CuBr were performed, using the same buffers and catalysts concentrations reported before. The variants BMP2 K3Plk (Tabisz 2016) was included in these experiments in order to identify side effects which are specific for the site mutation of the BMP variant. Reactions were performed for 60 min and stopped by addition of 100 mM EDTA (5 mM final concentration). 20 µl samples were separated by SDS-PAGE, visualized under Cy5 detection channel. The coupled proteins were then transferred to a nitrocellulose membrane and

visualized using anti BMP2 antibody. The use of Western blotting instead of Coomassie Brilliant Blue staining was performed in order to have a higher detection level on the protein after the reaction.

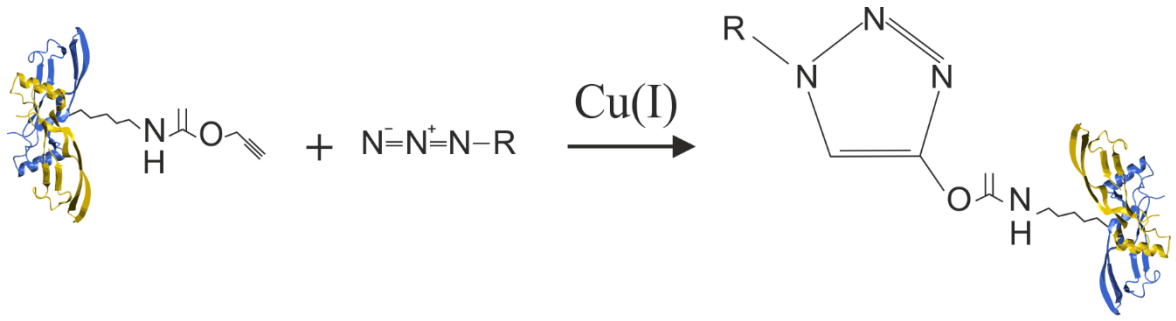

Figure 9: Copper catalyzed alkyne - azide cycloaddition - scheme of the reaction
The BMP2 variant, BMP2 E83Plk harboring the alkyne group reacts to an azide-functionalized counterpart in presence of copper I (Cu (I)). The azide-functionalized molecules used were: Sulfo-Cy5-Azide or 5/6-Texas Red-PEG_3-Azide.

3.2 Strain-Promoted Azide–Alkyne Cycloaddition (SPAAC): copper free reaction for BMP2 E83Azide

The BMP2 E83Azide was coupled via the strain-promoted azide–alkyne cycloaddition that involves the azide group of the protein and a dibenzocyclooctyne (DBCO) group of a reaction partner under copper-free conditions. 20 µM of BMP2 E83Azide were incubated for 60 min with different concentration of a DBCO-functionalized fluorophore (DBCO-Sulfo-Cy5), to test the efficacy of the reaction. The fluorophore concentrations used were: 1 mM, 100 µM, 10 µM, 1 µM, 0.1 µM, 0.01 µM, and 0 µM as control. 20 µl samples were separated by SDS-PAGE. The gels were analyzed under Cy5 detection channel and stained by Coomassie Brilliant Blue.

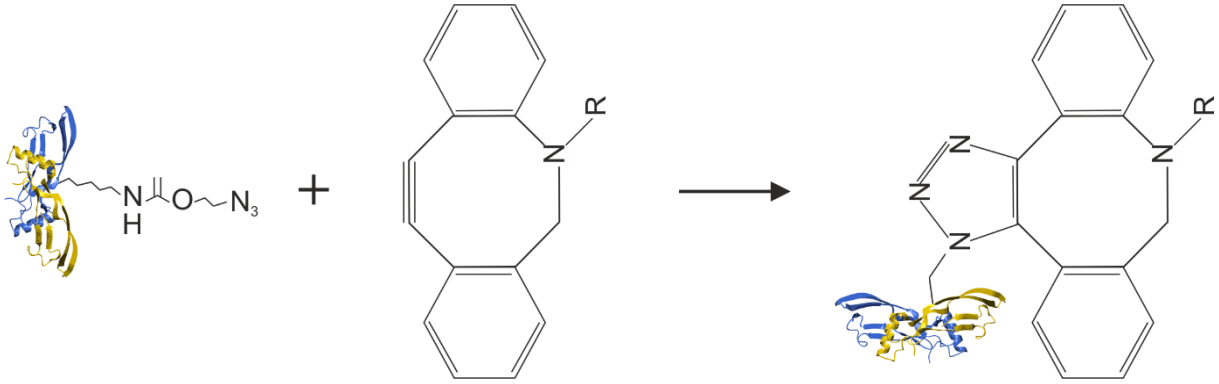

Figure 10: Strain-Promoted Azide–Alkyne Cycloaddition (SPAAC) – Scheme of reaction
BMP2 E83Azide harboring an azide group reacts with a dibenzocyclooctyne (DBCO) group without the requirement of copper to catalyze the reaction. The DBCO-functionalized molecules used were: DBCO-Sulfo-Cy5 and DBCO-PEG_4-5/6-Texas Red.

3.3 Biological activity of fluorophore coupled BMP2 variants after CuAAC or SPAAC reaction

Cy5, with the bulky structure, was found to inhibit the binding of the BMP2 variants to the receptors. The first experiments performed using Cy5 coupled proteins led to misinterpretation of the data due to a completely suppression of biological activity. The Sulfo-Cy5-Azide or DBCO-Sulfo-Cy5 were therefore substituted for biological tests with 5/6-Texas Red-PEG_3-Azide or DBCO-PEG_4-5/6-Texas Red, respectively These choice of fluorophores containing a spacer (PEG_3 or a PEG_4) was done in order to separate the protein from the bulky fluorophore structure that would prevent the blockage of the BMP2 variants' binding sites.

The biological activities of the different coupled BMP2 variants were tested by ALP assay as described in 2.5.3, in order to test if the reactions affected the bioactivity of the proteins. Uncoupled BMP2 variants and BMP2 WT were used as control.
Alkaline phosphatase expression of BMP2 E83Plk coupled to 5/6-Texas Red-PEG_3-Azide after CuAAC reactions was compared to BMP2 K3Plk after 30 min, 60 min or 120 min coupling time and the values at 50 nM were used to calculate the residual bioactivity in relation to the controls. Alkaline phosphatase expression was also detected using the 1-Step™ NBT/BCIP substrate solution (described in 2.5.3). In this case cells were treated with 200 nM coupled proteins

For the SPAAC reaction, BMP2 E83Azide was coupled to DBCO-PEG_4-5/6-Texas Red and incubated for 15 min, 30 min, 60 min, 120 min, or overnight at 4 °C. Samples were applied to C2C12 cells in a log-2 dilution and alkaline phosphatase expression measured as described in 2.5.3. Non-coupled BMP2 E83Azide was taken as control, and values at 50 nM were used to calculate the residual bioactivity of the reacted protein relative to the non-coupled control. Alkaline phosphatase expression was also detected by staining applying 200 nM of coupled BMP2 E83Azide and using non-coupled BMP2 E83Azide as control.

3.4 Functionalization of microspheres with azide- or DBCO- groups

Different microspheres were used to couple the BMP2 variants: recombinant collagen like peptide (RCP) microspheres produced from Fujifilm (Cellnest™), silica microspheres (Thermo Fisher Scientific), or agarose microspheres (azide- or DBCO- functionalized, according to the requirements for the click reaction, Jena Bioscience). RCP and silica microspheres expose amino groups on the surface that were used to couple a NHS-PEG_4-Azide (Jena Bioscence) or a NHS-PEG_4-DBCO linker by NHS ester-amine reaction. The RCP and silica microspheres were incubated for 2 h at room temperature with 4 mM NHS-PEG_4-Azide or NHS-PEG_4-DBCO linker in 0.1 M $NaHCO_3$ buffer (pH 7.4) in a total volume of 500 µl. The reactions were stopped by addition of 100 mM Tris (1 mM Tris final concentration). Microspheres were spun down for 30 sec at 20000 x g, the supernatant collected and the beads washed 3 times with dH_2O.

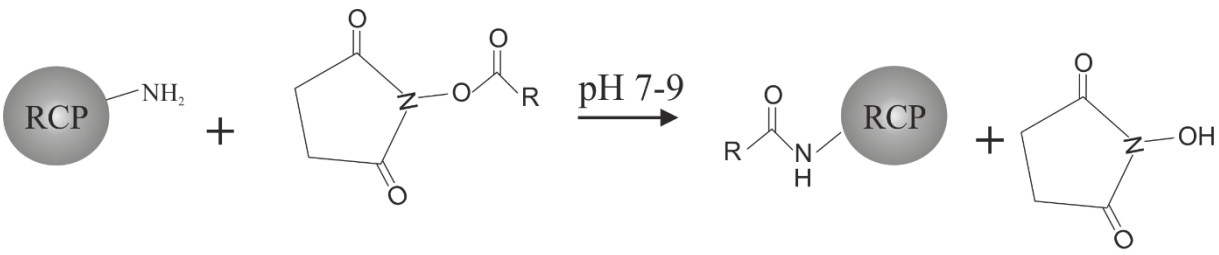

Figure 11: NHS - Amine reaction
The free amine present on the RCP microspheres were used for the NHS – amine reaction. The free amine were coupled to the NHS-functionalized linker in a pH~ 7-9. The bifunctional linker used were: NHS-PEG_4-Azide or NHS-PEG_4-DBCO.

RCP microspheres were produced by emulsification using calcium carbonate ($CaCO_3$) crystals as pore forming agent. Briefly a 20 % (w/v) aqueous RCP solution was mixed with

$CaCO_3$ powder in a 1:1 weight ration of RCP to $CaCO_3$. The suspension was added drop wise to preheated corn oil at 50 °C while stirring the emulsion at 800 rpm for 20 min. Then the emulsion was cooled using an ice bath and the emulsified microspheres were washed three times with acetone. After overnight drying at 60 °C, microspheres were sieved to the desired size (32-50 µm; 50-72 µm; 200-300 µm). Subsequently, the microspheres were crosslinked using different crosslinking reactions. Dehydrothermal (DHT) crosslinking was conducted at 160 °C in vacuum for 1 or 4 days, respectively. Hexamethylene diisocyanide (HMDIC) crosslinking was conducted by suspending 1 g of spheres and 1 ml of HMDIC or 30 µl of HMDIC in 100 ml ethanol for 1 day. After crosslinking, the $CaCO_3$ porogen was removed by suspending the microspheres in 0.23 M HCl for 30 min until the formation of carbon dioxide stopped. The microspheres were washed repeatedly with water until a neutral pH was achieved.

Carboxyl and amine groups of RCP are crosslinked by DHT; whereas HMDIC crosslinking only addresses amine groups. In both cases, the degree of crosslinking was determined by measuring the residual free amines on microspheres using a colorimetric assay, based on the incorporation of 2,4,6-trinitrobenzenesulfonic acid (TNBS). TNBS reacts with primary amines including both terminal α-amino groups and side chain ε-amino groups. The absorbance was measured at 345 nm. The described production of microspheres and measurements of free amine were performed at Fujifilm Manufacturing Europe (Tilburg, The Netherland).

Microsphere type	**Average free amino group ± SD (mmol/100 g)**
RCP 50-75 µm (high) HMDIC	14.6 ± 0.5
RCP 50-75 µm (low) HMDIC	28.0 ± 4.8
RCP 50-75 µm DHT 4 day	41.3 ± 2.1
RCP 200-300 µm (high) HMDIC high	26.6 ± 1.2

Table 10: Measurements of the residual free amines on the RCP microspheres based on the incorporation of 2,4,6-trinitrobenzenesulfonic acid (TNBS).

Based on the amounts of residual free amine groups, DHT crosslinked microspheres with a 50-75 µm diameter range (see Table 10) were chosen for the functionalization with the aforementioned NHS-PEG_4-Azide or NHS-PEG_4-DBCO linkers in order to maximize the functionalization rate.

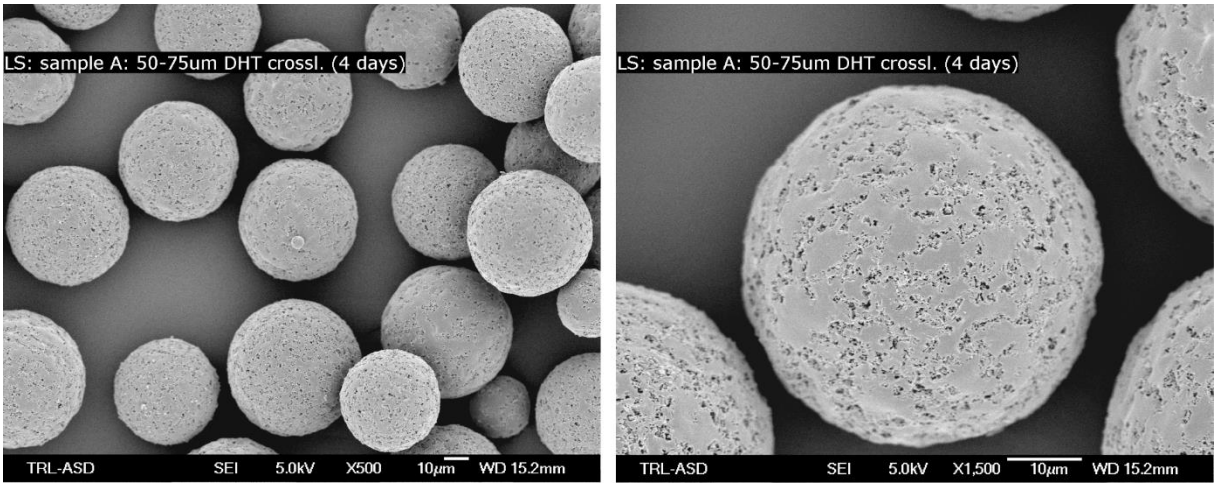

Figure 12: Scanning electron microscopy (SEM) of RCP microspheres
SEM images of RCP microspheres DHT crosslinked (4 days) with average size of 50 – 75 µm. SEM images were performed at Fujifilm Manufacturing Europe (Tilburg, The Netherland).

3.5 Coupling BMP2 variants to functionalized beads

3.5.1 CuAAC reactions: comparing the effects upon addition of $CuSO_4$ and CuBr

10 mg microspheres (azide-functionalized RCP or silica beads) or 20 µL (bed volume) of commercially available azide-functionalized agarose beads (Jena Bioscience), were incubated in reaction buffer (0.1 M HEPES pH 7.0, 3.9 M Urea, final concentration) with 20 or 50 µg BMP2 E83Plk. For the $CuSO_4$ CuAAC click reaction, 50µM $CuSO_4$, 5 mM NaAsc and 250µM THPTA were used. For the CuBr CuAAC reaction 100 µM CuBr and 250 µM THPTA were used. The reactions were performed in a total volume of 1 ml. Reactions were incubated for 1 h at room temperature on a rotating platform. BMP2 WT was used as negative control. Reactions were stopped by addition of a 100 mM EDTA solution (final EDTA concentration of 5 mM).

After reaction, microspheres were centrifuged for 1 min at 20000 x g and supernatants were collected. Beads were washed one time with 1 ml dH_2O and centrifuged again. Water was collected and 1 ml 6 M Urea was added to the beads and incubated overnight at 4 °C on a rotating platform. Beads were again centrifuged and urea supernatants collected and dialyzed against water in order to remove any possible chemical that could interfere with the following analyses. Coupled beads were kept at 4 °C in 1 ml dH_2O until use.

3.5.2 SPAAC reaction: coupling BMP2 E83Azide to DBCO-functionalized microspheres

20 µg BMP2 E83Azide were incubated with the different DBCO-functionalized microspheres (10 mg RCP, 10 mg silica microspheres or 20 µL (bed volume) agarose beads) in 1 ml dH_2O for 2 h at room temperature. After reaction, supernatants were collected and the beads washed with dH_2O. The supernatants were collected and beads incubated overnight in 6 M urea at 4 °C on a rotating platform. The following day, urea supernatants were collected and beads washed with dH_2O. Urea supernatants and beads were dialyzed against dH_2O. Beads were suspended in 1 ml dH_2O and kept at 4 °C until next use.

3.6 Quantification of the amount of protein coupled by CuAAC and SPAAC reactions

After click reaction the suspension mixtures composed of beads and protein was centrifuged and the supernatant was collected (= reaction supernatant (rs)). The other supernatants of the different washes are referred to as water wash supernatant (ws) and urea wash supernatant (us). The supernatants were dialyzed against dH_2O in order to remove any possible chemical that could interfere with the quantification measurements.

3.6.1 Western blot

20 µl samples (+ 4 µl 5x non-reducing loading buffer) of the individual supernatants of both CuAAC and SPAAC reactions were analyzed by SDS-PAGE and Western blot as described in 2.1.1.

3.6.2 ELISA

Samples of the supernatants of either reaction were also analyzed by ELISA (PeproTech). Samples of rs and us were diluted 1:1000, and ws 1:500 in the diluent which is included in the ELISA kit. The sandwich ELISA was performed according to the manufacturer's recommendations. Briefly, plates were incubated overnight with a solution containing the captured antibody at room temperature. On the next day, plates were washed 4 times with washing buffer (PeproTech ELISA Kit) and 300 µL/well blocking buffer (PeproTech ELISA Kit) was added. After a 2 h incubation at RT 100 µL of diluted samples were added. After further incubation for 2 h at RT the plates were washed 4 times, and the detection antibody (PeproTech ELISA Kit) added. After additional 2 h avidin peroxidase conjugate was added and incubated for 30 min. ABTS substrate (2,2'-azino-bis(3-ethylbenzothiazoline-6-sulphonic acid, (PeproTech ELISA Kit)) was added and absorbance was measured at 405 nm, using 650 nm as reference wavelength, in the ELISA plate reader (TECAN sunrise). A standard curve was prepared using the non-coupled BMP2 variant which was used for the respective click reactions (BMP2 E83Plk for CuAAC and BMP2 E83Azide for the SPAAC). As positive control, BMP2 WT provided from the manufacturer was used.

3.6.3 Using radioactively labelled BMP2

50 µCi (1.85 Mbq) of N-succinimidyl-[2,3-^{3}H]-propionate (^{3}H-NSP) were incubated with 20 µg of BMP2 WT, BMP2 E83Plk or BMP2 E83Azide in HBS_{500} buffer (10 mM Hepes, 500 mM NaCl, pH 8.4) for 2 h at room temperature. The NHS-ester reaction (Figure 11) occurred between the amine group of the BMP2 proteins and the NHS group of the linker ^{3}H-functionalized.

$$1 \text{ curie [Ci]} = 37 \times 10^{9} \text{ becquerel [bq]}$$

Tritium labeled proteins were separated from the uncoupled Tritium with an Amicon centrifugal tube (10 kDa - MWCO). Purified coupled proteins and flow through were collected and analyzed by scintillation counting. BMP2 E83Plk-^{3}H, BMP2 E83Azide-^{3}H and BMP2 WT-^{3}H were also analyzed photometrically. Absorbance was measured at 280 nm and the concentration was calculated. Click chemistry reactions were performed using 20000 counts per minutes (cpm) (~25 pg) of BMP2 E83Plk-^{3}H, BMP2 E83Azide-^{3}H or BMP2 WT-^{3}H together with unlabeled protein (20 µg or 50 µg BMP2 E83Plk, BMP2 E83Azide or BMP2 WT). After click reactions, rs, ws and us were collected. 100 µl samples were analyzed by scintillation counting. The measured cpm values were blank subtracted (reaction buffer, water or urea) and the values obtained for all samples were summed up. The amount of Tritium labeled protein coupled was measured indirectly: the sum of all measured values was subtracted from the 20000 cpm used for each reaction. Consequently the amount of protein that was coupled with the reaction was measured as a proportion of the amount of coupled Tritium labeled protein to the total amount of unlabeled protein used.

3.7 Evaluation of the osteogenic potential of BMP2 variants coupled to microspheres after click reactions

3.7.1 Alkaline Phosphatase assay of microspheres coupled protein

Alkaline phosphatase assay was performed as described in 2.5.3. BMP2 E83Plk or BMP2 E83Azide coupled microspheres suspended in 1 ml of PBS were diluted 1:10 in PBS. 10 µl of this suspension were added to the cells and covered with 90 µl DMEM medium containing 2

% FCS and 1 % Pen/Strep. In case of agarose and silica beads 20 µL of 0.9 % low melting agarose was added on top of the beads to ensure immobilization and direct contact with the cells. Plates were centrifuged for 5 min at 1200 rpm. 80 µL DMEM medium containing 2 % FCS and 1 % Pen/Strep was added on top. Cells with beads were incubated for 72 h and alkaline phosphatase expression was detected by staining as described before.

3.7.2 Alkaline Phosphatase assay of click reaction supernatants

Reaction supernatants of SPAAC click chemistry were applied to C2C12 to evaluate if the uncoupled protein also maintains its bioactivity after the reaction.
The concentration of the BMP variants in the reaction supernatants was measured by ELISA. C2C12 cells were cultured as described before 2.5.3 and 25 nM of BMP2 E83Azide or BMP2 WT samples of uncoupled protein contained in the reaction supernatant were applied. As positive control, untreated BMP2 E83Azide or BMP2 WT were used. Relative phosphatase expression was measured as described before and the relative bioactivity at 25 nM was calculated as percentage of the control.
The assay was performed only for the SPAAC reaction supernatants. The concentrations measured in CuAAC reaction supernatants were too low to achieve a 25 nM concentration (in the restricted volume of a 96 well plate) to be applied to the cells.

List of buffers – Click chemistry reaction

Buffer name	Composition
Reaction buffer – CuAAC – $CuSO_4$	0.1 M HEPES pH 7.0 3.9 M Urea 50 µM $CuSO_4$ 5 mM Sodium Ascorbate (NaAsc) 250 µM THPTA
Reaction buffer – CuAAC – CuBr	0.2 M HEPES pH 7.0 3.9 M Urea 100 µM CuBr 250 µM THPTA
HBS_{500} buffer	10 mM HEPES pH 7.4 500 mM NaCl 3.5 mM EDTA

Table 11: List of buffers – Click chemistry reaction

List of materials – Click chemistry reaction

Chemicals	Suppliers
1-Step™ NBT/BCIP	Thermo Fisher Scientific
5/6 – Texas Red – PEG_3 – Azide	Jena Bioscience
Agarose low melting point	Biozym
Agarose microspheres azide-functionalized	Jena Bioscience
Agarose microspheres DBCO-functionalized	Jena Bioscience
CuBr	BaseClick
$CuSO_4$	BaseClick
DBCO-PEG_4-5/6-Texas Red	Jena Bioscience
DBCO-Sulfo-Cy5	Jena Bioscience
EDTA	Sigma-Aldrich GmbH
ELISA kit	PeproTech
HEPES	Sigma-Aldrich GmbH
NaAsc	BaseClick
$NaHCO_3$	Sigma-Aldrich GmbH
NHS – PEG_4 – Azide	Jena Bioscience
NHS – PEG_4 – DBCO	Jena Bioscience
Recombinant collagen like peptide (RCP) Cellnest ™	Fujifilm
Silica microspheres	Sigma-Aldrich GmbH
Sulfo – Cy5 – Azide	Jena Bioscience
THPTA	BaseClick
Tritium NHS	
Urea	Sigma-Aldrich GmbH

Table 12: List of materials – Click chemistry reaction

4. Injection of a paste containing BMP2 coupled beads in a subcutaneous rat model

All animal experiments were performed with prior approval of the ethics committee for laboratory animal use (protocol number EMC 15-114-05) at Erasmus Medical Center, Rotterdam, The Netherlands. Nine week old male Sprague Dawley (SD) rats (Charles River) were used in this study. The animals were randomly assigned and housed in pairs in a specific pathogen free (SPF) facility and allowed to adapt to the conditions of the animal house for 7 days before implantation. The animals were maintained at 22 ± 5°C on a 12 h dark/light cycle with ad libitum access to standard rat chow and water. At 12 weeks after implantation, animals were euthanized with CO_2 and specimen were harvested for micro-CT analysis and histology.

The animal experiment was planned in order to compare ectopic bone formation induced by covalently coupled BMP2 E83Plk or BMP2 E83Azide, respectively, to wild type BMP2 being adsorbed onto microspheres. Additionally different doses of coupled or adsorbed protein were injected subcutaneously in order to identify the lowest protein dose being required to induce this process. RCP microspheres were used to prepare a subcutaneous injectable paste as carrier.

4.1 Samples preparation and microsphere-paste composition

10 different conditions were prepared: 10 µg, 1 µg, 0.1 µg adsorbed BMP2 WT; 10 µg, 1 µg, 0.1 µg BMP2 E83Plk covalently coupled to RCP microspheres; 10 µg, 1 µg, 0.1 µg BMP2 E83Azide covalently coupled to RCP microspheres and empty microspheres as control (n =7 per condition). CuAAC and SPAAC reactions were performed like described before: 10 mg of RCP microspheres, after functionalization with the azide or the DBCO linker, were reacted with 20 µg BMP2 E83Plk or BMP2 E83Azide. Each CuAAC or SPAAC reaction was performed 10 times in parallel (see Scheme Figure 13). Based on results obtained from ELISA experiments as well from those obtained by radioactive tracing, approximately 80 % of the protein was coupled to the microspheres (~ 16 µg protein). Each single reaction, containing ~ 16 µg protein coupled to the beads, was diluted to the final concentration needed for the animal experiment: (10 µg, 1 µg and 0.1 µg) and the dilutions were pooled in one single 5 ml Eppendorf tube, freeze-dried and mixed with 330 mg of empty microspheres.

BMP2 WT adsorbed RCP microspheres were prepared as following: 100 mg of RCP were incubated overnight at 4 °C with 100 µg BMP2 WT. Samples were lyophilized and mixed with 230 mg of empty RCP microspheres. At the day of injection each of the different RCP microspheres mixtures were resuspended with 1.2 ml saline (0.9 % NaCl) for at least 10 min using a spatula under sterile conditions. The freshly prepared paste was loaded into a 1 mL syringe and 100 µl of paste was injected subcutaneously into the dorsal part of the animal using a 19G needle.

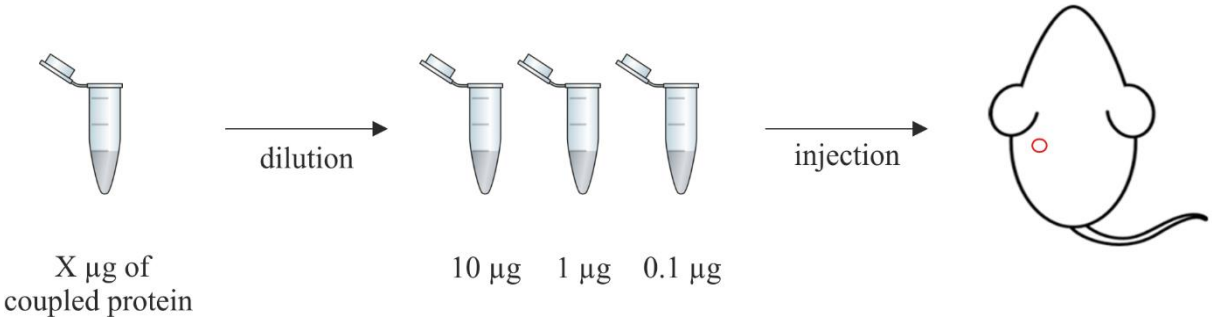

Figure 13: Scheme for the preparation of the samples for the animal experiment.
10 individual reactions were performed using 20 µg of BMP2 E83Plk or BMP2 E83Azide. The coupled protein after the reaction was calculated to be ~ 16 µg. Each reaction was diluted down to 10 µg, 1 µg or 0.1 µg, and all the dilutions collected in one 5 mL Eppendorf tube. Samples were lyophilized and 230 mg empty microspheres as well as 1.2 ml saline were added to create the paste. 100 µl of paste were then injected subcutaneously to the dorsal part of the animal.

4.2 Micro-computed tomography (micro-CT) analysis

A Quantum FX (Perkin Elmer, Waltham, MA, USA) micro-CT was used to image animals every two weeks until the end of the experiment (week 12) and also to image the implants retrieved at 12 weeks. To image ectopic bone *in vivo* the following parameters were used: Field of view: 73 mm, Voltage: 90 kV, Current: 160 µA, Scan Time: 120 sec. To image the implants *ex vivo* a field of view of 20 mm was used (other parameters were maintained).

4.3 Evaluation of bone density and bone volume

Trabecular and cortical bone mineral density (BMD) was measured on the basis of calibration scanning, using two phantoms with known density (0.25 g/cm^3 and 0.75 g/cm^3; Bruker

MicroCT) under identical conditions. For image processing, the software Analyze was used (Mayoclinic, Rochester, MN, USA), setting the threshold levels to 0.13 g/cm^3 *in vivo* and to 0.15 g/cm^3 *ex vivo*. These values have been chosen according to similar animal experiment previously performed (protocol number EMC 15-114-03) at Erasmus Medical Center, Rotterdam, The Netherlands.

Bone density was calculated as mean of the n=4 samples (BMP2 WT and BMP2 E83Azide) that formed bone, excluding the animals that did not show bone formation (zero values).

The bone volume was calculated as mean of the n=7 samples, including the zero values. Statistics were performed using a one-way ANOVA or an unpaired t-test with Welch correction assuming different standard deviation.

4.4 Histological evaluation of the explanted implants

For histological analyses, the ectopically formed ossicles were fixed in a 4 % formalin solution and decalcified using 10 % EDTA for 2-4 weeks. Implants were dehydrated and embedded in paraffin. 5 µm thick sections were prepared using a Leica microtome (Leica Biosystems Nussloch GmbH Germany) and mounted on subbed glass slides (Thermo Fisher Scientific). The sections were de-paraffinized and rinsed with distilled water to be subsequently stained according to the following standard procedures: hematoxylin and eosin (H&E), Masson´s Goldner, Alcian Blue, Movat Pentachrome, Safranin O, and Tartrate Resistant Acid Phosphatase (TRAP) staining. Samples were also immunohistochemically stained using anti vimentin, anti α-smooth muscle actin (α-SMA), and anti CD68 antibodies. The sections were imaged microscopically. For rehydration and dehydration standard protocols were used (see below).

Rehydration and dehydration steps:

Time (min)	**Solution**	**Aim/Notes**
10	Xylene I	Descending series: Deparaffining, rehydration
10	Xylene II	
3X dip in and out	EtOH 96 %	
3X dip in and out	EtOH 96 %	
3X dip in and out	EtOH 70 %	
3X dip in and out	EtOH 50 %	

	dH_2O	Swirl until turbulence disappear
Specific staining is performed		
2X dip in briefly	EtOH 70 %	Ascending series: dehydration
2	EtOH 96 %	
5	Isopropanol I	
5	Isopropanol II	
5	Xylene I	
5	Xylene II	

Hematoxylin & Eosin Staining:

Time (min)	**Solution**	**Aim/Notes**
Rehydration steps		
6	Hematoxylin	Staining of cell nuclei
	dH_2O	Flow weakly until no color is washed out any more
5	Tap water	Bluing
6	Eosin	Staining Extracellular matrix (ECM)
	dH_2O	Flow weakly until no color is washed out any more
Dehydration steps		

Nuclei: blue

ECM: pink

Masson´s Thricrome (12043, Morphisto):

Time (min)	**Solution**	**Aim/Notes**
Rehydration steps		
5	Hematoxylin	Staining of cell nuclei
10 sec	dH_2O	Flow weakly until no color is

		washed out any more
5	Tap water	Blueing
4	Acid Fuchsin – Ponceau (Goldner I)	Staining cytoplasm
30 sec	dH_2O	Flow weakly until no color is washed out any more
6	Phosphomolybdic acid – Orange G	Staining erythrocytes
30 sec	dH_2O	
8	Light Green (Goldner III)	Staining collagen
30 sec	dH_2O	
1	1 % Acetic acid	
1	Tap water	
Dehydration steps		

Nuclei: blue

Bone: green/turquoise

Osteoid: orange/red

Cartilage: Purple

Alcian Blue (13416, Morphisto):

Time (min)	**Solution**	**Aim/Notes**
Rehydration steps		
3	3 % Acetic acid	
30	1 % Alcianblue	Staining proteoglycans
	dH_20	
5	0.1 % nuclear fast red solution	Staining nuclei
	dH_2O	Flow weakly until no color is washed out any more
Dehydration steps		

Nuclei: red

Cartilage: blue

Movat Pentachrome (12057, Morphisto):

Time (min)	**Solution**	**Aim/Notes**
Rehydration steps		
12	1 % Alcianblue	Staining proteoglycans
5	dH_20	
60	Alkaline alcohol	
10	dH_2O	
10	Hematoxylin	Staining nuclei
15	dH_2O	
10	Crocein Scarlet Acid Fuchsin	Staining cytoplasm
30 sec	1% Acetic acid	
20	5 % Phostphotungstic acid	
2	1 % Acetic acid	
1	99 % EtOH	
6	99 % EtOH	
6	Saffron du Gatinais	Staining collagen
Dehydration steps		

Mature bone: dark yellow

Fibrous tissue: light yellow

Cartilage: green

Osteoids: red

TRAP (Acid Phosphatase, Leukocyte (TRAP) Kit, Sigma-Aldrich):

Time (min)	**Solution**	**Aim/Notes**
Rehydration steps		
Prepare 45 ml pre-warmed water at 37 °C and mix it with: 1 ml Diazotized Fast garnet GBC Solution, 0.5 ml Naphtol AS-BI Phosphate Solution, 2 ml Acetate solution, 1 ml Tartrate Solution		

90 (37 °C)	Prepared buffer	
	dH_2O	
30 sec	Hematoxylin (Morphisto)	Staining nuclei
	Tap water	
	dH_2O	
NO dehydration steps. Air dry and mount. Do not use xylene as this will dissolve the precipitated staining.		

Osteoclasts: pink/red

Nuclei: dark blue

Safranin O:

Time (min)	**Solution**	**Aim/Notes**
Rehydration steps		
5	Hematoxylin (Morphisto)	Staining nuclei
5	Tap water	
5	Fast Green (FCF)	
10 sec	1 % Acetic acid	
5	0.1 % Safranin O (S2255, Sigma-Aldrich)	Staining proteoglycans
Dehydration steps		

Nuclei: blue

Cartilage: orange/red

Vimentin, α-SMA and CD68:

Time (min)	**Solution**	**Aim/Notes**
Rehydration steps		
5	0.2 % Triton-X-100 in PBS	Staining nuclei
5 (3X)	PBS-T (PBS + 0.5 %	

	Tween-20)	
30	5 % BSA in PBS	
Overnight	Primary antibody	Antibodies used: rabbit monoclonal to vimentin, rabbit polyclonal to α-smooth muscle actin, and mouse monoclonal antibody to CD68. 1:100 dilution in antibody dilution buffer (DCS Innovative System).
5 (3X)	PBS-T	
10 min (RT)	Polymer enhancer (1-2 drops)	
5 (3X)	PBS-T	
20	HRP-Polymer	
5 (3X)	PBS-T	
5	DAB solution	
5	PBS-T	
30 sec	Hematoxylin	Staining nuclei
	Tap water	
Dehydration steps		

List of materials – Animal experiment

Material	Suppliers
19G needle	Braun
Alcian Blue Kit	Morphisto
EDTA	Sigma-Aldrich GmbH
Formalin	Sigma-Aldrich GmbH
Glass slides	Thermo Fisher Scientific
Hematoxylin & Eosin kit	Morphisto
Masson's Goldner Kit	Morphisto
Mouse monoclonal antibody to CD68	Abcam
Movat Pentachrome Kit	Morphisto
Rabbit monoclonal antibody to vimentin	Abcam (ab92547)
Rabbit polyclonal antibody to α-smooth muscle cells	Abcam (ab5694)
Safranin	Sigma-Aldrich GmbH
Syringe	BD Plastipak
Tartrate Resistant Acid Phosphatase (TRAP) Kit	Sigma-Aldrich GmbH
Xylen	Carl Roth GmbH

Table 13: List of materials – Animal experiment

List of laboratory equipment

Equipment	Model	Supplier/Producer
Agarose electrophoresis system	PerfectBlue™ Horizontal mini Gel System	Peqlab
Amicon concentrating cell 400ml	UFSC40001	Merck KGaA
Amicon concentrating cell 50ml	UFSC05001	Merck KGaA
Autoklav Tecnoclav Giessen Tischautoklav Varioklav	Biomedis Systec H+P	
Bacterial shaking incubator	Multitron Standard	Infors HT
Bacterial incubator 37°C		Memmert
Bench centrifuge	Heraeus Multifuge X1R Centrifuge	Thermo Fisher Scientific
Cell culture incubator	Heraeus Incubator	Thermo Fisher Scientific
Centrifuge	Avanti J-26 XP	Beckman Coulter
Chromatography system	ÄKTA avant FPLC BioLogic Duo-Flow Protein Purification System LaCHromUltraTM HPLC	GE Healthcare Bio-Rad Hitachi
Fluorescent microscope	BZ-9000 (BIOREVO)	Keyence
Fume hood		Prutscher
Microcentrifuge	Centrifuge 5417R	Eppendorf
Microscope	Keyence BZ – 9000 BIOREVO	Keyence
Microtome	Leica microtome	Leica Biosystems
pH-meter		Mettler Toledo
Plate reader	Infinite M200	Tecan Deutschland GmbH

QuantumFX		Perkin Elmer
QuickStand Benchtop System (Hollow Fiber Cartridge, 5000 NMWC, surface 650cm^2	UFP-5-C-4MA	GE Healthcare
Rotor	Rotor JA-10	Beckman Coulter
Rotor	Rotor JLA 8.1	Beckman Coulter
Rotor	Rotor JA-25.50	Beckman Coulter
Scale		Satorius
Scale	ABJ 220-4M	Kern&Sohn GmbH
Scale	EG 2200-2NM	Kern&Sohn GmbH
SDS-PAGE chamber system	PerfectBlue™ Doppel-Gelsystem Twin M	Peqlab
SDS-PAGE gel imaging system	FluorChemQ	Biozym Scientific GmbH/Cell Biosciences
Semi-dry blotting chamber	PerfectBlue™'Semi-Dry' Electro Blotter Sedec™M	Peqlab
Sterile hood	Safe 2020 class II safety cabinet EN 12469:2000	Thermo Fisher Scientific
Thermocycler	Labcycler Gradient	SensoQuest GmbH
Ultrasonic	Digital Sonifier 250	Branson
UV- Photometer	Evolution 60S	Thermo Fisher Scientific

Table 14: List of laboratory equipment

III. Results

1. Production of BMP2 E83Plk and BMP2 E94Plk

In order to achieve site directed immobilization of the BMP2 to scaffolds via click chemistry, two new constructs, BMP2 E83amber and BMP2 E94amber were generated. In contrast to the clone BMP2 K3amber, used to produce the protein BMP2 K3Plk (Tabisz 2016), the mutation in the new variants is either localized at the finger tips or on top, close to the symmetry axis of the dimeric BMP2 structure (Figure 14). If coupling to scaffolds is carried out via artificial amino acids residing in either one of these positions, the orientation of the receptors binding epitopes of the immobilized BMP2 molecule will be best matched to those of the receptor ectodomains of the cell surface, thus minimizing effects caused by steric hindrance.

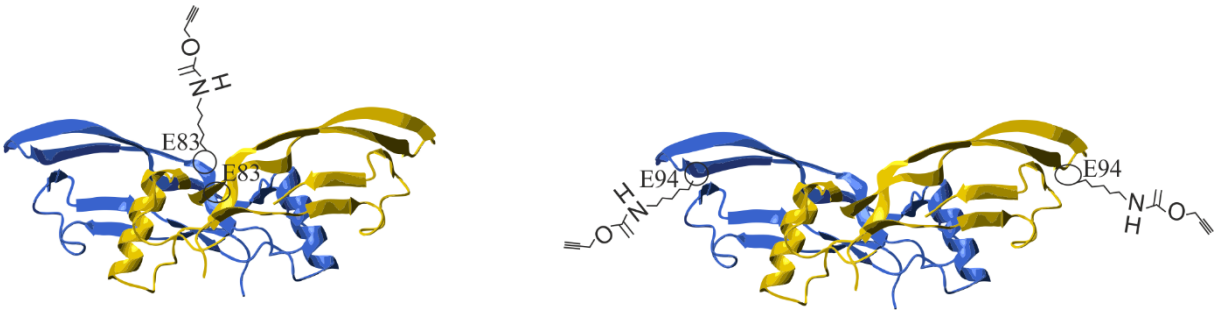

Figure 14: BMP2 variant structure - BMP2 E83Plk and BMP2 E94Plk
Images show the ribbon structures of the two BMP2 variants: BMP2 E83Plk and BMP2 E94Plk. Glutamic acid (E) was replaced by N-Propargyl-lysine at position E83 of the BMP2 or at position E94.

The previous BMP2 K3Plk variant (Tabisz 2016) was originally chosen in order to minimize possible problems related to protein expression, refolding or purification. However, soluble (i.e. non-coupled) BMP2 K3Plk revealed the same biological activities if compared to wild type BMP2, but after coupling to microspheres the access of the coupled BMP2 protein to cell receptors appeared limited. The generation of the new variants should allow, after introducing Plk as artificial amino acid, a direct comparison of these variants with that described by Tabisz et al. providing essential insights into position dependent effects on protein expression, refolding, purification, coupling efficacies, and residual bioactivities after coupling.

1.1 Cloning of BMP2 E83amber and BMP2 E94amber

As detailed described in the method section, the vector p25N-hmBMP2, which yields the cDNA encoding for human mature BMP2 (hmBMP2), was used to introduce mutations by site-directed mutagenesis. An amber TAG stop codon was introduced to either replace glutamic acid (E) 83 or E 94 of the hmBMP2 peptide sequence. The DNA containing the amber stop codon was amplified in a second PCR to introduce the restriction sites NdeI and BamHI and also to eliminate the TAG stop codon terminating protein expression in the template vector p25N-hmBMP2. To verify correct inserts sizes p25N-hmBMP2 E83amber and p25N-hmBMP2 E94amber were digested with NdeI and BamHI (Figure 15A). The resulting PCR products were first ligated to the backbone of pBluescript II SK (+), a transitory vector (Figure 15 B) and then into the backbone of the destination vector pET11a-pyrtRNA, carrying a sequence encoding for pyrrolysyl-tRNA. Plasmids were transformed in NovaBlue bacteria and analyzed by restriction digestion using BamHI and NdeI (Figure 15 C). The resulting vectors, pET11a-pyrtRNA BMP2 E83amber and pET11a-pyrtRNA BMP2 E94amber were analyzed by DNA sequencing.

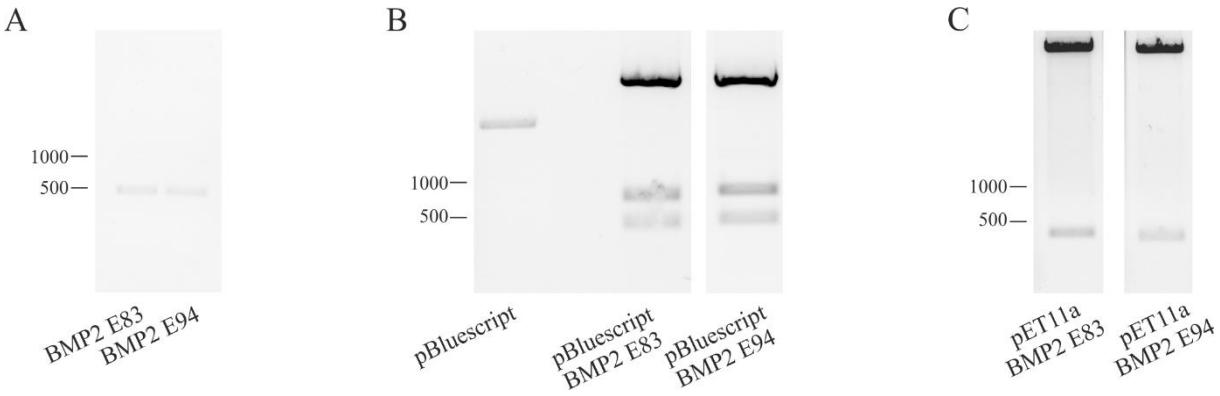

Figure 15: Cloning strategy of BMP2 E83amber and BMP2 E94amber.
(A) Agarose gel electrophoresis of inserts of pN25 BMP2 E83amber and pN25 BMP2 E94amber (BMP2 E83 and BMP2 E94, 400 bp) digested with NdeI and BamHI; (B) Image shows the pBluescript II SK (+) vector (pBluescript, 2962 bp) and restriction digestion of pBluescript vector after ligation with BMP2 E83amber and BMP2 E94amber inserts; (C) restriction digestion of pET11a BMP2 E83amber and pET11a BMP2 E94amber after ligation of pET11a-pyrtRNA vector with BMP2 E83amber and BMP2 E94amber inserts.

1.2 Evaluation of BMP2 E83Plk and BMP2 E94Plk protein expression

1.2.1 Validation of small scale protein expression using different concentration of N-Propargyl-lysine

The vectors, pET11a-pyrtRNA BMP2 E83amber and pET11a-pyrtRNA BMP2 E94amber, were used for protein expression in the *E. coli* strain BL21(DE3). Each construct was co-transformed with pRSFduet-pyrtRNAsynth containing the gene encoding the enzyme pyrrolysyl tRNA synthetase. The addition of tRNA/aminoacyl-tRNA synthetase (aaRS) pairs allows the site-specifically incorporation of artificial amino acids such as Plk into the protein at the target site in response to amber codons (TAG). When the amino acid is added to the growth medium, it must be efficiently transported into the cytoplasm, where tRNA/aaRs, the amino acid and the amber codon start the incorporation system.

Protein expression was performed overnight at 37 °C. Two different concentrations of N-Propargyl-lysine (Plk, 10 mM and 20 mM) were tested in order to identify the condition for most efficient protein expression. Both, Coomassie Brilliant Blue staining and Western blots showed successful expression at both Plk concentrations (Figure 16 A, B). No expression was observed in negative control samples which were induced with IPTG but Plk was omitted. For both variants, two distinct bands with an apparent molecular weight of approximately 13 kDa could be identified by Coomassie Brilliant Blue staining as well as by Western blotting (Figure 16 A, B). Both bands therefore represent monomeric forms of the particular BMP variant. The band with higher electrophoretic motility most likely represents a shortened variant resulting from a premature stop upon protein translation, most likely at the position where the amber codon has been introduced into the BMP2's primary protein, while the upper band most likely represents the full length form into which the Plk residue was correctly inserted. The upper band is indeed missing in the control without Plk. Application of 10 mM Plk resulted in higher yields of the short form (60 %) in case of BMP2 E83Plk, while a more equal ratio (50/50; short form/full length form) was observed for the variant BMP2 E94Plk. The increase in Plk concentration to 20 mM did not result in a pronounced increase of full length forms. For this reason 10 mM Plk was chosen for big scale expressions of both BMP2 variants.

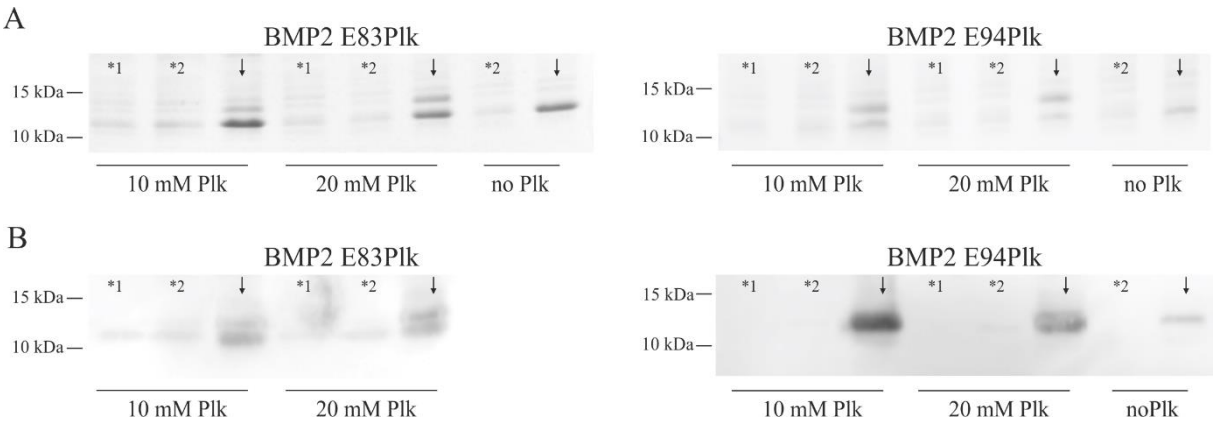

Figure 16: Small scale expression of BMP2 E83Plk and BMP2 E94Plk reveals the formation of two monomeric forms.
(A) Coomassie Brilliant Blue staining of the monomeric BMP2 variants (reducing conditions) using two different Plk concentrations (10 mM and 20 mM Plk) and negative control (no Plk). The double bands at ~13 kDa indicate the expression of two distinct BMP2 monomeric forms, one full length correct form including the Plk residue, and a short form most likely lacking the Plk. In the negative control (no Plk) only the band corresponding to lower molecular weight is visible. (B) Western blot of the BMP2 monomeric variants using an anti-BMP2 antibody. $*^1$ indicates samples before adding Plk at OD_{600} ~ 0.5 and $*^2$ indicates samples before IPTG induction at OD_{600} ~ 0.8. Arrows indicate samples after IPTG induction.

1.2.2 Large scale expression of BMP2 variants

The first results obtained from small scale expression approaches identified the essential parameters to allow expression of the two new variants in *E.coli*. Thus, the large scale expression was performed using the same conditions as for small scale expression (10 mM Plk, 37 °C overnight, 1 mM final concentration IPTG).

Coomassie Brilliant Blue staining and Western blotting were used to detect the expressed proteins (Figure 17 A, B). Samples after IPTG induction showed a strong expression compared to the samples without Plk.

Coomassie Brilliant Blue staining of BMP2 E83Plk, showed the presence of two bands at ~ 13 kDa as in the small scale, but here the yield of full length monomer was much higher than that of the shorter form, which is in line with the missing full length form in the negative control (without Plk addition) (Figure 17 A). In the Western blot the two bands were not electrophoretically separated for BMP2 E83Plk, while they were separated for BMP2 E94Plk (Figure 17 B). The BMP2 E94Plk showed a strong band correlated to the full length monomers (Figure 17 B). This might indicate a much higher yield of the full length variant. But when visualized by Coomassie Brilliant Blue staining no difference in signal intensity between the two bands could be observed. This discrepancy might rely on the used antibody

which despite of its polyclonal character might preferentially bind to the C-terminus of the BMP2 variants which is missing in the shorter forms of either variant.

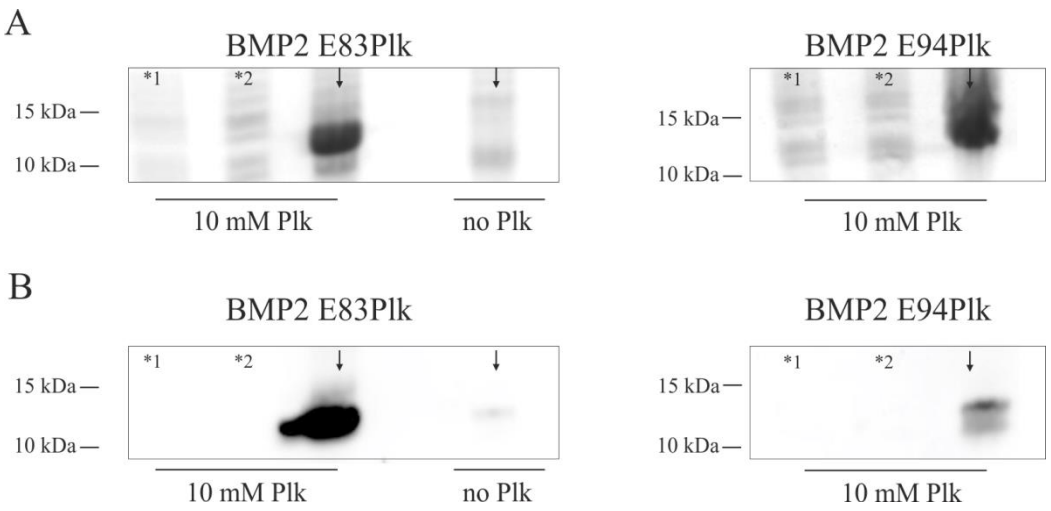

Figure 17: Large scale expression using 10 mM Plk leads to the production of higher amounts of full length BMP2 and lower amounts of the short form.
(A) Coomassie Brilliant Blue staining of monomeric BMP2 variants. The strong band correlated with the full length monomer (after IPTG induction, indicated by arrows) for the BMP2 E83Plk. In case of BMP2 E94Plk variant both bands appear not fully separated. (B) Western blotting of the monomeric BMP2 variants using an anti-BMP2 antibody. For BMP2 E94Plk a double band is visible, with a stronger signal for the full length monomer form. Arrows indicate samples after IPTG induction. $*^1$ indicate samples before adding the substrate (Plk) at OD_{600} ~ 0.5 and $*^2$ indicates samples before IPTG induction at OD_{600} ~ 0.8.

1.3 Purifications steps of BMP2 E83Plk and BMP2 E94Plk

Bacteria expressing BMP2 E83Plk or BMP2 E94Plk were centrifuged, the bacterial pellets weighted and inclusion bodies (IB) extracted (as described in Material and Methods 2.2.1). The intermediated products of the IB purification process (waste supernatants), the pellet of the last step and the purified product of the inclusion body, were analyzed by Coomassie Brilliant Blue staining (Figure 18). After the last centrifugation step, the unfolded monomeric BMP2 protein is contained in the supernatant and not in the pellet as in the previous steps. Strong bands were detected for the purified products, both BMP2 E83Plk and E94Plk, but traces of protein with an apparent molecular weight of approximately 13 kDa (monomeric weight of BMP2) were observed only for the BMP2 E94Plk discarded products (waste supernatant and pellet IB) but not for the BMP2 E83Plk variant.

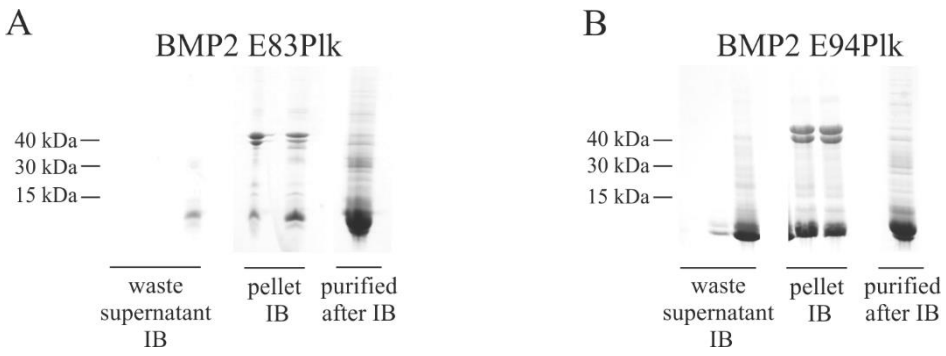

Figure 18: **Inclusion body purification of BMP2 E83Plk and BMP2 E94Plk indicates impurities in pellets and supernatants.**
Coomassie Brilliant Blue staining of BMP2 inclusion body purified products and discarded products (waste supernatant and pellet).

The monomeric BMP proteins obtained by inclusion body extraction were solubilized and further purified by size exclusion chromatography (SEC) (Figure 19). This step allows the separation of the BMP proteins from further impurities such as remaining nucleic acids. Each fraction obtained by SEC was analyzed by UV spectrophotometry. The fractions corresponding to the first peak (1A1 – 1B1) showed a nucleic acid like UV spectrum (spectrum peak ~ 260 nm), while all fractions of the second peak (1B4 – 2B4) showed a spectrum with a peak maximum at approximately ~ 280 nm, being characteristic for proteins. Only the fractions showing a peak at 280 nm were pooled, concentrated and used from renaturation.

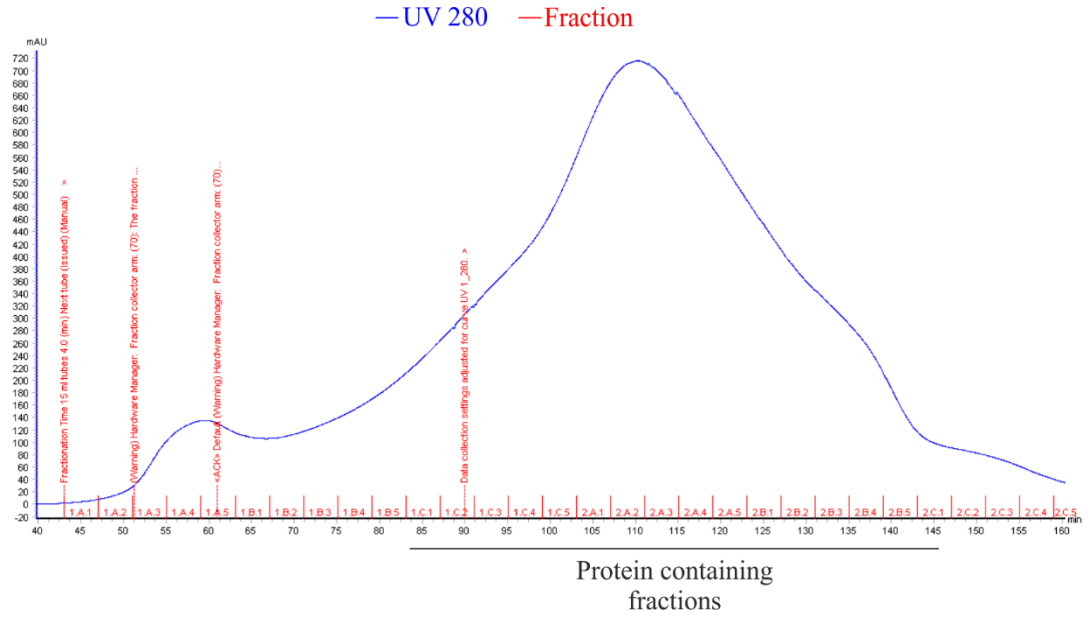

Figure 19: Size Exclusion Chromatography allows the separation of BMP2 variant from impurities.
Chromatogram of SEC of BMP2 E94Plk. The fractions corresponding to the first peak (1A1 – 1B1) showed a nucleic acid like UV spectrum (spectrum peak ~ 260 nm), while all fractions of the second peak (1B4 – 2B4)

showed a spectrum with a peak maximum at approximately ~ 280 nm, being characteristic for proteins. This chromatogram of BMP2 E94Plk represents an example of chromatogram for SEC. Also BMP2 E83Plk fractions were analyzed and only fractions with a peak ~ 280 nm were pooled, concentrated and renatured.

The refolding efficacy was evaluated by Coomassie Brilliant Blue staining analyzing samples under reducing and non-reducing conditions (Figure 20). Both BMP2 variants showed a high content of monomeric products (almost 50 %) (Figure 20). The multiple bands in the monomeric range (~13 kDa) or in the dimeric range (~25 kDa) might indicate again the presence of monomers of different lengths, suggesting also a possible formation of heterodimers (full length monomer plus short length monomer) or two different homodimers (two short length monomers or two full length monomers, respectively) during the refolding process.

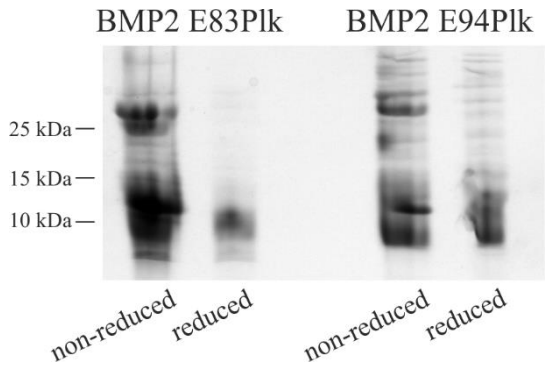

Figure 20: Refolding of BMP2 E83Plk and BMP2 E94Plk causes the formation of heterodimers as bi-product.
Coomassie Brilliant Blue staining of BMP2 variants after the refolding process. Both proteins were analyzed under reducing and non-reducing conditions. Both refolded products still show, under non-reducing conditions, the presence of monomers that can be removed by further purification processes.

1.4 Ion Exchange Chromatography of BMP2 E83Plk and BMP2 E94Plk

The refolded, dimeric proteins were separated from unfolded or incorrectly folded protein species by ion exchange chromatography.
Each fraction was analyzed by SDS Gel Electrophoresis and Coomassie Brilliant Blue staining. The BMP2 E83Plk dimer containing fractions, from D2 to D6, were pooled, dialyzed and concentrated (Figure 21 B). For BMP2 E94Plk, the two peaks containing monomers or dimers were not separated (Figure 22 A). As shown in the Coomassie Brilliant Blue, all

fractions mainly contain monomeric products ~13 kDa, while only fractions from D4 to D9 contained dimeric products at low yield staining (Figure 22 B). The fractions from D4 to D9 were pooled, dialyzed and concentrated.

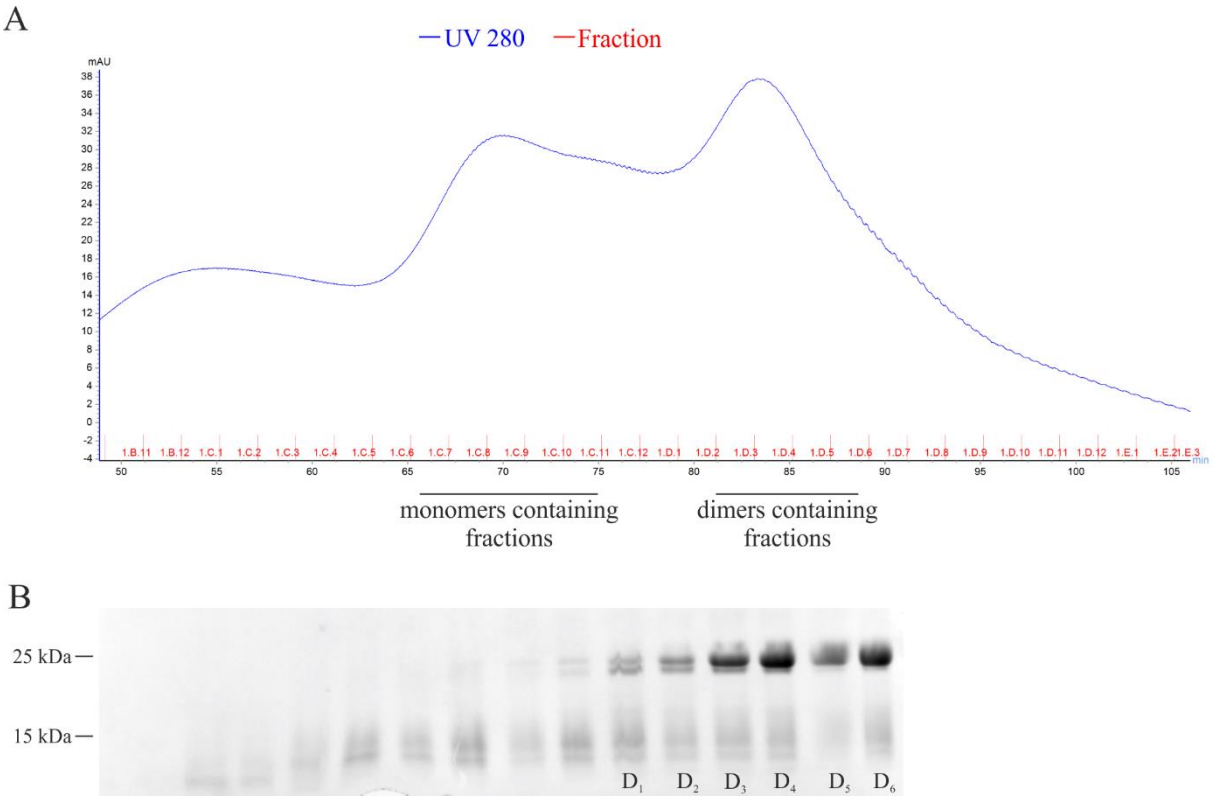

Figure 21: Ion Exchange Chromatography allows a clear separation of BMP2 E83Plk dimers from the monomeric forms.
(A) Chromatogram of BMP2 E83Plk showing two main peaks from C6 to C11 and from D2 to D6. Ion Exchange Chromatography performed by COO- cation exchange chromatography. Proteins were eluted in 2 ml fraction using a linear gradient of buffer IEX B_1 (see Table 4: List of buffers and solution – Protein production). Fractions were analyzed by Coomassie Brilliant Blue staining (B). The first peak showed the presence of monomers (C6 to C11) while the second peak showed the presence of dimers (D2 to D6). The fractions from D2 to D6 were pooled, dialyzed and concentrated.

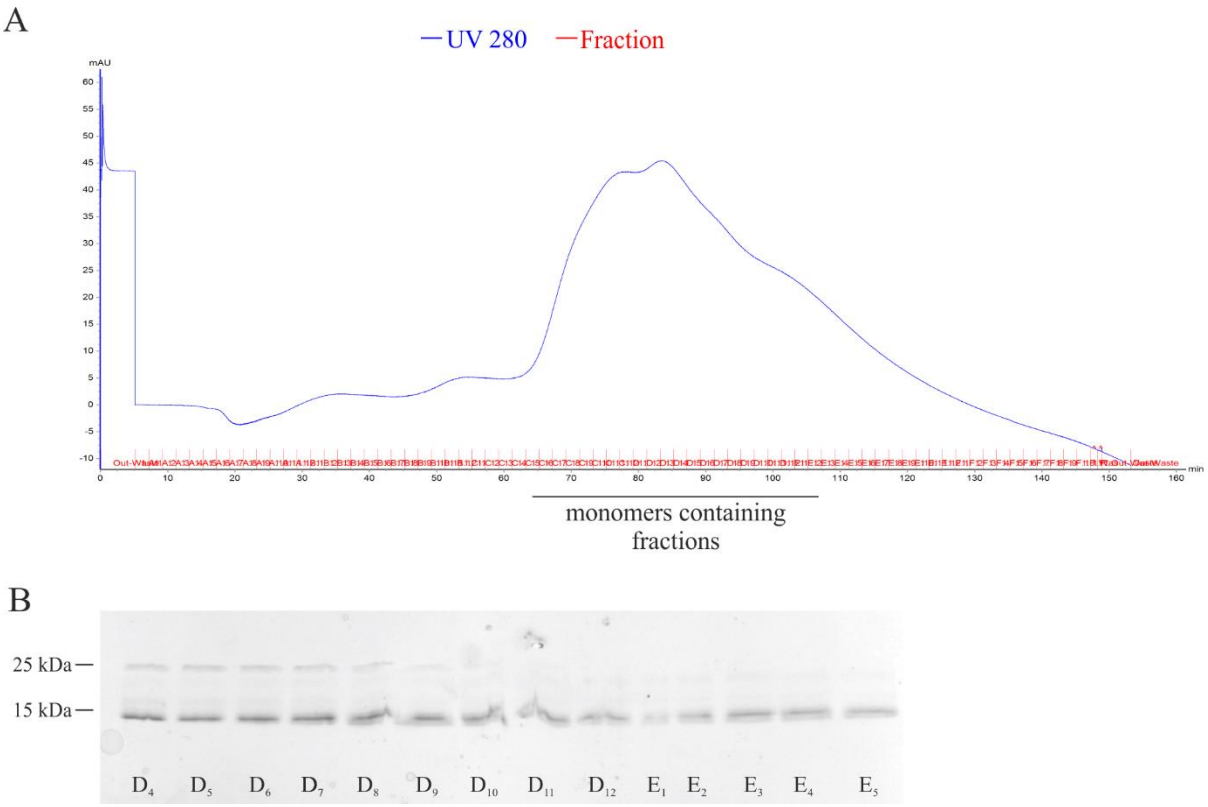

Figure 22: Ion Exchange Chromatography of BMP2 E94Plk reveals presence of dimeric products at low yield.
(A) Chromatogram of BMP2 E94Plk showing one main peak. Ion Exchange Chromatography performed by COO- cation exchange chromatography. Proteins were eluted in 2 ml fraction using a linear gradient of buffer IEX B_1 (see List of buffers – Protein production). Fractions were analyzed by Coomassie Brilliant Blue staining (B). Monomeric and dimeric protein variants could not be separated and were eluted together in one single peak. The fractions from D4 to D9 were pooled, dialyzed and concentrated.

1.5 Analyses of refolded BMP2 E83Plk and BMP2 E94Plk

1.5.1 SDS-PAGE and Western Blot

After pooling and concentrating the dimer containing fractions of each variant, concentrated protein pools were separated by SDS-PAGE and analyzed by Coomassie Brilliant Blue staining and by Western blotting under both, reducing and non-reducing conditions (Figure 23). Protein analysis by Coomassie Brilliant Blue staining showed a strong single band at ~13 kDa for BMP2 E83Plk variant, under reducing condition, indicating the presence of only one, most likely the full length form (Figure 23 A). In case of BMP2 E94Plk two bands were detected under these conditions, indicating that both, the full length and short length monomers are still present in the final refolded product (Figure 23 A). However, the signal

intensity of the two bands observed by Coomassie Brilliant Blue staining could not be detected at the same level by Western blotting (Figure 23 B). This discrepancy might rely on the used antibody which despite of its polyclonal character might preferentially bind to the C-terminus of the BMP2 variants which is missing in the shorter forms of either variant.
Under the non-reducing condition, BMP2 E83Plk showed only a dimeric product, while the BMP2 E94Plk still contained monomeric product (Figure 23A). By Western blotting multiple bands were also shown for BMP2 E83Plk, under both reducing and non-reducing conditions, indicating that the final protein contains homodimers but to lesser extend also heterodimers (Figure 23 B).

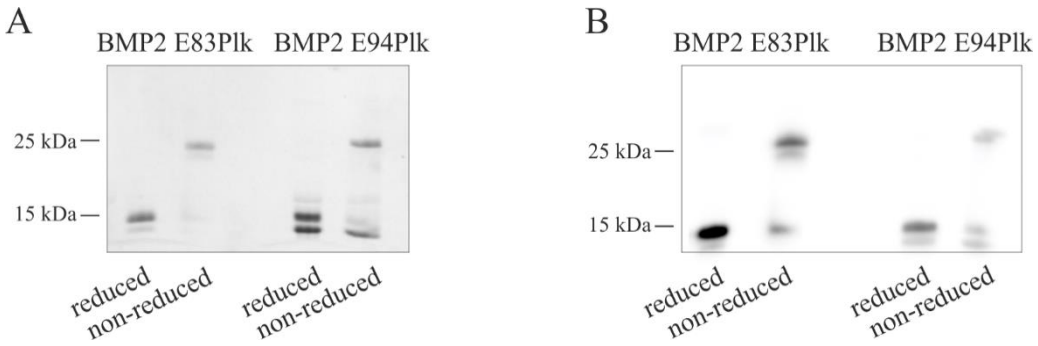

Figure 23: The Purified BMP2 E83Plk and BMP2 E94Plk products contain homo- and heterodimers.
(A) SDS-PAGE and Coomassie Brilliant Blue staining of refolded BMP2 E83Plk and BMP2 E94Plk; (B) Western blot of refolded BMP2 E83Plk and BMP2 E94Plk using an anti-BMP2 antibody. The final BMP2 E83Plk product shows strong band corresponding to the full length monomer (upper band) but also a weak band which corresponds to the short monomeric form (lower band) under reduced conditions. In contrast, under non-reducing conditions a double band at ~ 26 kDa could be identified by Western blotting indicating the presence of homo- and heterodimers. For BMP2 E94Plk the presence of both monomers forms could be visualized under reducing and non-reducing conditions suggesting that also the final product contains homo and heterodimers.

1.5.2 Mass Spectrometry

Mass spectrometry can provide both qualitative and quantitative information of molecules after their conversion to ions. The ESI-FT-ICR MS allows to ionize biological compounds such as peptides and proteins without inducing fragmentation providing high level of mass accuracy and sensitivity. The mass spectrum is a graphical display of the relative abundance of ion signals against the m/z ratio.
Do to the apparent inhomogeneity observed by SDS-GEL and Western blotting, a detailed analysis of the final products was performed by mass spectrometry. Unfortunately, for the BMP2 E94Plk no mass spectrum could be obtained. In case of BMP2 E83Plk the mass

spectrum showed two different peaks corresponding to a mass of 26102.04 Da and 26083.88 Da (Figure 24). The expected mass for the homodimer BMP2 E83Plk (with two full length monomers) is 26100.06 Da (without the first methionins). The calculated mass of Plk is 264.71 Da. The difference in mass of ~ 18 Da between the two peaks is therefore not connected to the Plk. These two peaks indicate only a difference in oxidation, and not the two monomeric forms detected by SDS-PAGE Electrophoresis. If heterodimers (one short form and one full length) were present in the final product a peak at 22396.74 Da would be detected. No monomeric forms were observed from the MS analyses.

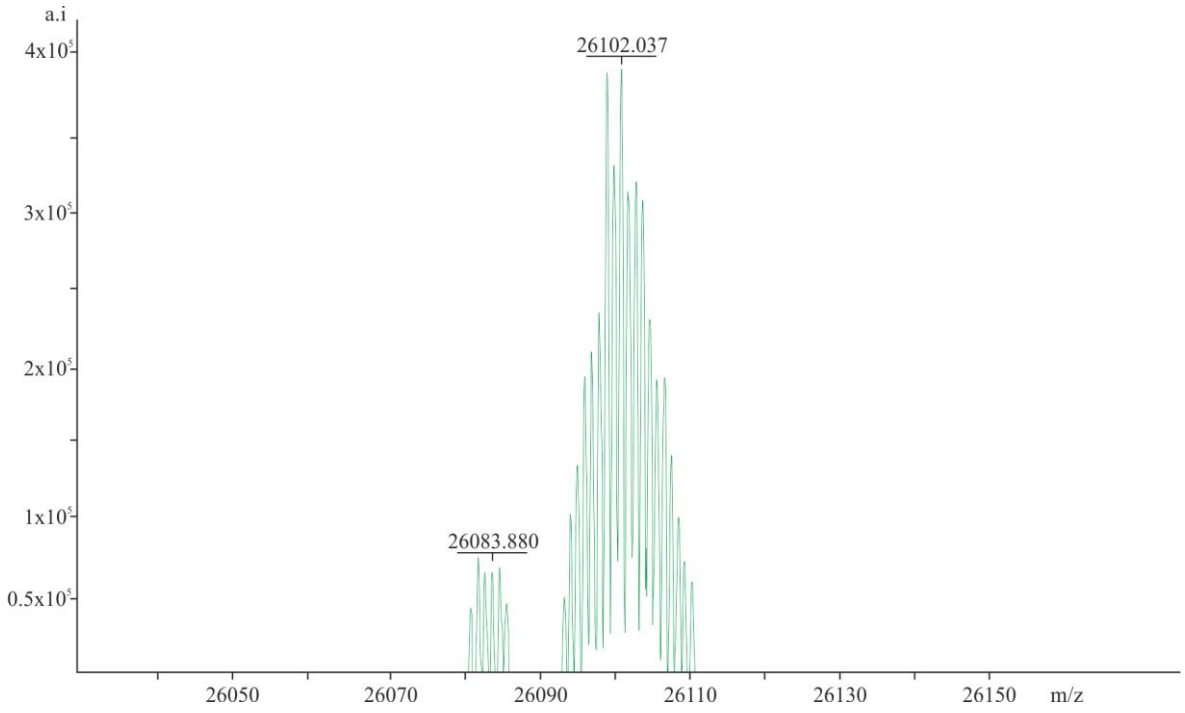

Figure 24: Mass spectrometry analysis of BMP2 E83Plk reveals the presence of homodimers
Refolded BMP2 E83Plk analyzed by mass spectrometry in order to validate the successful incorporation the N-Propargyl-lysine of each BMP2 E83Plk monomer. The peak corresponding to the higher molecular weight corresponds to the expected mass of a homodimer with one introduced Plk residue per monomer.

1.5.3 Alkaline Phosphatase (ALP) Expression

Ideally, the two produced BMP2 variants E83Plk and E94Plk should contain the artificial amino acid in each chain of the final homodimeric protein. The binding capability of the BMP2 variants to the BMP2 receptors at the cells surface might be affected by the presence of heterodimers and also by the presence of such an artificial amino acid. Therefore, the bioactivity of the produced proteins, BMP2 E83Plk and E94Plk, was verified using the well-

established C2C12-based ALP assay (described in Materials and Methods 2.5.3). ALP expression induced by BMP2 E83Plk and E94Plk was compared to that induced by wild type BMP2 as control (Figure 25).

The two BMP2 variants, revealed different biological activities *in vitro* as demonstrated by the calculated EC_{50} values. Data retrieved from fitting the dose-responses to a logistic fit model yielded EC_{50} values of 16.7 nM ± 3.5 nM for BMP2 WT, 43.9 nM ± 5.6 nM for BMP2 E83Plk, 84.1 nM ± 5.7 nM for BMP2 E94Plk. The calculated EC_{50} values indicated an approximately 3-fold lower bioactivity of the BMP2 E83Plk and a 6-fold lower bioactivity of the E94Plk variant if compared to wild type BMP2. In case of BMP2 E94Plk also the values for maximal ALP induction appeared reduced which is not true for the variant E83Plk.

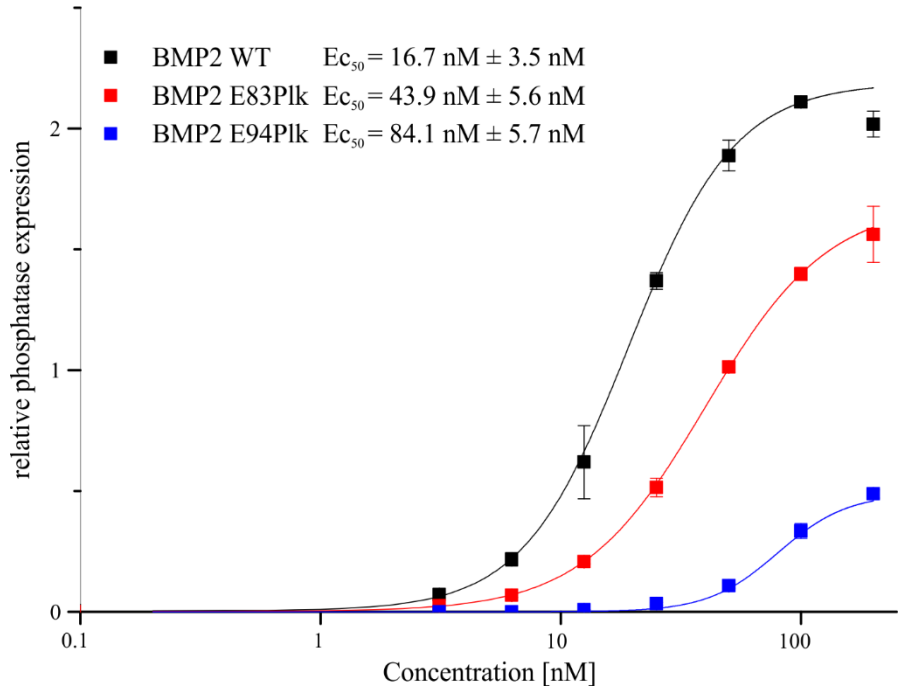

Figure 25: The produced BMP2 E83Plk and BMP2 E94Plk show reduced biological activities *in vitro* compared to wild type BMP2.
Biological activity was tested by ligand induced ALP expression in C2C12 cells, using the indicated ligand concentrations. EC_{50} corresponds to the concentration of ligand that gives half-maximal response.

Due to the intense impurities of the final BMP2 E94Plk product and its significantly reduced biological activity, the variant E83Plk was chosen as the one performing best in terms of renaturation efficacy and maintained bioactivity.

Subsequent productions of the BMP2 E83Plk variant showed a heterogeneous mix of monomers and dimers when analyzed by mass spectrometry (Figure 26), Coomassie Brilliant Blue staining (Figure 27) and a different relative alkaline phosphatase expression *in vitro*, with not comparable EC_{50} values (Figure 28) between the different batches.

Mass spectrometry analyses of the different batches showed presence of homodimers (formed by two full length monomers) for the first two baches, BMP2 E83Plk#1 and #2, with a single peak at ~ 26100 Da (Figure 26 A, B). The other two batches (BMP2 E83Plk Ches and E83Plk #3) showed presence of monomers at ~ 13000 Da (Figure 26 C, D). The detected monomeric forms correspond to the full length monomer (~ 13050 Da). The short length monomer would have a mass of 9343.71 Da, since the protein translation would stop at E83. These two batches showed also a peak corresponding to the homodimer mass of ~ 26100 Da. The heterodimer (one full length monomer and one short form monomer) would have a mass of 22396.74 Da.

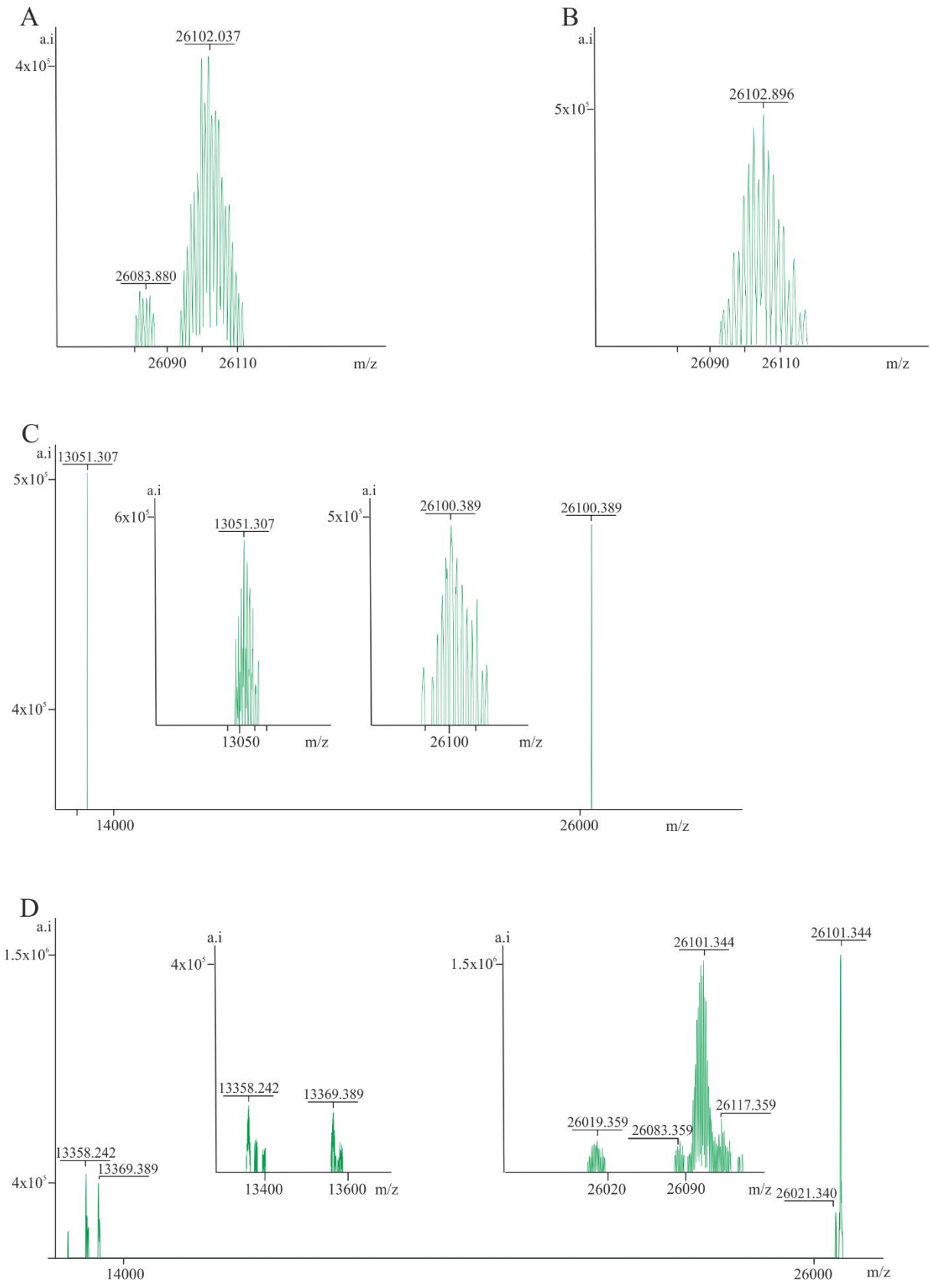

Figure 26: Mass spectrometrical analyses of all batches of BMP2 E83Plk shows differences in mass and highlight the presence of monomers in some of the batches.

Different production of BMP2 E83Plk analyzed by mass spectrometry. (A) BMP2 E83Plk #1, (B) BMP2 E83Plk #2, (C) BMP2 E83Plk Ches (the refolding procedure has been performed with Ches and not with Chaps), (D) BMP2 E83Plk #3.

Beside the mass spectrometry, Coomassie Brilliant Blue revealed the presence of heterogenic products containing multiple homo/hetero dimeric products (BMP2 E83Plk #1 and #2) and also monomers (BMP2 E83Plk Ches and #3) (Figure 27 A, B). The several batches were pooled and additionally purified again using Ion Exchange Chromatography by $SO3^-$ cation exchange chromatography. The final product (BMP2 E83Plk final) shows no presence of monomers under non-reducing conditions.

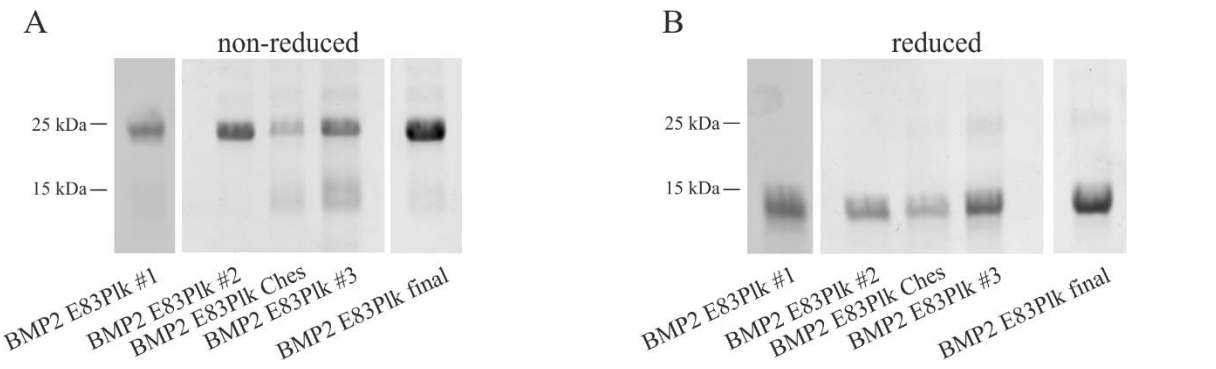

Figure 27: Coomassie Brilliant Blue staining of all the batches of BMP2 E83Plk shows the presence of monomers.
Different productions of BMP2 E83Plk were separated by SDS-PAGE under non-reducing (A) and reducing (B) conditions. Four batches of BMP2 E83Plk were produced: BMP2 E83Plk #1, BMP2 E83Plk #2, BMP2 E83Plk Ches (the refolding procedure has been performed with Ches and not with Chaps), and BMP2 E83Plk #3. These different batches were pooled and purified by IEX Chromatography. BMP2 E83Plk final indicates the purified batch.

The different batches produced and the final pooled product was analyzed using the well-established alkaline phosphatase assay (Figure 28). The calculated EC_{50} values of the different bathes show comparable EC_{50} values of the wild type protein for BMP2 E83Plk #1 or #3. The other bathes showed instead much higher EC_{50} values. The final BMP2 E83Plk indicated 2-fold lower bioactivity compared to the wild type BMP2. This BMP2 E83Plk final product was used for the animal experiment.

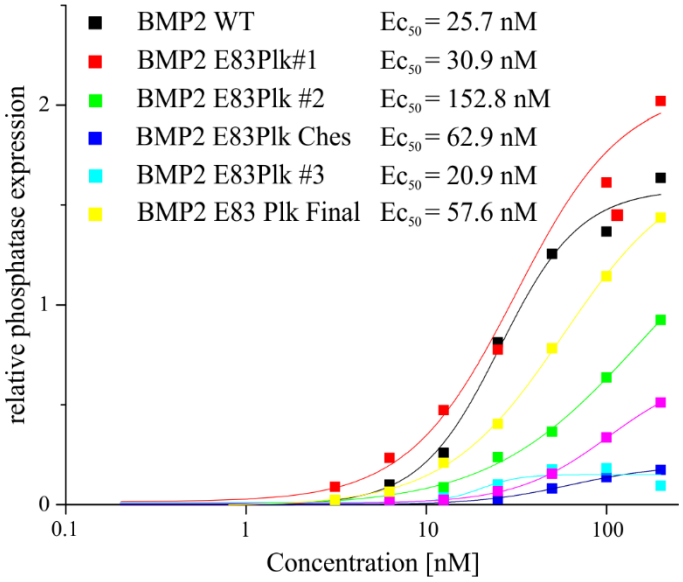

Figure 28: The biological activity of the different batches of BMP2 E83Plk is compromised by the purity of the protein.

BMP2 E83Plk batches were analyzed *in vitro* by alkaline phosphatase expression. Compared to the BMP2 WT all the batches and the final purified product show higher EC_{50} values. The calculated EC_{50} values indicated an approximately 2-fold lower bioactivity of the BMP2 E83Plk final product compared to the wild type BMP2.

2. Production of BMP2 E83Azide

A different BMP2 variant, harboring another artificial amino acid (H-L-Lys(EO-N3)-OH), was generated in order to perform different site directed immobilization techniques. The new variant was expressed using the pET11a-pyrtRNA BMP2 E83amber vector since previous observations revealed that the E83 mutation for the BMP2 E83Plk was the best performing variant in term of protein expression, refolding and purification.

2.1 Evaluation of BMP2 E83Azide protein expression

2.1.1 Validation of BMP2 E83Azide small scale expression using different concentrations of H-L-Lys(EO-N3)-OH.

The BMP2 Azide83 harboring H-L-Lys(EO-N3)-OH, at position E83 of the hmBMP2, was produced by co-transforming the pET11a-pyrtRNA BMP2 E83amber vector with pRSFduet-pyrtRNAsynth. Expression was performed using the same conditions as for BMP2 E83Plk in the E.coli strain BL21(DE3). Different concentrations of the substrate (H-L-Lys(EO-N3)-OH) were tested for the most efficient expression. Coomassie Brilliant Blue staining showed expression in presence of 10 mM, 15 mM, and 20 mM Azide (Figure 29). Different SDS-PAGE electrophoresis gels were performed in order to achieve a clear band separation in the 13 kDa range, which was not possible. A substrate concentration higher or equal to 15 mM revealed an increase in band intensity compared to lower concentration and the negative control. Based on these data, the 15 mM Azide concentration showed a better expression compared to the 10 mM concentration that was previously used for the BMP2 E83Plk expression. Therefore, for the consecutive large scale expression, 15 mM substrate concentration was used.

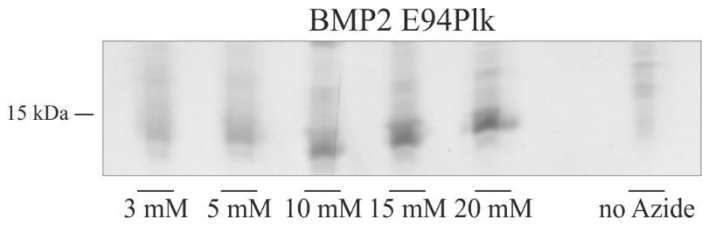

Figure 29: Coomassie Brilliant Blue staining of BMP2 Azide83 small scale expression confirms the possibility to express the BMP2 azide variant.
Coomassie Brilliant Blue staining of BMP2 monomeric variant using 5 different concentrations of H-L-Lys(EO-N3)-OH substrate. Arrows indicate samples after IPTG induction.

2.1.2 Expression of BMP2 E83Azide variant using 15 mM substrate.

The small scale expression of the BMP2 E83Azide identified the parameters to express this BMP2 variant. The large scale expression was performed under the same conditions of the small scale expression (37 °C overnight, 15 mM substrate, 1 mM final concentration IPTG). Coomassie Brilliant Blue staining and Western blot confirmed protein expression using 15 mM substrate (Figure 30). BMP2 E83Azide induced samples show the presence of two bands around 13 kDa indicating the presence of the full and short length monomers, as observed for the BMP2 E83Plk or E94Plk variants (Figure 30 A), while in the Western blot only a strong single band is visible (Figure 27 B). The "smeary" might be connected to the antibody used, indicating products of undefined molecular weights. Negative controls without substrate did not express any protein.

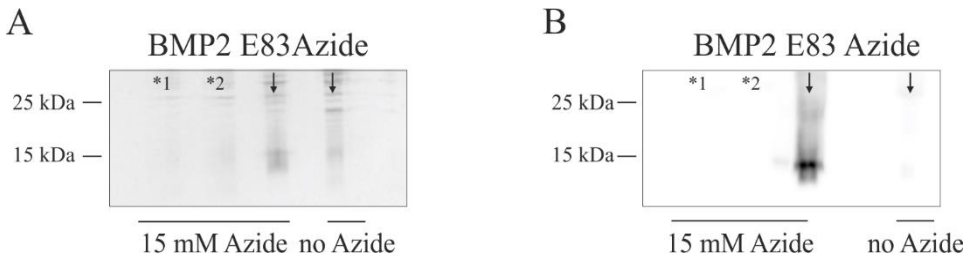

Figure 30: BMP2 E83Azide large scale expression is confirmed by Coomassie Brilliant Blue staining and Western blot.
(A) Coomassie Brilliant Blue staining of BMP2 monomeric variants; (B) Western blot of BMP2 monomeric variants using BMP2 antibody. Arrows indicate samples after IPTG induction. $*^1$ indicate samples before adding the substrate (H-L-Lys(EO-N3)-OH) at OD_{600} ~ 0.5 and $*^2$ indicate samples before IPTG induction at OD_{600} ~ 0.8. Arrows indicate samples after IPTG induction.

2.2 Purification steps of BMP2 E83Azide

Bacteria expressing BMP2 E83Azide were centrifuged, the bacterial pellets weighted and inclusion bodies (IB) extracted. The monomeric BMP proteins obtained by inclusion body extraction were solubilized and further purified by SEC (Figure 31). This step allows the separation of the BMP proteins from further impurities such as remaining nucleic acids. Each fraction obtained by SEC was analyzed by UV spectrophotometry. The fractions corresponding to the first part of the main peak (indicated by arrow) showed a nucleic acid like UV spectrum (spectrum peak ~ 260 nm), while all fractions of the peak showed a spectrum with a peak maximum at approximately ~ 280 nm, being characteristic for proteins.

Only the fractions showing a peak at 280 nm were pooled, concentrated and used for renaturation. The chromatogram did not show separated peaks, as observed for the BMP2 E83Plk, but the use of UV spectrophotometry allowed the separation of the protein containing fractions from the impurities such as nucleic acid.

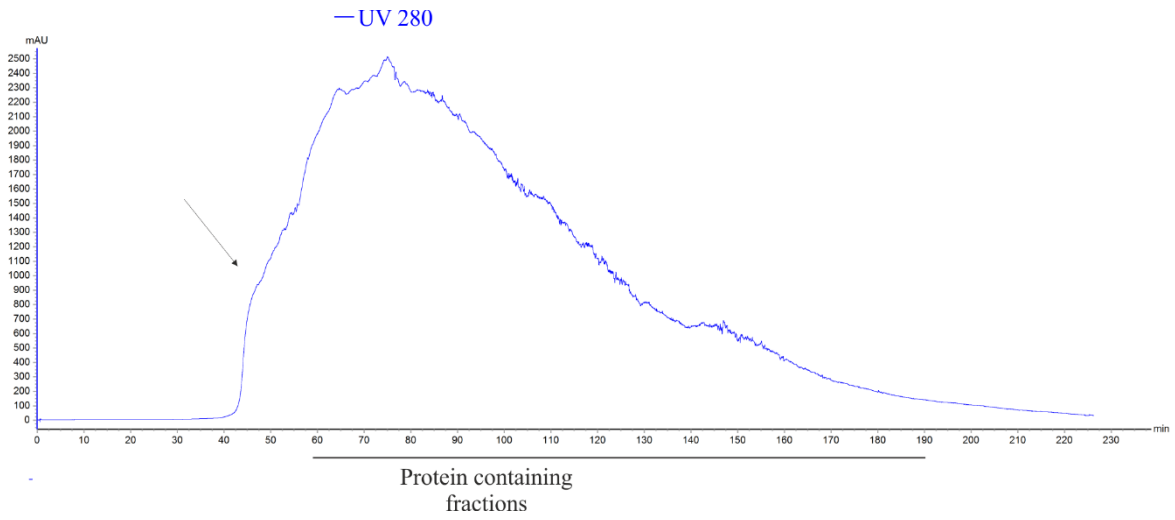

Figure 31: Size Exclusion Chromatography of BMP2 E83Azide shows one single peak consisting of protein containing fractions.
The fractions of the main peak were analyzed by UV spectrophotometry and only a protein spectrum with a peak at 280 nm was observed. These fractions were pooled together for renaturation.

2.3 Analysis of BMP2 E83Azide refolded proteins by SDS Gel Electrophoresis

The refolded BMP2 E83Azide was analyzed by Coomassie Brilliant Blue staining under reducing and non-reducing conditions (Figure 32). Under reducing conditions one strong band and a “smeary” higher band were detected at 13 kDa. Under non-reducing conditions, a band corresponding to the mobility of the dimer could be detected representing approximately 50 % of total protein aside of different monomeric products. The two different bands detected at ~ 13 kDa in the non-reduced samples suggested the presence of the two monomeric forms.

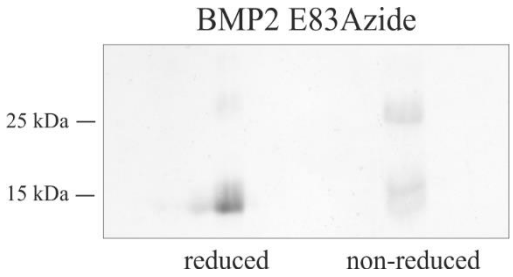

Figure 32: Analysis BMP2 E83Azide revealed monomers presence after refolding process.
Coomassie Brilliant Blue staining of BMP2 E83Azide after renaturation under reducing and non-reducing conditions. The refolded protein contains some monomers after the renaturation process.

2.4 Ion Exchange Chromatography of BMP2 E83Azide

The refolded protein was further purified by IEX using SO_3^- cation exchange chromatography (Figure 33 A) and eluted fractions analyzed by SDS-PAGE and Coomassie Brilliant Blue staining (Figure 33 B).

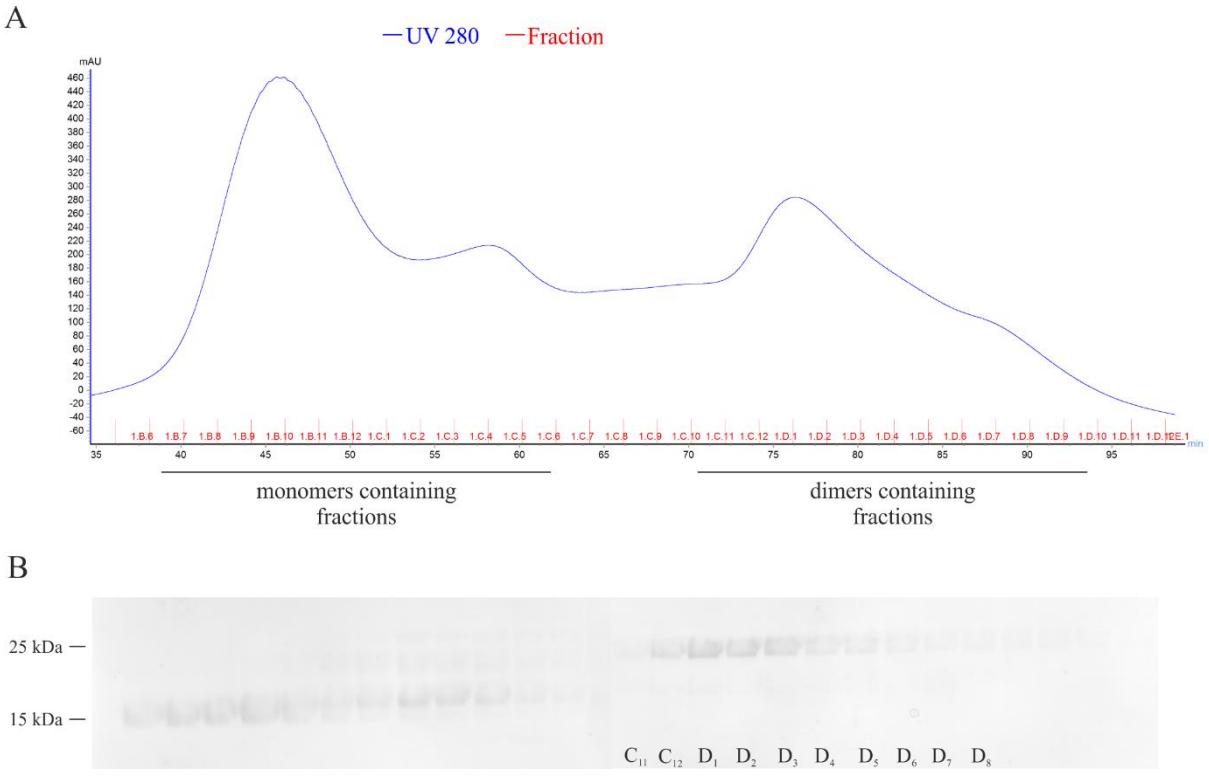

Figure 33: Separation of BMP2 E83Azide dimers from monomers by Ion Exchange Chromatography.
(A) Chromatogram of BMP2 E83Azide. The different peaks represent the monomer and dimers containing fractions that were analyzed by (B) Coomassie Brilliant Blue staining. The separation between monomers and dimers was clear and fractions from C12 to D8, containing only dimers, were pooled.

Dimers were mainly present in the second peak of the chromatogram, even though a low presence was observed also in the first peak together with the monomers containing fractions. Only dimer containing fractions, from C11 to D8 were pooled, dialyzed and concentrated.

2.5 Analyses of the BMP2 E83Azide final product

2.5.1 SDS-PAGE and Western blot

The final product was separated by SDS-PAGE Electrophoresis and stained by Coomassie Brilliant Blue as well as analyzed by Western blot under reducing and non-reducing conditions (Figure 34). Coomassie Brilliant Blue stained SDS gel under non-reducing and reducing conditions showed the presence of two separated bands at around 13 kDa, indicating the presence of short form and long form monomers in the final product (Figure 34 A). Western blotting analysis did not provide evidence of this double band in non-reducing conditions (Figure 34 B). This discrepancy might rely on the used antibody which despite of its polyclonal character might preferentially bind to the C-terminus of the BMP2 variants which is missing in the shorter forms of either variant. On the other side, the absence of both bands might indicate that, the detection of the lower band is connected to a possible missing binding site in the short form. While the higher band, detected by Coomassie Brilliant Blue, might be an incorrectly refolded monomer, and not the full length monomeric protein, that would be otherwise detected by the antibody.

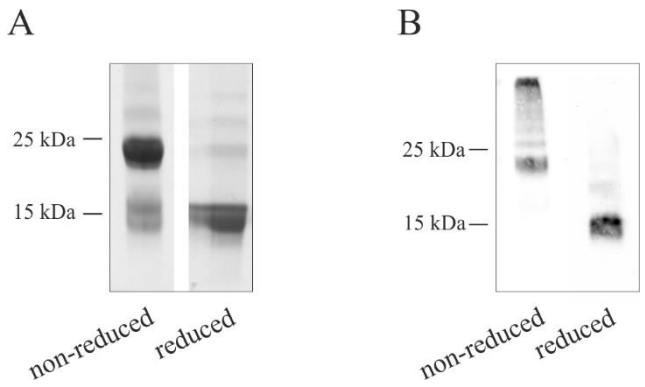

Figure 34: Analysis of BMP2 E83Azide revealed presence of monomers in the final product by Coomassie Brilliant Blue staining that could not be identified by Western blotting.
(A) SDS-PAGE and Coomassie Brilliant Blue staining and (B) Western blot of the refolded final product BMP2 E83Azide. The reducing and non-reducing conditions showed the presence of a double band at ~ 13 kDa (A) not detected by Western Blot (B).

2.5.2 Mass Spectrometry

The MS analysis of the BMP2 E83Azide showed a homogeneous population with a mass of 26138.602 Da (Figure 35). The calculated mass of BMP2 E83Azide correctly incorporating (H-L-Lys(EO-N3)-OH) at position E83 of each monomeric chain is 26162.08 Da. Therefore the detected protein is a homodimer that correctly incorporates the artificial amino acid. The amount of heterodimeric protein and monomeric forms that were observed by SDS-GEL could not be detected by MS, possibly due to the low amount.

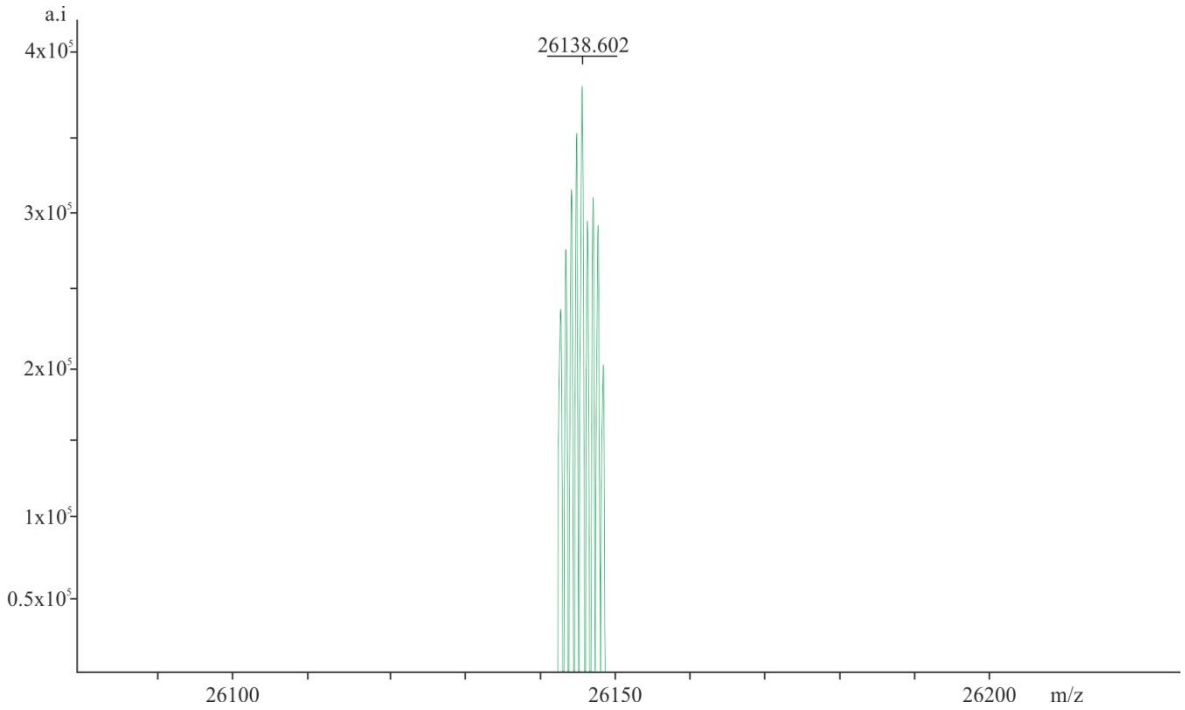

Figure 35: Mass spectrometry validates the correct incorporation of the substrate in BMP2 E83Azide variant.
Refolded BMP2 E83Azide analyzed by mass spectrometry in order to validate the successful incorporation the H-L-Lys(EO-N3)-OH of each BMP2 E83Azide monomer.

2.5.3 Biological activity testing by alkaline phosphatase (ALP) expression *in vitro*

The biological activity of the new BMP2 variant was tested by its ability to induce ALP expression in C2C12 cells and was compared to both BMP2 WT and the first BMP2 E83Plk (Figure 36). The calculated EC_{50} value for BMP2 E83Azide is 2-fold higher compared to those of BMP2 WT or BMP E83Plk.

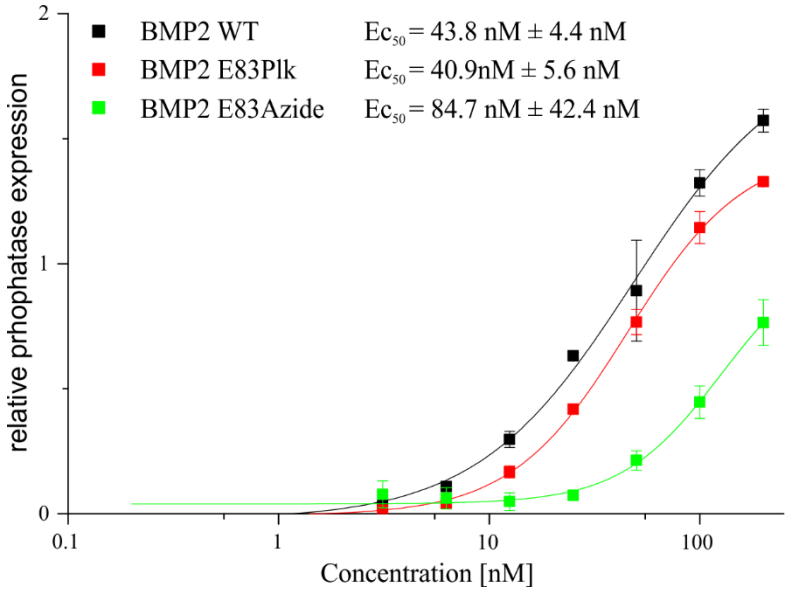

Figure 36: BMP2 E83Azide is less bioactive than BMP2 WT *in vitro*.
Alkaline phosphatase expression was used to evaluate the biological activity of the BMP2 E83Azide compared to that of the wild type protein and BMP2 E83Plk. The new BMP2 E83Azide shows a 2-fold lower bioactivity compared to the BMP2 WT.

In accordance with BMP2 E83Plk, BMP2 E83Azide was produced in different batches and all the final products showed the presence of monomers. For this reason, a further purification step using IEX by SO_3^- cation exchange chromatography was performed. Figure 37 shows the last purified batch of BMP2 E83Plk and E83Azide used for subsequent animal experiment. The removal of the monomeric component from the final product highly increased the biological activity as proven by the alkaline phosphatase assay. The BMP2 E83Azide shows the same bioactivity of the wild type protein, while the BMP2 E83Plk is 2-fold less bioactive compared to the wild type (Figure 37 A). The Coomassie Brilliant Blue staining of the final protein reveals the absence of monomers for the BMP2 E83Plk, while the BMP2 E83Azide contains some monomers that had no impact on the biological activity (Figure 37 B).

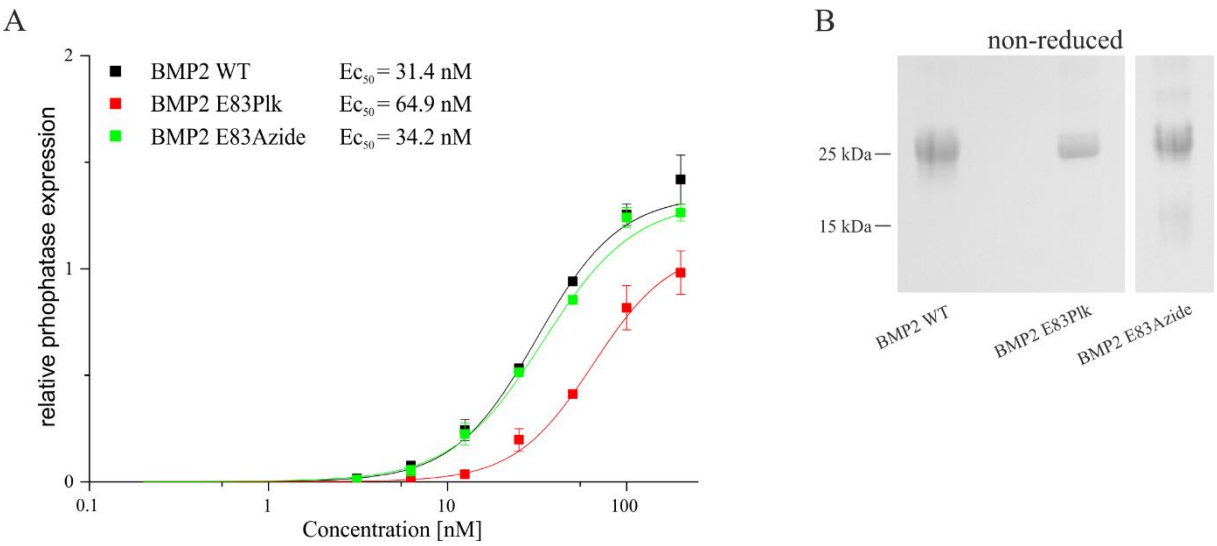

Figure 37: BMP2 E83Plk and BMP2 E83Azide, used for the animal experiments, are as bioactive as the wild type protein *in vitro* after an extra purification step.
The final purified batches of BMP2 variants produced were tested *in vitro* in the ALP assay (A) prior to the animal experiment. BMP2 WT served as positive control. (B) Coomassie Brilliant Blue staining of the BMP2 variants and the BMP2 WT.

3. Copper catalyzed azide-alkyne cycloaddition (CuAAC)

Creating new BMP2 variants harboring artificial amino acids, enables the covalent binding of the protein to the scaffold in a site directed manner by click chemistry reaction. The use of this approach was performed with a previously produced BMP2 variant, BMP2 K3Plk, which revealed the same biological activity if compared to wild type BMP2. However, the coupling to the beads affected the protein by limiting the access of the coupled BMP2 protein to cell receptors (Tabisz 2016). The generation of the BMP2 E83Plk variant should allow a direct comparison with BMP2 K3Plk as described by Tabisz et al. to provide insights into position-dependent effects and residual bioactivities after coupling.

The CuAAC reaction is known for its specificity and good reaction efficiency, which benefits from higher reaction temperatures, neutral pH and high concentrations of the reactants (Hong et al. 2009). However, conjugation of biomolecules using the CuAAC reaction is challenging because of the sensitivity of proteins to reducing and oxidizing conditions and limited applicable protein concentrations. CuAAC occurs e.g. between the alkyne group of the BMP2 E83Plk and the azide group of e.g. azide-functionalized microspheres in presence of copper (Cu). Two different catalysts were used in this work: $CuSO_4$ and CuBr. As copper in $CuSO_4$ represents a Cu (II) ion, it requires the use of sodium ascorbate (NaAsc) as a reducing agent to trigger the reduction Cu (II) to Cu (I), which is not necessary for CuBr. Both techniques were used to couple the BMP2 E83Plk to azide-functionalized microspheres. An initial analysis of effects on the protein relying on the used coupling conditions was performed.

3.1 CuAAC – proof of the efficacy of the reaction with $CuSO_4$ and CuBr

In order to prove the individual reaction conditions for the BMP2 E83Plk, the ideal corresponding reaction partners are represented by defined compounds which are not difficult to handle (e.g. in terms of solubility, toxicity, etc.) and additionally would allow to monitor coupling in at least semi-quantitative manner. Thus, fluorophores functionalized with the required reactive groups were chosen. For BMP2 E83Plk, an azide-functionalized fluorophore (Sulfo-Cy5Azide) was used which was coupled to the ligand and different incubation times in presence or absence of Cu ions (either, $Cu(II)SO_4$ or Cu(I)Br) were compared. The optimization of the protocol, regarding buffers and concentrations of catalysts to use, was

partially established by previous experiments (Tabisz 2016). The reaction between BMP2 E83Plk and the azide-functionalized fluorophore in presence of $CuSO_4$ led to the formation of products with higher molecular weight as shown by slower migrating bands (corresponding to the mass of ~ 40 kDa) by SDS-PAGE, which could not be detected if CuBr was used (Figure 38 A). Furthermore, for all conditions a smeary background staining could be detected under non-reducing conditions which extended up to the gel's pockets (not shown) indicating protein assemblies of high, but not defined molecular weight. As control, the same reaction was carried out with BMP2 WT, where no fluorescent signal was detected. As expected, the lack of signal is due to the inability of the wild type protein to couple to azide groups. The presence of structures with higher molecular weights which appear upon reaction with Cu (II) as catalyst, might indicate that the sodium ascorbate is used to reduce Cu (II) to Cu (I) also partially reduces the disulfide bonds within BMP2 E83Plk. This allows the subsequent formation of new cysteine bridges which, if different ligands are interconnected, leads to formation of unidentified structures with higher molecular weights.

THPTA acts as a protectant during the CuAAC reaction by intercepting the radicals resulting from the $CuSO_4$/NaAsc redox reaction. Upon reaction with $CuSO_4$ and NaAsc, BMP2 E83Plk appeared indeed more "smeary" if THPTA was omitted from the reaction. In contrast, the CuAAC reaction performed in presence of CuBr and without NaAsc produced a single band with a molecular weight of ~ 25 kDa. No multimers at higher molecular weights could be detected (Figure 38 B).

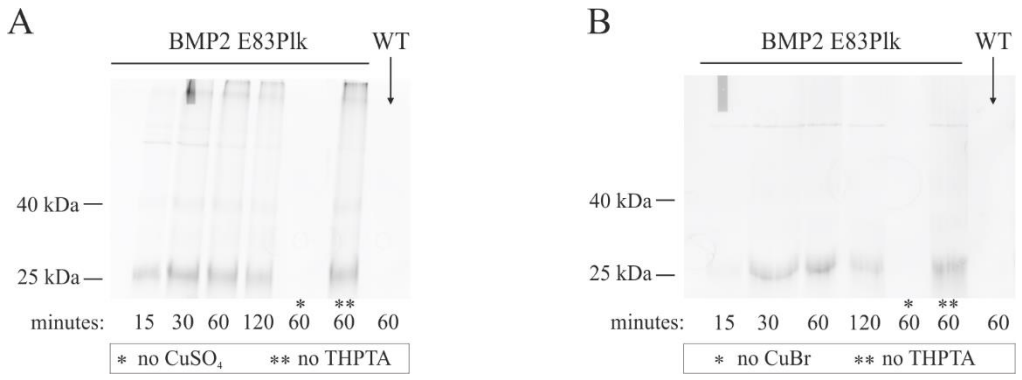

Figure 38: The CuAAC catalysts, $CuSO_4$ or CuBr, affect the BMP2 E83Plk in a different manner.
20 µM BMP2 E83Plk and BMP2 WT were coupled to 100 µM Cy5-azide and reactions were performed for 15, 30, 60 and 120 minutes. Control reactions without $CuSO_4$ (A *) or CuBr (B *) or without THPTA (A **, B **) were included. Samples were separated by SDS-PAGE and analyzed under Cy5 detection channel.

In order to compare the effect of the two catalysts for the CuAAC reaction employing BMP2 proteins, a previous produced BMP2 variant was also used. BMP2 K3Plk contains the Plk group at the N-terminus of the BMP2 sequence. For a basic analysis on structural changes comparing BMP2 E83Plk, BMP2 K3Plk and BMP2 WT, CuAAC reactions catalyzed by either $CuSO_4$/NaAsc or CuBr were performed. For these experiments, another fluorophore was used: 5/6-Texas Red-PEG_3-Azide. This fluorophore with the PEG_3 spacer might avoid problems related to steric hindrance.

As previously observed, proteins coupled to azide-functionalized fluorophore showed a fluorescent signal under Cy3 detection channel (Figure 39). The $CuSO_4$/NaAsc redox reaction caused the formation of multimers at ~ 40 kDa and the smear at higher molecular weights in case of both BMP2 variants (BMP2 E83Plk and BMP2 K3Plk), while the CuBr catalyzed reaction produced only one single band with a molecular weight reflecting the protein dimer (Figure 39 A). The use of an anti-BMP2 antibody allowed a more precise visualization of proteins since the BMP2 WT does not react with the azide-functionalized fluorophore, but might also be affected by the reaction conditions (Figure 39 B). Both BMP2 variants and the wild type protein showed formation of multimers at ~ 40 kDa upon $CuSO_4$ or CuBr treatment, but only with $CuSO_4$, a distinctive and strong protein aggregation was observed.

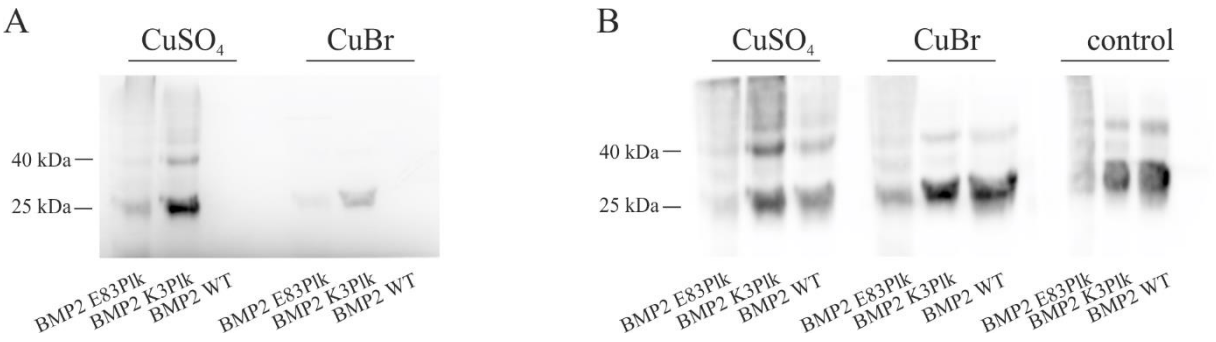

Figure 39: The catalysts $CuSO_4$ or CuBr individually affect the CuAAC reaction efficacy.
20 µM BMP2 E83Plk, BMP2 K3Plk and BMP2 WT were coupled to 100 µM 5/6-Texas Red-PEG_3-Azide and reactions were performed for 60 minutes. Coupled proteins were separated by SDS-PAGE and the gel analyzed under Cy3 detection channel (A). Proteins were transferred onto a nitrocellulose membrane and visualized using anti BMP2 antibody (B).

The two different catalysts, $CuSO_4$ and CuBr, also caused a noticeable difference in reaction efficacy. Stronger signals were detected when BMP2 E83Plk and BMP2 K3Plk was coupled by using of $CuSO_4$ as catalyst if compared to the signals of CuBr catalyzed reaction. This clearly indicated that the CuAAC reaction catalyzed by $CuSO_4$ has a higher efficacy. As

Western blotting detected both coupled and uncoupled BMP2 variants, it could be used as loading control, showing that the amount of loaded protein was the same, but the amount of fluorescently labelled protein clearly differed between the two methods (Figure 39 B). BMP2 E83Plk showed a distinctive smear also in the control, presumably due to a protein precipitation which occurred before performing the experiment.

After this first analysis potential changes in biological activities which might occur upon reaction were investigated using cell-based assays. 5/6-Texas Red-PEG_3-Azide was used as fluorophores since the insertion of a PEG_3 linker should provide enough flexibility to allow the exposure of the receptor binding sites (wrist and knuckle epitopes) of the BMP2 variant to the receptors on the cell surface. This is especially important for the BMP2 E83Plk variant, since the side chain of Plk 83 is located at close proximity to the type II receptor binding sites. In preliminary experiments using Sulfo-Cy5-Azide, as coupling fluorophore for the BMP2 E83Plk, the resulting protein failed to induce ALP expression. The fluorophore Cy5, being a bulky structure, covers the receptors binding sites, leading to a reduced biological activity and subsequent misinterpretation of the obtained data.

All BMP2 variants showed decreased bioactivity after the CuAAC reactions using either $CuSO_4$ or CuBr when compared to the positive control (uncoupled protein) (Figure 40). After 30 min of reaction both BMP2 E83Plk and BMP2 K3Plk preserved only 20 % of bioactivity when using $CuSO_4$ and 40 % or ~ 60 %, respectively, with CuBr. The results were comparable for both BMP2 variants at both conditions, with ~ 40 % of retained bioactivity after 60 min reaction time. After 120 min of reaction, the bioactivity remained at ~ 40 % for all conditions, apart from BMP2 K3Plk that dropped down to ~ 20 % when treated with $CuSO_4$.

In parallel to the ALP assay, histochemical staining of ALP activity of the treated cells was also performed in order to visualize a qualitative aspect of the effects of the differently treated BMP2 variants on cells. The staining did not allow a precise distinction of the differences between methods and variants (Figure 41). In any case, compared to the controls, both BMP2 variants showed less bioactivity in this qualitative analysis, confirming the quantitative data obtained from ALP assays.

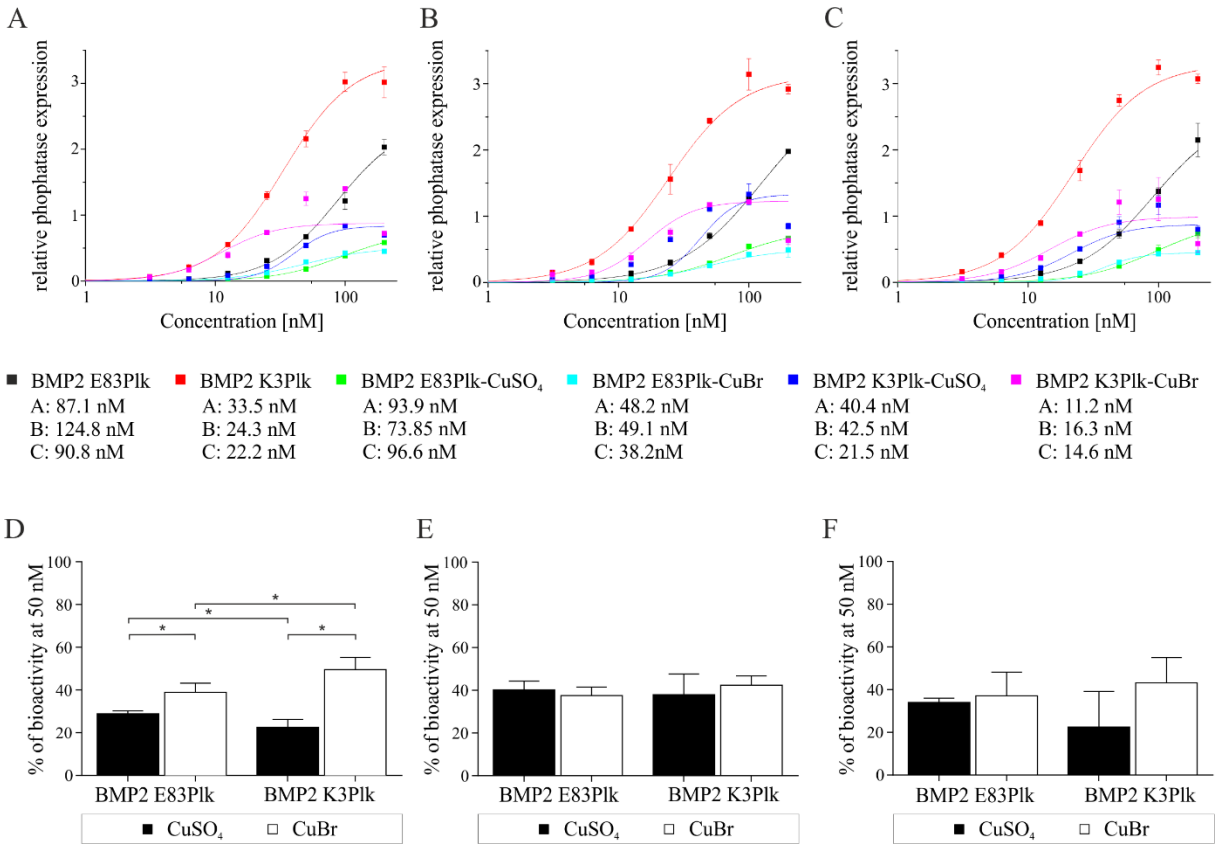

Figure 40: The bioactivity of BMP2 variants upon click reaction depends of the catalysts used.
(A, B and C) Figures show alkaline phosphatase expression with increasing concentration of BMP2 variants coupled to 5/6-Texas Red-PEG$_3$-Azide. (D, E and F) Graphs show bioactivity at 50 nM as percentage relative to native (unreacted) protein. Different reaction times were analyzed: (A, D) 30 min, (B, E) 60 min, (C, F) 120 min. Significances were carried out by a non-parametric Mann-Whitney test. * = $P < 0.05$. n = 4.

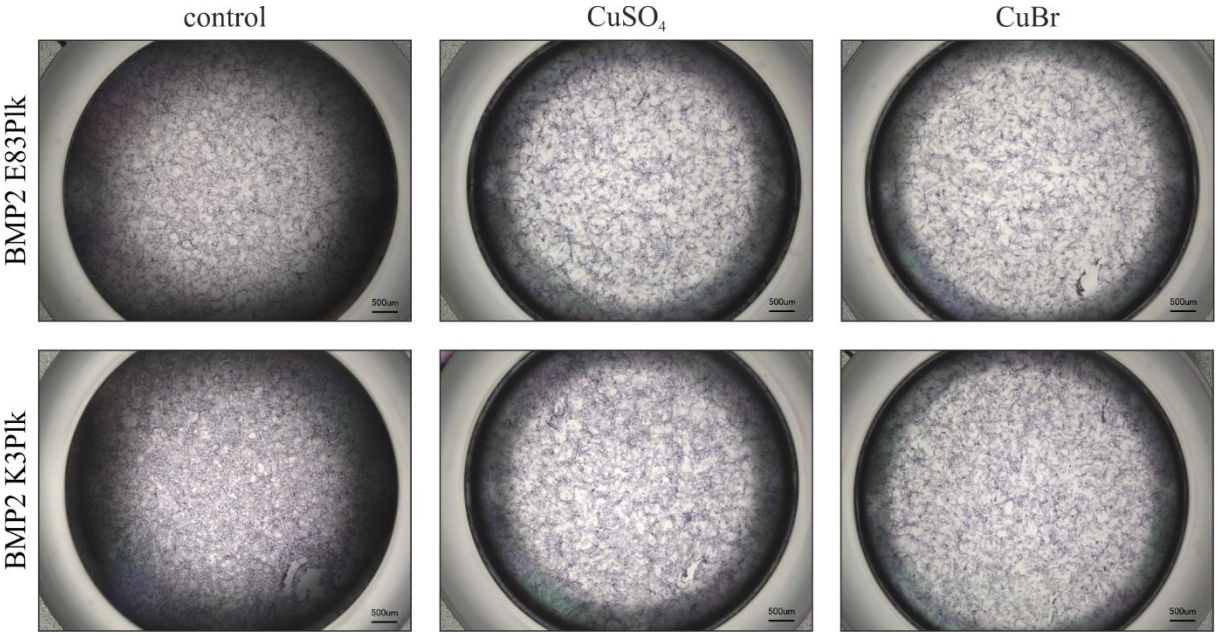

Figure 41: BMP2 variants coupled to 5/6-Texas Red-PEG$_3$-Azide induce Alkaline Phosphatase staining of C2C12.
C2C12 cells were treated with 200 nM of BMP2 (E83Plk or K3Plk) coupled to 5/6-Texas Red-PEG$_3$-Azide. The positive alkaline phosphatase staining indicates that the BMP variants after the reaction are less bioactive

compared to the native proteins (control). However, ALP staining is a qualitative measurement that does not allow a quantification of the protein's bioactivity. Representative images of alkaline phosphatase staining after 60 min of CuAAC reaction.

3.2 Analyses of efficacy of the coupling reaction of BMP2 E83Plk to azide-functionalized microspheres with $CuSO_4$ and CuBr.

In order to test coupling to microscopic structures BMP2 E83Plk was coupled to different microspheres consisting either of a recombinant collagen like peptide (RCP), silica or agarose. RCP and silica microspheres were first functionalized using a bivalent linker providing NHS as well as azide functional groups (NHS-PEG_4-Azide). The linker was coupled to the beads by NHS ester-amino reaction (Figure 11). The commercially available agarose were already azide-functionalized, thus did not require further modification.

50 µg of BMP2 E83Plk or BMP2 WT were coupled to the azide-functionalized microspheres by CuAAC using either $CuSO_4$ or CuBr as catalysts. The supernatants of the individual reactions containing the excess of protein which did not bind to the beads (non-bound protein) as well as supernatants of subsequent wash steps (containing the non-covalently coupled protein) were analyzed by Western blotting (Figure 42).

The amount of protein being not coupled mainly depends on the particular type of microsphere used, but also on the catalyst applied in the CuAAC reaction.

Proteins got coupled or adsorbed almost completely during the time the coupling reaction took place. Adsorbed proteins that could be removed with the urea washes are shown in Figure 42 D, E and F. In all cases, the signal of the BMP2 WT contained in the harsh wash was stronger compared to the BMP2 E83Plk. However, the BMP2 WT used as negative control, was not completely removed from the beads even with the harsh urea wash step, because the detected differences in signal intensity are not so evident between the BMP2 E83Plk and BMP2 WT. BMP2 WT might be strongly adsorbed to the different microspheres meaning that it cannot be removed even by washing with 6 M urea.

By comparing the two catalysts ($CuSO_4$ or CuBr) used for the coupling reaction strong differences in the Western blot signals could be observed (Figure 42). These differences did not depend on the type of the particular microspheres. For both catalysts, the bands corresponding to a molecular weight of ~ 40 kDa and the already described smear could be generally observed. For CuBr both, the band at 40 kDa and the smear were more pronounced indicating higher protein amounts in the individual supernatants. The bands visible at even

higher molecular weight that were not observed in the experiments testing the coupling efficacy with functionalized fluorophores (Figure 38, 39) could be detected (Figure 42). This might be due to the use of higher reaction volumes. Another possibility would be connected to a partial degradation of the microspheres, caused by the harsh washing conditions.

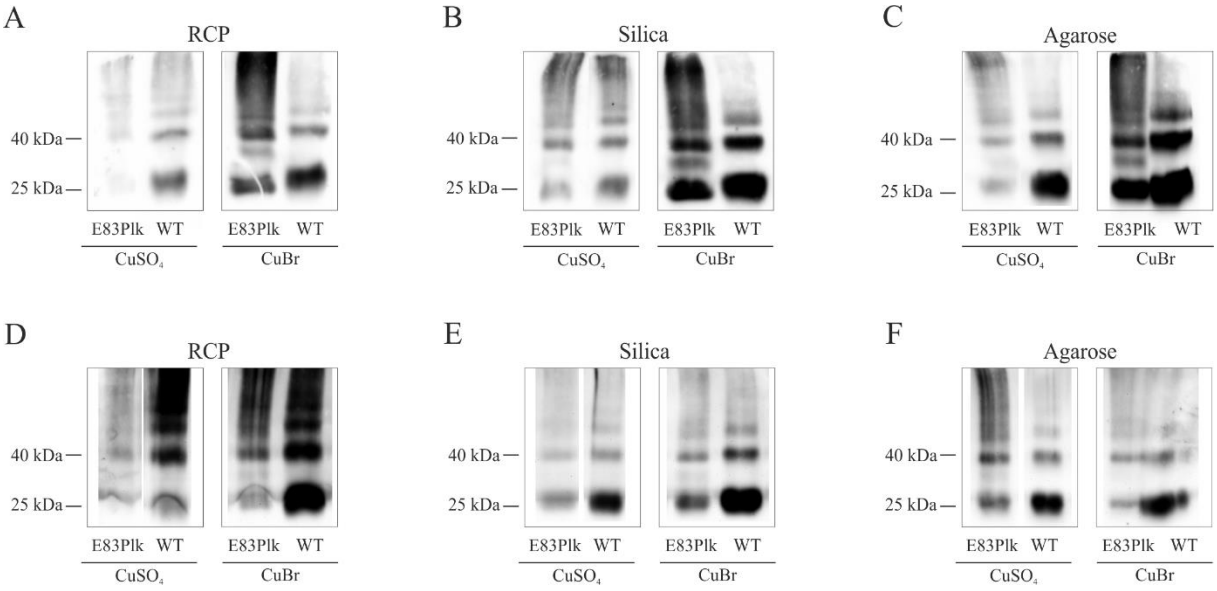

Figure 42: Coupling BMP E83Plk to different microspheres by CuAAC: $CuSO_4$ and CuBr show differences in coupling efficacies and differently affect the protein's structure.
Western blot analyses of supernatants of the reaction (A – C) and wash supernatants (D – F) using an anti-BMP2 antibody. 50 µg of each indicated protein was coupled to RCP, silica or agarose beads, respectively. The pictures used in this figure have a high contrast, both for supernatants and for urea washes. The difference in the obtained signals between the $CuSO_4$ and CuBr catalyzed reactions observed in the supernatants of reactions of all the microspheres is important to note. The supernatants of urea washes show that unspecific coupled or adsorbed protein is removed.

The evaluation of the click chemistry efficacy and a determination of the amount of coupled protein can qualitatively be described by Western blot analysis of the supernatants, or by analyzing resolved proteins e.g. after solubilization of the spheres. Alternatively, a quantification of coupled protein can be performed indirectly by a quantification of the uncoupled protein using ELISA or, if the protein can be radioactively labeled, simply by scintillation counting of the supernatants.

As mentioned, the quantification by ELISA or by the use of radioactively labeled proteins is an indirect measurement, since the values of what is coupled to the beads after the reaction and the washing steps were calculated by the determination of unbound protein in the supernatants.

In detail, in case of radioactively labeled proteins it is essential to know how many counts per minutes (cpm) of ^{3}H labeled protein have been used in the initial coupling reaction. Subsequently, the cpm counted in the supernatants of the reaction and in the supernatants of washes were subtracted. Assuming that ^{3}H labeling of the BMP2 proteins did not affect their ability to be covalently coupled to the microspheres, a proportion of the cpm measured to the µg of protein allows the calculation of the amount of protein being indeed coupled.
The values in Table 15 show that from the initial 50 µg of protein used for the reaction around 82 % - 95 % were found to be bound to the microspheres after the reaction.
Almost the same numbers were measured for the wild type protein. As already claimed before it might be possible that BMP2 wild type is also strongly bound to the microspheres and hardly removed after the harsh washes.

		RCP	Silica	Agarose
BMP2 E83Plk	$CuSO_4$	47.6 µg	41.3 µg	43.7 µg
	CuBr	46.7 µg	35.8 µg	41.5 µg
BMP2 WT	$CuSO_4$	46.3 µg	45.1 µg	39.7 µg
	CuBr	47.5 µg	28.2 µg	43.4 µg

Table 15: Quantification of the amount of BMP2 E83Plk and BMP2 WT coupled to the different microspheres after the click chemistry reaction using radioactively labeled protein.
Tritium labeled protein, BMP2 WT or BMP2 E83Plk were used for the click reaction. 20000 cpm of ^{3}H labeled protein (~ 26 pg) were mixed with 50 µg of unlabeled protein and the amount of coupled protein was measured as a proportion of the cpm measured to the total µg used for the reaction.

3.3 Coupling BMP2 E83Plk to azide-functionalized microspheres

The first studies on the efficacy of the reaction were performed with higher amounts of protein, starting from 200 µg and scaling it down to 10 µg. This procedure was performed in order to estimate to which point the evaluation and quantification of data appears feasible in terms of reproducibility and significance for the future *in vivo* study.
As shown before, the data obtained by Western blotting gave a first impression on the efficacy of the reaction (Figure 43 A, B). The signals for BMP2 WT that in theory cannot be coupled during the reaction and hence removed with the urea wash were found to be stronger in the supernatant compared to the unbound BMP2 E83Plk. The quantitative analyses performed with ELISA and radioactive tritium were expected to show similar values (Figure

43 C, D). However, the results were divergent. Also a comparison of data obtained by ELISA and those experiments using the ^{3}H-labeled protein showed unexpectedly quantitative differences in determined protein amounts being coupled. However, these differences might be explained as follows: ELISA utilizes antibodies to detect target protein in the supernatants. The obtained values might be underestimated because of masked or destroyed antigen binding epitopes being the results of the harsh conditions used for coupling. On the other hand, ^{3}H-labeled protein used for the click reaction, might still contain unbound ^{3}H linker molecules which certainly behave different in terms of microspheres binding. This certainly would lead to an overestimation of the proteins amounts being present in the supernatant. However, both methods did not show any significant difference in the coupling efficacies comparing BMP2 WT and BMP2 E83Plk, which is in clear contrast to what was observed by Western blotting. In summary, from the obtained results described above it is not clear whether at all, or to what extent, the BMP2 variant E83Plk is covalently coupled to the used microspheres. Since the calculated coupling efficacy measured by ELISA is 93 %, while the obtained one from measurements using radioactively labeled protein is ~ 55 %, an average of the two measurements was used as the basis to calculate the protein amounts. Based on this assumption it could be concluded that from 20 µg of BMP2 E83Plk used for the reaction, 16 µg were coupled to 10 mg of microspheres.

To test whether the coupled protein maintained its biological activity after coupling, the protein functionalized microspheres were tested by ALP staining. C2C12 cells were treated with BMP2 E83Plk-coupled RCP or silica microspheres (Figure 43 E, F). The latter were covered with 0.4 % of low melting agarose in order to keep the microspheres in place during the 72 h of incubation. The staining developed around those beads decorated with the osteoinductive protein. Both RCP and silica microspheres induce alkaline phosphatase expression in those cells in contact with the BMP2 E83Plk coupled beads.

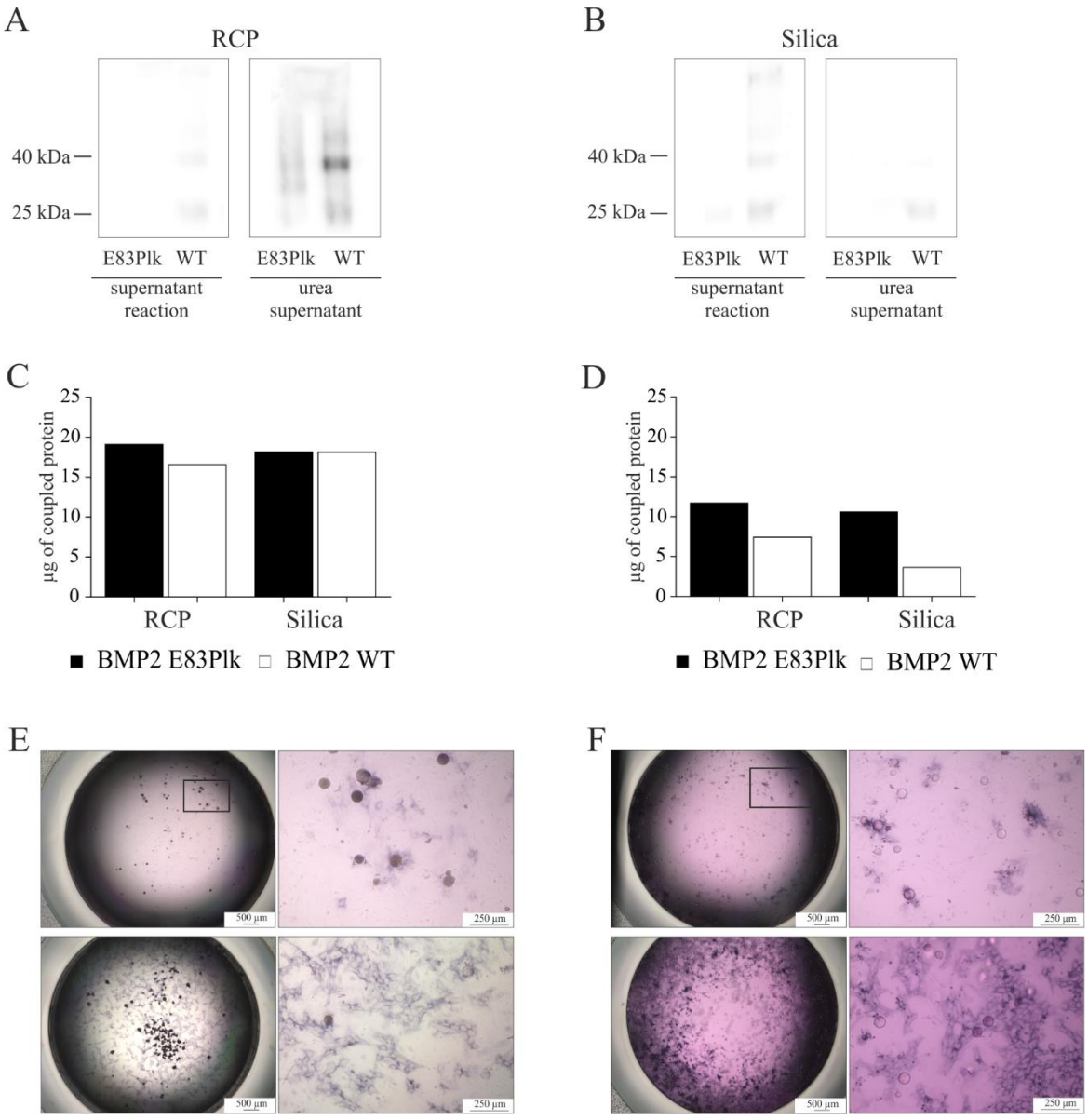

Figure 43: Quantification of immobilized BMP2 variants by $CuSO_4$ catalyzed reaction reveals discrepancies between ELISA and radioactive labeling.
20 µg of BMP2 E83Plk or BMP2 WT were coupled by CuAAC reaction to RCP or silica microspheres. (A) Supernatant and urea wash of RCP, (B) Supernatant and urea wash of silica; (C) ELISA calculation of protein coupled to the microspheres; (D) Radioactive measurement of amount of protein coupled to the microspheres; (E) (F) Alkaline phosphatase staining of C2C12 with BMP2 E83Plk coupled RCP (E) and silica (F) beads.

4. Copper free click chemistry

Accordingly to the coupling experiments described above the same set of experiments was performed but using the second variant, BMP2 E83Azide. Conventional click chemistry requires the presence of a Cu (I) catalyst that, as shown in the previous chapter, is a highly specific reaction as observed for the experiments using the azide-functionalized fluorophore, but can provoke conformational, structural and biological changes in the BMP2 protein.
The novel copper free click chemistry is based on the reaction of a cyclooctyne (DBCO) moiety with an azide-labeled reaction partner, known as strain-promoted alkyne azide cycloaddition (SPAAC). This reaction is very fast at room temperature and does not require Cu (I) as catalyst. Cyclooctynes are thermostable with very narrow and specific reactivities toward azides, resulting in almost quantitative yields of stable triazoles.

4.1 Proof of the efficacy of the reaction

The second BMP2 variant produced, BMP2 E83Azide was used as the azide reaction partner to the dibenzocyclooctyne (DBCO) counterpart. First, the efficacy of the reaction was proven with a DBCO coupled fluorophore, Sulfo-Cy5- DBCO, as was done for the copper catalyzed reaction.

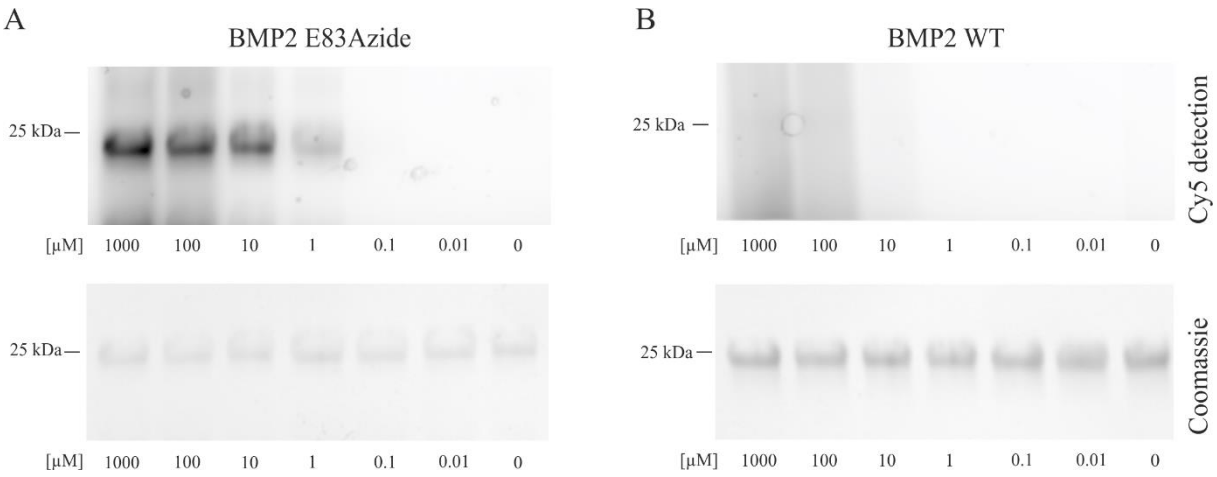

Figure 44: SPAAC reaction is specific and efficient.
20 µM BMP2 E83Azide was coupled to different concentrations to azide-functionalized Cy5. Samples were separated by SDS-PAGE and then analyzed under Cy5 detection channel (upper panel). As negative control BMP2 wild type (BMP2 WT) was used (upper right panel). Gels were afterwards stained with Coomassie Brilliant Blue in order to visualize the total proteins (lower panels).

The specificity and efficacy of the reaction are observed in the positive fluorescent signals which could be detected if 1 mM to 1 µM azide-functionalized Cy5 were used (Figure 44). BMP2 WT, which was used as negative control, was not fluorescently labeled thus confirming the specificity of this reaction. The presence of both loaded proteins could be confirmed by Coomassie Brilliant Blue staining.

As for the CuAAC reaction, the Cy5 fluorophore was substituted by DBCO-PEG$_4$-5/6-Texas Red in order to avoid the concealment of the receptor binding sites. The reaction was performed for different incubation times, starting from 15 min to 120 min or overnight, and samples were analyzed for their capability to induce alkaline phosphatase expression in C2C12 (Figure 45).

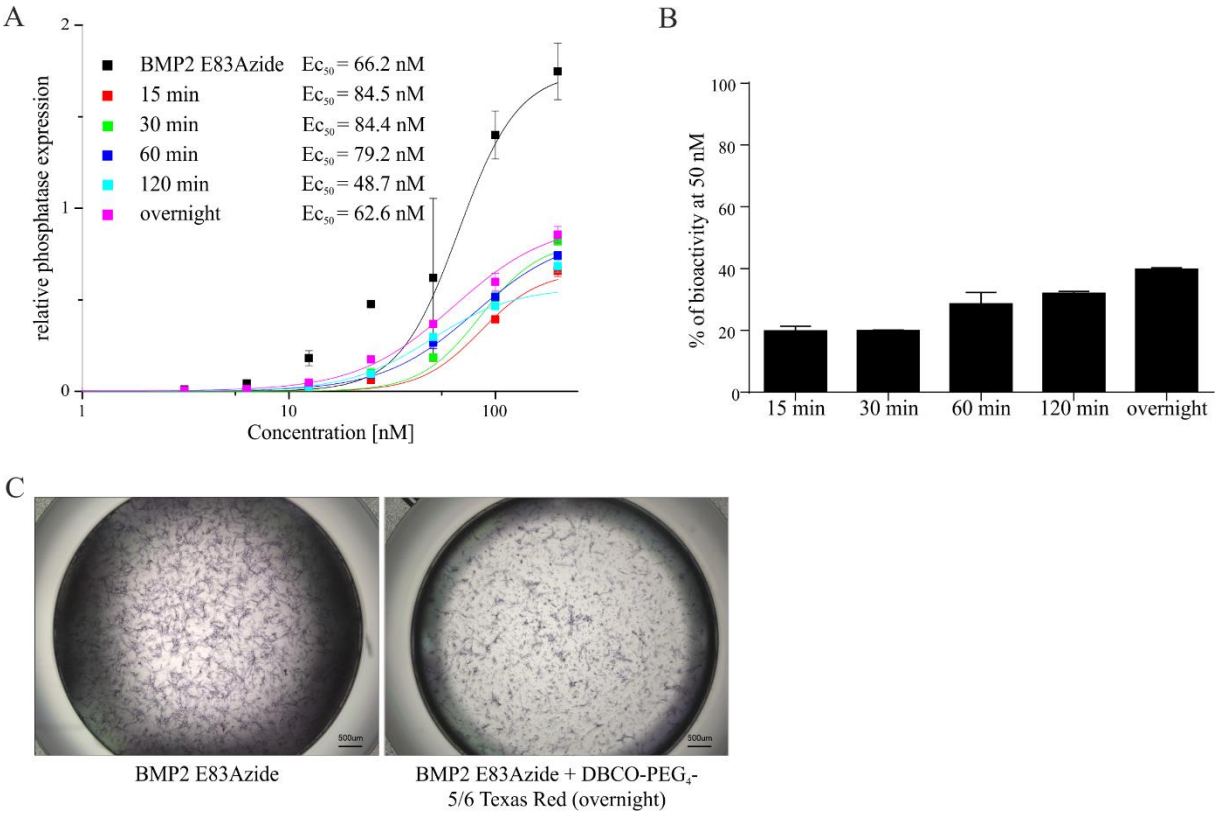

Figure 45: BMP2 E83Azide coupled to DBCO-PEG$_4$-5/6-Texas Red induces ALP activity.
C2C12 cells were treated with BMP2 E83Azide coupled to DBCO-PEG$_4$-5/6-Texas Red after being incubated for different reaction times (15 min, 30 min, 60 min, 120 min and overnight). (A) Alkaline phosphatase expression using 200 nM coupled protein (log-2 dilution) and using BMP2 E83Azide as positive control; (B) percentages are calculated considering the native protein as 100 % of bioactivity; (C) Alkaline phosphatase staining of C2C12 using 200 nM native BMP2 E83Azide and BMP2 E83Azide coupled to the DBCO fluorophore after overnight reaction. Statistic was not performed because of low n (n=2).

The overall trend of the reacted samples revealed similar EC_{50} values (Figure 45 A). Minor changes in bioactivity depending on reaction time were obtained when comparing the ALP

activities induced at 50 nM ligand concentrations (Figure 45 B). The bioactivity was reduced to 20 % in the first 15 or 30 min reaction time, which further increased to 30 % after 1 hour and reaching a reduction to 40 % after incubation overnight. These effects can also be visualized microscopically by ALP staining (Figure 45 C). The decreased staining induced by sampled which were exposed to the reaction conditions compared to the BMP2 E83Azide control, confirmed the observation made in ALP assay.

4.2 Analyses of the efficacy of the BMP2 E83Azide – DBCO reaction

After validating the reaction efficacy, BMP2 E83Azide was coupled to different microspheres, as was done for BMP2 E83Plk after the CuAAC reaction. RCP and silica microspheres were DBCO-functionalized, using a NHS-PEG_4-DBCO linker as describe before for the azide functionalization. Commercially available DBCO-functionalized agarose beads were used as third microsphere type.

The qualitative and quantitative analysis of the reaction was based on the four main methods described before: Western blotting, ELISA, the use of radioactively labelled proteins and the induction of ALP in cell-based assays. Western blot analysis confirmed coupling of BMP2 E83Azide to the beads since weaker signals were obtained in supernatants if compared to the one observed for BMP2 WT (Figure 46 A, B, C). For the RCP and silica microspheres, the urea wash supernatants confirmed a further removal of unspecific bound protein, while the absence of signal for the agarose beads, indicating that any protein that did not get coupled, adsorbed or unspecifically bound is already contained in the reaction supernatant.

The quantification methods of ELISA and radioactively labeled proteins show the amount of protein coupled by subtracting the cumulative release (protein content of reaction supernatant and washes) from the initial amount of protein used (Figure 46 D, E). As already observed for the CuAAC reaction, the quantitative analysis performed with ELISA and radioactive tritium showed quantitative differences in determining protein amounts being coupled (Figure 46 D, E). However, these differences might be explained as follows: ELISA utilizes antibodies to detect target protein in the supernatants. The obtained values might be underestimated because of masked or destroyed antigen binding epitopes being the results of the coupling. On the other hand, ^{3}H labeled protein used for the click reaction might still contain unbound ^{3}H linker molecules which certainly behave different in terms of microspheres binding. This certainly would lead to an overestimation of the proteins amounts being present in the

supernatant. However, those results are not in line with what observed by Western blotting, mainly for the silica and agarose beads, where the signal for BMP2 WT is stronger compared to the one of BMP2 E83Azide, indicating a higher amount of protein contained in the supernatants (Figure 46 B, C).

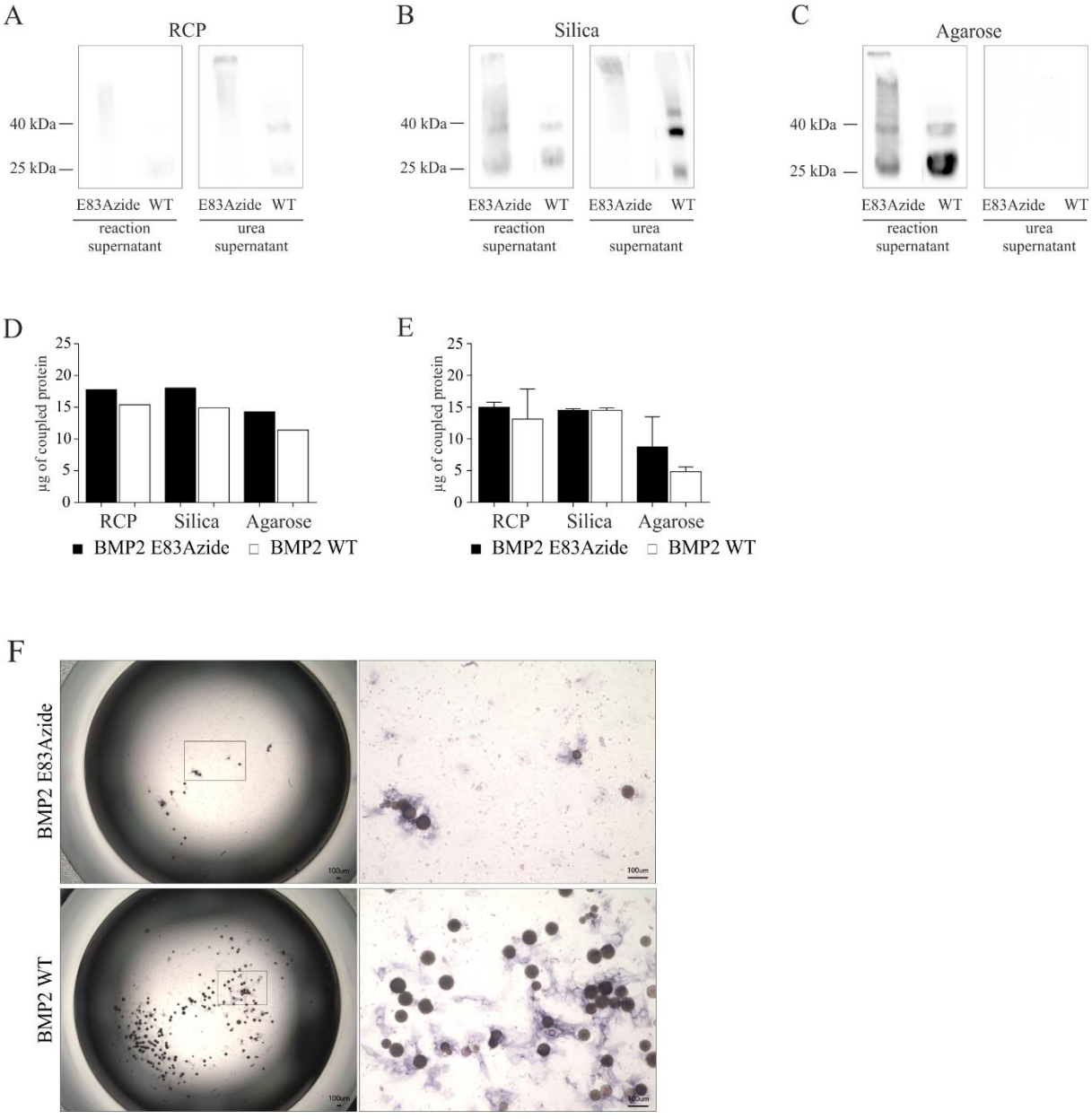

Figure 46: SPAAC mediated coupling of BMP2 E83Azide to different DBCO-functionalized microspheres shows coupling efficacy up to 90 %.

20 µg of BMP2 E83Azide or BMP2 WT (negative control) were reacted with 10 mg DBCO-functionalized microspheres. (A, B, C) Western blot of supernatants of reactions and urea wash supernatants of RCP, Silica and Agarose microspheres. (D) ELISA of ^{3}H labeled samples using supernatants of reactions, supernatants of water and urea washes (E) cpm quantification of ^{3}H labeled sample using supernatants of reactions, supernatants of water and urea washes (F) Alkaline phosphatase staining of BMP2 E83Azide and BMP2 WT coupled RCP. Statistical analysis was performed using a t-test between the BMP2 E83Azide and BMP2 WT of each microsphere type, but no significant difference was shown.

In summary, from the obtained results it is not possible to conclude if the BMP2 E83Azide is coupled to the microspheres and if at which extend. The calculated coupling efficacy measured by ELISA was almost ~ 90 % for the BMP2 E83Azide and ~ 70 % for the BMP2 WT. For the agarose beads on the other hand, coupling efficacy was calculated to be 75 % of BMP2 E83Azide and 50 % of BMP2 WT. In contrast to the ELISA, the scintillation measurements showed an efficacy of ~ 75 % for the SPAAC reaction with RCP and silica microspheres, without significant differences between BMP2 E83Azide and BMP2 WT. While for the agarose beads a coupling efficacy of ~ 40 % for BMP2 E83Azide and ~ 20 % for BMP2 WT was calculated. For the animal experiment an average of the two measurements (ELISA and radioactive labeled protein) was used as the basis to calculate the protein amounts. Based on this assumption it could be concluded that from 20 µg of BMP2 E83Azide used for the reaction, ~ 16 µg were coupled to 10 mg of RCP microspheres.
ALP staining confirmed the preserved biological activity of the protein after coupling (Figure 46 F). It is important to underline that only the cells in close contact to the microspheres expressed alkaline phosphatase, while all other cells in further distance were not stimulated. This is a clear indication that the protein is covalently coupled and not released, as is shown for the BMP2 WT that induce alkaline phosphatase expression also in cells not in close contact (Figure 46 G).

As last experiment the biological activity of uncoupled ligands which were released from the spheres and found in the supernatant was tested. The concentration of BMP2 WT and BMP2 E83Azide were determined by ELISA. The values measured for BMP2 E83Azide were: 0.86 µg/ml (RCP9, 1.5 µg/ml (silica), 11.6 µg/ml (agarose) (Figure 47 A). In addition, for BMP2 WT: 2.1 µg/ml was measured for RCP, 3.2 µg/ml for silica and 14.3 µg/ml for agarose (Figure 47 B). 25 nM of these uncoupled proteins contained in the supernatant were applied to C2C12 cells and compared with the same amount of native protein. The ALP assay revealed that only the supernatants of SPAAC reactions with agarose beads maintained biological activity of up to ~ 90 % if compared to native BMP2 E83Azide (Figure 47). Reaction supernatants from the RCP and silica beads instead indicated a substantial decrease, which might be explained by a possible fragmentation of RCP/silica beads during the reaction, resulting in BMP2 E83Azide protein coupled to small pieces of microspheres, and thus showing lower biological activities. However, the same observation was done for BMP2 WT that showed a decreased biological activity possibly due to fragmentation of the RCP or silica beads. The bioactivity of BMP2 WT was observed to be slightly higher than 100 % for the

agarose beads. This relies on an inaccurate protein determination by ELISA, meaning that a higher amount of protein was applied to the cells.

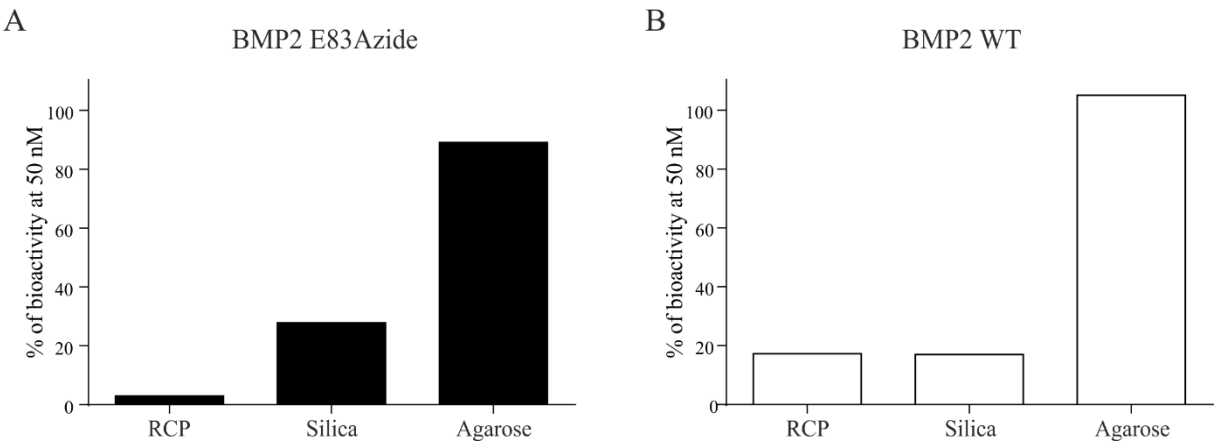

Figure 47: Supernatants of the SPAAC reaction revealed changes in the uncoupled BMP2 E83Azide protein

C2C12 cells were treated with 25 nM BMP2 E83Azide or BMP2 WT. The concentrations of the supernatants were determined by ELISA. BMP2 WT and BMP2 E83Azide native proteins were used as positive control and values at 25 nM set as 100 %. Static was not performed because of the low n (n=1).

5. Animal experiment

The detailed analyses of effects caused by the applied click chemistry reaction conditions, on structure and bioactivity of the different BMP2 variants, was appropriately taken into account for conducting animal experiment using BMP2 decorated RCP microspheres. The RCP microspheres were subcutaneously injected as a paste into the back of rats. Four cohorts of conditions were included within this study: BMP2 WT adsorbed to the RCP microspheres, BMP2 E83Azide coupled via SPAAC and BMP2 E83Plk coupled via CuAAC using $CuSO_4$ as catalyst. Unloaded ("empty") microspheres were used as negative control (Figure 48). Each BMP2 protein variant was applied in 3 different concentrations: 10 µg, 1 µg and 0.1 µg.
The main aim of the animal experiment was to prove whether the covalently coupled proteins are capable to induce ectopic bone formation and whether differences either in a qualitative and/or quantitative manner between the two application forms can be observed. In order to avoid any possible influence of released protein (e.g. from samples containing just adsorbed BMP2 wild type), these samples were grouped and applied together in a separated group of animals (Group 1), while covalently coupled proteins were distributed within Group 2 and Group 3. Since the coupled protein is supposed not to be released and dispersed into the surrounding tissue and therefore not influencing the outcome of the nearby implants, the three concentrations were indeed applied to a single animal. The last group (Group 4) contained only 0.1 µg of either coupled or adsorbed protein, which considering the low concentrations, would most likely not influence the outcome being triggered by the neighboring implants (Figure 48).

The general outcome of the animal experiment should lead to considerations concerning the applicability of the different chemistries used here but also to validate the usability of the applied scaffold/paste formulation. Sample containing BMP2 E83Plk coupled RCP microspheres did not show any formation of ectopic bone during the whole duration of the experiment (12 weeks). For BMP2 E83Azide and BMP2 WT, only at highest doses (10 µg) bone formation occurred after four weeks. Application of lower doses (1 µg and 0.1 µg) did not result in the formation of any bone. The implants containing lower doses and the negative control could not be retrieved from the animals at week 12, apparently because they degraded within the course of the experiment.

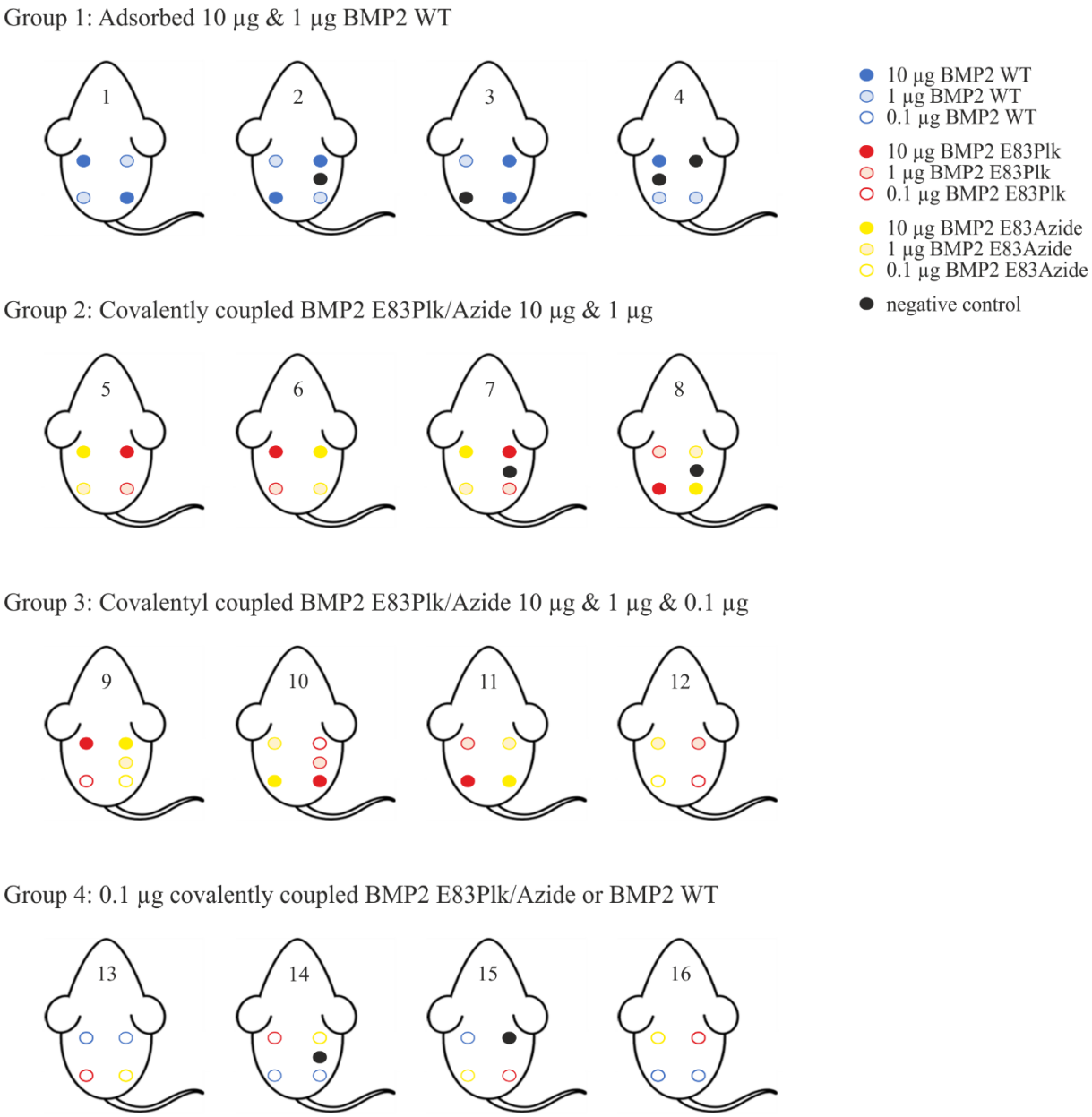

Figure 48: Schematic distribution of the groups according to the amount of protein and type of protein or chemistry used.
Three concentrations were used: 10 µg, 1 µg and 0.1 µg per implant. BMP2 WT was adsorbed into RCP microspheres, BMP2 E83Plk coupled by CuAAC using $CuSO_4$ as catalyst, and BMP2 E83Azide coupled by SPAAC reaction.

5.1 Analysis of bone formation by micro-CT

Micro-CT scans of all animals were performed every second week (Figure 49). Ectopic bone formation was evaluated in terms of bone volume and bone density. Over the 7 injection performed for each condition, only 4 produced bone in both BMP2 WT and BMP2 E83Azide groups using 10 µg protein. In Group 1, containing adsorbed BMP2 WT, rat 1 (upper and

lower injection) and rat 2 (upper and lower injection) started to form bone at week 4. In Group 2 and 3 (10 µg BMP2 E83Azide coupled samples) rat 7, 8, 9, and 11 formed bone.

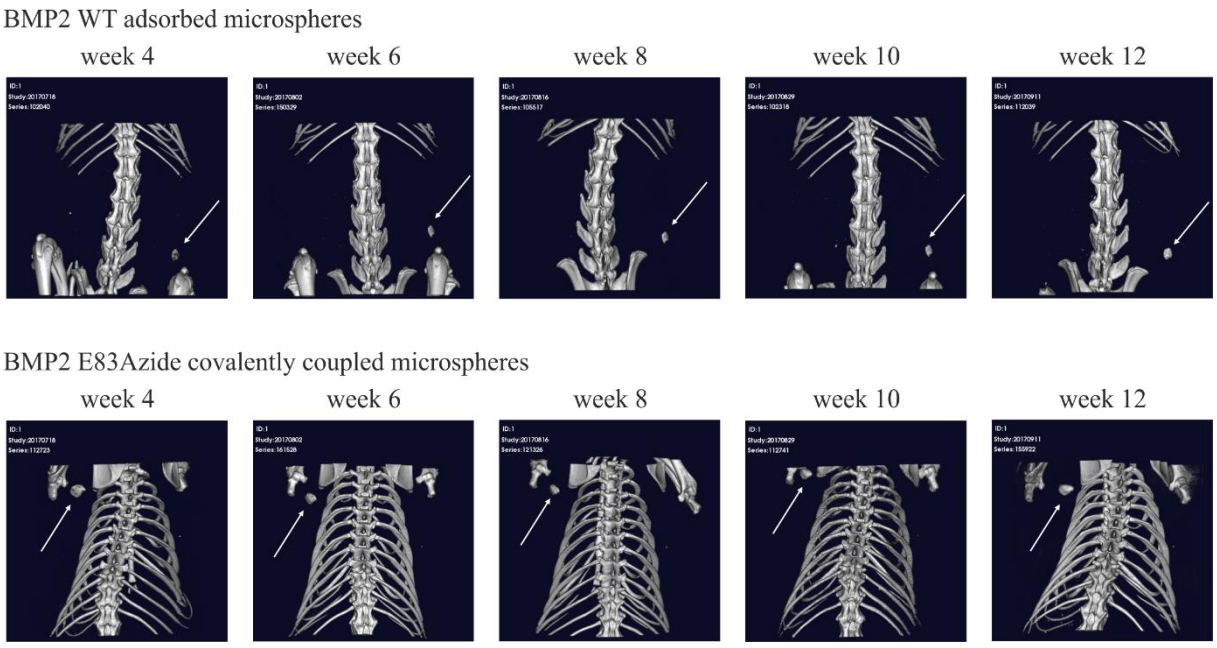

Figure 49: Micro-CT scans show increased ectopic bone formation over 12 weeks.
Representative images of rat treated with 10 µg BMP2 adsorbed WT (Rat 1) and covalently coupled BMP2 E83Azide (Rat 7). The arrows indicate the ectopic bone formed subcutaneously.

From the microCT analysis values of bone density and bone volume were calculated. Bone density was calculated as mean of the n=4 samples (BMP2 WT and BMP2 E83Azide) that formed bone, excluding the animals that did not show bone formation (zero values). The bone volume was calculated as mean of the n=7 samples, including the zero values. Already from the microCT scan it is possible to distinguish an increase in bone density based on the intensity of white color over the black background (Figure 49).

The minimum bone volume formed was 2.16 mm^3 and the maximum 7.28 mm^3 for the BMP2 WT, while for BMP2 E83Azide the minimum was 2.45 mm^3 and maximum 33.33 mm^3 (*ex vivo* data) (Figure 50). The bone volume measured was in general much lower compared to the total volume of the implant, since the injection volume was of 100 µl, a volume of 100 mm^3 could ideally be expected.

The bone volume reached a peak at 6 weeks and maintained a steady state for both wild type BMP2 and BMP2 E83Azide until week 12 (Figure 50).

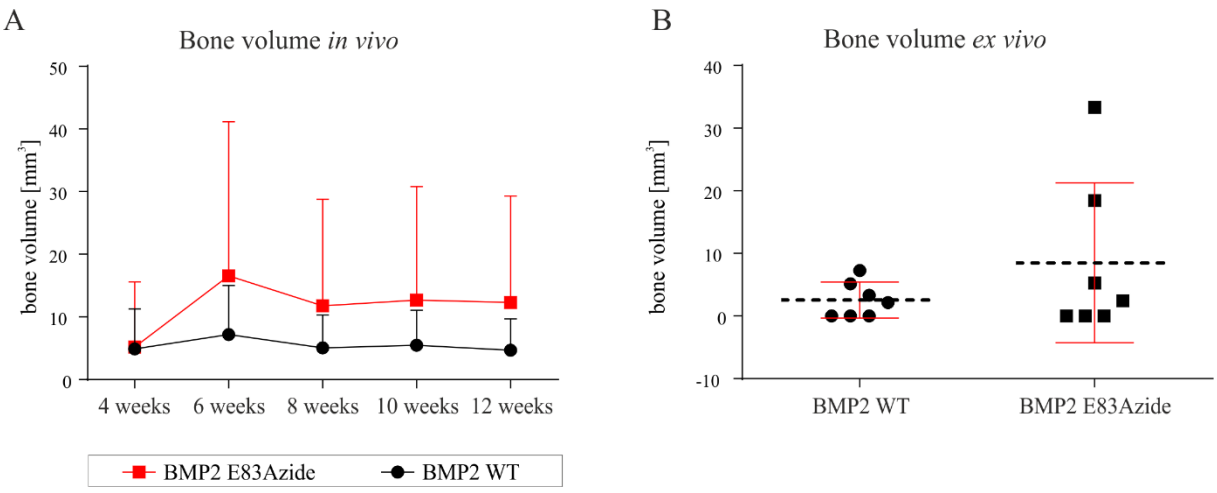

Figure 50: Bone volume measurements indicate a maximum volume at week 6 and a steady state until week 12.
(A, B) Graphs show ectopic bone formation that was evaluated by microCT *in vivo* over a duration of 12 weeks and at the end of the animal experiment *ex vivo*. The maximum volume was measured at week 6 with a value of 7.5 mm^3 for BMP2 WT and 16.8 mm^3 for BMP2 E83Azide. The statistics was performed using (A) a one-way ANOVA and (B) an unpaired t-test with Welch correction. No significance was detected in these analyses. n=7.

The bone density clearly showed a constant increase over the duration of the experiment (Figure 51). Also for the bone density no significant differences between the density values of the ossicles induced by both conditions could be observed (Figure 51).

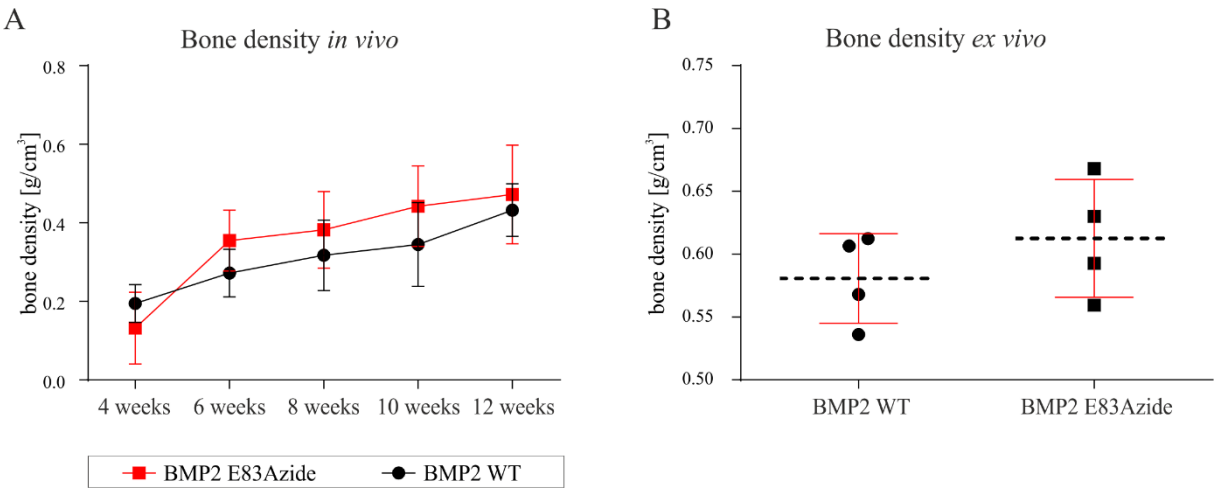

Figure 51: Bone density increases over the 12 weeks and confirms that the ectopic bone formed has no differences in quality.
(A, B) Graphs show bone density that was evaluated by microCT *in vivo* over duration of 12 weeks and at the end of the animal experiment *ex vivo*. The statistics was performed using (A) a one-way ANOVA and (B) an unpaired t-test with Welch correction. No significance was detected in these analyses. n=4.

These analyses strongly indicate that the quality and/or the structure of the produced ectopic bone might differ if it formed upon induction by BMP2 WT or BMP2 E83Azide.

5.2 Analysis of bone by histology

Because of the aforementioned differences observed by µCT analyses a detailed histochemical and immunohistochemical analysis was performed employing all retrieved implants. At first Hematoxylin & Eosin (H&E) staining was performed to get an overview on the overall structure of the explants (Figure 52). Formation of cortical bone was observed in all the implants but differences were observed if these structures were induces by BMP2 WT or BMP2 E83Azide.

All explanted ossicles which were formed by induction with BMP2 WT revealed a shell-like structure, with an external cortical bone structure and internal marrow filling the hollow space. The BMP2 E83Azide induced ossicles, showed a more uniform bone formation throughout the implant with several RCP microspheres still present after 12 weeks.

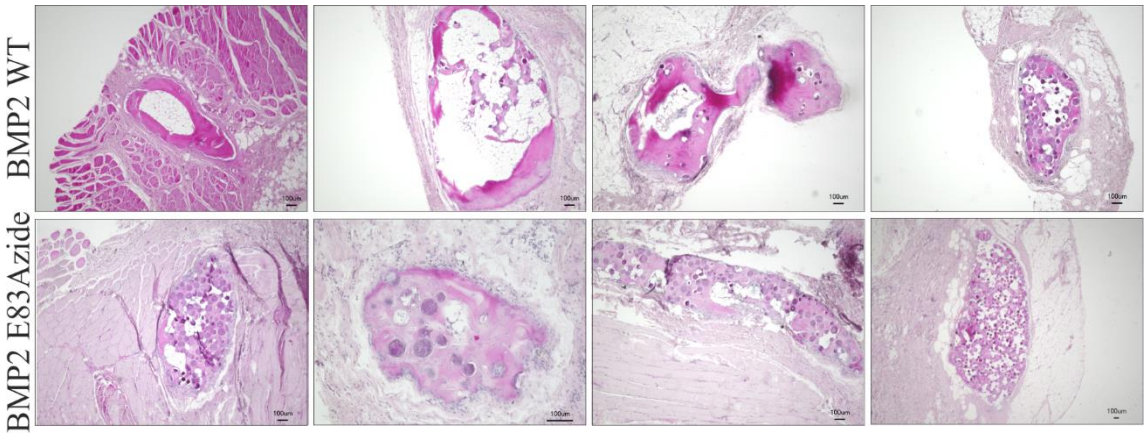

Figure 52: Comparison of ectopic bone formation between BMP2 WT and BMP2 E83Azide.
Four implants over seven induced ectopic bone formation for BMP2 WT or for BMP2 E83Azide. The H&E staining represent each retrieved implant at 12 weeks after implantation. The upper panel shows the BMP2 WT-induced ossicles, where a shell like structure can be observed with void filling part in the inner part. The lower panel instead represents the BMP2 E83Azide-induced ossicles were an abundant presence of microspheres can still be observed at week 12 after implantation.

When analyzing the bone induced by BMP2 WT in detail, it was possible to distinguish several structures applying different histological stainings (Figure 53). The external part of the ossicles was constituted by cortical bone with osteocytes in lacunae spread within the bone

matrix. Non-mineralized, organic portions of bone matrix, so-called osteoids, could also be observed by H&E staining (Figure 53). A more detailed picture can be obtained by staining these structures by Movat Pentachrome. The red color stains osteoids and the yellow color represents the bone matrix. Cartilaginous tissue was identified by various staining. Those stainings showed cartilage tissue in purple (Masson's Goldner), in green (Movat Pentachrome), in blue (Alcian Blue), on in purple (Safranin O) (Figure 53). Safranin O specifically stains the cartilaginous part (articular cartilage) in purple which is proportional to its proteoglycan content.

Other cell types which could be identified are bone lining cells (inactive osteoblasts) indicated by asterisks in the H&E staining (Figure 53). In addition, distribution of osteoclasts at the implantation site was investigated by the tartrate resistant acid phosphatase (TRAP, specific marker expressed in mature osteoclasts) staining (Figure 53). Representative stained sections showed a large production of this resorbing enzyme around the newly formed bone (highlighted by black arrows in Figure 53).

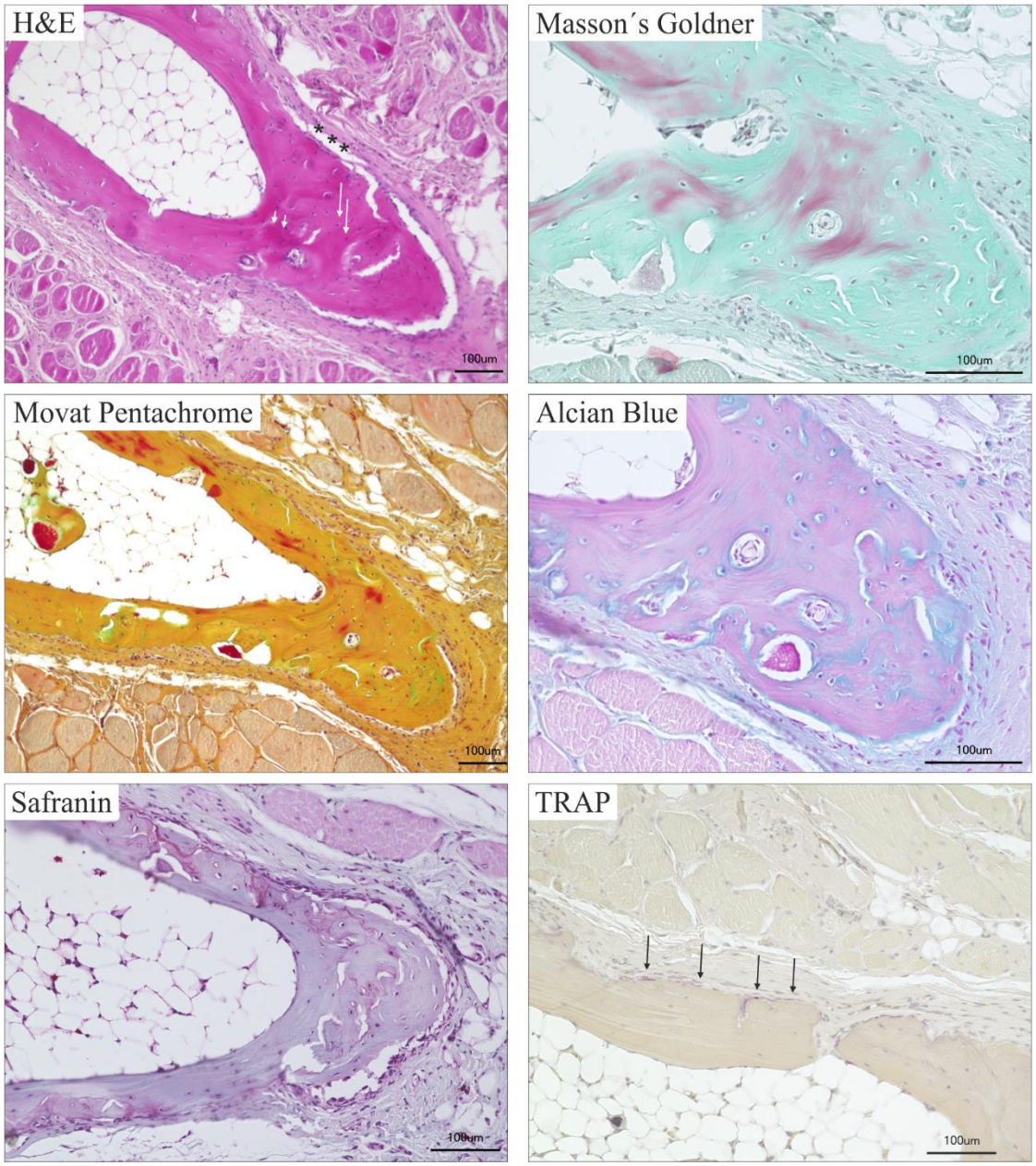

Figure 53: Histology evaluation of ectopic bone formation in BMP2 WT implants.
Representative images of various staining techniques analyzing ectopic bone formation in rat 1. H&E (long arrows indicates osteocytes, short arrows indicate osteoid and asterisks indicate bone lining cells), Masson´s Goldner (purple cartilage residue), Movat Pentachrome (green cartilage residue, yellow bone matrix, red osteoid), Alcian Blue (blue cartilage), Safranin O (purple cartilage), and TRAP (black arrows highlight osteoclasts).

The implants were also stained immunohistochemically using anti-vimentin, anti-α-smooth muscle actin (SMA) and anti-CD68 antibodies. Vimentin was used to prove whether the implant surrounding layer of cells are fibroblasts. Indeed this layer was positively stained for vimentin (Figure 54). Vimentin^{+} staining could also be detected in the newly bone structure since vimentin is expressed in several cell types (Lian et al. 2009). However, the specificity of

vimentin^{+} cells is not further characterized in this study. Additionally, the presence of newly formed vessels in the implants was also indicated by immunostaining with α-SMA (Figure 54) (Kusuma et al. 2015). CD68 is a marker for macrophages and was detected in some cells surrounding the implants. CD68^{+} cells were shown to be osteomacs, cells present in the bone tissue and involved in bone remodeling (Chang et al. 2008). Therefore, it might be that the detected CD68^{+} cells around the implant are involved in the osteoclastogenesis process and therefore indicating a remodeling activity. However, identification of remodeling events was not the focus of this study.

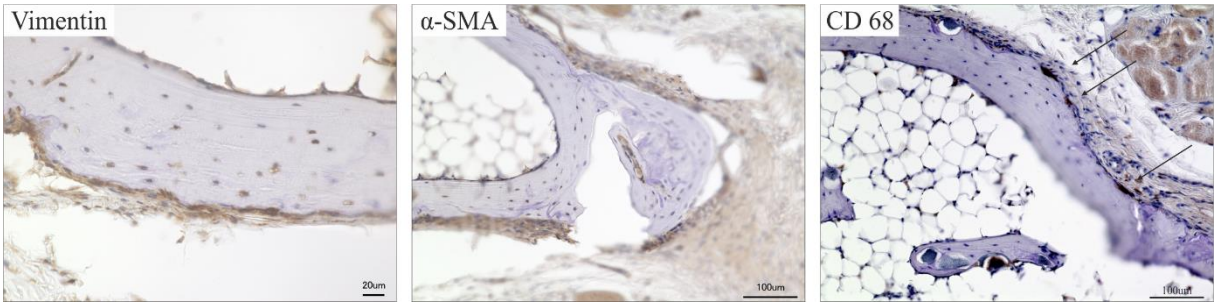

Figure 54: Immunohistochemical analyses of BMP2 WT implants
Representative images of BMP2 WT induced ossicle from rat 1. Immunohistochemical analyses were performed using anti-vimentin, anti α-smooth muscle actin (α-SMA), and CD68 antibody. CD68^{+} cells are indicated by black arrows.

Importantly, the BMP2 E83Azide implants which accordingly to µCT analysis appeared similar in bone density but showed a trend to higher bone volume if compared to BMP2 WT, however, they differ in their general appearance. These bone part of these implants cannot be described as "nut-shell"-like architecture. Here, the bony structures are more uniformly distributed throughout the implant's cross sections (Figure 55). The newly formed bone was shown to contain osteocytes in lacunae distributed within the bone matrix. Unmineralized, organic portions of the bone matrix (osteoid) were detected as red stained areas using Movat Pentachrome staining (Figure 55). The presence of cartilaginous tissue was observed by Masson's Goldner, Movat Pentachrome Alcian Blue, and Safranin O staining (Figure 55).
Positive vimentin and α-SMA cells could also be observed surrounding the outer implant layer of the implants. CD68^{+} cells were also observed in this outer layer but also intruding into the inner part of the implant.
The remnants of RCP beads observed in BMP2 E83Azide explants were completely absent in 3 out of 4 BMP2 WT samples representing the most pronounced difference between the two

application types. These are surrounded by thin layers of bony tissue, possibly protecting them from degradation.

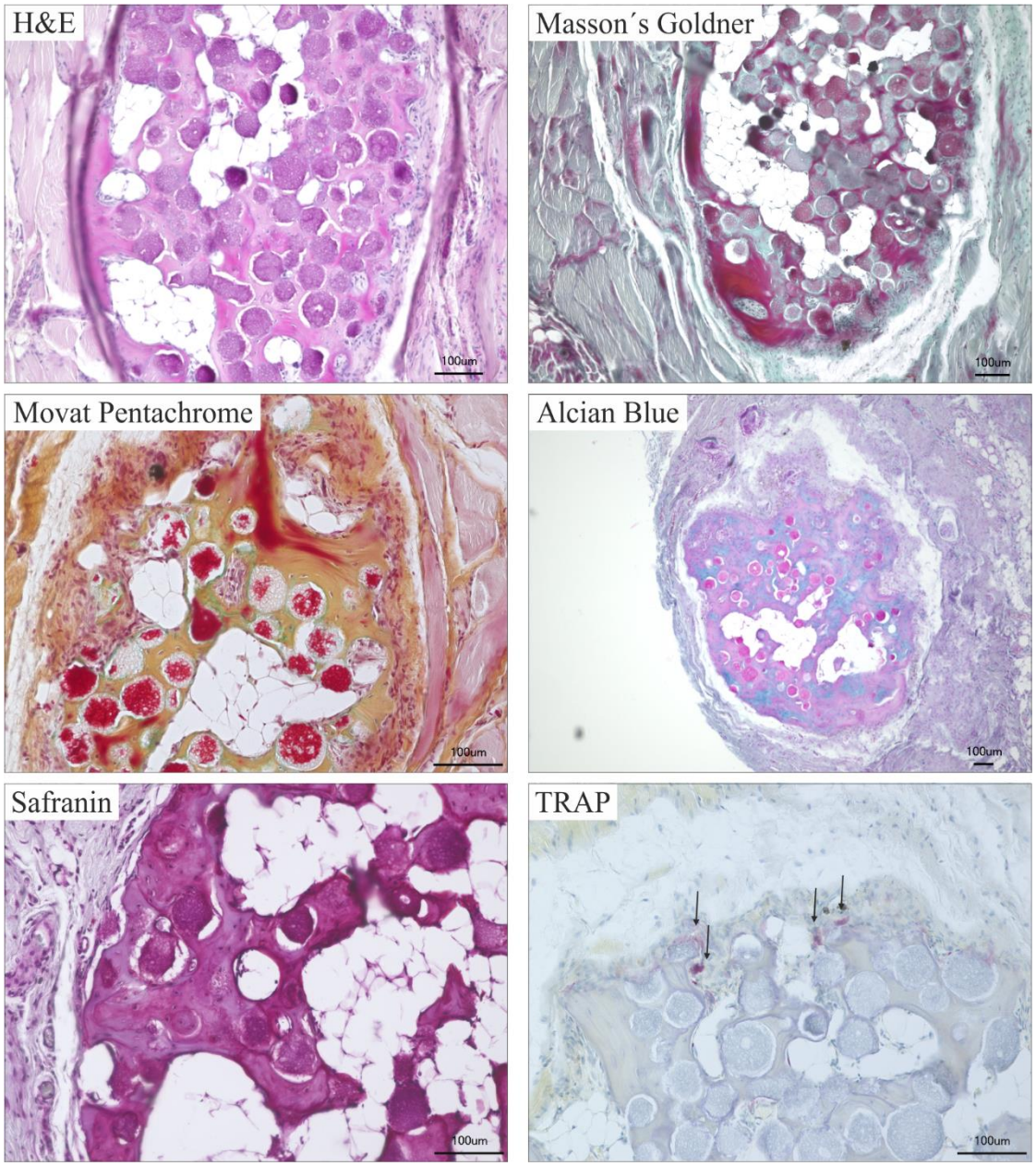

Figure 55: Histology evaluation of ectopic bone formation in BMP2 Azide83 implants.
Representative images of various staining techniques analyzing ectopic bone formation in rat 7, rat 8 and rat 11. H&E (long arrows indicates osteocytes, short arrows indicate osteoid and asterisks indicate bone lining cells), Masson´s Goldner (purple cartilage residue), Movat Pentachrome (green cartilage residue, yellow bone matrix, red osteoid), Alcian Blue (blue cartilage), Safranin O (purple cartilage), and TRAP (black arrows highlight osteoclasts).

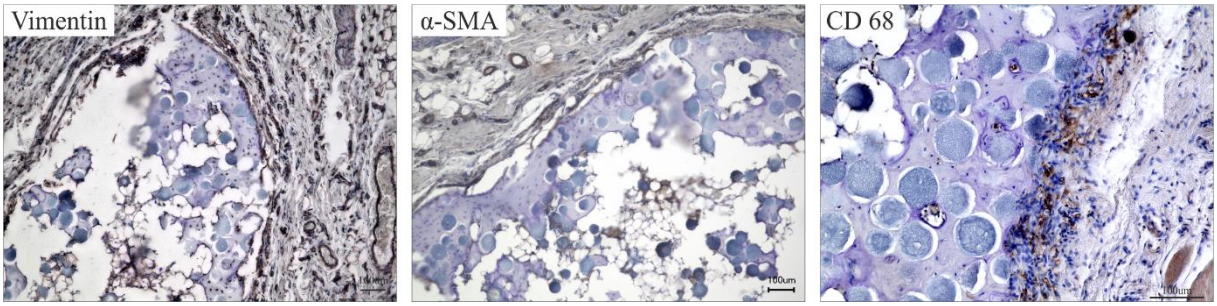

Figure 56: Immunohistochemical analysis of BMP2 E83Azide implants
Representative images of BMP2 E83Azide induced ossicle from rat 8. Immunohistochemical analysis was performed using anti-vimentin, anti α-smooth muscle actin (α-SMA), and CD68 antibody.

In summary, the new BMP2 variants harboring either N-Propargyl-lysine or (H-L-Lys(EO-N3)-OH) artificial amino acids were intensively analyzed in terms of expression and refolding ability, purity and bioactivity. The produced BMP2 variants were coupled to microspheres by site directed immobilization techniques. Each reaction was then investigated in terms of coupling efficacy and possible effects caused on the coupled protein upon reactions. In the last step, the BMP2 variants coupled microspheres were compared to BMP2 WT adsorbed microspheres in an animal experiment.

IV. Discussion

The long history of research on BMP2 involved dozens of investigators over a period of more than half a century. Intensive work was done in order to define the conceptual, physical, chemical, and biological nature of this bone derived molecule, that is involved in bone homeostasis and repair but it is also capable to induce the formation of ectopic bone in a variety of soft tissues (Sanchez-Duffhues et al. 2015, Salazar et al. 2016). A detailed characterization of this bone-inducing protein included the identification of its three dimensional structure, the associated signaling pathways and cell surface receptors, the modulating agonists and antagonists, the discovery of naturally occurring mutations to related disorders as well as its biological role in embryonic development and tissue homeostasis (Katagiri et al. 2015). The intricate interaction between BMP2 and several tissues and molecules initiates the entire osteoinductive process.

Due to its bone forming potential, the use of BMP2 was exploited in preclinical and clinical studies for spinal fusion and for many other applications where the generation of bone tissue is desired (Faundez et al. 2016, McKay et al. 2007).

The short half-life of BMP when systemically administered (16 minutes in rat and 7 minutes in non-human primates) led to the investigation and application of different methods for protein delivery at a bone defect site. A successful delivery system should retain the growth factor at the defect site for the duration of time being required for homing the appropriate cells to the defect area and to induce and regulate cell proliferation and differentiation and thereby to induce bone regeneration (Hollinger et al. 1998, Haidar et al. 2009). The use of innovative, cutting edge biomaterials might improve the retention of the protein at the defect site thus increasing the quality of the newly formed bone. Since the use of supraphysiological protein doses is associated with high cost and, importantly, causes severe side effects, scaffolds with higher protein-entrapment capabilities are needed to decrease the conventionally applied doses.

As these necessities can be regulated by the scaffolds and the BMP molecules, intensive research focused on the improvement of the material characteristics and/or on the generation of so-called second generation BMPs with superior bioactivities. Chemically-modified BMPs functionalized with reactive groups or modified to have higher affinities to their functionalized carriers have been investigated. These modifications would allow coupling using particular techniques. However, it has always to be considered that these protein

modifications might result in altered stability, solubility, bioactivity and biospecificity (Gautschi et al. 2007).
A successful clinical BMP therapy depends on the equilibrium of parameters that control the localized and controlled release of the factor from its particular delivery system. Some parameters are: protein dose, protein release kinetics, the release mechanism, and nature as well as structure geometry of the used scaffold material.

The aforementioned parameters were all addressed in this study mainly focusing on altering the release of the investigated modified protein.
Porous microspheres made of a recombinant collagen-like peptide (RCP) were investigated within an EU founded consortium (BIO-INSPIRE) in terms of their potential to maintain a sustained and controlled release of BMP2 as the release is the general problem that causes the severe side effects. By tuning pore and/or particle sizes, crosslinking times and the applied crosslinking methods, Mumcuoglu et al. could show that the release kinetics can be modified by altering these parameters. These microspheres showed a lower initial burst release kinetics (Mumcuoglu et al. 2018a) if compared to other systems. The use of a hydrogel-microspheres combination in an injectable form allowed a tight control of the BMP2 release *in vivo* (Mumcuoglu et al. 2018b). The alginate hydrogel reduced the BMP2 release from the microspheres *in vitro* and possibly also *in vivo* as shown by fluorescently label BMP2 WT that was detected at the injection site 4 week post-implantation (Mumcuoglu et al. 2018b). In addition, it was shown that an initial marginal release of the growth factor might be required to recruit osteoinductive progenitors cells towards the implantation site, but also a sustained release that triggers their osteoblastic differentiation should be guaranteed (Haidar et al. 2009). This "ideal" release kinetic of BMP2, assumed as the "ideal pharmacokinetic", is in line with other studies (Brown et al. 2011). Even though it implies the use of high doses of protein necessary to trigger the osteogenic capabilities.

The use of this new material produced several positive outcome both *in vitro* and *in vivo*. Therefore, it was used also in this study but with the focus on different immobilization techniques addressing the growth factor rather than on the material.
Using covalently immobilized proteins, initial burst release cannot occur but, in the long-term, the osteogenic activity of the growth factor remains constant along with the degradation of the microspheres. It was hypothesized that the amount of protein to be injected most likely represents the minimal effective dose being required to induce bone formation.

1. Creating new BMP2 variants: how mutations influence protein characteristics

As already introduced, the common adsorption techniques aim to improve the control of the burst release in order to reduce the related severe side effects. Development of materials with improved retention ability and thereby higher osteoinductive properties are still very limited.
Several different functionalization techniques involved the chemical modification and activation of the biomaterial surface followed by attachment of the bioactive protein. For example, the use of the heparin binding sites of BMP constituted a step forward in bone regeneration and repair (Ruppert et al. 1996). Heparin binding sites were identified in several growth factors and are involved in various physiological processes. However, an additional function of heparin binding sites could be to localize active growth factors by restricting their diffusion. Several studies have indeed used heparin sulfate (HS) to have a higher control of the protein during *in vivo* studies by modifying the material with HS (Liang and Kiick 2014) and/or by increasing the number of heparin binding sites in modified recombinant BMP2 variants (Wurzler et al. 2004). The increase in heparin binding sites induced and enhanced osteogenic activity of BMP2 *in vivo*, possibly due to a longer retention period in the tissue and thus better bioavailability (Depprich et al. 2005). It could also be shown that heparin stimulates BMP activity by protecting ligands from the inhibitory microenvironment around target cells. These findings suggest that simultaneous administration of BMPs with sulfated polysaccharides might be clinically useful at least for local bone regeneration. Moreover it was found that HS acts as a catalyst for the formation of BMP2 signaling complexes (Kuo et al. 2010).
Another immobilization technique requires only the activation of the carboxyl or amino groups of the biomaterial, allowing a conjugation with the biomolecule by a simple chemistry, the 1-ethyl-3-(3-dimethylaminopropyl)carbodiimide hydrochloride (EDC)/ N-Hydroxysuccinimide (NHS) reaction. In case of BMP2 coupled to scaffold by EDC/NHS chemistry, the reaction occurs between the amine groups provided by either the N-terminal alpha amine or also by those present in e.g. side chains of lysine residues within the peptide chain, and the activated carboxyl group of the scaffolds (Pohl et al. 2013). The activation is usually done on the carboxyl groups of the scaffold because this could cause internal crosslinking if performed on the protein. However, this technique results in a random immobilization that might compromise the growth factor bioactivity.

These coupling techniques rely on the modification and activation of the material and on the immobilization of the protein.

A different way for protein immobilization can be achieved by protein modification. The introduction of protein modifications needs a strong experience in the handling of the unmodified target protein, which requires knowledge of the target protein's structure, its general biochemical characteristics and its (bio-) activities. The insertion of a mutation at any position of the amino acids sequence might lead to altered characteristics impeding the production of active protein. Problems might occur regarding protein expression, refolding as well as a reduction of its overall solubility.

Existing methods to modify proteins with the aim to couple them to e.g. solid structure include the insertion of naturally occurring amino acids such as cysteine, lysine, serine, histidine and tyrosine residues but also of unnatural amino acids (UAAs) (Gunnoo and Madder 2016). Both methods require the modification of the cDNA sequence encoding for the desired target protein. By the use of two revolutionary techniques, *in vitro* synthesis of oligonucleotides and polymerase chain reaction (PCR), site directed mutagenesis (Weiner et al. 1994) has become a robust and versatile method being used in several studies with the aim to examine the essential molecular mechanisms of gene and protein function (Ho et al. 1989, Higuchi et al. 1988, Wang et al. 2015).

Although the genetic code theoretically allows protein synthesis using more than 60 different amino acids, just 20 amino acids (or 22 if including selenocystein and pyrrolisine (Zhang et al. 2005)) were shown to be sufficient for life. The incorporation of unnatural amino acids at a defined site within the protein sequence marked a step in the evolution of proteins, or even entire organisms, with new properties (Xie and Schultz 2006). It appeared feasible to modify the translation machinery in order to develop a method that allows to encode extra amino acids which can then already be introduced upon protein synthesis. Moreover, the introduction of amino acids with a defined three dimensional orientation and charge at unique sites in proteins will contribute to the investigation of protein structure and function *in vitro* and *in vivo*. The technique described by the Shultz's group (Xie and Schultz 2006), utilizes non-natural tRNAs which are individually recognized by mutated aminoacyl tRNA synthetases (AaRS). These synthetases accept a limited set of artificial amino acids as substrates which then can be used in protein translation. However, from the 64 possible triplet sequences only three are non-coding (TAA, TGA, TAG, named ochre, opal, and amber codon, respectively).

For codon expansion usually the TAG (amber) codon is used allowing an expansion of the genetic code with over 30 additional UAAs, such as those with alkyl- and azido-appended functionalities for click and Staudinger based investigations, photo-reactive sidechains for crosslinking and intrinsically fluorescent coumaryl- and dansyl-moieties, allowing insight into the localization and trafficking at the cellular level (Foley and Burkart 2007).

Modified proteins were created by the use of affinity tags fused to the protein to allow immobilization on scaffolds. The use of a rare amino acid dihydroxy phenylalanine (DOPA) allows the non-covalent bond to titanium dioxide surfaces. By preparing a poly-Tyr-tagged rhBMP2 (N-terminal tetra tyrosyl fusion protein) which is converted into a poly-DOPA-tagged BMP2 by hydrolization of tyrosine, the BMP2 variant might be immobilized only by the use of the DOPA high affinity to titanium (Jennissen and Laub 2007).

Site directly modified proteins were generated by the insertion of additional cysteine residues in order to couple the mutated protein to functionalized materials by e.g. maleimide or iodoacetimide groups. Cysteine has a unique nucleophilicity in comparison with other reactive side chains and under physiological conditions it has a high tendency to form nucleophilic thiolate ions (Gunnoo and Madder 2016). Modified proteins have been applied in different areas, from tracking of protein fluorophore conjugates (Paarmann et al. 2016) to the polyethylene glycol (PEG)ylation of therapeutic proteins to reduce immunogenicity, from the production of materials with novel properties to test the mechanism of pathological enzymes (Spicer and Davis 2014).

In particular, BMP2 cysteine analogues were created in order to enable the attachment of SH-reactive PEG (Hu et al. 2010), to couple them to sulfhydryl-reactive dye fluorescent dye (Paarmann et al. 2016) or to covalently couple them by thioether formation between the SH group of the protein and the iodoacetamide group that is present on crosslinked acrylamide beads (Tabisz 2016). Hu et al. evaluated the characteristics of three different BMP2 cysteine analogues: BMP2 A2C (also used in (Tabisz 2016)), BMP2 N56C and BMP2 E96C (Hu et al. 2010). The importance of cysteines in BMP proteins is connected to their role in the formation of disulfide bridges. Each of the BMP 2 monomers contains seven cysteines. Six of them form three intramolecular disulfide bridges (Cys 43/Cys 111, Cys 47/Cys 113, and Cys 14/Cys 79), constituting a so-called cysteine knot, that is crucial for the structure stabilization and thus for the activity of the BMP2. The seventh cysteine residue (Cys 78) forms an intermolecular disulfide bond with the other monomer, constituting the dimer (Scheufler et al. 1999). The mentioned BMP2 cysteine analogues (BMP2 A2C, N56C, and E96C) showed only slight differences in expression, refolding and analysis by mass spectrometry and

exhibited 2- to 3-fold lower bioactivities if compared to wild type BMP2. Dose-response curves were similar for the A2C and E96C variants, while the BMP2 N56C was the least active (Hu et al. 2010). Also Surface Plasmon Resonance (SPR) measurements indicated similar affinity interactions to the receptors, in case of BMP2 A2C and E96C, while for the N56C analogue, the binding affinity is reduced about 5-fold with BMPR-IA and less than 2-fold with ActR-IIB (Hu et al. 2010) . The introduced cysteine residues were located at positions within the mature part of human BMP2 outside of the known receptor binding sites (the so-called wrist and knuckle epitopes) thus most likely not impeding interaction with the cell surface receptors. However, the PEGylated BMP2 cysteine analogues exhibited different behaviors. Some showed an increase in bioactivity, possibly related to the enhanced solubility of the PEGylated analogues, while some had strongly decreased bioactivity caused by the attached PEG that could interact with the receptor binding sites. Hence, the decreased bioactivity observed for the uncoupled cysteine analogue proteins is most likely not related to the position of the mutation but rather to structural and conformational changes of BMP2 as a consequence of the additional cysteine. The presence of an additional "free" cysteine residue might led to the formation of multimers and also improperly folded dimers (Tabisz 2016). The use of cysteine might not be the perfect choice if site directed immobilization of these proteins to other structures is desired.

The aforementioned immobilization approaches were mainly restricted to the N-terminus. Our approach aimed instead on the insertion of artificial amino acid in positions that would not interfere on the bioactivity of the mutated protein in its free form and overall after its reaction with scaffold.

The comprehensive study of Kirsch et al. analyzed more than 57 human BMP2 variants addressing the mature part of the protein (Kirsch et al. 2000). The BMP2 variants described by Kirsch et al. represented single amino acid substitutions replacing the particular amino acids with alanine (Kirsch et al. 2000). The alanine-scanning mutational analysis of BMP2 allowed the identification and characterization of two distinct binding epitopes in human BMP2 as well as the detection of antagonistic BMP2 variants providing new insights into the mechanism of BMP receptor activation. On the basis of this study, the crystal structures of ternary complexes comprising BMPR-IA, ActR-IIB ectodomains and either wild type BMP2 or other BMP2 variants have been investigated in order to understand specificity and affinity of ligand and receptors interaction (Weber et al. 2007). Using these studies as starting point, positions in the BMP2 molecules which allow the best possible linkage without diminishing the bioactivity of the resulting construct could be identified.

The first BMP2 variant harboring an artificial amino acid was the variant BMP2 K3Plk (Tabisz et al. 2017). Even though a mutation at this position was not previously investigated, it was thought that a replacement of this lysine residue by e.g. N-Propargyl-lysine (Plk) would not affect the overall protein structure, refolding and bioactivity of the resulting "free" protein". To produce BMP2 K3Plk, the unnatural amino acid Plk was introduced by genetic codon expansion directly during bacterial protein expression (Tabisz 2016). The produced BMP2 variant showed biological activity being comparable to the wild type protein. However, coupling of BMP2 K3Plk to bulky structures utilizing the Plk residue at its N-terminus might impede the interaction of the coupled protein with receptors on the cells surface by steric hindrance.

To overcome this problem, this work focused on improving the whole process, starting from the identification of ideal positions for the introduction of the mutation, the production of different protein variants, up to the improvement and validation of the coupling process.

Analyzing the BMP2 structure on the basis of the work performed by Kirsch et al. it was decided to introduce the mutation at two individual positions of the mature BMP2 sequence that most likely would not have compromising effects on the overall bioactivity of the resulting BMP2 variants. Glutamic acid (E) 83 and E94 are localized either at the finger tips or on top, close to the symmetry axis of the dimeric BMP2 structure hence outside of the known receptor binding interfaces. At these positions, the effects caused by steric hindrance should be minimal after linkage to solid scaffold. Furthermore, these positions were chosen because they did not indicate any measurable alterations in function when substituted by alanine (Kirsch et al. 2000).

In order to test whether the two new BMP2 variants can be produced in *E. coli*, protein expression was first proven in small scale using different concentrations of Plk. In agreement with previous results, a concentration of 10 mM Plk was found to be the most effective in terms of protein expression (Luhmann et al. 2015).

Analysis of the expressed BMP2 variants BMP2 E83Plk and BMP2 E94Plk under reducing conditions, revealed the presence of two bands with an apparent molecular weight of ~ 13 kDa that is the size of the monomeric BMP2. The bands with lower molecular weight represent shorter forms of the BMP2 monomers which most likely originated from a pre-mature translational stop of the introduced amber stop codon. The full length monomeric forms indicate therefore the successful introduction of the Plk since, this band is in fact missing in the negative control without substrate. In case of BMP2 K3Plk, this effect could not be observed as a shortened product would only comprise two amino acids.

The presence of two monomeric forms might result from refolding in the formation of heterodimer. Indeed, heterodimers were observed after the refolding process and in the consecutive purification via ion exchange chromatography. The final products thus contained a mix of homodimeric and heterodimeric protein species as indicated by separation via SDS-GEL electrophoresis where a double band at the dimeric size (~ 26 kDa) and a double band in reduced conditions was detected. This heterogeneity was not confirmed by mass spectrometry analysis. Spectra of the different batches of produced BMP2 E83Plk show the presence of only one type of dimeric product consisting of two full length monomers. The heterodimers are not detected by mass spectrometry possibly due to the low quantity. In case of BMP2 E83Plk only two batches showed also the presence of full length monomers in the final products. The final purified products, BMP2 E83Plk and E83Azide, also used for the animal experiment did not show monomeric components in the final product and therefore they were not analyzed by mass spectrometry.

The two mutations, E83amber and E94amber, showed great differences already from the expression step. During expression a more pronounced formation of short form monomers was shown in case of BMP2 E94Plk compared to BMP2 E83Plk. Moreover, a low efficacy of the renaturation procedure was noticed during the purification step by ion exchange chromatography, where the fractions were mainly constituted of monomers with low amounts of dimers. The difficulties in the production of BMP2 E94Plk brought to a mixed final product constituted by homodimers, heterodimers and high amounts of monomers.

The distinct separation of the two monomeric forms under reducing conditions that was more pronounced for the BMP2 E94Plk highlighted the difference between the amount of protein detected by Coomassie Brilliant blue staining and Western blot. The antibody might have more affinity and specificity for the full length monomer, suggesting that it binds to the epitope where the mutations are located and at every C-terminal end. Additionally, the low protein yield of the negative control might rely on a blockade within the translational machinery, since “empty” (without Plk) tRNAs/tRNA synthetase might occupy the ribosomes at the amber stop codon. Therefore, also in the positive control, where Plk was indeed introduced, the presence of short form monomers indicates a lower efficiency in translation, at the same substrate concentration, that was noticed between the two variants.

This heterogeneity of BMP2 E94Plk strongly compromised its biological activity resulting 6-fold less bioactive if compared to the wild type protein. The BMP2 E83Plk results only 3-fold less bioactive comparted to wild type BMP2.

Even though no receptor affinity interaction analyses were performed by SPR, the mutation position and moreover the orientation of the artificial amino acid at those specific positions should not interfere with the receptor binding sites. Therefore the decreased biological activity should mainly be related to the impurities of both final products. As further demonstrated, the additional purification step, performed to reduce impurities such as monomers or heterodimers of the final products, resulted in a slight increase in bioactivity for the BMP2 E83Plk.

Despite substitution of E94 by alanine (Kirsch et al. 2000) or by cysteine (Hu et al. 2010) did not apparently affect refolding and bioactivity, replacement with Plk resulted the high content of short monomer form, which obviously causes low efficiency in the refolding process and consequently high decrease the biological activity.

Due to these observations the production of the BMP2 variants was only continued with the E83 variant. In all the batches of BMP2 E83Plk the outcome always resulted in a mixed population of homodimers and heterodimers. The use of several purification methods allowed an almost complete removal of the monomeric component from the final product.

As previously described, the site directed mutagenesis method allows to adapt the functionalization of the protein according to the desired chemistry. On this basis, BMP2 was produced with another artificial amino acid (H-L-Lys(EO-N3)-OH) harboring, instead of the alkyne group present in Plk, an azide as functional group, which allows the reaction with other reaction partners such as e.g. dibenzocyclooctyne (DBCO).

BMP2 E83Azide was produced following the standard protocol that was established for BMP2 E83Plk. In contrast to the expression of BMP2 E83Plk, 15 mM of the substrate (H-L-Lys(EO-N3)-OH) showed highest protein expression levels. A clear band separation at the size of the expected monomers was not achieved. Also in this case the antibody used for Western blot analysis did not recognize the shorter monomeric form, as observed for the Plk variants.

Possibly connected to the increase in substrate concentration, the expression and purification steps yielded in higher protein amounts if compared to the Plk variant.

Even though the final product still contained a low percentage of monomers, they were not detected by mass spectrometry analysis. However, BMP2 E83Azide showed a 2-fold less bioactivity if compared to the wild type protein.

The possibility to produce functionalized proteins according to the desired application has been investigated for different proteins (Nguyen et al. 2009). From what was discussed above

it is clear that protein modification has not only to do with the structure but also on the consequences that structure modifications might cause on signaling and interaction with other molecules.
In summary, how, where and what to introduce an additional amino acid requires intense background knowledge and experience in protein chemistry.

2. Site direct immobilization of BMP2 variants: different chemistries and different scaffolds

After proving that the introduced reactive group did not strongly affect the biological activity of the produced proteins, some questions arose: (1) are the reactive groups available for the reaction with the corresponding functional groups present on scaffolds, such as microspheres, (2) does binding of the protein to these structures inhibit the interaction with cell surface receptors and thus (3) is the coupled protein still biologically active?

Former experiments already demonstrated that, independent of the covalent coupling method used, growth factors were able to maintain their biological activity (Pohl et al. 2013, Di Luca et al. 2017, Schwab et al. 2015, Budiraharjo et al. 2013).
The various immobilization chemistries differ within each other according to the targeted reactive groups, the use of spacer arms and the different chemistries used for coupling. However, immobilization techniques are restricted to those requiring the use of aqueous-based chemistry, as most growth factors are either not soluble in organic solvents in or become damaged therein (Masters 2011).
The most common method (EDC/NHS) for conjugating biomolecules to compounds utilizes the zero length crosslinking agent EDC. This reaction occurs between a carboxyl group and an amine group creating a stable amide bond. This method is simple, inexpensive, effective, and performed under mild conditions. In the BMP protein, the C-terminus is buried into the protein structure and activation of carboxyl groups can cause internal protein crosslinking. Therefore, carboxyl groups are activated on the scaffolds and these react with the amine groups of the BMP2. This method results in a random immobilization of the protein with a strong possibility of altering the growth factor bioactivity by impeding its recognition by its receptors (Masters 2011).

The approach suggested in this study proposes instead to site direct immobilize the protein to the scaffold allowing a reproducible outcome in terms of protein orientation and bioactivity.

As one possible option, the copper catalyzed azide-alkyne cycloaddition (CuAAC) reaction has been extensively used in the field of pharmaceutics and chemical biology as an efficient method for the modification of different molecules by covalent binding of other compounds (McKay and Finn 2014, Meyer et al. 2016). The reaction occurs between an alkyne and an azide generating 1,4-disubstituted 1,2,3-triazoles in presence of Cu (I) salts. A number of Cu (I) sources can be used directly. However it was suggested that the use of a catalyst produced by *in situ* reduction of Cu (II) salts, seems better and more effective, and are also less costly and often purer than Cu (I) salts (Rostovtsev et al. 2002). However, the use of Cu (II) requires ascorbic acid and/or sodium ascorbate as reductant, as it converts oxidized Cu (II) species to the catalytically active +1 oxidation state (Hein and Fokin 2010).

This redox cycle continuously generates reactive oxygen species (ROS) until the reducing agent is consumed. Excessive ROS may degrade delicate biomolecules to different extents, including the oxidative modification of certain amino acid residues, particularly histidine, cysteine, methionine, tryptophan, and tyrosine (Li et al. 2016). Several studies have reported the decrease in biological activity of proteins after CuAAC bioconjugation (Lallana et al. 2011). Loss in enzymatic activity of 31 % was reported after labeling the enzyme *Candida antarctica* lipase B (CalB) with an alkynated dansyl probe (Schoffelen et al. 2008). Another study reported a decrease in the immunoreactivity of an antibody used to stain a glycoprotein GlyCAM-Ig that was previously coupled by CuAAC (Agard et al. 2004).

An optimization of the bioconjugation protocol involved the application of tris(3-hydroxypropyltriazolylmethyl)amine (THPTA) that not only accelerated the CuAAC reaction, but also inhibited protein degradation by ROS (Hong et al. 2009). Despite the use of THPTA, oxidation was still registered in cysteine residues and free histidine in proteins (Nairn et al. 2015).

Reduced bioactivities and protein aggregation was also observed in our experiments utilizing CuAAC. The reaction of BMP2 E83Plk with an azide-functionalized fluorophore showed the high specificity of the reaction in presence of copper but at the same time, the intensive degree of protein multimerization when $CuSO_4$/NaAsc were used as reaction catalysts. THPTA acted as a protector in the reaction. Products of unidentified molecular weights were indeed created, appearing in the Coomassie Brilliant Blue staining as “smear” at the expected size of the protein dimer (~ 26 kDa) and also at higher molecular weight.

Moreover, the biological activity of BMP2 E83Plk coupled to the fluorophore was compromised, as shown by a decrease to ~ 40 % after 60 min of reaction. If the $CuSO_4$/NaAsc redox pair was substituted by CuBr, that being in the +1 catalytically active oxidation state does not require NaAsc, the azide conjugated BMP2 E83Plk only showed moderate aggregate formation. However, the biological activity of reaction catalyzed by CuBr was affected at a similar level if compared to the $CuSO_4$/NaAsc CuAAC after 60 min reaction. Surprisingly, the CuAAC reactions influenced the biological activity of the two Plk variants, BMP2 E83Plk and BMP2 K3Plk, in a different manner. BMP2 K3Plk was more affected by the presence of the reducing agent in the $CuSO_4$ catalyzed reaction compared to BMP2 E83Plk, but the effect was less pronounced in the CuBr catalyzed reaction in comparison to BMP2 E83Plk, using the native (unreacted) protein variants as control. The different mutation positions or altered amino acid side chains adjacent to the mutation site possibly could possibly affect the stability of the dimeric protein in response to reducing agents. An effect that could also influence the decreased bioactivity could result from fluorophore-derived steric hindrance. The use of a PEG_3 spacer between the azide group, reacting with the alkyne of the BMP2 E83Plk or K3Plk and the fluorophore, prevent the masking of the protein receptors binding sites. In case of BMP2 K3Plk, the azide-functionalized fluorophore is coupled to the alkyne of the N-terminal end that might have a higher flexibility compared to the one coupled at E38. The fluorophore at the N-terminus might then mask the wrist binding epitope avoiding the interaction with the type I receptor. In a previous study a fluorophore (without PEG) was also coupled to the N-terminal end of a BMP2 variant (BMP2 A2C), but in this case it did not mask the binding sites, possibly due to tighter bonds and with less flexibility (Paarmann et al. 2016). Another possibility for the overall decrease in activity of both variants upon reaction is that PEG_3 is known to unspecifically interact with the protein (wrapping) hence causing steric hindrance effects (Wu et al. 2014).

The use of copper (I) sources, like CuBr, was shown to be a less effective catalyst when compared to catalysts that result from *in situ* reduction of Cu (II) salts, such as $CuSO_4$. Both BMP2 Plk variants (E83Plk and K3Plk) coupled to the azide fluorophore showed a lower reaction efficacy when using CuBr. Also the coupling reaction to azide-functionalized microspheres highlighted the differences in reaction capabilities. On one hand CuBr catalyzed click chemistry caused only moderate aggregates formation, and on the other the efficacy of the reaction is highly compromised.

The need of copper ions as catalyst for the reaction makes this method ambiguous for its use in biomedical applications. The concentration of copper compounds in biological samples has

to be tightly controlled because of their cytotoxic effects. The recommended upper threshold of copper ions concentrations in biological materials should not exceed 15 ppm (parts per million, 1 mg/l = 1 ppm) (Ahmad Fuaad et al. 2013). The concentration of copper in the particular coupling reactions was approximately 8 ppm. Taking into account that after reaction the BMP2 coupled microspheres were thoroughly washed using stringent conditions, the copper concentration in final samples cannot exceed the recommended standards.

In light of the limitations of the CuAAC ligation, researchers have turned to a handful of "second generation" click reactions that are biorthogonal and catalyst-free. The strain-promoted azide – alkyne cycloaddition (SPAAC) is reaction in which the ring strain built into a cyclic alkyne drives the reaction and eliminates the need for a catalyst (van Hest and van Delft 2011). Commonly used cyclooctyne reagents are: difluorocyclooctynes (DIFO), biarylazacyclooctynones (BARAC), dibenzocyclooctynes (DBCO), dibenzoazacyclooctynes (DIBAC) on which optimization of the reactivity and development of more efficient synthetic routes for their preparation have been objectives of different groups (Lallana et al. 2011).

One of the two counterparts of the SPAAC reaction, either the strained alkyne or the azide part have to be incorporated into the protein of choice to enable SPAAC reactions. Not surprisingly, the majority of the modifications were done using functional azide groups considering its non-toxicity, relative inertness and small size, which lead to minimal perturbation of protein structure (van Hest and van Delft 2011).

The bulky and hydrophobic dibenzocyclooctynes introduced by the SPAAC ligation caused significant changes in the release kinetics of DBCO-functionalized molecules (Meyer et al. 2016). Due to a possible steric hindrance from the bulky DBCO group, the BMP2 was functionalized with the azide reactive group, while the DBCO was coupled to the scaffold.

The high specificity and efficacy of the reaction was also proven by the use of a DBCO-functionalized fluorophore. The steric hindrance caused by the presence of the bulky fluorophore in the close proximity of the receptor binding sites was circumvented by the use of spacers (PEG_4). The DBCO coupled BMP2 E83Azide maintained its biological activity *in vitro* showing a decrease to ~ 40 % compared to the unreacted protein. The same decrease in biological activity (~ 40 %) was also observed for the CuAAC reactions suggesting that the azide- or alkyne- functionalized BMP2 variants might be perturbed from the covalent coupling reaction itself or there might be a steric hindrance effect caused by the unspecific binding of PEG_3 or PEG_4. This might cause the observed decreases in bioactivity for both reactions. However, if in the case of CuAAC the presence of copper and reducing agents caused changes in the structure and therefore in the biological activity of the protein, for the

SPAAC reaction there are no data available that support the assumption that the decrease in activity is related to structural protein modifications.

It is most likely that the *in vitro* analysis of the biological activity might be influenced by other external factors that are not strictly related to the coupling technique.

An important part of this work focused on quantification methods for the evaluation of the efficacy of the CuAAC and SPAAC reactions. The analysis of protein coupled to microspheres was done in an indirect way, meaning that the amount of coupled protein was calculated by measuring the quantity of uncoupled protein in the supernatants of the particular reaction or wash steps. A direct quantification of coupled protein by common e.g. BCA (Bicinchoninic Acid) protein assays could not be performed because this method was not applicable in case of CuAAC reactions as the buffers used in the reaction interfere with the BCA method set up. Furthermore, the low amount of protein to be detected and the high variability due to the presence of microspheres made the method to be considered not accurate. However, the recombinant collagen-like peptide (RCP) microspheres consist of protein what made it impossible to distinguish between the coupled protein and the microspheres-derived protein.

Differences between the applied reaction conditions, materials or used proteins could be visualized on a qualitative basis by Western blotting, to verify the content of the particular BMP variant in the supernatants. The analysis of the supernatants gives a first impression of the uncoupled protein after the click chemistry reaction. The difference in signal detected between the BMP2 variants and the wild type BMP2 confirmed at first glance the specificity of either CuAAC or SPAAC reaction. Only a slight difference in signal between the BMP2 E83Plk83 or BMP2 E83Azide and the BMP2 WT was detected, suggesting that the wild type protein gets strongly adsorbed to the microspheres and seems hardly removable even with stringent washes. Anyhow, signals in Western blot are quite sensitive and differences observed are often overestimated. Furthermore, the outcome of the reaction depends from the type of microspheres being used. Differences in signal intensity could be observed if comparing RCP, silica and agarose microspheres. The first two types of spheres were functionalized by NHS chemistry using bivalent, PEG_3-spaced linkers with either an additional azide or DBCO group. This has a double meaning, from one side the presence of a spacer decreased the probability to mask the receptor binding sites of the protein after coupling but from the other side, the linkers needed to be coupled covalently to the microspheres. If the linkers would behave similarly as the used proteins, there is a possibility that also the linkers are just adsorbed and not coupled, thus decreasing the reaction efficacy of

protein coupling as second step. The third type of microspheres composed of agarose and already functionalized should give a more accurate information concerning this aspect. However also in this case, the differences in signal intensity detected by Western blot were not conclusive.

The first qualitative difference within the microspheres observed by Western blot analysis was then analyzed quantitatively by ELISA and radioactive labeled protein measurements.

A clear tendency with similar values was observed for the RCP and silica microspheres and different results were obtained for the agarose beads when using the above mentioned measuring techniques. The lower amount of protein being coupled to the agarose beads cannot result from the limited available DBCO functional groups/mg that are indicated from the company where the product is purchased.

This difference can still be connected to the use of the functional linker for RCP and silica beads that might provoke a different reaction efficacy compared to the agarose beads. In addition, the observed differences between the two quantification methods might be correlated with the method itself. It was previously shown that BMP2 is a sensitive protein that easily aggregates and undergoes conformational changes under physiological conditions (Luca et al. 2010). Although, some of these changes may be reversible *in vivo*, but they could be sufficient to make BMP2 less detectable by antibodies. In experiments where release studies and bioactivity analysis were included, the sensitivity of BMP2 or any other protein included in the study as well as the protein handling conditions have to be considered (Luca et al. 2010)

Several release studies showed the percentages of BMP2 released from the carriers *in vitro* after a certain period of time (Bergman et al. 2009). What was usually not shown is the amount of protein that is still present upon complete digestion of the scaffold itself. 12 % of the loaded BMP2 could be detected by ELISA in an *in vitro* release study after 28 days, but upon digestion the remaining 88 % could not be detected (Bergman et al. 2009). A large fraction of the BMP2 may be assumed to be not detected by ELISA. It is likely that the protein was adsorbed to the surface of the sample tubes during dilution or underwent conformational changes in the release medium, what make it undetectable by the antibodies (Piskounova et al. 2014).

To avoid the virtual protein loss in case of a quantification by ELISA, caused by adsorption to surfaces, sampling and dilutions, protein can be radiolabeled by e.g. ^{125}I to monitor the protein (Piskounova et al. 2014). By comparing the results obtained by ^{125}I labeled BMP2 and ELISA, a significant difference in measurements of the released protein was calculated. After

4 weeks of measurements, roughly 80 % of the protein was released (Piskounova et al. 2014), which is significantly more than the ~ 12 % measured previously by ELISA as claimed by Bergman et al..

These results support the data presented in this work, even though not to such an incongruent extend. Protein multimerization was already detected by Western blot, therefore is not surprising that the ELISA detection method revealed in general lower values of protein contained in the supernatants caused by a decreased antibody accessibility. The tritium labeled protein instead revealed higher values of uncoupled BMP2 thus resulting in lower amounts of protein being instead coupled to the microspheres therefore indicating a lower reaction efficacy.

In summary, the amount of coupled protein seems overestimated by ELISA, while the radioactive quantification method might result in an underestimation of the coupled protein. The labeled protein might contain traces of the used small tritium, despite harsh washing steps and therefore can still be detected in the reactions.

Albeit, the validation of the reaction efficacy by radioactive labeled protein might provide more accuracy, this method was not sensitive enough to show differences between the two CuAAC catalyzed methods. The efficacy of the CuAAC reaction performed with CuBr as catalyst was much lower if compared to $CuSO_4$/NaAsc catalyzed reactions. These results were proven by the significantly lower fluorescence signal after SDS-PAGE when BMP2 E83Plk was coupled to the azide-functionalized fluorophore and in the stronger Western blot signals that were observed for the supernatants of the CuBr reactions after coupling to the azide-functionalized microspheres. However, these efficacy differences between $CuSO_4$ and CuBr catalyzed reactions did not correspond to evaluations performed by radioactively labeled proteins, where no difference between the two used catalysts was shown. Therefore, the quantification by radioactive labeled protein might be disturbed by traces of free tritium and hence not being accurate enough, it was concluded that the $CuSO_4$ was the most efficient reaction relying on the fluorophore experiments. The following CuAAC reactions were performed by using $CuSO_4$ as catalyzer.

Another important difference was noticed when comparing the amount of coupled protein (BMP2 E83Plk or BMP2 E83Azide) to the control BMP2 WT. When comparing ELISA and radiolabeled protein, the amount of BMP2 E83Plk or BMP2 E83Azide coupled to the microspheres was not significantly different if compared to that of the wild type protein. According to these results obtained by two different detection methods, it could be concluded that the majority of the applied proteins is just adsorbed to the beads and could not be

removed by washing with 6 M urea buffers. Additionally, the use of harsher conditions such as 6 M GuCl were tested but causing a strong degradation of the microspheres.
This conclusion could be easily excluded by referring to the reaction specificity observed with the azide- or DBCO- functionalized fluorophores. For either CuAAC or SPAAC reaction any fluorescent signal was detected for the BMP2 WT.
Therefore, it is more plausible that also in the reaction with the microspheres the BMP2 variant are, at least partially, covalently coupled and not just adsorbed. What remains still open and could not be determined by the quantification methods is the portion of covalently coupled protein over the adsorbed one. An additional hint on this result is given from the ALP staining using BMP2 variant coupled beads compared to the wild type one. The staining restricted to the close proximity of the beads for the BMP2 E83Plk or BMP2 E83Azide confirms that the protein are indeed covalently coupled, because as observed for the wild type protein a more diffuse staining at further distance would be observed.

In summary, the *in vitro* analyses of the CuAAC and SPAAC reactions provided an overview on the coupling reaction mechanisms, on the effects of the reactions on protein structure and biological activities and highlighted the difficulties related to the determination of the reaction efficacy which is influenced by several factors. CuAAC reactions caused the formation of multimers at a higher extend in the $CuSO_4$ catalyzed reaction than the CuBr but influencing the biological activity in the same way. The higher efficacy of the $CuSO_4$ reactions proposed to use this catalyst for the *in vitro* analysis and final animal experiment. SPAAC reactions showed high efficacy and specificity without affecting protein structure and biological activity. This section described in detail all aspects of BMP2 application and the difficulties to exactly monitor the production of implants and the individual product outcome.

3. The new variant BMP2 E83Azide induces formation of ectopic bone tissue *in vivo*

Ectopic bone refers to ossification of tissues away from their original place, where the word “ectopic” originates from the Greek word *ektopos* (away from a place) (Scott et al. 2012). Ectopic bone formation has mainly been connected to congenital or inherited malformation or to complication of various conditions such as paraplegia, post burn or traumatic injury (Scott et al. 2012). Such pathologic formation of bone in soft tissues such as muscle, subcutaneous

tissue, and fibrous tissue adjacent to joints is called heterotopic ossification (HO). One of the most severe forms of ectopic bone formation is represented by the inheritable disease fibrodysplasia ossification progressiva (FOP) being caused by mutations in the ACVR1 gene (Shore et al. 2006).

The underlying mechanism of heterotopic ossification is not well understood. One theory is that HO results from the differentiation of osteogenic progenitors that are induced by various local and/or systemic factors. Theoretically cells from ectodermal or endodermal origin could give rise to osteogenic lineage cells and directly contribute to HO through the process of epithelial to mesenchymal transition (EMT) (Mani et al. 2008) or endothelial to mesenchymal transition (EndMT) (Kovacic et al. 2012). Current data suggest that epithelial cells may secrete BMPs or other osteogenic factors and thereby contribute to HO indirectly, but they do not directly give rise to osteogenic lineage cells. Instead, several observations on the ability of endothelial cells to undergo EndMT and generate ectopic calcification have suggested that cells of endodermal origin could contribute to HO (Ranchoux et al. 2015, Dudley et al. 2008). Endothelial cells highly express BMP receptors, and BMP receptor/SMAD activation stimulates endothelial cells migration and tube formation, indicating a role for BMP in regulating the organization and differentiation of the newly formed endothelial cells in a capillary network (Valdimarsdottir et al. 2002). In addition, BMPs have the ability to redirect the differentiation of endothelial progenitor cells to orchestrate EndMT in these cells, often through inflammatory cell intermediates (Matsumoto et al. 2008, Valdimarsdottir et al. 2002). Furthermore, misexpression of constitutively active ACVR1/ALK2, a BMP type-I receptor encoded by the gene being mutated in FOP, caused morphological changes of endothelial cells to a mesenchymal like cells and induced co-expression of mesenchymal (Fibroblast specific protein 1, FSP-1) and endothelial marker (Tie2) (Medici et al. 2010).

These observations were interpreted as evidence that endothelial cells could contribute to HO. Unfortunately, Tie2 is expressed also in other endothelial cells types, including pro-angiogenic monocytes of hematopoietic origin (Matsubara et al. 2013, De Palma et al. 2005) but also in pericytes precursors (Teichert et al. 2017) being of mesenchymal origin. Other data also suggest that endothelial cells might regulate osteogenic differentiation of other cells, like mesenchymal cells, thus contributing to HO indirectly by an endothelial-mesenchymal cells crosstalk (Bidarra et al. 2011, Saleh et al. 2011). These facts propose that cells of mesodermal origin are the main candidate for HO.

The characteristic features of MSCs are the abilities to self-renew and to differentiate into all mesodermal lineage cells, including osteoblasts, chondrocytes, adipocytes, smooth muscle

cells, and myocytes, but not hematopoietic cells (Kan and Kessler 2014). The lack of MSC-specific markers prevents the unequivocal demonstration of MSC contribution to HO. Wosczyna el al. found $Tie2^+$ cells in HO models in mice, and further analyses revealed a non-endodermal origin of these cells as 90 % of these cells were $PDGFRa^+$ and $Sca1^+$ (both are MSC progenitor cell markers) (Wosczyna et al. 2012, Lounev et al. 2009). The $Tie2^+PDGFRa^+Sca1^+$ cells showed multipotency and exhibited the capacity for both BMP-dependent osteogenic and spontaneous adipogenic differentiation (Wosczyna et al. 2012). These cells were shown to be located in the interstitial spaces within skeletal muscle of both mouse and human (Oishi et al. 2013, Wosczyna et al. 2012, Uezumi et al. 2010). Another study suggested that different subpopulation of mesenchymal progenitors cells, glutamate aspartate transporter (GLAST)-expressing cells, may also contribute to HO (Kan et al. 2013).
Among the overall mesenchymal progenitor cell pool that contribute to HO, muscle satellite cells that are muscle-specific stem cells responsible for skeletal muscle growth and regeneration, have received considerable attention for their capacity of BMP-dependent osteogenic differentiation in cell-based assays (Katagiri et al. 1994). It is questionable whether the muscle environment provides unique and essential growth, survival or differentiation factors required for the differentiation into the osteogenic lineage of more widely distributed progenitor cell populations, or that the osteoprogenitor cells responsible for heterotopic ossification are restricted to skeletal muscle and associated soft tissues. The osteogenic *in vitro* response of satellite cells, was not confirmed *in vivo*, where they showed having a minimal role in the development of HO (Wada et al. 2002, Lounev et al. 2009, Oishi et al. 2013), whereas the evidence for others, such as circulating osteogenic mesenchymal precursors, is stronger. Recent studies identified the existence of different osteogenic mesenchymal precursors in the circulation such as bone marrow-derived osteoblast progenitor cells (MOPCs) for their contribution to HO. In a BMP-induced model, GFP^+ MOPCs were transplanted in mice and after 3 weeks a significant number of GFP^+ osteoblastic cells were found in the newly generated HO (Otsuru et al. 2007). This suggests that bone marrow-derived osteoblasts progenitors cells could be an important contributor to HO *in vivo*.

Recalling the use of Greek it is possible to explain also the other form of bone formation called orthotopic bone formation. The word *orthos* means “straight, right”, indicating studies in which bone is formed at its correct anatomical location. Injection of material into the long bone periosteum or into calvarial defects, involves different mechanisms if compared to ectopic bone formation. Transplantation into a long bone defect of biomaterials supplemented

with cells or growth factors is subjected to significant stress/strain forces with weight-bearing and locomotion. The presence of biomechanical forces involves a cascade of signaling events leading to the formation of bone tissue by a process called “mechanotransduction” (Allori et al. 2008).

In contrast, ectopic bone models are completely lacking mechanical forces. The absence of mechanotransduction signals, allows the removal of potential extraneous experimental variables (Scott et al. 2012). Subcutaneous or intramuscular implantation models represent the two mainly used ectopic models.

Subcutaneous implantation is the easiest experimental model to study ectopic bone formation. It is easy to perform from a surgical point of view and can be applied to a variety of mammalian animal models, such as mouse, rat, rabbit, dog, pig and many others. Rodents are most widely used due to the low costs, soft skin that allows the insertion of implants of larger volume, easy handling and availability of immune-deficient rodents for xenograft-based experiments (Scott et al. 2012). Bone marrow-derived mesenchymal stem cells (BMSCs) represent the most studied cell type, however, the lack of an osteogenic environment when implanted subcutaneously brings up the necessity to add growth factors such as BMP2 and/or vascular endothelial growth factor (VEGF) (Zhang et al. 2014a, Tadokoro et al. 2012). The theoretical lack of native bone forming stem cells within the intradermal environment needs also to be considered. Studying the effects induced by exogenous stem cells or by the used biomaterials on ectopic bone formation might be advantageous or disadvantageous, respectively. Additionally, the reduced vascularization and blood flow, together with the lack of cells able to send osteogenic differentiation signals could result in inferior bone forming capacities if compared to other ectopic models, such us the intramuscular model (Scott et al. 2012).

However, studies concerning this topic are controversial discussed. For instance, the use of BMP2 loaded scaffolds was reported to induce higher bone formation in an intramuscular model if compared to a subcutaneous model (Yoshida et al. 1998), whereas others did not observe any differences. It is important to note that different doses have been applied: the first group used 5 µg (Yoshida et al. 1998) and the second 20 µg (Ma et al. 2015). It cannot be excluded that different dosages caused differential effects comparing the two models. The highest dosage of 20 µg did not show any difference in bone formation between the intramuscular and subcutaneous site, probably related to a saturation effect thus preventing a further increase in bone formation.

The use of intramuscular implantation models, as the first one being used after the discovery of BMPs, has been exploited also in human patients. BMP7 loaded collagen mixed with donor bone marrow was used to fill a titanium mesh cage and implanted into the patient`s latissimus dorsi muscle and after 7 weeks implantation the bone-muscle flap was transplanted into the mandibular defect site (Warnke et al. 2004).

The choice of the most conclusive animal model should be taken according to the experimental questions that need to be answered by the particular model. The use of animal models is essential to evaluate biocompatibility, tissue responses and mechanical function of e.g. orthopedic or dental implants prior to clinical use in human (Pearce et al. 2007).

In vitro testing should be primarily used as a first stage test in order to avoid the unnecessary use of animals in the testing of cytologically inappropriate materials. The first information regarding cytotoxicity, genotoxicity, cell proliferation and differentiation and as well as material screening in terms of potentially harmful additives incorporated during the manufacturing process it is based on *in vitro* testing.

Cell-based assays were used at first to evaluate the biological activity of the new BMP2 variants. The mouse pre-myoblast cell line (C2C12) were used to test ALP expression after exposure to both BMP2 E83Plk83 or BMP2 E83Azide always using the wild type BMP2 as positive control. The biological activity of the new BMP2 variants BMP2 E83Azide (EC_{50} 34.2 nM) was identical to that of wild type BMP2 (EC_{50} 31.4 nM), while BMP2 E83Plk appeared 1.9-fold less bioactive (EC_{50} 64.9 nM) than wild type BMP2. The introduction of the artificial amino acids in close proximity of the receptor binding sites did not or just marginally influence the variant’s bioactivity.

A similar outcome was shown after the coupling. BMP2 E83Plk coupled to the azide-functionalized microspheres or BMP2 E83Azide coupled to DBCO-functionalized microspheres, induced ALP expression in C2C12 cells after exposure to the osteoinductive microspheres. Alkaline phosphatase staining was restricted to the cells in direct contact with the microspheres in case of the BMP2 variants, while for the wild type protein, staining could also be observed in further distances indicating that ALP expression was induced by diffusible BMP2 molecules. The presence of wild type protein on the microspheres after the stringent washes might be attributed to the highly adsorptive capacity of the microspheres.

The *in vitro* tests by ALP staining confirmed the maintained biological activity of the two BMP2 variants after the click chemistry reactions. Moreover, the restricted staining, in case of the BMP2 variants, indicates that the majority of the protein seems indeed covalently

immobilized with a portion of adsorbed protein. The possible presence of adsorbed protein seems not enough to induce ALP even in close neighborhood of the applied microspheres.

According to the outcome of the *in vitro* studies, a subcutaneous animal model was planned in order to test the ability of the covalently coupled protein to induce bone formation, investigating also the effects of different applied protein dosages. A paste only composed of RCP microspheres coupled with one of the BMP2 variants or adsorbed with BMP2 WT was used as bone inducing injectable material.

Different studies already explored the diversity of reactions in bone formation in terms of quality and quantity (Park et al. 2012) in various ectopic and orthotopic models in relation to the applied dosages (Ben-David et al. 2013, Lee et al. 2010, Zara et al. 2011, Mumcuoglu et al. 2018b, Yoshida et al. 1998, Park et al. 2012). The use of high doses of BMP2 was proven to induce structurally abnormal bone, indicating that increasing BMP2 doses beyond certain thresholds does not further improve bone healing, and is indeed producing a lower bone quality with abnormal structure. Cyst-like bone voids filled with adipose tissue were found instead of trabecular bone impeding e.g. complete bone union (Zara et al. 2011). In this study, three concentrations of the coupled BMP2 variants were tested and compared to the same doses of just adsorbed BMP2 WT: 10 µg, 1 µg and 0.1 µg. Four weeks after implantation, only for the highest doses (10 µg) formation of bone tissue could be observed. Surprisingly only the BMP2 E83Azide variant and wild type BMP2 induced formation of ectopic bone whereas BMP2 E83Plk did not. The reasons of the negative outcome of this experiment still remain elusive. The complete absence of bone formation could be connected to the observed effects that copper induced on the BMP2 E83Plk. Distinctive multimers formation was detected after the reaction; nevertheless the coupled BMP2 E83Plk variant appeared biologically active *in vitro* as shown by ALP expression staining. It might be possible that the real dose injected into the animals did not correspond to the quantities calculated by ELISA or radioactive labeled protein and therefore maybe much less was applied in the animals. Therefore, the concentration of the protein could have been too low or with lower bioactivity caused by the $CuSO_4$/NaAsc to initiate the required process which at long term result in the formation of ossicles. In contrast to BMP2 E83Plk, the BMP2 E83Azide and the BMP2 WT were able to induce ectopic formation of bone but only at the highest concentration (10 µg), while the lowest dosages (1 µg and 0.1 µg) did not induce any bone formation.

In the previous study performed with the same range of doses, BMP2 WT of the same batch was adsorbed onto RCP microspheres and then embedded in alginate hydrogel (Mumcuoglu

et al. 2018b). Ectopic bone formation was observed already from week 2 for the highest dose (10 µg) and a dose-dependent increase in bone volume and density was shown over the 10 weeks of implantations. In this study instead, the RCP microspheres were used as a direct injectable paste. The use of the hydrogel was avoided since the protein is supposed to be covalently coupled and therefore, cannot ideally diffuse. The protein trapped in the hydrogel would be masked and possible not be able to induce any signal in the environment until the hydrogel is degraded.

The injection of RCP microspheres encapsulated in hydrogel of different nature, such as alginate or hyaluronic acid hydrogels, provoke an inflammation which was detected already after one week post-implantation ((Fahmy-Garcia et al. 2018) unpublished data). The inflammatory milieu is indeed required for the development of ectopic bone formation (Kunihiro Tsuchida 2013) since injury in soft tissues triggers the upregulation of BMP signaling in the inflammatory environment, which together with increased expression of other osteogenic cytokines induces ectopic and heterotopic ossification (Yu et al. 2008).

The study of Fahmy-Garcia et al. showed that hyaluronic acid induced high levels of inflammation over the whole experimental time (up to 10 weeks) indicated by $iNOS^+$ and $CD206^+$ cells infiltrating the implant while the alginate hydrogel induced an initial inflammatory phase that declined over time. The strong inflammatory effect of the hyaluronic acid implants influenced also the quality of the formed bone that was much lower compared to the alginate. Other studies have shown that the implantation of a collagen sponge loaded with BMP2 WT induced an inflammation lasting the first 7 days. The inflammatory volume that is represented from the edema measured by magnetic resonance imaging scanner showed a peak at day 2. The inflammatory area that represented by inflammatory cellular infiltration evaluated by histology registered a peak at day 7. After a rapid initial extravasation, the inflammatory edema is reabsorbed in a time-dependent manner (Xiong et al. 2013). The fibrotic tissue surrounding the implant consists of fibroblasts and granulated tissue that replaces the edematous exudate. The presence of fibrotic tissue around the implant was observed also in this study by $vimentin^+$ cells detected around the implant. $Vimentin^+$ cells were also found in proximity to and within the implants. This suggests that not all stained cells represent fibroblasts since vimentin expression is not restricted to fibroblasts bus also in proliferative cells of mesenchymal origin (Lian et al. 2009). $CD68^+$ cells were found in both BMP2 WT and BMP2 E83Azide implants, mainly outside of the implants but also surrounding remnants of RCP microspheres in the inner part of the implant, probably due to an infiltration processes. However, CD68 is not a specific inflammatory marker, as iNOS or

CD206. $CD68^+$ cells were associated with osteomacs, cells involved in the remodeling process (Chang et al. 2008). Therefore, it is not possible to conclude whether or not, an inflammatory process was also induced and still present in our study at the end of the animal experiment. The absence of a hydrogel in our paste formulation might have triggered a lower host inflammatory response or induced a similar reaction like the alginate hydrogel ((Fahmy-Garcia et al. 2018) unpublished data).

The timeline of bone formation was comparable to other subcutaneous implantation studies (Meretoja et al. 2014, Bae et al. 2013, Todeschi et al. 2017, Lee et al. 2010). The common time frame for the evaluation of ectopic bone forming processes in subcutaneous models is typically 4 to 8 or 12 weeks. The previous study from Fahmy-Garcia et al. (unpublished data) and from Mumcuoglu et al. showed initial bone formation already at week 2, possibly due to the strong inflammation reaction induced by the hydrogels and by the consequent dense material formation reminiscent to calcification that did not always result in bone formation as it was observed in other studies (Kim et al. 2005).

The initial inflammatory process seems beneficial in terms of cell recruitment homing osteoinductive cells to the implantation site already in the first weeks. The intensity of a stronger inflammation reaction might also set an earlier timeline in the recruitment of osteoinducing cells. The presence of PEGylated functional linkers used to couple the protein to the microspheres in both click reactions might provoke immune reaction (Schellekens et al. 2013). Tetra(ethylene glycol) (PEG_4) used here as a backbone of the heterobifunctional linker, NHS-PEG_4-DBCO, has no exposed terminus upon conjugation, and its short length greatly minimizes the immunogenic potential (Saifer et al. 2014). The PEG_4 spacer is very hydrophilic. The 30 Å (25 atoms) long linker acted as a spacer between the protein and the microspheres, thus allowing an easier interaction of the protein with the cellular receptors. The absence of the linker would have arranged the BMP2 E83Azide and the RCP microspheres at minimal distances, probably masking the receptors binding sites on the coupled BMP2 protein. In any case, even after binding BMP2 E83Azide to the DBCO group of the linker, the possible steric hindrance effects are minimized due to the orientation of the azide functional group on the BMP2 variant.

This resulted in the maintained biological activity of the coupled BMP2 Azide83 to RCP microspheres *in vivo* as shown by the positive outcome of our subcutaneous rat model. Assessment with microCT revealed the presence of ossified implants from week 4 until week 12. Evaluation of bone density (BD) and bone volume (BV) was performed during the whole experimental time. Although not statistically significant, BMP2 E83Azide-functionalized

microspheres, showed a trend to produce larger total BV while the BD resulted in the same range. The bone volume for both, BMP2 E83Azide and BMP2 WT registered a peak at week 6 with a steady state until week 12. On the other side BD continued to increase over the 12 weeks.

Albeit, it was not possible to conclude the real amount of covalently coupled protein after the click reaction, the outcome of the animal experiment revealed a difference in the two formed ossicles. The different bone morphologies observed in the two conditions, suggested that the different "release kinetics" of the proteins had significantly influenced cell recruitment and bone formation. The BMP2 WT adsorbed within the paste induced the formation of dense cortical bone, while covalently coupled protein demonstrated a more uniform, sponge-like bone formation throughout the entire sample. Even though the biomaterial has the same characteristics and should allow an easier cell infiltration, the shorter diffusion distance given from the absence of an encapsulating hydrogel might be connected with the observed outcome (Hulsart-Billstrom et al. 2013). The histological examination showed remarkable differences in bone formation connected to the different immobilization techniques.

The release profile of the adsorbed wild type protein is directed from the implant to the subcutaneous environment. The newly formed bone has indeed this structure, the bone shell outside formed from the osteogenic stimuli given from the released protein and abundant adipose tissue inside. While in the BMP2 E83Azide implants, the bone formed around the single microspheres, encapsulating them in the newly formed bone, with less adipose tissue. The final ossicles showed a much higher percentage of microspheres throughout the implants compared to the wild type induced ones, where almost no microspheres could be detected.

The observed differences indicate that the BMP2 E83Azide seems indeed covalently coupled. However, the proportion between coupled and adsorbed protein is still unknown. In any case, independently from the percentage of coupled protein over the just adsorbed one, it was possible to detect different bone morphologies. Supposing that the protein is released also in the BMP2 E83Azide situation, the cells infiltrated into the implant driven by the chemotactic signals of the potentially released BMP2 Azide83, inducing new bone formation also in the inner part of the implant.

The lowest concentrations (1 µf and 0.1 µg) of either BMP2 WT or BMP2 E83Azide, did not induce ectopic bone formation. In case of adsorbed BMP2 WT, this could be connected to the absence of hydrogel, because as observed by Mumcuoglu et al. the presence of hydrogel minimized the release of protein *in vivo* that then induced bone formation. In case of the

covalently coupled protein, the portion of protein that might be released would show most likely the same fast release profile of the wild type protein, therefore not able to recruit cells at the implantation site where covalently coupled protein was available.

Histological evaluation of the implants focused on the identification of cells involved in the bone formation process. Osteocytes embedded in lacunae are spread within the cortical bone matrix where also the unmineralized organic portion, the osteoid, is detectable.
Knowing that, bone development occurs by two distinct processes: intramembranous ossification (IMO) and endochondral ossification (ECO). The IMO process is characterized by mesenchymal stem cells differentiating directly into osteoblasts and eventually producing bone (Shapiro 2008). While ECO, is characterized by a cartilaginous template anlage and it is involved in fracture healing. Regions of cartilage formation were detected in all histological sections of the newly formed bone indicating endochondral ossification process.
Osteocytes, bone lining osteoblast and remaining cartilaginous tissue could be distinguished in the hard tissue components whereas vimentin$^+$ fibroblasts were located around the implants. Blood vessels could be well distinguished in the hematoxylin & eosin staining, and where possible by α-SMA$^+$ cells. CD68$^+$ cells were detected around the BMP2 WT induced ossicles, while in case of BMP2 E83Azide were around the implant and also in the inner part surrounding the still available microspheres. CD68 is a macrophage marker (lysosomal-associated transmembrane glycoprotein) highly expressed by human tissue macrophages. Its expression was associated with osteomacs, cells that are involved in bone homeostasis (Chang et al. 2008). In this study, the presence of these cells was connected with a possible osteoclastogenesis process occurring at the time of the implants retrieval.
Osteoclasts activity was visualized by TRAP positive staining which scattered along the edge of newly formed bone matrix, demonstrating an active cartilage and bone remodeling. The inflammatory response is not unexpected, as BMP2 is a known chemoattractant for lymphocytes, monocytes, and macrophages (Cunningham et al. 1992), even though it was unexpected to be detectable at 12 weeks after implantation.

In summary, the first subcutaneous *in vivo* experiment of covalently coupled BMP2 could show the maintained bioactivity of the protein and the generation of ectopic bone in a more uniform way compared to the wild type protein. This study showed several limitations that have to be addressed in future animal experiment.

V. Conclusion

This work demonstrated the successful generation of BMP2 variants harboring artificial amino acids at specific positions of the BMP2 protein. However, the position of the mutation impacted on the protein expression, refolding and bioactivity of BMP2 E94Plk while the other BMP2 variants E83Azide and E83Plk showed similar bioactivities as the wild type protein. The functionalized proteins revealed high reaction efficacy when coupled to the respective functionalized fluorophores by either CuAAC or SPAAC reactions. Despite showing multimers formation upon CuAAC reaction, BMP2 E83Plk was able to induce ALP expression in a cell-based assay. However, this protein coupled to microspheres failed to induce ectopic bone formation *in vivo*. The BMP2 E83Azide coupled by copper free reaction to microspheres induced ALP expression *in vitro* and ectopic bone formation *in vivo*.

The validation of the coupling efficacy was the main limitation. Different possible methods for protein quantification were investigated such as ELISA and scintillation counting of radioactively labeled proteins. Nevertheless, both methods were not able to reveal the exact quantity of protein on the microspheres after the coupling reactions. In detail, the main limiting problem was that it was impossible to state what amount of protein was covalently coupled and how much protein was adsorbed from the microspheres. The outcome of the animal experiment revealed a different bone morphology between the BMP2 E83Azide-functionalized microspheres and the BMP2 WT microspheres were the protein is just adsorbed. The histological examination of the ectopic bone suggested indeed a different release mechanism between the wild type protein and the BMP2 variant. The released wild type BMP2 induced a shell-like structure as indication of a protein release from the implant to the environmental tissue, while the BMP2 E83Azide induced a more uniform bone formation throughout the implants and not just restricted to the outer layer. From these observations it can be concluded that BMP2 E83Azide is at least partially covalently coupled but to what extend is unknown and need to be elucidated in future experiments. The main aim of the animal experiment was to prove the possibility to induce bone formation with lower doses compared to the adsorbed wild type protein. Different from the above mentioned hypothesis, microspheres coupled with low amounts of BMP2 variants were unable to induce bone formation whereas high doses were shown to mediate subcutaneous ectopic bone formation.

The outcome of this study provides interesting results in the BMP2-driven bone regeneration field. However, it remains elusive how much protein is actually coupled to the microspheres. To answer this question, further investigations or alternative approaches are urgently needed.

VI. Outlook

The outcome of this study revealed the need for further investigations on different aspects regarding the protein variants and the coupling methods. Considering the coupling reactions, a detailed investigation of the effects on the protein upon coupling reaction could be performed. However, further studies should mainly focus on the BMP2 E83Azide coupled by SPAAC to microspheres and the osteoinductive properties in follow-up animal experiment. In detail, it would be more useful to investigate this method in orthotopic models rather than ectopic, since the final aim of future clinical applications is to use BMP2 for critical size bone defects and to avoid the severe side effects associated with the high amount of protein currently used. One of the main modifications would be applied to the protein itself by removing the heparin binding site at the N-terminus. As was previously proven BMP2 variants without heparin binding site showed a lower binding ability to scaffolds. Therefore, this would certainly decrease the observed unspecific adsorptive binding. Moreover, using these new BMP2 variants in an extra animal experiment, bone formation should be evaluated at different time points in order to investigate cells infiltration and bone formation mechanisms. For this aim, in order to study the different release kinetics *in vivo*, fluorescently labeled proteins could be used to trace the release during experimental time. Furthermore, radiolabeled proteins could also be used *in vivo* to quantify the amounts of BMP that is still contained in the ossicles at different time points.

Several aspects still need to be investigated; however, the first results obtained from the animal study indicated that covalently immobilized protein could represent the promising strategy for translational bone regeneration applications.

Bibliography

AGARD NJ, PRESCHER JA AND BERTOZZI CR. 2004. A strain-promoted [3 + 2] azide-alkyne cycloaddition for covalent modification of biomolecules in living systems. J Am Chem Soc 126: 15046-15047.

AGARWAL R AND GARCIA AJ. 2015. Biomaterial strategies for engineering implants for enhanced osseointegration and bone repair. Adv Drug Deliv Rev 94: 53-62.

AHMAD FUAAD AA, AZMI F, SKWARCZYNSKI M AND TOTH I. 2013. Peptide conjugation via CuAAC 'click' chemistry. Molecules 18: 13148-13174.

AI-AQL ZS, ALAGL AS, GRAVES DT, GERSTENFELD LC AND EINHORN TA. 2008. Molecular mechanisms controlling bone formation during fracture healing and distraction osteogenesis. J Dent Res 87: 107-118.

ALLORI AC, SAILON AM, PAN JH AND WARREN SM. 2008. Biological basis of bone formation, remodeling, and repair-part III: biomechanical forces. Tissue Eng Part B Rev 14: 285-293.

BAE IH, JEONG BC, KOOK MS, KIM SH AND KOH JT. 2013. Evaluation of a thiolated chitosan scaffold for local delivery of BMP-2 for osteogenic differentiation and ectopic bone formation. Biomed Res Int 2013: 878930.

BALTZER AW, LATTERMANN C, WHALEN JD, WOOLEY P, WEISS K, GRIMM M, GHIVIZZANI SC, ROBBINS PD AND EVANS CH. 2000. Genetic enhancement of fracture repair: healing of an experimental segmental defect by adenoviral transfer of the BMP-2 gene. Gene Ther 7: 734-739.

BAUER S, PARK J, PITTROF A, SONG YY, VON DER MARK K AND SCHMUKI P. 2011. Covalent functionalization of TiO2 nanotube arrays with EGF and BMP-2 for modified behavior towards mesenchymal stem cells. Integr Biol (Camb) 3: 927-936.

BEGAM H, NANDI SK, KUNDU B AND CHANDA A. 2017. Strategies for delivering bone morphogenetic protein for bone healing. Mater Sci Eng C Mater Biol Appl 70: 856-869.

BEHR B, SORKIN M, LEHNHARDT M, RENDA A, LONGAKER MT AND QUARTO N. 2012. A comparative analysis of the osteogenic effects of BMP-2, FGF-2, and VEGFA in a calvarial defect model. Tissue Eng Part A 18: 1079-1086.

BEN-DAVID D, SROUJI S, SHAPIRA-SCHWEITZER K, KOSSOVER O, IVANIR E, KUHN G, MULLER R, SELIKTAR D AND LIVNE E. 2013. Low dose BMP-2 treatment for bone repair using a PEGylated fibrinogen hydrogel matrix. Biomaterials 34: 2902-2910.

BERGMAN K, ENGSTRAND T, HILBORN J, OSSIPOV D, PISKOUNOVA S AND BOWDEN T. 2009. Injectable cell-free template for bone-tissue formation. J Biomed Mater Res A 91: 1111-1118.

BESSA PC, CASAL M AND REIS RL. 2008. Bone morphogenetic proteins in tissue engineering: the road from laboratory to clinic, part II (BMP delivery). J Tissue Eng Regen Med 2: 81-96.

BESSHO K, TAGAWA T AND MURATA M. 1989. Purification of bone morphogenetic protein derived from bovine bone matrix. Biochem Biophys Res Commun 165: 595-601.

BETZ OB, BETZ VM, NAZARIAN A, PILAPIL CG, VRAHAS MS, BOUXSEIN ML, GERSTENFELD LC, EINHORN TA AND EVANS CH. 2006. Direct percutaneous gene delivery to enhance healing of segmental bone defects. J Bone Joint Surg Am 88: 355-365.

BIDARRA SJ, BARRIAS CC, BARBOSA MA, SOARES R, AMEDEE J AND GRANJA PL. 2011. Phenotypic and proliferative modulation of human mesenchymal stem cells via crosstalk with endothelial cells. Stem Cell Res 7: 186-197.

BISHOP GB AND EINHORN TA. 2007. Current and future clinical applications of bone morphogenetic proteins in orthopaedic trauma surgery. Int Orthop 31: 721-727.

BOERCKEL JD, KOLAMBKAR YM, DUPONT KM, UHRIG BA, PHELPS EA, STEVENS HY, GARCIA AJ AND GULDBERG RE. 2011. Effects of protein dose and delivery system on BMP-mediated bone regeneration. Biomaterials 32: 5241-5251.

BONAFE L ET AL. 2015. Nosology and classification of genetic skeletal disorders: 2015 revision. Am J Med Genet A 167A: 2869-2892.

BONEWALD LF. 2007. Osteocytes as dynamic multifunctional cells. Ann Ny Acad Sci 1116: 281-290.

BONFIELD W. 2006. Designing porous scaffolds for tissue engineering. Philos Trans A Math Phys Eng Sci 364: 227-232.

BOYAN BD, HUMMERT TW, DEAN DD AND SCHWARTZ Z. 1996. Role of material surfaces in regulating bone and cartilage cell response. Biomaterials 17: 137-146.

BOYNE PJ, MARX RE, NEVINS M, TRIPLETT G, LAZARO E, LILLY LC, ALDER M AND NUMMIKOSKI P. 1997. A feasibility study evaluating rhBMP-2/absorbable collagen sponge for maxillary sinus floor augmentation. Int J Periodontics Restorative Dent 17: 11-25.

BRAZIL DP, CHURCH RH, SURAE S, GODSON C AND MARTIN F. 2015. BMP signalling: agony and antagony in the family. Trends Cell Biol 25: 249-264.

BROWN KV, LI B, GUDA T, PERRIEN DS, GUELCHER SA AND WENKE JC. 2011. Improving bone formation in a rat femur segmental defect by controlling bone morphogenetic protein-2 release. Tissue Eng Part A 17: 1735-1746.

BUDIRAHARJO R, NEOH KG AND KANG ET. 2013. Enhancing bioactivity of chitosan film for osteogenesis and wound healing by covalent immobilization of BMP-2 or FGF-2. J Biomater Sci Polym Ed 24: 645-662.

BURKUS JK, TRANSFELDT EE, KITCHEL SH, WATKINS RG AND BALDERSTON RA. 2002. Clinical and radiographic outcomes of anterior lumbar interbody fusion using recombinant human bone morphogenetic protein-2. Spine (Phila Pa 1976) 27: 2396-2408.

CAHILL KS, CHI JH, DAY A AND CLAUS EB. 2009. Prevalence, complications, and hospital charges associated with use of bone-morphogenetic proteins in spinal fusion procedures. JAMA 302: 58-66.

CARRAGEE EJ, HURWITZ EL AND WEINER BK. 2011. A critical review of recombinant human bone morphogenetic protein-2 trials in spinal surgery: emerging safety concerns and lessons learned. Spine J 11: 471-491.

CELESTE AJ, IANNAZZI JA, TAYLOR RC, HEWICK RM, ROSEN V, WANG EA AND WOZNEY JM. 1990. Identification of transforming growth factor beta family members present in bone-inductive protein purified from bovine bone. Proc Natl Acad Sci U S A 87: 9843-9847.

CHACKO BM, QIN B, CORREIA JJ, LAM SS, DE CAESTECKER MP AND LIN K. 2001. The L3 loop and C-terminal phosphorylation jointly define Smad protein trimerization. Nat Struct Biol 8: 248-253.

CHANG MK, RAGGATT LJ, ALEXANDER KA, KULIWABA JS, FAZZALARI NL, SCHRODER K, MAYLIN ER, RIPOLL VM, HUME DA AND PETTIT AR. 2008. Osteal tissue macrophages are intercalated throughout human and mouse bone lining tissues and regulate osteoblast function in vitro and in vivo. J Immunol 181: 1232-1244.

CHARLES JF AND ALIPRANTIS AO. 2014. Osteoclasts: more than 'bone eaters'. Trends Mol Med 20: 449-459.

CHATZINIKOLAIDOU M, LICHTINGER TK, MULLER RT AND JENNISSEN HP. 2010. Peri-implant reactivity and osteoinductive potential of immobilized rhBMP-2 on titanium carriers. Acta Biomater 6: 4405-4421.

CHEN D, JI X, HARRIS MA, FENG JQ, KARSENTY G, CELESTE AJ, ROSEN V, MUNDY GR AND HARRIS SE. 1998. Differential roles for bone morphogenetic protein (BMP) receptor type IB and IA in differentiation and specification of mesenchymal precursor cells to osteoblast and adipocyte lineages. J Cell Biol 142: 295-305.

CHENG H ET AL. 2003. Osteogenic activity of the fourteen types of human bone morphogenetic proteins (BMPs). J Bone Joint Surg Am 85-A: 1544-1552.

CHO TJ, GERSTENFELD LC AND EINHORN TA. 2002. Differential temporal expression of members of the transforming growth factor beta superfamily during murine fracture healing. J Bone Miner Res 17: 513-520.

CLARKE B. 2008. Normal bone anatomy and physiology. Clin J Am Soc Nephrol 3 Suppl 3: S131-139.

CRANE JL AND CAO X. 2014. Bone marrow mesenchymal stem cells and TGF-beta signaling in bone remodeling. J Clin Invest 124: 466-472.

CUNNINGHAM NS, PARALKAR V AND REDDI AH. 1992. Osteogenin and recombinant bone morphogenetic protein 2B are chemotactic for human monocytes and stimulate transforming growth factor beta 1 mRNA expression. Proc Natl Acad Sci U S A 89: 11740-11744.

DE PALMA M, VENNERI MA, GALLI R, SERGI SERGI L, POLITI LS, SAMPAOLESI M AND NALDINI L. 2005. Tie2 identifies a hematopoietic lineage of proangiogenic monocytes required for tumor vessel formation and a mesenchymal population of pericyte progenitors. Cancer Cell 8: 211-226.

DEPPRICH R, HANDSCHEL J, SEBALD W, KUBLER NR AND WURZLER KK. 2005. [Comparison of the osteogenic activity of bone morphogenetic protein (BMP) mutants]. Mund Kiefer Gesichtschir 9: 363-368.

DI LUCA A, KLEIN-GUNNEWIEK M, VANCSO JG, VAN BLITTERSWIJK CA, BENETTI EM AND MORONI L. 2017. Covalent Binding of Bone Morphogenetic Protein-2 and Transforming Growth Factor-3 to 3D Plotted Scaffolds for Osteochondral Tissue Regeneration. Biotechnol J 12.

DUDLEY AC, KHAN ZA, SHIH SC, KANG SY, ZWAANS BM, BISCHOFF J AND KLAGSBRUN M. 2008. Calcification of multipotent prostate tumor endothelium. Cancer Cell 14: 201-211.

EHRLICH M, HORBELT D, MAROM B, KNAUS P AND HENIS YI. 2011. Homomeric and heteromeric complexes among TGF-beta and BMP receptors and their roles in signaling. Cell Signal 23: 1424-1432.

EL-GHANNAM A. 2005. Bone reconstruction: from bioceramics to tissue engineering. Expert Rev Med Devices 2: 87-101.

ELSABAHY M, NAZARALI A AND FOLDVARI M. 2011. Non-viral nucleic acid delivery: key challenges and future directions. Curr Drug Deliv 8: 235-244.

EVANS C. 2011. Gene therapy for the regeneration of bone. Injury 42: 599-604.

EVANS CH. 2012. Gene delivery to bone. Adv Drug Deliv Rev 64: 1331-1340.

FAHMY-GARCIA S ET AL. 2018. Novel in situ gelling hydrogels loaded with recombinant collagen peptide microspheres as a slow release system induce ectopic bone formation.

FAUBER J. 2010. Doctors question journal articles: Medtronic paid surgeons millions for other products. Journal Sentinel

FAUNDEZ A, TOURNIER C, GARCIA M, AUNOBLE S AND LE HUEC JC. 2016. Bone morphogenetic protein use in spine surgery-complications and outcomes: a systematic review. International Orthopaedics 40: 1309-1319.

FDA INFUSE™ BONE GRAFT/LT-CAGE™ LUMBAR TAPERED FUSION DEVICE. 2002. Summary of Safety and Effectiveness Data Premarket Approval Application P000058.

FDA PUBLIC HEALTH NOTIFICATION. 2014. United States Food and Drug Administration, Department of Health and Human Services, Center for Devices and Radiological Health. InFUSE bone Graft/LT-CAGE? Lumbar tapered fusion Devices—P000058. 2002.

FLORENCIO-SILVA R, SASSO GR, SASSO-CERRI E, SIMOES MJ AND CERRI PS. 2015. Biology of Bone Tissue: Structure, Function, and Factors That Influence Bone Cells. Biomed Res Int 2015: 421746.

FOLEY TL AND BURKART MD. 2007. Site-specific protein modification: advances and applications. Curr Opin Chem Biol 11: 12-19.

GARRISON KR, DONELL S, RYDER J, SHEMILT I, MUGFORD M, HARVEY I AND SONG F. 2007. Clinical effectiveness and cost-effectiveness of bone morphogenetic proteins in the non-healing of fractures and spinal fusion: a systematic review. Health Technol Assess 11: 1-150, iii-iv.

GAUTSCHI OP, FREY SP AND ZELLWEGER R. 2007. Bone morphogenetic proteins in clinical applications. ANZ J Surg 77: 626-631.

GLOWACKI J AND MIZUNO S. 2008. Collagen scaffolds for tissue engineering. Biopolymers 89: 338-344.

GOTHARD D, SMITH EL, KANCZLER JM, RASHIDI H, QUTACHI O, HENSTOCK J, ROTHERHAM M, EL HAJ A, SHAKESHEFF KM AND OREFFO RO. 2014. Tissue engineered bone using select growth factors: A comprehensive review of animal studies and clinical translation studies in man. Eur Cell Mater 28: 166-207; discussion 207-168.

GOVENDER S ET AL. 2002. Recombinant human bone morphogenetic protein-2 for treatment of open tibial fractures: a prospective, controlled, randomized study of four hundred and fifty patients. J Bone Joint Surg Am 84-A: 2123-2134.

GREEN D, WALSH D, MANN S AND OREFFO RO. 2002. The potential of biomimesis in bone tissue engineering: lessons from the design and synthesis of invertebrate skeletons. Bone 30: 810-815.

GUNNOO SB AND MADDER A. 2016. Chemical Protein Modification through Cysteine. Chembiochem 17: 529-553.

GUO X, ZHENG Q, KULBATSKI I, YUAN Q, YANG S, SHAO Z, WANG H, XIAO B, PAN Z AND TANG S. 2006. Bone regeneration with active angiogenesis by basic fibroblast growth factor gene transfected mesenchymal stem cells seeded on porous beta-TCP ceramic scaffolds. Biomed Mater 1: 93-99.

HAIDAR ZS, HAMDY RC AND TABRIZIAN M. 2009. Delivery of recombinant bone morphogenetic proteins for bone regeneration and repair. Part A: Current challenges in BMP delivery. Biotechnol Lett 31: 1817-1824.

HAMILTON PT, JANSEN MS, GANESAN S, BENSON RE, HYDE-DERUYSCHER R, BEYER WF, GILE JC, NAIR SA, HODGES JA AND GRON H. 2013. Improved bone morphogenetic protein-2 retention in an injectable collagen matrix using bifunctional peptides. PLoS One 8: e70715.

HARTUNG A, BITTON-WORMS K, RECHTMAN MM, WENZEL V, BOERGERMANN JH, HASSEL S, HENIS YI AND KNAUS P. 2006. Different routes of bone morphogenic protein (BMP) receptor endocytosis influence BMP signaling. Mol Cell Biol 26: 7791-7805.

HEIN JE AND FOKIN VV. 2010. Copper-catalyzed azide-alkyne cycloaddition (CuAAC) and beyond: new reactivity of copper(I) acetylides. Chem Soc Rev 39: 1302-1315.

HELDIN CH, MIYAZONO K AND TEN DIJKE P. 1997. TGF-beta signalling from cell membrane to nucleus through SMAD proteins. Nature 390: 465-471.

HIGUCHI R, KRUMMEL B AND SAIKI RK. 1988. A general method of in vitro preparation and specific mutagenesis of DNA fragments: study of protein and DNA interactions. Nucleic Acids Res 16: 7351-7367.

HINCK AP. 2012. Structural studies of the TGF-beta s and their receptors - insights into evolution of the TGF-beta superfamily. Febs Letters 586: 1860-1870.

HINCK AP, MUELLER TD AND SPRINGER TA. 2016. Structural Biology and Evolution of the TGF-beta Family. Cold Spring Harb Perspect Biol 8.

HO CS, LAM CW, CHAN MH, CHEUNG RC, LAW LK, LIT LC, NG KF, SUEN MW AND TAI HL. 2003. Electrospray ionisation mass spectrometry: principles and clinical applications. Clin Biochem Rev 24: 3-12.

HO SN, HUNT HD, HORTON RM, PULLEN JK AND PEASE LR. 1989. Site-Directed Mutagenesis by Overlap Extension Using the Polymerase Chain-Reaction. Gene 77: 51-59.

HOLLINGER JO, SCHMITT JM, BUCK DC, SHANNON R, JOH SP, ZEGZULA HD AND WOZNEY J. 1998. Recombinant human bone morphogenetic protein-2 and collagen for bone regeneration. J Biomed Mater Res 43: 356-364.

HONG V, PRESOLSKI SI, MA C AND FINN MG. 2009. Analysis and optimization of copper-catalyzed azide-alkyne cycloaddition for bioconjugation. Angew Chem Int Ed Engl 48: 9879-9883.

HORBELT D, DENKIS A AND KNAUS P. 2012. A portrait of Transforming Growth Factor beta superfamily signalling: Background matters. Int J Biochem Cell Biol 44: 469-474.

HU J, DUPPATLA V, HARTH S, SCHMITZ W AND SEBALD W. 2010. Site-specific PEGylation of bone morphogenetic protein-2 cysteine analogues. Bioconjug Chem 21: 1762-1772.

HULSART-BILLSTROM G, PISKOUNOVA S, GEDDA L, ANDERSSON BM, BERGMAN K, HILBORN J, LARSSON S AND BOWDEN T. 2013. Morphological differences in BMP-2-induced ectopic bone between solid and crushed hyaluronan hydrogel templates. J Mater Sci Mater Med 24: 1201-1209.

HUSTEDT JW AND BLIZZARD DJ. 2014. The controversy surrounding bone morphogenetic proteins in the spine: a review of current research. Yale J Biol Med 87: 549-561.

ISRAEL DI, NOVE J, KERNS KM, KAUFMAN RJ, ROSEN V, COX KA AND WOZNEY JM. 1996. Heterodimeric bone morphogenetic proteins show enhanced activity in vitro and in vivo. Growth Factors 13: 291-300.

ITOH K ET AL. 2001. Bone morphogenetic protein 2 stimulates osteoclast differentiation and survival supported by receptor activator of nuclear factor-kappa B ligand. Endocrinology 142: 3656-3662.

JAMES AW, LACHAUD G, SHEN J, ASATRIAN G, NGUYEN V, ZHANG X, TING K AND SOO C. 2016. A Review of the Clinical Side Effects of Bone Morphogenetic Protein-2. Tissue Eng Part B Rev 22: 284-297.

JANG JH, SCHAFFER DV AND SHEA LD. 2011. Engineering biomaterial systems to enhance viral vector gene delivery. Mol Ther 19: 1407-1415.

JENNISSEN HP AND LAUB M. 2007. Development of an universal affinity fusion tag (Poly-DOPA) for immobilizing recombinant proteins on biomaterials. Materialwiss Werkst 38: 1035-1039.

JONES AA, BUSER D, SCHENK R, WOZNEY J AND COCHRAN DL. 2006. The effect of rhBMP-2 around endosseous implants with and without membranes in the canine model. J Periodontol 77: 1184-1193.

KAIGLER D, WANG Z, HORGER K, MOONEY DJ AND KREBSBACH PH. 2006. VEGF scaffolds enhance angiogenesis and bone regeneration in irradiated osseous defects. J Bone Miner Res 21: 735-744.

KAN L AND KESSLER JA. 2014. Evaluation of the cellular origins of heterotopic ossification. Orthopedics 37: 329-340.

KAN L, PENG CY, MCGUIRE TL AND KESSLER JA. 2013. Glast-expressing progenitor cells contribute to heterotopic ossification. Bone 53: 194-203.

KANG Q ET AL. 2004. Characterization of the distinct orthotopic bone-forming activity of 14 BMPs using recombinant adenovirus-mediated gene delivery. Gene Ther 11: 1312-1320.

KAPS C, HOFFMANN A, ZILBERMAN Y, PELLED G, HAUPL T, SITTINGER M, BURMESTER G, GAZIT D AND GROSS G. 2004. Distinct roles of BMP receptors Type IA and IB in osteo-/chondrogenic differentiation in mesenchymal progenitors (C3H10T1/2). Biofactors 20: 71-84.

KARFELD-SULZER LS, SIEGENTHALER B, GHAYOR C AND WEBER FE. 2015. Fibrin Hydrogel Based Bone Substitute Tethered with BMP-2 and BMP-2/7 Heterodimers. Materials (Basel) 8: 977-991.

KASHIWAGI K, TSUJI T AND SHIBA K. 2009. Directional BMP-2 for functionalization of titanium surfaces. Biomaterials 30: 1166-1175.

KATAGIRI T, OSAWA K, TSUKAMOTO S, FUJIMOTO M, MIYAMOTO A AND MIZUTA T. 2015. Bone morphogenetic protein-induced heterotopic bone formation: What have we learned from the history of a half century? . Japanese Dental Science Review 51: 42-50.

KATAGIRI T, YAMAGUCHI A, KOMAKI M, ABE E, TAKAHASHI N, IKEDA T, ROSEN V, WOZNEY JM, FUJISAWA-SEHARA A AND SUDA T. 1994. Bone morphogenetic protein-2 converts the differentiation pathway of C2C12 myoblasts into the osteoblast lineage. J Cell Biol 127: 1755-1766.

KIM CS, KIM JI, KIM J, CHOI SH, CHAI JK, KIM CK AND CHO KS. 2005. Ectopic bone formation associated with recombinant human bone morphogenetic proteins-2 using absorbable collagen sponge and beta tricalcium phosphate as carriers. Biomaterials 26: 2501-2507.

KING WJ AND KREBSBACH PH. 2012. Growth factor delivery: how surface interactions modulate release in vitro and in vivo. Adv Drug Deliv Rev 64: 1239-1256.

KIRSCH T, NICKEL J AND SEBALD W. 2000. BMP-2 antagonists emerge from alterations in the low-affinity binding epitope for receptor BMPR-II. EMBO J 19: 3314-3324.

KNAUS P AND SEBALD W. 2001. Cooperativity of binding epitopes and receptor chains in the BMP/TGFbeta superfamily. Biol Chem 382: 1189-1195.

KOVACIC JC, MERCADER N, TORRES M, BOEHM M AND FUSTER V. 2012. Epithelial-to-mesenchymal and endothelial-to-mesenchymal transition: from cardiovascular development to disease. Circulation 125: 1795-1808.

KULAR J, TICKNER J, CHIM SM AND XU J. 2012. An overview of the regulation of bone remodelling at the cellular level. Clin Biochem 45: 863-873.

KUNIHIRO TSUCHIDA TO, AKIYOSHI UEZUMI AND HARUMOTO YAMADA. 2013. Origin and Therapeutic Strategies for Ectopic Bone Formation in Skeletal Muscle. Human Genetics & Embryology 3: 3.

KUO WJ, DIGMAN MA AND LANDER AD. 2010. Heparan Sulfate Acts as a Bone Morphogenetic Protein Coreceptor by Facilitating Ligand-induced Receptor Hetero-oligomerization. Mol Biol Cell 21: 4028-4041.

KUSUMA GD, MENICANIN D, GRONTHOS S, MANUELPILLAI U, ABUMAREE MH, PERTILE MD, BRENNECKE SP AND KALIONIS B. 2015. Ectopic Bone Formation by Mesenchymal Stem Cells Derived from Human Term Placenta and the Decidua. PLoS One 10: e0141246.

LALLANA E, RIGUERA R AND FERNANDEZ-MEGIA E. 2011. Reliable and Efficient Procedures for the Conjugation of Biomolecules through Huisgen Azide-Alkyne Cycloadditions. Angew Chem Int Edit 50: 8794-8804.

LAMPLOT JD ET AL. 2013. BMP9 signaling in stem cell differentiation and osteogenesis. Am J Stem Cells 2: 1-21.

LEE JH, KIM CS, CHOI KH, JUNG UW, YUN JH, CHOI SH AND CHO KS. 2010. The induction of bone formation in rat calvarial defects and subcutaneous tissues by recombinant human BMP-2, produced in Escherichia coli. Biomaterials 31: 3512-3519.

LEE KB, JOHNSON JS, SONG KJ, TAGHAVI CE AND WANG JC. 2013. Use of autogenous bone graft compared with RhBMP in high-risk patients: a comparison of fusion rates and time to fusion. J Spinal Disord Tech 26: 233-238.

LI S, CAI H, HE J, CHEN H, LAM S, CAI T, ZHU Z, BARK SJ AND CAI C. 2016. Extent of the Oxidative Side Reactions to Peptides and Proteins During the CuAAC Reaction. Bioconjug Chem 27: 2315-2322.

LIAN N, WANG W, LI L, ELEFTERIOU F AND YANG X. 2009. Vimentin inhibits ATF4-mediated osteocalcin transcription and osteoblast differentiation. J Biol Chem 284: 30518-30525.

LIANG Y AND KIICK KL. 2014. Heparin-functionalized polymeric biomaterials in tissue engineering and drug delivery applications. Acta Biomater 10: 1588-1600.

LIN HY AND WANG XF. 1992. Expression cloning of TGF-beta receptors. Mol Reprod Dev 32: 105-110.

LOUIS-UGBO J, KIM HS, BODEN SD, MAYR MT, LI RC, SEEHERMAN H, D'AUGUSTA D, BLAKE C, JIAO A AND PECKHAM S. 2002. Retention of 125I-labeled recombinant human bone morphogenetic protein-2 by biphasic calcium phosphate or a composite sponge in a rabbit posterolateral spine arthrodesis model. J Orthop Res 20: 1050-1059.

LOUNEV VY, RAMACHANDRAN R, WOSCZYNA MN, YAMAMOTO M, MAIDMENT ADA, SHORE EM, GLASER DL, GOLDHAMER DJ AND KAPLAN FS. 2009. Identification of Progenitor Cells That Contribute to Heterotopic Skeletogenesis. Journal of Bone and Joint Surgery-American Volume 91a: 652-663.

LUCA L, CAPELLE MA, MACHAIDZE G, ARVINTE T, JORDAN O AND GURNY R. 2010. Physical instability, aggregation and conformational changes of recombinant human bone morphogenetic protein-2 (rhBMP-2). Int J Pharm 391: 48-54.

LUHMANN T, JONES G, GUTMANN M, RYBAK JC, NICKEL J, RUBINI M AND MEINEL L. 2015. Bio-orthogonal Immobilization of Fibroblast Growth Factor 2 for Spatial Controlled Cell Proliferation. Acs Biomater Sci Eng 1: 740-746.

LYNCH MP, CAPPARELLI C, STEIN JL, STEIN GS AND LIAN JB. 1998. Apoptosis during bone-like tissue development in vitro. J Cell Biochem 68: 31-49.

MA JL, YANG F, BOTH SK, PRINS HJ, HELDER MN, PAN JL, CUI FZ, JANSEN JA AND VAN DEN BEUCKEN JJJP. 2015. Bone Forming Capacity of Cell- and Growth Factor-Based Constructs at Different Ectopic Implantation Sites. Journal of Biomedical Materials Research Part A 103: 439-450.

MANI SA ET AL. 2008. The epithelial-mesenchymal transition generates cells with properties of stem cells. Cell 133: 704-715.

MANOLAGAS SC. 2006. Choreography from the tomb: an emerging role of dying osteocytes in the purposeful, and perhaps notso purposeful, targeting of bone remodeling. BoneKEy-Osteovision 3: 5-14.
MASSAGUE J. 1998. TGF-beta signal transduction. Annu Rev Biochem 67: 753-791.
MASTERS KS. 2011. Covalent growth factor immobilization strategies for tissue repair and regeneration. Macromol Biosci 11: 1149-1163.
MATSUBARA T ET AL. 2013. TIE2-expressing monocytes as a diagnostic marker for hepatocellular carcinoma correlates with angiogenesis. Hepatology 57: 1416-1425.
MATSUMOTO T ET AL. 2008. Fracture induced mobilization and incorporation of bone marrow-derived endothelial progenitor cells for bone healing. J Cell Physiol 215: 234-242.
MCKAY CS AND FINN MG. 2014. Click chemistry in complex mixtures: bioorthogonal bioconjugation. Chem Biol 21: 1075-1101.
MCKAY WF, PECKHAM SM AND BADURA JM. 2007. A comprehensive clinical review of recombinant human bone morphogenetic protein-2 (INFUSE Bone Graft). Int Orthop 31: 729-734.
MEDICI D, SHORE EM, LOUNEV VY, KAPLAN FS, KALLURI R AND OLSEN BR. 2010. Conversion of vascular endothelial cells into multipotent stem-like cells. Nature Medicine 16: 1400-U1480.
MERETOJA VV, TIRRI T, MALIN M, SEPPALA JV AND NARHI TO. 2014. Ectopic bone formation in and soft-tissue response to P(CL/DLLA)/bioactive glass composite scaffolds. Clin Oral Implants Res 25: 159-164.
MEYER JP, ADUMEAU P, LEWIS JS AND ZEGLIS BM. 2016. Click Chemistry and Radiochemistry: The First 10 Years. Bioconjug Chem 27: 2791-2807.
MILLER SC, DE SAINT-GEORGES L, BOWMAN BM AND JEE WS. 1989. Bone lining cells: structure and function. Scanning Microsc 3: 953-960; discussion 960-951.
MISHINA Y ET AL. 2004. Bone morphogenetic protein type IA receptor signaling regulates postnatal osteoblast function and bone remodeling. J Biol Chem 279: 27560-27566.
MUELLER TD AND NICKEL J. 2012. Promiscuity and specificity in BMP receptor activation. FEBS Lett 586: 1846-1859.
MUMCUOGLU D, DE MIGUEL L, JEKHMANE S, SIVERINO C, NICKEL J, MUELLER TD, VAN LEEUWEN JP, VAN OSCH GJ AND KLUIJTMANS SG. 2018a. Collagen I derived recombinant protein microspheres as novel delivery vehicles for bone morphogenetic protein-2. Mater Sci Eng C Mater Biol Appl 84: 271-280.
MUMCUOGLU D, FAHMY-GARCIA S, RIDWAN Y, NICKE J, FARRELL E, KLUIJTMANS SG AND VAN OSCH GJ. 2018b. Injectable BMP-2 delivery system based on collagen-derived microspheres and alginate induced bone formation in a time- and dose-dependent manner. Eur Cell Mater 35: 242-254.
MUMCUOGLU D, SIVERINO C, TABISZ B, KLUIJTMANS SG AND NICKEL J. 2017. How to use BMP-2 for clinical applications? A review on pros and cons of existing delivery strategies. Journal of Translational Science 3(5): 1-11.
MURRAY SS, BROCHMANN MURRAY EJ, WANG JC AND DUARTE ME. 2016. The history and histology of bone morphogenetic protein. Histol Histopathol 31: 721-732.
MUSGRAVE DS, BOSCH P, GHIVIZZANI S, ROBBINS PD, EVANS CH AND HUARD J. 1999. Adenovirus-mediated direct gene therapy with bone morphogenetic protein-2 produces bone. Bone 24: 541-547.
NAIRN NW, BARIOLA PA, GRADDIS TJ, VANBRUNT MP, WANG A, LI G AND GRABSTEIN K. 2015. Cysteine as a Monothiol Reducing Agent to Prevent Copper-Mediated Oxidation of Interferon Beta During PEGylation by CuAAC. Bioconjug Chem 26: 2070-2075.

NGUYEN DP, LUSIC H, NEUMANN H, KAPADNIS PB, DEITERS A AND CHIN JW. 2009. Genetic encoding and labeling of aliphatic azides and alkynes in recombinant proteins via a pyrrolysyl-tRNA Synthetase/tRNA(CUA) pair and click chemistry. J Am Chem Soc 131: 8720-8721.

NICKEL J, KOTZSCH A, SEBALD W AND MUELLER TD. 2005. A single residue of GDF-5 defines binding specificity to BMP receptor IB. J Mol Biol 349: 933-947.

NICKEL J, SEBALD W, GROPPE JC AND MUELLER TD. 2009. Intricacies of BMP receptor assembly. Cytokine Growth Factor Rev 20: 367-377.

NIYIBIZI C, BALTZER A, LATTERMANN C, OYAMA M, WHALEN JD, ROBBINS PD AND EVANS CH. 1998. Potential role for gene therapy in the enhancement of fracture healing. Clin Orthop Relat Res: S148-153.

NOHE A, HASSEL S, EHRLICH M, NEUBAUER F, SEBALD W, HENIS YI AND KNAUS P. 2002. The mode of bone morphogenetic protein (BMP) receptor oligomerization determines different BMP-2 signaling pathways. J Biol Chem 277: 5330-5338.

O'LOUGHLIN PF, MORR S, BOGUNOVIC L, KIM AD, PARK B AND LANE JM. 2008. Selection and development of preclinical models in fracture-healing research. J Bone Joint Surg Am 90 Suppl 1: 79-84.

OISHI T, UEZUMI A, KANAJI A, YAMAMOTO N, YAMAGUCHI A, YAMADA H AND TSUCHIDA K. 2013. Osteogenic differentiation capacity of human skeletal muscle-derived progenitor cells. PLoS One 8: e56641.

ORYAN A, MONAZZAH S AND BIGHAM-SADEGH A. 2015. Bone injury and fracture healing biology. Biomed Environ Sci 28: 57-71.

OTSURU S, TAMAI K, YAMAZAKI T, YOSHIKAWA H AND KANEDA Y. 2007. Bone marrow-derived osteoblast progenitor cells in circulating blood contribute to ectopic bone formation in mice. Biochem Biophys Res Commun 354: 453-458.

OZKAYNAK E, RUEGER DC, DRIER EA, CORBETT C, RIDGE RJ, SAMPATH TK AND OPPERMANN H. 1990. OP-1 cDNA encodes an osteogenic protein in the TGF-beta family. EMBO J 9: 2085-2093.

PAARMANN P, DORPHOLZ G, FIEBIG J, AMSALEM AR, EHRLICH M, HENIS YI, MULLER T AND KNAUS P. 2016. Dynamin-dependent endocytosis of Bone Morphogenetic Protein2 (BMP2) and its receptors is dispensable for the initiation of Smad signaling. Int J Biochem Cell B 76: 51-63.

PARK JC, KIM JC, KIM BK, CHO KS, IM GI, KIM BS AND KIM CS. 2012. Dose- and time-dependent effects of recombinant human bone morphogenetic protein-2 on the osteogenic and adipogenic potentials of alveolar bone-derived stromal cells. J Periodontal Res 47: 645-654.

PARK YJ, KIM KH, LEE JY, KU Y, LEE SJ, MIN BM AND CHUNG CP. 2006. Immobilization of bone morphogenetic protein-2 on a nanofibrous chitosan membrane for enhanced guided bone regeneration. Biotechnol Appl Biochem 43: 17-24.

PATEL ZS, YOUNG S, TABATA Y, JANSEN JA, WONG ME AND MIKOS AG. 2008. Dual delivery of an angiogenic and an osteogenic growth factor for bone regeneration in a critical size defect model. Bone 43: 931-940.

PEARCE AI, RICHARDS RG, MILZ S, SCHNEIDER E AND PEARCE SG. 2007. Animal models for implant biomaterial research in bone: A review. Eur Cells Mater 13: 1-10.

PELED E, BOSS J, BEJAR J, ZINMAN C AND SELIKTAR D. 2007. A novel poly(ethylene glycol)-fibrinogen hydrogel for tibial segmental defect repair in a rat model. J Biomed Mater Res A 80: 874-884.

PISKOUNOVA S, GEDDA L, HULSART-BILLSTROM G, HILBORN J AND BOWDEN T. 2014. Characterization of recombinant human bone morphogenetic protein-2

delivery from injectable hyaluronan-based hydrogels by means of 125I-radiolabelling. J Tissue Eng Regen Med 8: 821-830.
POHL TL, SCHWAB EH AND CAVALCANTI-ADAM EA. 2013. Covalent binding of BMP-2 on surfaces using a self-assembled monolayer approach. J Vis Exp.
RAGGATT LJ AND PARTRIDGE NC. 2010. Cellular and molecular mechanisms of bone remodeling. J Biol Chem 285: 25103-25108.
RAHMAN MS, AKHTAR N, JAMIL HM, BANIK RS AND ASADUZZAMAN SM. 2015. TGF-beta/BMP signaling and other molecular events: regulation of osteoblastogenesis and bone formation. Bone Res 3: 15005.
RANCHOUX B ET AL. 2015. Endothelial-to-mesenchymal transition in pulmonary hypertension. Circulation 131: 1006-1018.
RATANAVARAPORN J, FURUYA H AND TABATA Y. 2012. Local suppression of pro-inflammatory cytokines and the effects in BMP-2-induced bone regeneration. Biomaterials 33: 304-316.
REDDI AH. 2005. BMPs: from bone morphogenetic proteins to body morphogenetic proteins. Cytokine Growth Factor Rev 16: 249-250.
RIHN JA, PATEL R, MAKDA J, HONG J, ANDERSON DG, VACCARO AR, HILIBRAND AS AND ALBERT TJ. 2009. Complications associated with single-level transforaminal lumbar interbody fusion. Spine J 9: 623-629.
ROACH P, FARRAR D AND PERRY CC. 2006. Surface tailoring for controlled protein adsorption: Effect of topography at the nanometer scale and chemistry. Journal of the American Chemical Society 128: 3939-3945.
ROSTOVTSEV VV, GREEN LG, FOKIN VV AND SHARPLESS KB. 2002. A stepwise huisgen cycloaddition process: copper(I)-catalyzed regioselective "ligation" of azides and terminal alkynes. Angew Chem Int Ed Engl 41: 2596-2599.
RUPPERT R, HOFFMANN E AND SEBALD W. 1996. Human bone morphogenetic protein 2 contains a heparin-binding site which modifies its biological activity. Eur J Biochem 237: 295-302.
SAIFER MG, WILLIAMS LD, SOBCZYK MA, MICHAELS SJ AND SHERMAN MR. 2014. Selectivity of binding of PEGs and PEG-like oligomers to anti-PEG antibodies induced by methoxyPEG-proteins. Mol Immunol 57: 236-246.
SALAZAR VS, GAMER LW AND ROSEN V. 2016. BMP signalling in skeletal development, disease and repair. Nat Rev Endocrinol 12: 203-221.
SALEH FA, WHYTE M, ASHTON P AND GENEVER PG. 2011. Regulation of mesenchymal stem cell activity by endothelial cells. Stem Cells Dev 20: 391-403.
SAMPATH TK, MUTHUKUMARAN N AND REDDI AH. 1987. Isolation of osteogenin, an extracellular matrix-associated, bone-inductive protein, by heparin affinity chromatography. Proc Natl Acad Sci U S A 84: 7109-7113.
SANCHEZ-DUFFHUES G, HIEPEN C, KNAUS P AND TEN DIJKE P. 2015. Bone morphogenetic protein signaling in bone homeostasis. Bone 80: 43-59.
SCHELLEKENS H, HENNINK WE AND BRINKS V. 2013. The immunogenicity of polyethylene glycol: facts and fiction. Pharm Res 30: 1729-1734.
SCHEUFLER C, SEBALD W AND HULSMEYER M. 1999. Crystal structure of human bone morphogenetic protein-2 at 2.7 A resolution. J Mol Biol 287: 103-115.
SCHOFFELEN S, LAMBERMON MH, VAN ELDIJK MB AND VAN HEST JC. 2008. Site-specific modification of Candida antarctica lipase B via residue-specific incorporation of a non-canonical amino acid. Bioconjug Chem 19: 1127-1131.
SCHWAB EH, POHL TL, HARASZTI T, SCHWAERZER GK, HIEPEN C, SPATZ JP, KNAUS P AND CAVALCANTI-ADAM EA. 2015. Nanoscale control of surface immobilized BMP-2: toward a quantitative assessment of BMP-mediated signaling events. Nano Lett 15: 1526-1534.

SCHWARTZ Z, LOHMANN CH, OEFINGER J, BONEWALD LF, DEAN DD AND BOYAN BD. 1999. Implant surface characteristics modulate differentiation behavior of cells in the osteoblastic lineage. Adv Dent Res 13: 38-48.

SCIADINI MF AND JOHNSON KD. 2000. Evaluation of recombinant human bone morphogenetic protein-2 as a bone-graft substitute in a canine segmental defect model. J Orthop Res 18: 289-302.

SCOTT MA, LEVI B, ASKARINAM A, NGUYEN A, RACKOHN T, TING K, SOO C AND JAMES AW. 2012. Brief review of models of ectopic bone formation. Stem Cells Dev 21: 655-667.

SEEHERMAN H, WOZNEY J AND LI R. 2002. Bone morphogenetic protein delivery systems. Spine (Phila Pa 1976) 27: S16-23.

SEEHERMAN H AND WOZNEY JM. 2005. Delivery of bone morphogenetic proteins for orthopedic tissue regeneration. Cytokine Growth Factor Rev 16: 329-345.

SEYEDIN SM, THOMAS TC, THOMPSON AY, ROSEN DM AND PIEZ KA. 1985. Purification and characterization of two cartilage-inducing factors from bovine demineralized bone. Proc Natl Acad Sci U S A 82: 2267-2271.

SHAPIRO F. 2008. Bone development and its relation to fracture repair. The role of mesenchymal osteoblasts and surface osteoblasts. Eur Cell Mater 15: 53-76.

SHI Y AND MASSAGUE J. 2003. Mechanisms of TGF-beta signaling from cell membrane to the nucleus. Cell 113: 685-700.

SHIELDS LB, RAQUE GH, GLASSMAN SD, CAMPBELL M, VITAZ T, HARPRING J AND SHIELDS CB. 2006. Adverse effects associated with high-dose recombinant human bone morphogenetic protein-2 use in anterior cervical spine fusion. Spine (Phila Pa 1976) 31: 542-547.

SHIMAZU C, HARA T, KINUTA Y, MORIYA K, MARUO Y, HANADA S AND MINAGI S. 2006. Enhanced vertical alveolar bone augmentation by recombinant human bone morphogenetic protein-2 with a carrier in rats. J Oral Rehabil 33: 609-618.

SHORE EM ET AL. 2006. A recurrent mutation in the BMP type I receptor ACVR1 causes inherited and sporadic fibrodysplasia ossificans progressiva. Nat Genet 38: 525-527.

SIEBER C, KOPF J, HIEPEN C AND KNAUS P. 2009. Recent advances in BMP receptor signaling. Cytokine Growth Factor Rev 20: 343-355.

SPICER CD AND DAVIS BG. 2014. Selective chemical protein modification. Nat Commun 5: 4740.

SUN P, WANG J, ZHENG Y, FAN Y AND GU Z. 2012. BMP2/7 heterodimer is a stronger inducer of bone regeneration in peri-implant bone defects model than BMP2 or BMP7 homodimer. Dent Mater J 31: 239-248.

TABISZ B. 2016. Site directed immobilization of BMP2: two approaches for the production of osteoinductive scaffolds. Thesis.

TABISZ B, SCHMITZ W, SCHMITZ M, LUEHMANN T, HEUSLER E, RYBAK JC, MEINEL L, FIEBIG JE, MUELLER TD AND NICKEL J. 2017. Site-Directed Immobilization of BMP-2: Two Approaches for the Production of Innovative Osteoinductive Scaffolds. Biomacromolecules 18: 695-708.

TADOKORO M, MATSUSHIMA A, KOTOBUKI N, HIROSE M, KIMURA Y, TABATA Y, HATTORI K AND OHGUSHI H. 2012. Bone morphogenetic protein-2 in biodegradable gelatin and beta-tricalcium phosphate sponges enhances the in vivo bone-forming capability of bone marrow mesenchymal stem cells. J Tissue Eng Regen Med 6: 253-260.

TAKADA I, YOGIASHI Y AND KATO S. 2012. Signaling Crosstalk between PPARgamma and BMP2 in Mesenchymal Stem Cells. PPAR Res 2012: 607141.

TANAKA-KAMIOKA K, KAMIOKA H, RIS H AND LIM SS. 1998. Osteocyte shape is dependent on actin filaments and osteocyte processes are unique actin-rich projections. J Bone Miner Res 13: 1555-1568.

TANNOURY CA AND AN HS. 2014. Complications with the use of bone morphogenetic protein 2 (BMP-2) in spine surgery. Spine Journal 14: 552-559.

TARASSOLI P, KHAN WS, HUGHES A AND HEIDARI N. 2013. A review of techniques for gene therapy in bone healing. Curr Stem Cell Res Ther 8: 201-209.

TEICHERT M ET AL. 2017. Pericyte-expressed Tie2 controls angiogenesis and vessel maturation. Nat Commun 8: 16106.

TEN DIJKE P, MIYAZONO K AND HELDIN CH. 1996. Signaling via hetero-oligomeric complexes of type I and type II serine/threonine kinase receptors. Curr Opin Cell Biol 8: 139-145.

TERPE K. 2003. Overview of tag protein fusions: from molecular and biochemical fundamentals to commercial systems. Appl Microbiol Biotechnol 60: 523-533.

TODESCHI MR, EL BACKLY RM, VARGHESE OP, HILBORN J, CANCEDDA R AND MASTROGIACOMO M. 2017. Host cell recruitment patterns by bone morphogenetic protein-2 releasing hyaluronic acid hydrogels in a mouse subcutaneous environment. Regen Med 12: 525-539.

UEZUMI A, FUKADA S, YAMAMOTO N, TAKEDA S AND TSUCHIDA K. 2010. Mesenchymal progenitors distinct from satellite cells contribute to ectopic fat cell formation in skeletal muscle. Nat Cell Biol 12: 143-152.

ULUDAG H, D'AUGUSTA D, GOLDEN J, LI J, TIMONY G, RIEDEL R AND WOZNEY JM. 2000. Implantation of recombinant human bone morphogenetic proteins with biomaterial carriers: A correlation between protein pharmacokinetics and osteoinduction in the rat ectopic model. J Biomed Mater Res 50: 227-238.

URIST MR. 1965. Bone: formation by autoinduction. Science 150: 893-899.

URIST MR, SILVERMAN BF, BURING K, DUBUC FL AND ROSENBERG JM. 1967. The bone induction principle. Clin Orthop Relat Res 53: 243-283.

URIST MR AND STRATES BS. 1971. Bone morphogenetic protein. J Dent Res 50: 1392-1406.

VAIDYA R, CARP J, SETHI A, BARTOL S, CRAIG J AND LES CM. 2007. Complications of anterior cervical discectomy and fusion using recombinant human bone morphogenetic protein-2. Eur Spine J 16: 1257-1265.

VALDIMARSDOTTIR G, GOUMANS MJ, ROSENDAHL A, BRUGMAN M, ITOH S, LEBRIN F, SIDERAS P AND TEN DIJKE P. 2002. Stimulation of Id1 expression by bone morphogenetic protein is sufficient and necessary for bone morphogenetic protein-induced activation of endothelial cells. Circulation 106: 2263-2270.

VAN HEST JC AND VAN DELFT FL. 2011. Protein modification by strain-promoted alkyne-azide cycloaddition. Chembiochem 12: 1309-1312.

WADA MR, INAGAWA-OGASHIWA M, SHIMIZU S, YASUMOTO S AND HASHIMOTO N. 2002. Generation of different fates from multipotent muscle stem cells. Development 129: 2987-2995.

WAN Y, CHONG LW AND EVANS RM. 2007. PPAR-gamma regulates osteoclastogenesis in mice. Nat Med 13: 1496-1503.

WANG C, WANG TY, ZHANG LY, GAO XJ, WANG XW AND JIN CJ. 2015. Cut-and-paste-based cloning strategy for large gene site-directed mutagenesis. Genet Mol Res 14: 5585-5591.

WANG EA, ROSEN V, CORDES P, HEWICK RM, KRIZ MJ, LUXENBERG DP, SIBLEY BS AND WOZNEY JM. 1988. Purification and characterization of other distinct bone-inducing factors. Proc Natl Acad Sci U S A 85: 9484-9488.

WANG EA ET AL. 1990. Recombinant human bone morphogenetic protein induces bone formation. Proc Natl Acad Sci U S A 87: 2220-2224.

WARNKE PH ET AL. 2004. Growth and transplantation of a custom vascularised bone graft in a man. Lancet 364: 766-770.

WARNOCK JN, DAIGRE C AND AL-RUBEAI M. 2011. Introduction to viral vectors. Methods Mol Biol 737: 1-25.

WEBER D, KOTZSCH A, NICKEL J, HARTH S, SEHER A, MUELLER U, SEBALD W AND MUELLER TD. 2007. A silent H-bond can be mutationally activated for high-affinity interaction of BMP-2 and activin type IIB receptor. Bmc Struct Biol 7.

WEINER MP, COSTA GL, SCHOETTLIN W, CLINE J, MATHUR E AND BAUER JC. 1994. Site-directed mutagenesis of double-stranded DNA by the polymerase chain reaction. Gene 151: 119-123.

WINET H AND HOLLINGER JO. 1993. Incorporation of polylactide-polyglycolide in a cortical defect: neoosteogenesis in a bone chamber. J Biomed Mater Res 27: 667-676.

WOSCZYNA MN, BISWAS AA, COGSWELL CA AND GOLDHAMER DJ. 2012. Multipotent progenitors resident in the skeletal muscle interstitium exhibit robust BMP-dependent osteogenic activity and mediate heterotopic ossification. J Bone Miner Res 27: 1004-1017.

WOZNEY JM. 2002. Overview of bone morphogenetic proteins. Spine (Phila Pa 1976) 27: S2-8.

WOZNEY JM, ROSEN V, CELESTE AJ, MITSOCK LM, WHITTERS MJ, KRIZ RW, HEWICK RM AND WANG EA. 1988. Novel regulators of bone formation: molecular clones and activities. Science 242: 1528-1534.

WRANA JL, ATTISANO L, CARCAMO J, ZENTELLA A, DOODY J, LAIHO M, WANG XF AND MASSAGUE J. 1992. TGF beta signals through a heteromeric protein kinase receptor complex. Cell 71: 1003-1014.

WU J, ZHAO C, LIN WF, HU RD, WANG QM, CHEN H, LI LY, CHEN SF AND ZHENG J. 2014. Binding characteristics between polyethylene glycol (PEG) and proteins in aqueous solution. J Mater Chem B 2: 2983-2992.

WURZLER KK, EMMERT J, EICHELSBACHER F, KUBLER NR, SEBALD W AND REUTHER JF. 2004. [Evaluation of the osteoinductive potential of genetically modified BMP-2 variants]. Mund Kiefer Gesichtschir 8: 83-92.

XIE J AND SCHULTZ PG. 2006. A chemical toolkit for proteins--an expanded genetic code. Nat Rev Mol Cell Biol 7: 775-782.

XIONG C ET AL. 2013. BMP-2 adverse reactions treated with human dose equivalent dexamethasone in a rodent model of soft-tissue inflammation. Spine (Phila Pa 1976) 38: 1640-1647.

YOSHIDA K, BESSHO K, FUJIMURA K, KUSUMOTO K, OGAWA Y, TANI Y AND IIZUKA T. 1998. Osteoinduction capability of recombinant human bone morphogenetic protein-2 in intramuscular and subcutaneous sites: an experimental study. J Craniomaxillofac Surg 26: 112-115.

YU PB ET AL. 2008. BMP type I receptor inhibition reduces heterotopic [corrected] ossification. Nat Med 14: 1363-1369.

YUASA K, KOKUBU E, KOKUBUN K, MATSUZAKA K, SHIBA K, KASHIWAGI K AND INOUE T. 2014. An artificial fusion protein between bone morphogenetic protein 2 and titanium-binding peptide is functional in vivo. J Biomed Mater Res A 102: 1180-1186.

ZARA JN ET AL. 2011. High doses of bone morphogenetic protein 2 induce structurally abnormal bone and inflammation in vivo. Tissue Eng Part A 17: 1389-1399.

ZHANG Q, HE QF, ZHANG TH, YU XL, LIU Q AND DENG FL. 2012. Improvement in the delivery system of bone morphogenetic protein-2: a new approach to promote bone formation. Biomed Mater 7: 045002.

ZHANG W, ZHU C, WU Y, YE D, WANG S, ZOU D, ZHANG X, KAPLAN DL AND JIANG X. 2014a. VEGF and BMP-2 promote bone regeneration by facilitating bone marrow stem cell homing and differentiation. Eur Cell Mater 27: 1-11; discussion 11-12.

ZHANG X, GUO J, ZHOU YS AND WU G. 2014b. The Roles of Bone Morphogenetic Proteins and Their Signaling in the Osteogenesis of Adipose-Derived Stem Cells. Tissue Eng Part B-Re 20: 84-92.

ZHANG Y, BARANOV PV, ATKINS JF AND GLADYSHEV VN. 2005. Pyrrolysine and selenocysteine use dissimilar decoding strategies. Journal of Biological Chemistry 280: 20740-20751.

ZHAO Y, ZHANG J, WANG X, CHEN B, XIAO Z, SHI C, WEI Z, HOU X, WANG Q AND DAI J. 2010. The osteogenic effect of bone morphogenetic protein-2 on the collagen scaffold conjugated with antibodies. J Control Release 141: 30-37.

ZHENG Y, WU G, ZHAO J, WANG L, SUN P AND GU Z. 2010. rhBMP2/7 heterodimer: an osteoblastogenesis inducer of not higher potency but lower effective concentration compared with rhBMP2 and rhBMP7 homodimers. Tissue Eng Part A 16: 879-887.

Affidavit

I hereby confirm that my thesis entitled: “Induction of ectopic bone formation by site directed immobilized BMP2 variants *in vivo*” is the result of my own work. I did not receive any help or support from commercial consultants. All sources and / or materials applied are listed and specified in the thesis.

Furthermore, I confirm that this thesis has not yet been submitted as part of another examination process neither in identical nor in similar form.

Place, Date Signature

Eidesstattliche Erklärung

Hiermit erkläre ich an Eides statt, die Dissertation: “ Induktion ektoper Knochenbildung durch gerichtet immobilisierte BMP2-Varianten *in vivo* ” eigenständig, d.h. insbesondere selbständig und ohne Hilfe eines kommerziellen Promotionsberaters, angefertigt und keine anderen als die von mir angegebenen Quellen und Hilfsmittel verwendet zu haben.

Ich erkläre außerdem, dass die Dissertation weder in gleicher noch in ähnlicher Form bereits in einem anderen Prüfungsverfahren vorgelegen hat.

Ort, Datum Unterschirift

List of publications

PUBLICATIONS

"Site-Directed Immobilization of Bone Morphogenetic Protein 2 to Solid Surfaces by Click Chemistry". Siverino C*, Tabisz B, Lühmann T, Meinel L, Müller T, Walles H, Nickel J. Journal of visualized experiments 2018.

"How to Use BMP-2 for Clinical Applications? A Review on Pros and Cons of Existing Delivery Strategies". Didem Mumcuoglu*, Claudia Siverino*****, Barbara Tabisz*, Bas Kluijtmans, and Joachim Nickel. Journal of Translational Science, November 2017.

"Collagen I based recombinant peptide microspheres as novel delivery vehicles for bone morphogenetic protein-2". Didem Mumcuoglu*, Laura de Miguel*, Shehrazade Jekhmane, Claudia Siverino, Joachim Nickel, Thomas D. Mueller, Johannes P. van Leeuwen, Gerjo J. van Osch, Sebastiaan G. Kluijtmans. Materials Science and Engineering C, 2017.

THIS WORK HAS BEEN PRESENTED AT THE FOLLOWING CONFERENCES:

2015 – 4th International Conference "Strategies in Tissue Engineering", Würzburg
Poster: "Site-directed Immobilization of BMP-2 and Noggin Inhibitory Peptides onto Collagen Beads for Bone Regeneration"

2015 - 4th TERMIS World Congress – Boston, USA
Poster: "Site-directed Immobilization of BMP-2 and Noggin Inhibitory Peptides onto Collagen Beads for Bone Regeneration"

2016 - 11th International BMP Conference, Boston USA
Poster: "Site-directed Immobilization of BMP-2 and Noggin Inhibitory Peptides onto Collagen Beads for Bone Regeneration"

2017 – TERMIS EU Conference, Davos, Switzerland
Oral presentation: "Site-directed immobilization of BMP-2 and noggin inhibitory peptides onto collagen I based recombinant peptide microspheres for bone regeneration"

2017 - 7th KMM-VIN Industrial Workshop, Erlangen, Germany
Oral presentation: "Site directed immobilization of BMP-2 onto collagen beads for bone regeneration"

Acknowledgement

I would like to thank Prof. Dr. Heike Walles for giving me the opportunity to conduct my doctoral research at the Chair of Tissue Engineering and Regenerative within the BIO-INSPIRE Marie Curie Project. Thank you for your advice during our meetings and creating a friendly and respectful working environment. I am really happy of being a part of the TERM team.

I would like to express my deepest gratitude to my supervisor and mentor Dr. Joachim Nickel. Thank you for being a great and patient supervisor, for all the help and support during these years. Thanks for sharing your enthusiasm and passion for research. You have always believed in me and constantly kept me motivated. Thank you for the huge input during correcting this dissertation, I could always count on an honest opinion from your side. It was an honor and pleasure to work with you and thank you for that!

My gratitude goes to Prof. Dr. Thomas Müller for valuable participation in my thesis committee meetings and providing adequate and valuable feedback.

I would like to thank Dr. Tessa Lühmann for personal attendance at my thesis committee meetings and thanks also to Prof. Dr. Lorenz Meinel for kindly providing N-Propargyl-lysine, sharing pET11a-pyrtRNA and pRSFduet-pyrtRNAsynth vectors.

I would like to thank Dr. Werner Schmitz for performing mass spectrometry analysis and his help in the interpretation of the data.

I would like to thank Sabine Graiff for the technical support and taking care of the protein lab and Heike Oberwinkler for her great help in the histological analyses.

Being part of an international group within the BIO-INSPIRE project made these years full of inspiring scientific conversations and friendly environment during all the meetings and secondments. I would like to thank Fujifilm and Didem for the production of the biomaterial used in my experiments and for having me during the research collaboration period.

I would like to thank Prof. Dr. Gerjo van Osch and Dr. Eric Farrell for having me at the Erasmus medical center for the animal experiment and always providing scientific support. A warm thank goes to Shorouk for the great help during the animal experiment.

I would like to thank all my colleagues working at TERM for a nice and friendly atmosphere, as well as the secretarial and technical assistants for taking care of the perfect organization of the lab. A big thank goes to Barbara for the knowledge transfer and help in the lab.

A warm thank goes to all the friends around the world for being always there for me!

From my whole heart I would like to thank my family for unlimited love, support and care during my all life. Everything I accomplished until now was possible just because of you.

Ringrazio con tutto il cuore la mia famiglia, per avermi sempre supportato e amato incodizionatamente. Tutto quello che sono riuscita ad ottenere nella mia vita lo devo a voi.

Finally, the biggest thank goes to Markus for being a colleague, a friend and my beloved partner. Thanks for the joy, happiness and love that you brought into my life!